Faculté des Sciences - Aix-Marseille Université
163 Avenue de Luminy - Case 901
13288 Marseille

Laboratoire de Chimie Bactérienne
31 Chemin Joseph Aiguier
13009 Marseille

Thèse

En vue d'obtenir le grade de Docteur d'Aix-Marseille Université
Biologie, spécialité Microbiologie

Présentée et soutenue publiquement par

Morgane Wartel

Le Mercredi 18 Décembre 2013

A novel class of bacterial motors involved in the directional transport of a sugar at the bacterial surface: The machineries of motility and sporulation in *Myxococcus xanthus*.

Une nouvelle classe de moteurs bactériens impliqués dans
le transport de macromolécules à la surface bactérienne:
Les machineries de motilité et de sporulation de *Myxococcus xanthus*.

Membres du Jury :

Dr. Christophe Grangeasse	Rapporteur
Dr. Patrick Viollier	Rapporteur
Pr. Pascale Cossart	Examinateur
Dr. Francis-André Wollman	Examinateur
Dr. Tâm Mignot	Directeur de Thèse
Pr. Frédéric Barras	Président du Jury

Faculté des Sciences - Aix-Marseille Université
163 Avenue de Luminy - Case 901
13288 Marseille

Laboratoire de Chimie Bactérienne
31 Chemin Joseph Aiguier
13009 Marseille

Thèse

En vue d'obtenir le grade de Docteur d'Aix-Marseille Université
Biologie, spécialité Microbiologie

Présentée et soutenue publiquement par

Morgane Wartel

Le Mercredi 18 Décembre 2013

A novel class of bacterial motors involved in the directional transport of a sugar at the bacterial surface: The machineries of motility and sporulation in *Myxococcus xanthus*.

Une nouvelle classe de moteurs bactériens impliqués dans
le transport de macromolécules à la surface bactérienne:
Les machineries de motilité et de sporulation de *Myxococcus xanthus*.

Membres du Jury :

Dr. Christophe Grangeasse	Rapporteur
Dr. Patrick Viollier	Rapporteur
Pr. Pascale Cossart	Examinateur
Dr. Francis-André Wollman	Examinateur
Dr. Tâm Mignot	Directeur de Thèse
Pr. Frédéric Barras	Président du Jury

Après quasiment cinq années passées au LCB, j'ai évidemment plein de personnes à remercier, pour leur participation, de près ou de loin, à cette thèse.

Tout d'abord, je tiens à remercier Frédéric Barras, directeur du LCB et Président de mon jury de thèse, de m'avoir accueilli au sein de son laboratoire.

Je tiens également à remercier les membres de mon jury pour l'intérêt qu'ils ont porté à mon manuscrit et pour leurs commentaires constructifs : le Dr. Christophe Grangeasse et le Dr. Patrick Viollier, mes rapporteurs ; le Pr. Pascale Cossart et le Dr. Francis-André Wollman, mes examinateurs.

Cette thèse aurait sans doute été différente, voire plus difficile sans les membres « géniaux » (et je pèse mes mots) de l'équipe Mignot. Je pense vraiment avoir eu énormément de chance de faire partie d'une équipe comme celle-là. Même s'il y a eu des moments difficiles, je ne garde que des bons souvenirs, et surtout beaucoup de fous rires (que Patrice Moreau, Mireille Ansaldi et l'équipe Dolla ont dû subir…). Je vais commencer par mes Liliane et Catherine : Le Gall et Luciano. A nous trois, on formait les trois « grasses » (que ce soit pour la nourriture ou pour nos blagues de bon goût), et on dominait le monde (enfin Marseille) du haut de nos « marches Mignot ». Merci pour tout les filles, merci pour votre écoute, votre attention, votre gentillesse, vos paquets de mouchoirs dans les moments difficiles. Mais merci aussi pour tout les bons moments partagés (aux paillasses ou au bureau, autour de bières ou de mojitos, avec Céline Dion ou Francky Vincent). Ensuite, il y a mes Sophie et Sophie : Guzzo et Laura, mes dernières voisines de bureau. Chouchou-Guzzo, évidemment, merci de m'avoir fait découvrir HG et Geny G (que j'imite parfaitement bien maintenant), merci aussi pour tes remontages de moral et tes tentatives de redonnage de confiance en soi (avec moi, il y avait beaucoup de boulot). Où que je sois en post-doc, j'espère que tu viendras me voir et qu'on se fera une bonne quiche (comme on sait si bien les faire). Ma petite Laura, ma voisine de dos, j'ai vraiment été contente de partager ce bureau de la joie avec toi. J'espère que tu as apprécié mes vibes et qu'elles ne vont pas trop te manquer. Comme pour Guzzo, si tu viens me voir en post-doc, promis, je te ferais des vibes à la Céline ! Merci aussi pour ton soutien pendant la rédaction. Dernière personne avec qui j'ai partagé ce bureau, et pas des moindres, Jean-Phillipe Castaing, ou Jean-Phi, ou JP pour les intimes. Ton arrivée et ta présence masculine dans cette équipe purement féminine a été une bonne chose pour nous toutes. J'ai vraiment été contente de partager le bureau avec toi (mais aussi et surtout les Twix). Merci pour tes blagues, tes gâteaux, ta bonne humeur, mais merci aussi

pour les discussions plus sérieuses sur l'avenir. Un grand merci aussi à ma napolitaine préférée, Emi ! Merci d'avoir été à mes côté pendant une bonne partie de ma thèse, merci d'avoir été là dans les moments difficiles (que ce soit pour la thèse ou plus personnel) et merci pour tous tes conseils pour la suite. Même si on n'a pas toujours été d'accord sur tout, tu comptes vraiment beaucoup pour moi, et j'espère qu'on se reverra (à Marseille, à Naples, ou ailleurs). Baci, mia amica. Je remercie également les autres filles de l'équipe : Rym, pour son aide en matière de phylogénomie, son oreille attentive, et sa gentillesse (et aussi pour les bonnes pâtisseries qu'elle nous ramenait de Tunisie, dans la petite boite violette avec un « M ») ; Aurélie (ou Nathalie P.), ma jumelle de confiance en soi, merci pour ton aide et ton expertise sur le système Tol-Pal, et pour tes sourires; et Audrey, merci pour ta légendaire bonne humeur et pour tes clafoutis (à lire ces remerciements, je me rends compte que j'ai beaucoup mangé pendant ma thèse). Je remercie aussi tous mes collaborateurs de Princeton pour avoir participé aux travaux de cette thèse : Joshua, Mingzhai, Fabian et Shashi.

Je remercie aussi Spider-Leon (pour tes blagues de bon goût et ton expertise en microscopie), Romé (d'avoir été mon parrain de thèse, pour nos discussions scientifiques et pour ton écoute), Anouchka (heureusement que tu étais là cet été, merci beaucoup pour ton soutien et pour ta gentillesse), Eric (pour ta gentillesse et ton aide tout au long de mon parcours), toutes les personnes du sous-sol: Thierry, Anne, Elodie, Jordan, Frédérique, François, Maïa, Audrey et Annick (l'autre Corse du LCB), Laurent, Béatrice, Vanessa (pour ta bonne humeur, tes cartes postales, tes porte-clefs, et tes adaptateurs américains), Delphine, Isabelle, Martine, Aurélia, Jean-Pierre et Claude (pour m'avoir prêté à plusieurs reprises de la « colle-contact », m'évitant ainsi de marcher pieds nus dans tout l'Institut), Philippe et tous les autres (que j'oublie involontairement).

Pour clore en beauté le volet laboratoire, je tenais évidemment à remercier mon génie de chef : Tâm ! Merci de m'avoir accueilli dans ton équipe en master et merci de t'être « battu » avec moi pour que je puisse faire une thèse chez toi. Je suis bien consciente que j'ai eu énormément de chance de faire une thèse à tes côtés. Merci de m'avoir transmis (une partie de) ton savoir, ta passion, et (une partie de) ton optimisme. Merci de m'avoir donné la chance de partir en congrès, de rencontrer d'autres gens passionnés, et de voir ce qui se fait ailleurs comme Science. Evidemment, merci de m'avoir appris à faire de savants calculs mathématiques (les moles, MSD, dérivés, et constante d'Avogadro n'ont presque plus de secrets pour moi maintenant ; à chaque fois que je ferai un produit en croix, je penserai à toi). Merci aussi pour ton oreille attentive (pas seulement pour les problèmes scientifiques), merci d'avoir pris le temps de discuter avec moi de

mon avenir, et de m'avoir aidé à prendre des décisions quant à mon futur post-doc. Malgré tes « coups de gueule » (souvent justifiés, ou pas), tu es un chef exceptionnel, et j'ai vraiment adoré travailler avec toi ces quasi-5 dernières années.

Merci à mes précieux amis, vous avez été une vraie famille pour moi à Marseille pendant ces 4 années de thèse : Nico et Ferdinand, merci de m'avoir supportée (dans les bons et les mauvais moments), et merci de m'avoir embarquée dans tous vos bons plans : Tignes, le GR20 (encore merci Nico d'avoir accepté de prendre le déo, Ph, si tu veux, je t'aiderais à finir le GR Nord), Stockholm (dédicace aux pieds de PH), Giens, le petit chalet en Savoie, et bien d'autres… Grâce à vous, ces 4 années de thèse sont remplies de bons souvenirs, de fous rires, de bonne musique (ou pas), de superbes panoramas. Vous allez me manquer et j'espère que malgré nos différentes destinations post-doctorales, on se reverra ! Merci aussi à mon Fabrice Mouhamar, merci pour pleins de choses (je vais forcément en oublier) : merci pour tes fameux plats en sauces, nos repas avec le Ferdinand à Marseille (chez vous) sont de superbes souvenirs, merci de m'avoir prêté tes tee-shirts à plusieurs reprises pour me moucher, merci pour ta gentillesse et pour m'avoir écouté pleurnicher (c'est écrit dans tes remerciements), et je profite de ces remerciements pour m'excuser de ne pas encore être venu te voir chez toi, mais promis, j'essaie de corriger ça rapidement. Merci ma Anne-Lise, la SuperWoman du Nebraska (et je te souhaite bientôt de l'Alaska), d'être toujours là, même si ces dernières années, je n'ai pas été très disponible pour toi. Tu es une fille en or, et j'ai beaucoup de chance de t'avoir comme amie. Merci aussi à Marie-Cécile, Louise, Aurélie, Hamza, Thibault, Mélissa, Catarina, Lisa, Sébastien, Sylvain, Jennifer, Julien, et Yonathan d'avoir été là pour moi.

Merci à mon Bernard, plus connu sous le nom de Baptiste. Tu le sais, je ne suis pas douée pour les remerciements (tu appréhendais, et moi aussi, cette partie de la thèse), mais je suis obligée de mettre ton nom dans cette partie car sans toi, je ne suis pas sûre que je serais venue à bout de cette thèse. Merci d'avoir sacrifié ton été, tes soirées, tes week ends pour moi. Je suis prête à sacrifier le prochain été pour ta thèse (et même mes soirées, et mes week ends) ! J'ai beaucoup de chance de t'avoir rencontré (enfin, toi aussi…).

Evidemment un grand merci à ma famille, et surtout à mes parents pour m'avoir soutenue (dans tous les sens du terme), depuis la Corse ou la Bretagne, pendant cette thèse et même avant. Merci d'être là pour moi, et même si je ne suis pas la fille la plus expressive de la Terre, je voulais vous dire que vous me manquez énormément depuis Marseille et que je vous aime. Merci à mon frère

Romain, pour tous les bons moments passés à Molini ou à Bodeux. Et merci à ma Mamie Rose, pour tout son amour et pour tous ses bons colis remplis de fromages, de charcuteries corses et de confitures maison, ça fait du bien au moral !

Merci à vous tous d'avoir rendu cette « aventure » possible !

TABLE OF CONTENTS

ARTICLES

ABBREVIATIONS

Å: Ångström

AAA+: ATPase associated with diverse cellular activities

ADP: adenosine diphosphate

A-motility: adventurous motility

ATP: adenosine triphosphate

ATPase: adenosine triphosphatase

bp: base pairs

CCCP: carbonyl cyanide *m*-chlorophenylhydrazone

CTP: cytidine triphosphate

DNA: deoxyribonucleic acid

EM: electron microscopy

EPS: exopolysaccharides

ER: endoplasmic reticulum

FA: focal adhesion

FAC: focal adhesion complexes

F-actin: filamentous actin

G-actin: globular actin

GFP: green fluorescent protein

GTD: globular tail domains

GTPase: guanosine triphosphatase

i.e.: id est

KDa: kilodalton

Mbp: megabase pairs

μm: micrometer

miRNA: micro RNA

mm: millimeter

mRNA: messenger RNA

mRNP: mRNA protein complexes

MT: microtubules

MTOC: microtubule-organizing center

nm: nanometer

NPC: nuclear pore complex

OMA: outer membrane auxiliary

PG: peptidoglycan

Pi: inorganic phosphate

PMF: proton motive force

PorSS: Porphyromonas secretion system

RER: rough endoplasmic reticulum

RNA: ribonucleic acid

rRNA: ribosomal RNA

SER: smooth endoplasmic reticulum

sfGFP: super folder green fluorescent protein

SIM: structure illumination microscopy

S-motility: social motility

snRNA: small nuclear RNA

TEM: transmission electron microscopy

TIRF: total internal reflection fluorescence

TPR: tetratricopeptide repeat

tRNA: transfer RNA

T3SS: type III secretion system

T4P: type IV pilus

T9SS: type IX secretion system

UTP: uridine triphosphate

UV: ultraviolet

Wet-SEEC: surface enhanced ellipsometric contrast microscopy in wet condition

WT: wild type

YFP: yellow fluorescent protein

INTRODUCTION

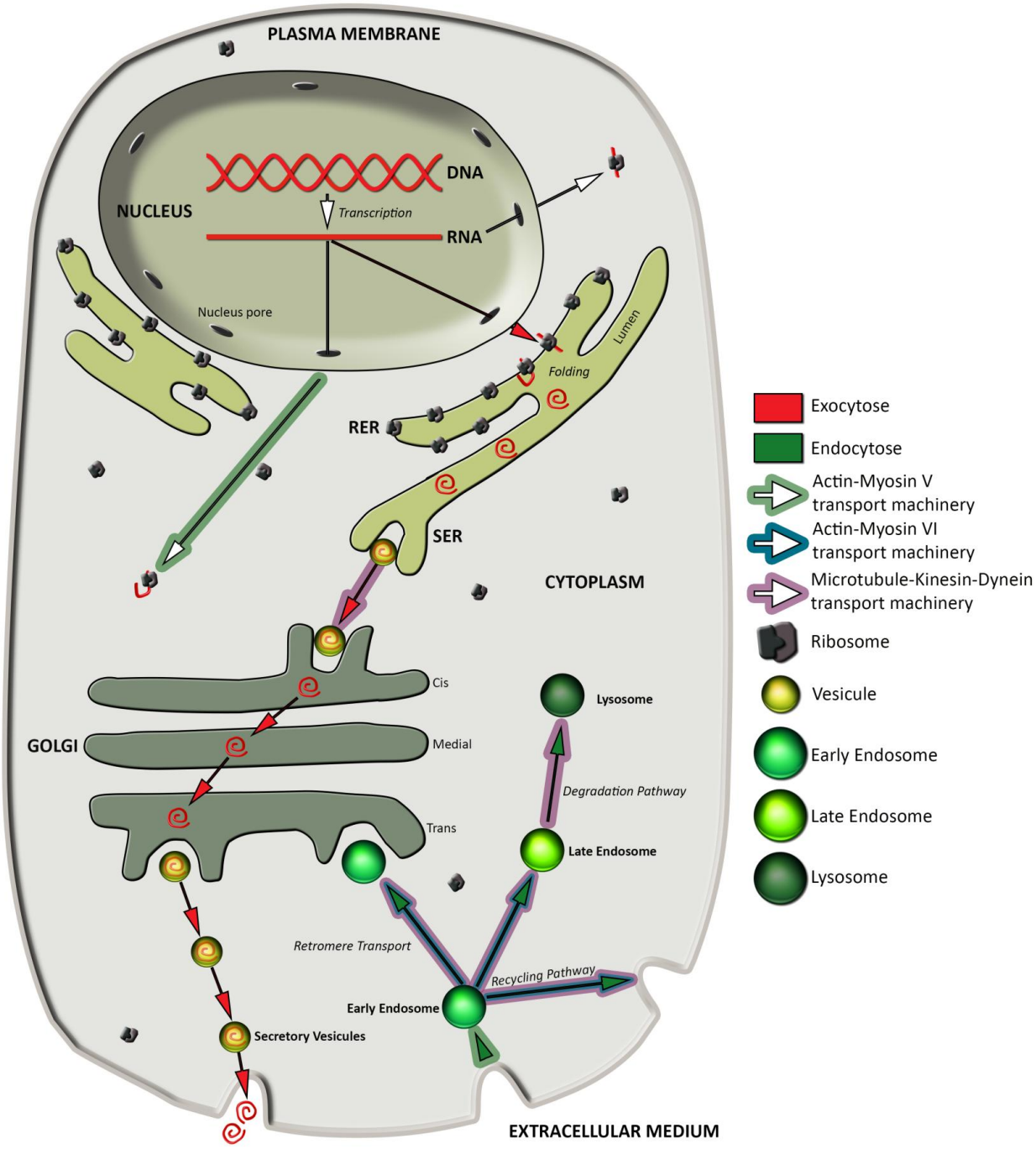

Figure 1. Schematic representation of a eukaryotic cell.

1. Intracellular Transport in Living Cells

In eukaryotic cells, intracellular transport is fundamental for cellular functions, survival and morphogenesis. Because the cells are compartmentalized into distinct membranous organelles and possess defined subcellular regions, the molecules and the organelles themselves have to be transported to the right compartment and to the right subcellular regions respectively, to exert their functions.

Because of the large eukaryotic cell size (10 to 100 µm), and because of the varying dimensions of the molecules and organelles, these latter cannot only simply diffuse in the cytoplasm to reach their destination. For fast and efficient transport of cargos (here and for the rest of the text, cargos refer to the transported molecules/organelles), cells have evolved sophisticated molecular motors that move along cytoskeletal filaments. These transport machineries (molecular motors + cytoskeleton) will be described below, but to understand where and when this transport is required, I will first make a brief description of the exocytic and endocytic pathways and discuss where active transport is involved in these pathways. As we will see, directed transport mechanisms are involved in all basic processes from protein synthesis, to protein maturation and to the delivery of proteins to their final destination.

1.1. Protein Sorting and Targeting Require Dedicated Transport in Eukaryotic Cells

1.1.1. Paths to Protein Synthesis and Exocytosis

To survive, eukaryotic cells produce proteins that could have different final destinations: they can exert their functions in the cytoplasm or in the membranous organelles, or they can be secreted in the extracellular medium *via* the exocytose pathway (Figure 1). In parallel, cells can also import molecules from the extracellular medium *via* the endocytic pathway (Figure 1). For these essential processes, cells require active transport to carry molecules and organelles to different places.

Protein synthesis starts in the nucleus with the transcription of DNA into RNA. After processing and splicing, the RNA exits the nucleus through the nuclear pore complex (NPC) to reach the cytoplasm (Figure 1). Passive diffusion could be at the origin of this export. However, with

increasing molecule size, passive diffusion becomes quickly inefficient. Thus, large molecules, such as large RNAs (≥ 30 KDa), are transported across the NPC actively. Besides, these export machineries allow transport to occur in a controlled manner. The export of transfer RNA (tRNA), micro RNA (miRNA), ribosomal RNA (rRNA) and small nuclear RNA (snRNA) is ensured by exportins of the karyopherin family, regulated by the small GTPase Ran (Katahira, 2012; Köhler and Hurt, 2007). On the contrary, the export of messenger RNA (mRNA) results from another class of transporters called Tap-p15 in metazoans and Mex67–Mtr2 in *Saccharomyces cerevisiae* (Katahira, 2012). Moreover, numerous additional export factors cooperate with the mRNA export receptor (Katahira, 2012; Köhler and Hurt, 2007). It has also been shown that exceptionally, large mRNA protein complexes (mRNPs) exit the nucleus through nuclear membrane budding (Speese et al., 2012).

Translation takes place at ribosomes, which can be free in the cytoplasm, or embedded in the endoplasmic reticulum (thus called rough endoplasmic reticulum or RER) membrane. RNA transcripts can thus be addressed to two localizations for their translation: they can be transported to the ribosomes embedded in RER if the protein encoded by the RNA needs to be matured (Figure 1); or they can be transported to specific subcellular regions where free ribosomes will translate them. Indeed, a large part of the expressed transcripts are translated at specific subcellular localizations where the protein is required (Lécuyer et al., 2007). The transport of these RNAs can occur *via* acto-myosin motors (Figure 1). This active localization of mRNA provides spatial control of protein expression and function (Jansen and Niessing, 2012; Sladewski et al., 2013).

When translation takes place in the RER, embedded ribosomes extrude protein chains into the lumen of the RER (Figure 1). Then, vesicles deriving from the smooth endoplasmic reticulum (SER, endoplasmic reticulum without ribosomes) and containing the newly synthesized proteins, leave the endoplasmic reticulum (ER). These vesicles, coated by COPII complex, are transported in a directional manner to the Golgi apparatus. This export of cargo from the ER to the Golgi apparatus involves microtubules filaments and its plus- and minus-end-directed motors, kinesin and dynein respectively (Figure 1) (Brownhill et al., 2009; Gupta et al., 2008). In the Golgi apparatus, proteins are modified and processed. The Golgi apparatus also packages proteins in vesicles, which could have different cellular destinations. They could be addressed to the cytoplasm to fuse with the membrane of organelles (endosome, ER). They could be involved in exocytosis, a process where a vesicle and its content are targeted to the plasma membrane, fuse with it to release the content in the extracellular medium (secretion) (Figure 1) (Brownhill et al., 2009).

1.1.2. Endocytosis

At the same time, but by a reverse route, cells can internalize molecules from the surface through a process called endocytosis. The endocytosis pathway starts at the plasma membrane, where an extracellular molecule becomes engulfed in early endosomes. Immediately after internalization, these early endosomes can have different destinations: (i), they may be transported back to the plasma membrane *via* the recycling pathway; (ii), they can be sent to the degradative pathway *via* its transition into late endosomes and lysosomes; (iii), finally, they can reach the Golgi apparatus through the retromer transport pathway (Figure 1) (Brownhill et al., 2009; Hunt and Stephens, 2011). Whatever pathway the early endosome follows, the distribution of this organelle depends on active transport driven among other by microtubule-kinesin/dynein actin-myosin VI (Figure 1) (Baluska et al., 2004; Loubéry et al., 2008; Tumbarello et al., 2013).

As discussed above, endocytosis and exocytosis are driven by passive diffusion, acto-myosin motors and microtubule-associated motors. In the next chapter, I will describe the mechanisms that govern the movement of molecules and organelles in eukaryotic cells.

1.2. How Molecules and Organelles Move in the Cytoplasm?

As discussed above, molecules and membranous organelles move throughout cytoplasm to reach subcellular regions where they will exert their function. These intracellular displacements could be currently divided in two categories: passive movement (which is also called Brownian motion) and active transport.

1.2.1. Brownian Motion

1.2.1.1. Principle

Brownian motion is the stochastic movement of particles suspended in a solution and it is ubiquitous at the molecular and cellular scale (for example, movement of small molecules in the cytoplasm, or movement of a non-motile organism in a liquid medium). In the cytoplasm, Brownian motion gives rise to the diffusive movement of molecules and membranous organelles throughout the cell. These random movements depend on different factors: the composition/viscosity of the cytoplasm, the organization and the geometry of the cell, and the

size of the diffusing particles (indeed, the effective viscosity of the cytoplasm increases with particle size) (Misteli, 2001; Verkman, 2002).

Brownian movement is essential for the cell survival because protein collisions drive many essential protein interactions and enzyme-substrate reactions (Misteli, 2001; Verkman, 2002). For example, DNA replication and transcription in the nucleus necessitates many proteins to interact with DNA and RNA (Scialdone and Nicodemi, 2010). This nuclear mobility of proteins is largely energy-independent and therefore likely occurs by a diffusion-based mechanism (Misteli, 2001; Phair and Misteli, 2000). Moreover, Brownian motion also drives many processes in the cytoplasm such as protein-protein interactions and enzyme-reactions (Verkman, 2002).

1.2.1.2. Limitations and Constraints

Although Brownian motion drives several processes in many cell compartments, this process is often too slow for the long distance transport of cargos and/or for their concentration at specific subcellular regions.

While proteins typically diffuse throughout the cytoplasm with diffusion coefficients in the range of tens of $\mu m^2/s$ and therefore explore the volume of a cell within a few minutes to several tens of minutes (for a cell size of a tens of microns), a 100 nm sized organelle (Figure 1, a vesicle measure around 100 nm) typically has a diffusion coefficient of $10^{-3}\mu m^2/s$ within the cell, and would need 10 days to diffuse over the length of the same cell (Klumpp et al., 2006). Thus, for large objects, such as chromosomes (Figure 1, the X chromosome measures around 7 μm and a lysosome measures around 1 μm) or organelles which need to be moved over long distances, or for some small molecules which need to be transported faster in the cell, other efficient transport systems are required.

1.2.2. Active and Directed Transports

For directed, efficient and fast transport of cargos or to carry large objects (such as chromosomes, membrane organelles, secretory vesicles…), eukaryotic cells use active transport based on a two-component complex: a cytoskeletal fiber that serves as a track, and a motor protein that does the work. The molecular motor converts the chemical energy (ATP) into a mechanical work producing directed motion.

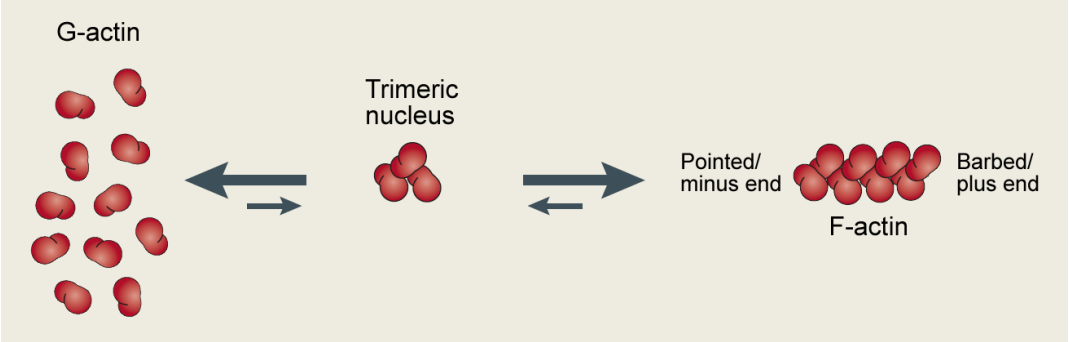

Figure 2. Schema of the actin polymerization (modified from Goley and Welch, 2006).

Two classes of mechanisms are used to actively transport cargos in eukaryotic cells: actin-based mechanisms that involve myosin motors pulling on actin fibers, and microtubule-based mechanisms that involve dynein or kinesin motors pulling on microtubules.

1.2.2.1. Actin-Based Transport

1.2.2.1.1. Actin Structure & Function

The eukaryotic actin cytoskeleton is highly conserved and actin is the most abundant protein in many eukaryotic cells (about 5% or more of the total cell protein). It is involved in several processes, including cell migration, endocytosis, the trafficking of cargos and cytokinesis, many of which are essential for the survival of the cell (Alberts et al., 2002).

The core component of the actin cytoskeleton is the monomeric globular G-actin (G for globular), a 43-kDa ATPase. G-actin can self-assemble into filamentous F-actin (F for filamentous), under the control of ATP hydrolysis (Figure 2). The filament forms a right-handed helix, with a helical pitch of 36 nm (Warshaw, 2012). The filaments arrange as double helical polymers of G-actin, in a head-to-tail conformation and thus the filaments are polarized (Figure 2). Indeed, each asymmetric filament possesses a fast growing barbed end, called the plus-end, and a slower growing pointed end, called the minus-end, that are distinguishable by their structural characteristics and kinetic properties (Figure 2) (Goley and Welch, 2006; Pollard and Borisy, 2003). This filament polarity is essential for the mechanism of actin assembly and also for the directional movement of the myosin motors. Besides, F-actin is oriented in the eukaryotic cell: the plus-ends are oriented toward the edge of the cell. The polarity of F-actin is therefore essential for cargos transport, as myosin V and VI motors move preferentially toward the plus- or the minus-end respectively, allowing for example, the oriented transport of mRNA.

1.2.2.1.2. Myosin Motors

Myosins, which are able to move on actin filaments, are involved in various cellular functions like movement of pigment granules, cytokinesis, cell adhesion, exocytose, endocytose, movement of mRNA and cell motility. The versatile functions of myosins are reflected by their diversity: 35 distinct classes of myosin were characterized by their kinetic properties and structural adaptations (Odronitz and Kollmar, 2007). Here, I will only describe class V and VI myosins, which are adapted to transport cargos.

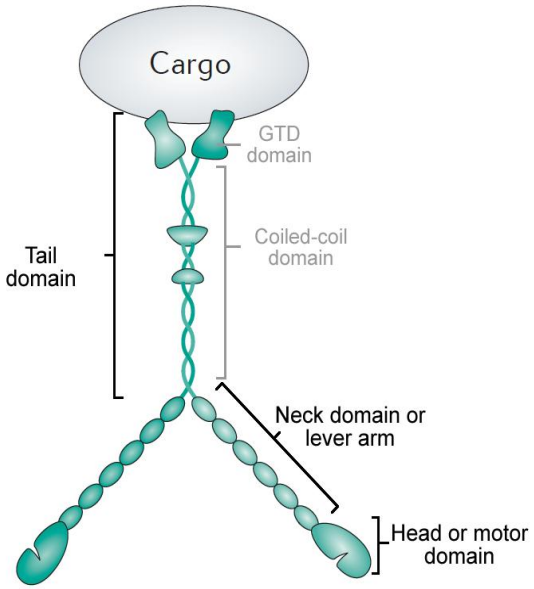

Figure 3. Domain structure of myosin V (modified from Hammer and Sellers, 2012).

Properties of myosin V

Myosin V is found in almost all eukaryotic genomes sequenced to date (Odronitz and Kollmar, 2007). It is composed of three domains: the head, the neck and the tail (Figure 3).

The head domain, often called the motor domain is located at the N-terminus and contains the nucleotide and the actin binding sites (Figure 3).

The neck domain is also called the lever arm because it moves as a rigid body to generate the power stroke (which is the distance that the lever arm moves in a single event) (Figure 3). The power stroke is due to a response to small ATP-dependent changes in the conformation of the motor domain (Hammer and Sellers, 2012; Sakamoto et al., 2003).

The tail domain contains the most class-specific variations and consists of coiled-coil motifs and two globular tail domains (GTDs) (Figure 3). The coiled-coil forming sequences dimerize to form a two headed motor, allowing the molecule to walk along actin filaments by alternating the positions of the leading and lagging head (Hammer and Sellers, 2012; Warshaw et al., 2005). The GTDs, located at the C-terminus, mediate the binding of the myosin to the cargo (Figure 3).

Processive movement of myosin V along actin

Myosins V are one of the most highly studied processive molecular motor, which have the ability to travel long distances (> 1 μm) by taking multiple 36 nm steps without detaching from their actin tracks. This ability, called processivity, makes this motor well suited for directed and efficient intracellular cargo transport along the actin cytoskeleton, traveling from the cell center toward the cell periphery (Warshaw, 2012). Indeed, myosin V is characterized to move directionally toward the F-actin plus-end, in a "hand-over-hand" manner (akin to human walking), at a velocity of 0,5 μm/s (Pierobon et al., 2009; Yildiz et al., 2003).

Myosin V dimers form a coordinated two-headed motors, allowing it to "walk" along actin filaments by alternating the positions of its leading and lagging heads (Figure 4b). The directionality of myosin originates in periodic asymmetries of the actin filament, a consequence of the head-to-tail conformation of G-actin in the filament. As a result, myosin V moves directionally toward the plus-end of the actin filament and cannot step back (Hammer and Sellers, 2012; Rief et al., 2000).

The affinity of myosin for actin is at the heart of the processive and directional movement and it depends on the kinetic cycle of ATP hydrolysis at the myosin heads (Figure 4a). Myosin has a high affinity for actin when it is nucleotide-free or when it is bound to ADP alone, whereas it has a low affinity for actin when it is bound to ATP or to ADP and inorganic phosphate (Pi) (Figure 4a) (Hammer and Sellers, 2012; De La Cruz et al., 1999). In the resting state, myosin V dwells

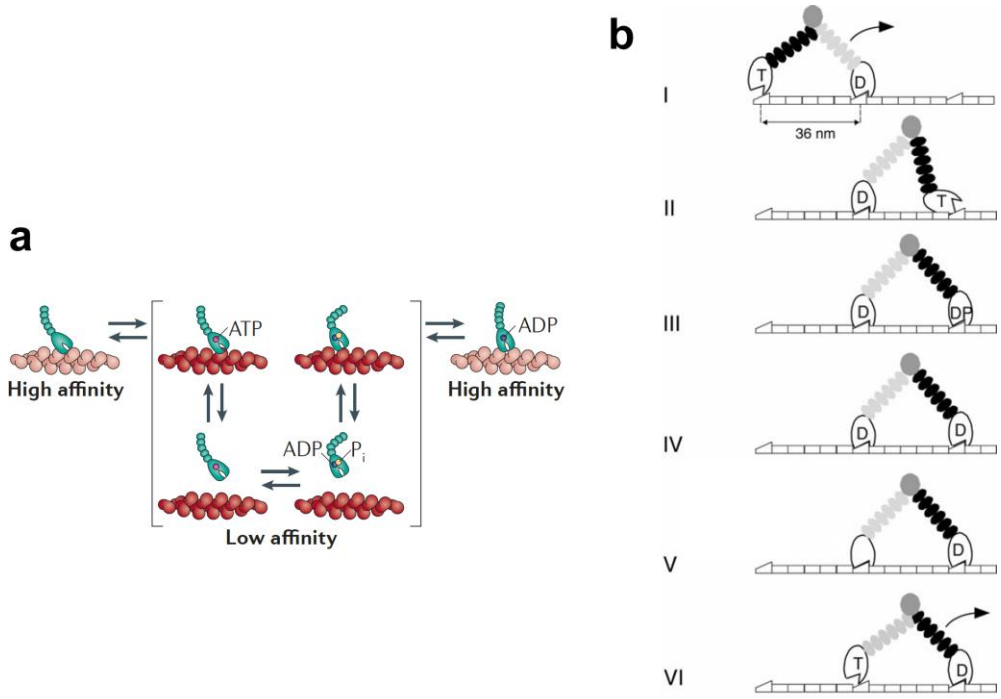

Figure 4. Processive movement of myosin V along actin. a. Variation of the myosin affinity for actin filament depends on the kinetic cycle of ATP hydrolysis of myosin (from Hammer and Sellers, 2012). b. Model of the processive movement of myosin V along actin filament. D = ADP; T = ATP; DP = ADP + Pi (modified from Rief et al., 2000).

with both heads attached to the actin filament in an ADP-bound form. ATP binding to the lagging head promotes its dissociation from actin (Figure 4b, step I), and forward movement of the released head (Figure 4b, step II). Thus, the previous leading head then becomes the lagging head. The newly detached leading head quickly hydrolyzes ATP and subsequently binds actin (Figure 4b, step III). Inorganic phosphate (Pi) release occurs concomitant or immediately after actin binding (Figure 4b, step IV). Because the two heads exert intramolecular strain on each other, leading head-binding induces the lagging head to release its ADP and thus detach from actin (Figure 4b, step V). The released lagging head binds a new ATP and the cycle is reproduced (Figure 4b, step VI) (Hammer and Sellers, 2012; Kull and Endow, 2013; Muretta et al., 2013; Rief et al., 2000).

Properties of the myosin VI

I will not detail myosin VI because it has been discovered more recently and it is similar to the myosin V. It is involved in variety of intracellular processes such as vesicular membrane traffic, cell migration and mitosis. Moreover, like myosin V, dimers of myosin VI are processive motors. However, the interesting property of myosin VI is its capacity to move in the opposite direction compared to myosin V. Indeed, myosin VI traffic directionally toward the minus-end of actin filaments (Buss et al., 2004; Sweeney and Houdusse, 2010). The principal difference between myosin V and VI is that the myosin VI has an insert localized at the end of the motor domain (or head domain). This insert is the unique determinant of the myosin VI directionality because when it is absent, myosin VI becomes a plus-end directed motor (Park et al., 2007). The presence of this insert may allow the repositioning/rotation of the lever arm, projecting the motor head toward the minus-end (Ménétrey et al., 2005; Wells et al., 1999).
In conclusion, myosin V and myosin VI promote bidirectional transport along the actin filament. Such actin-based transport allows the cargos to be transported throughout the cytoplasm, in the direction of the plasma membrane (toward the plus-end), for example during exocytosis; or in the direction of the "center of the cell" (toward the minus-end), during endocytosis.

1.2.2.2. Microtubule-Based Transport

1.2.2.2.1. Microtubule Organization

Microtubules (MT) are essential cytoskeletal polymers present in all eukaryotic cells. They extend throughout the cytoplasm and are involved in mitosis, cell motility, intracellular transport,

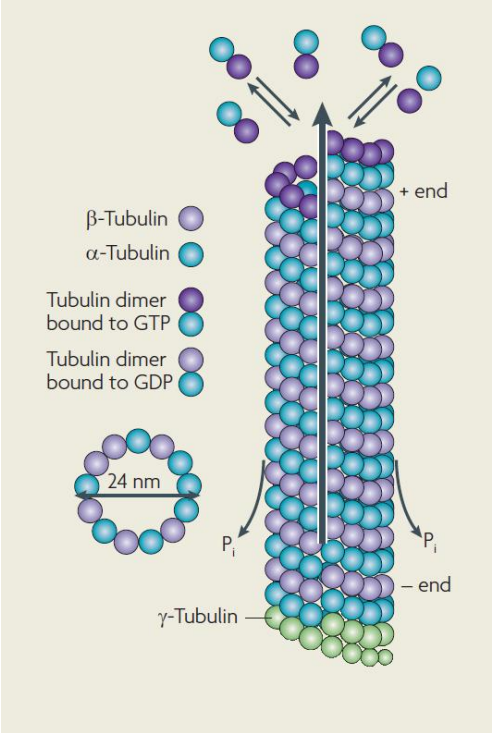

Figure 5. Structure of a microtubule (modified from Conde and Cáceres, 2009).

secretion, maintenance of cell shape and cell polarization. Microtubules are polarized structures composed of α and β tubulin heterodimer subunits assembled into linear protofilaments. A single microtubule is built from 13 protofilaments that associate laterally to form a 24 nm wide hollow cylinder (Figure 5). Because of the head-to-tail association of the αβ heterodimers, microtubules are polar structures with different rates of polymerization at the two ends. Indeed, it is possible to distinguish a plus-end (faster-growing end) and a minus-end (slower-growing end): the β-tubulin monomer pointing towards the plus-end and the α-tubulin monomer exposed at the minus-end (Figure 5). A third tubulin isoform, the γ-tubulin, acts as a template for the correct assembly of microtubules (Figure 5) (Alberts et al., 2002; Conde and Cáceres, 2009; Nogales and Wang, 2006). As for F-actin, microtubules are oriented in the eukaryotic cell: they are anchored at the microtubule-organizing center (MTOC) by their minus-ends, while their plus-ends continue to grow into the cell periphery. Thus, the polarity of microtubules is important for cellular transport, as their kinesin and dynein motors move preferentially and directionally toward the plus- or the minus-end, respectively, allowing for example, vesicles to be directed to or from the ER and the Golgi apparatus.

1.2.2.2.2. Kinesin and Dynein Motors

Kinesin and dynein are microtubule-based motors that also drive the intracellular transport of molecules and membranous organelles. As for myosin V and VI for actin-based movement, kinesins use microtubule rails to transport cargo towards the plus-end and dyneins use microtubule to drive transport toward the minus-end (Hunt and Stephens, 2011).

Although kinesin and dynein are distinct from one another and from myosin, they are both two-headed motor protein systems that use ATP energy to transport a variety of intracellular cargos. Both kinesin and dynein move along microtubules processively (Gennerich and Vale, 2009).

Like myosin, kinesin is an ATPase. It is composed of two identical heavy chains and two associated light chains (Figure 6). Each heavy chain includes an N-terminal motor domain that carries the catalytic activity followed by a region predicted to form a α-helical coiled-coil leading to heavy chains dimerization. The light chains are involved in cargo specificity (Wade, 2009). Kinesin moves forward the microtubules plus-end at a velocity about 1 μm/s (Gagliano et al., 2010). The mechanical cycle of kinesin has been well characterized and resembles that of myosin: movement is driven by the ATPase cycle and directed by the polarity of the MTs.

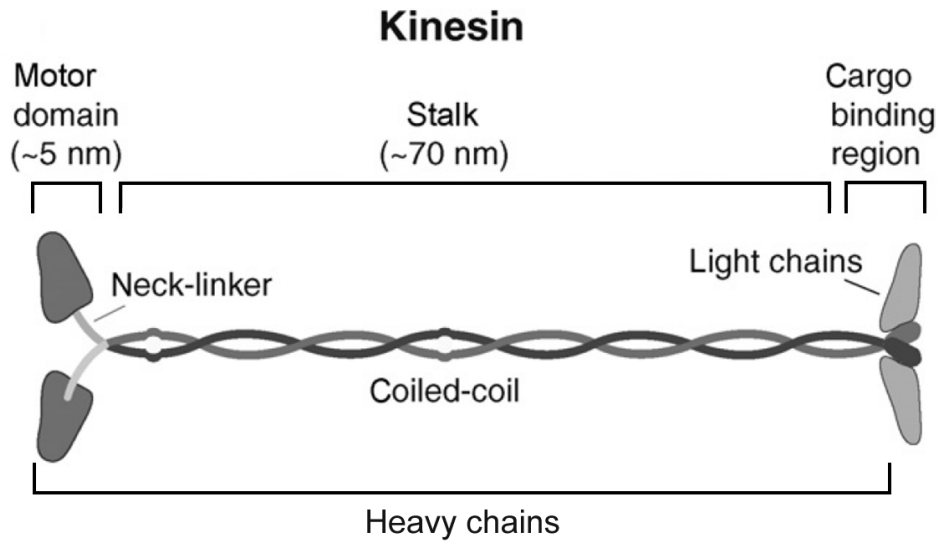

Figure 6. Domain structure of kinesin (Gennerich and Vale, 2009).

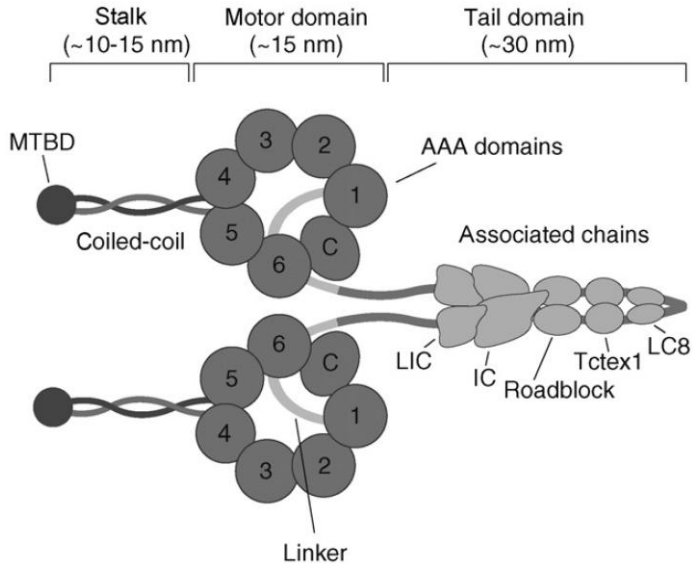

Figure 7. Domain structure of cytoplasmic dynein (Gennerich and Vale, 2009).

Dynein is involved in various biological functions, such as axonal transport, mitosis, and cilia/flagella movement. Although dynein was discovered 50 years ago, the progress of dynein research has been slow due to its large size and flexible structure. Dynein belongs to the AAA+ family (ATPase associated with diverse cellular activities) and can be divided into four domains: a tail (in N-terminus), a linker, a head or motor domain, and stalk (in C-terminus) (Figure 7). Contrary to the motor domain of kinesin which is located in N-terminus, the motor domain of dynein is closer to the C-terminus. Moreover, this motor domain does not carry the microtubule-binding domain as observed in the motor domain of kinesin. These structural differences are thought to be responsible of the different orientation taken by both of these microtubule-based motors. The tail is involved in cargo binding and the linker changes its conformation depending on the nucleotide state. The head (motor) domain of dynein is the site of ATP hydrolysis and is composed of six AAA+ modules and a coiled-coil domain, arranged in a ring. Among the six AAA+ domains, hydrolysis at the first AAA+ domain mainly provides the energy for dynein motility. The stalk domain of dynein was identified as the microtubule-binding domain chain (Figure 7) (Gennerich and Vale, 2009; Kikkawa, 2013). Dynein move toward the microtubule minus-end at a velocity about 2 μm/s but its mechanical cycle is still poorly understood (Wade, 2009).

1.3. Conclusions

In this introductory chapter, I argued the molecular organization of eukaryotic cells depends on a complex network of cytoskeletal filaments and associated molecular motors to compensate for the limitations of Brownian motion and to move large size particles. Indeed, these active transports require energy (hydrolysis of ATP and GTP) but allow a fast, efficient and directed movement (around 1 μm/s for both transport machineries) throughout the cytoplasm, when the Brownian movement is not sufficient.

Bacterial cells are thought to differ from eukaryotes because: first, their organization as long been thought to be much simpler and secondly, their small size may not justify the need for active intracellular transport. In the next chapter, I will review recent literature showing that the bacterial is in fact highly organized and ask whether active transport mechanisms and motors participate in this organization.

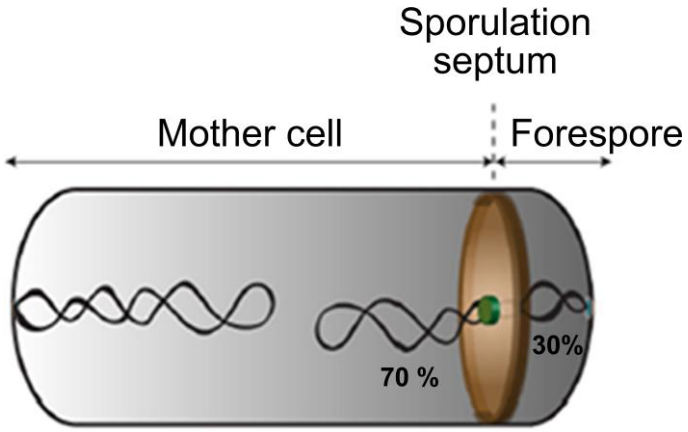

Figure 8. Sporulation of *B. subtilis*. Formation of the asymmetric sporulation septum (brown disc) divides the cell into mother cell and forespore compartments, and traps 30 % of the forespore chromosome (black ribbon) inside the forespore (modified from Fiche et al., 2013).

2. Architecture of the Prokaryotic Cell

Given that eukaryotes are highly compartmentalized cells, containing many membranous organelles, active transport mechanisms are required for the complex trafficking of macromolecules and even the organelles themselves. In bacterial cells, the cytosol is thought to be uncompartmentalized (except for rare exceptions such as bacterial magnetosomes and carboxysomes; Komeili, 2012; Yeates et al., 2008). Therefore bacteria have been mostly considered as non-organized cells, wherein proteins simply diffuse throughout the cytoplasm to reach randomly their sites of action. However, this lack of compartmentalization does not preclude organization. Indeed, improvements in cell imaging revealed that despite the absence of organelles, DNA, RNA and proteins are targeted to specific subcellular regions in bacteria, where they are spatially constricted to exert their function. In this view, intracellular transport could contribute to organization.

In this chapter, I will describe different degrees of bacterial cell organization and I will present the mechanisms evolved by bacteria to localize properly their molecules.

2.1. The Bacterial Cell is Highly Organized

2.1.1. Structural Organization of the Bacterial Chromosome

Given the small size of the bacterial cell, the bacterial chromosome needs to be compacted. For example, the *Caulobacter crescentus* cell must package a 1,3 mm genome (4,0 Mbp) in a 2 micron cell (Toro and Shapiro, 2010). However, this compaction must allow the normal progression of the cell cycle (genes expression, DNA replication, chromosomes segregation). Recent advances in fluorescent microscopy revealed that bacterial chromosomal loci are not localized randomly within the cytoplasm (see below).

Indeed, several studies conducted in different bacteria indicate that the bacterial chromosome has a specific orientation within the cell. First evidence comes from the study of *Bacillus subtilis*. Under starvation, this bacterium triggers a sporulation program that divides the cell asymmetrically into a large mother cell and a small forespore (Figure 8). This asymmetric division naturally traps approximately 30 % of the forespore chromosome in the forespore and 70 % of the forespore chromosome stays in the mother cell. Wu and Errington showed that the portion

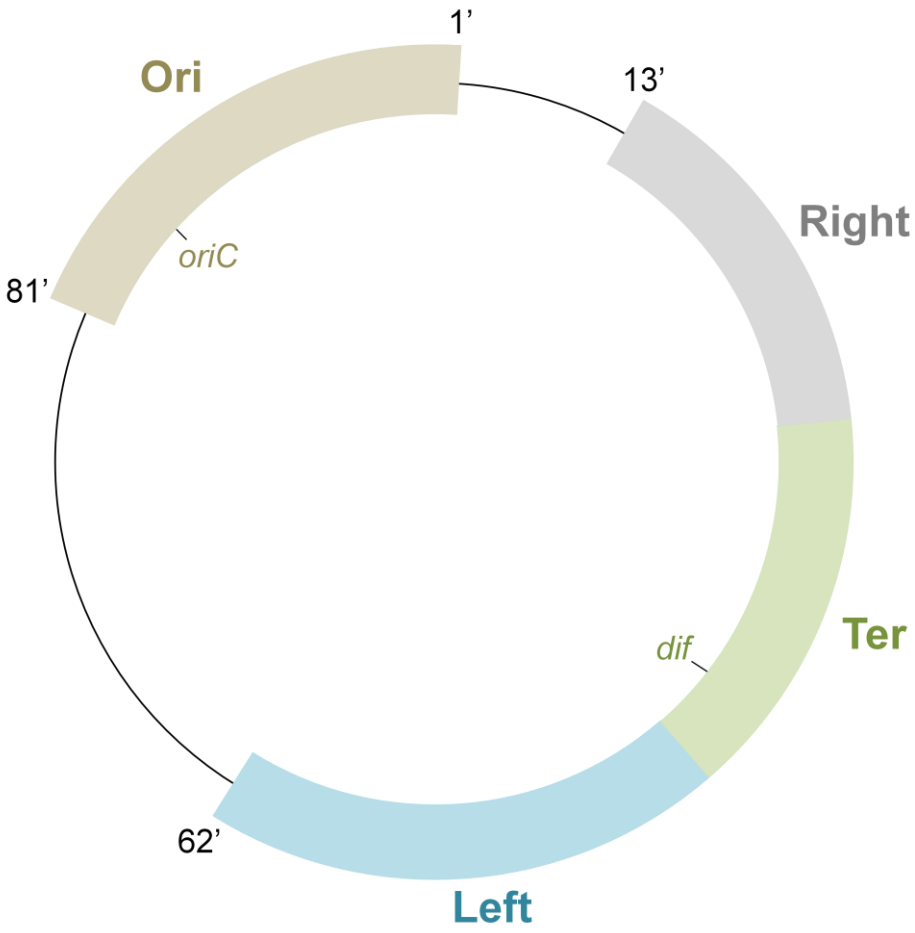

Figure 9. Organization of the *E. coli* chromosome into four macrodomains (thick lines: Ori, Right, Ter and Left) and two non-structured regions (thin lines) (adapted from Mercier et al., 2008; Valens et al., 2004).

of the chromosome found in the forespore (the 30 %) was reproducible from cell to cell, showing that the chromosome is spatially organized during sporulation (Wu and Errington, 1994). This chromosomal organization is important and it has been shown that the chromosomal position of certain sporulation genes could govern the timing and level of their expression during sporulation, and is therefore crucial for efficient spore formation in *B. subtilis* (Khvorova et al., 2000; Zupancic et al., 2001).

It was also found that the *Escherichia coli* chromosome is organized into four structured regions called macrodomains: the Ori macrodomain that contains *oriC*, the Ter macrodomain that contains the replication terminus and the chromosome dimer resolution *dif* site, and the left and right macrodomains (Valens et al., 2004). *E. coli* chromosome also contains two non-structured regions that flanks the Ori macrodomain (Figure 9) (Valens et al., 2004). Each macrodomain occupies a specific territory inside the nucleoid (Espeli et al., 2008). Moreover, if this chromosomal organization is perturbed, a viability defect is observed: cells are no longer able to properly segregate their chromosome (Mercier et al., 2008). This predetermined cellular positioning of chromosomal loci was also characterized in *Caulobacter crescentus* wherein 112 individual segments were shown to have a specific subcellular address (Viollier et al., 2004). In all these organisms, this organization is maintained over successive rounds of replication, segregation and cell division and is essential for the cell cycle.

This striking organization raises the question of how the chromosome is kept in place. Studies in *C. crescentus* and *B. subtilis* showed that a connection between the cell envelope and DNA exists and ensures proper localization of the chromosome. Indeed, the polar localization of the origin of replication of *B. subtilis* during sporulation, results from the connection between different components. Ben-Yehuda *et al.* demonstrated that the RacA protein binds preferentially to a large region around the origin of replication and also that RacA interacts directly with DivIVA (Ben-Yehuda et al., 2005). Since DivIVA, in turn, binds to negatively curved membranes, such as those present on the cytoplasmic side of the cell pole (developed below), the origin of replication is directly tethered to the cell pole (Lenarcic et al., 2009).

A similar mechanism was proposed to explain the polar localization of the origin of replication in *C. crescentus*. It involves a protein, PopZ, which is known to localize at the cell pole. This protein is also described to interact with the protein ParB, a DNA-binding protein. ParB binds specifically to the *parS* sequences, which are localized close to the origin of replication (Ebersbach et al., 2008). Thus, in *C. crescentus*, indirect interactions also allow the polar localization of the origin of replication.

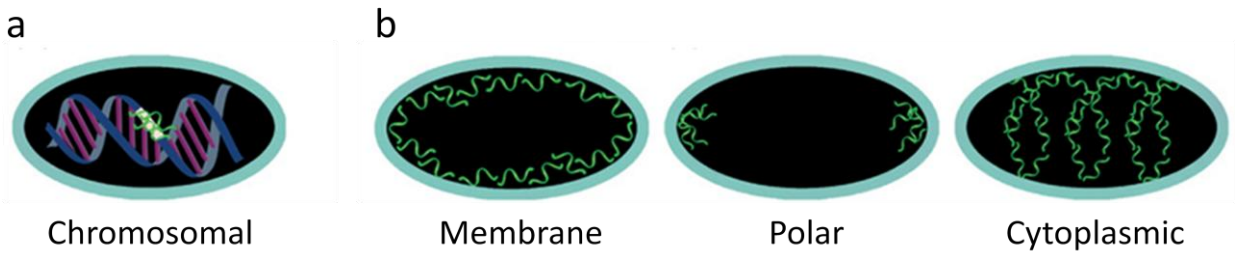

Figure 10. Patterns of mRNAs localization observed in bacteria. a. Several mRNAs in *C. crescentus* and *E. coli* were shown to localize near the chromosomal loci from which they are transcribed. b. Several mRNAs in *C. crescentus* and *E. coli* were shown to localize to the subcellular regions where their protein products are required, that is, to the membrane, the poles or the cytoplasm (modified from Govindarajan et al., 2012).

Recently, the structure of a bacterial genome was observed at high resolution in live imaging series and shown to have a mostly helical organization (Fisher et al., 2013). These authors also observed that the chromosome is bundled longitudinally and confined radially. By using rapid image acquisition, the authors found that the nucleoid exhibits waves of density changes that propagate from end to end. The authors proposed that these periodic undulations act to massage the nucleoid, thereby relieving tension such as super-coils and entanglements. Thus, their results confirmed that the nucleoid possesses an internal organization that could play critical governing roles, such as in the accessibility of the DNA and RNA polymerases to specific genes.

All these data support that bacterial chromosome is not a simple "ball of wool", floating in the cytoplasm, but rather a highly organized structure maintained at specific places within the bacterial cell.

2.1.2. Transcription and Translation are Spatially Organized

The high topological organization of the bacterial chromosome also implies that fundamental processes such as transcription and translation are spatially organized. Indeed, recent studies conducted by the Jacobs-Wagner and the Amster-Choder laboratories showed that mRNAs could adopt different patterns of localization in bacterial cells.

By using a sensitive method based on quantitative fluorescence *in situ* hybridization, Montero Llopis *et al.* observed a very limited dispersion of the transcripts from their sites of transcription during their lifetime both in *C. crescentus* and *E. coli*, (Figure 10a). mRNAs localization was also observed to restrict ribosomal mobility. The authors proposed that bacteria use the chromosome layout to localize post-transcriptional processes, locally increasing the subcellular concentration of the encoded proteins and their probability to interact and form complexes (Montero Llopis et al., 2010). This model could explain the frequent clustering of genes encoding interacting proteins because if interacting proteins encoded by clustered genes are synthesized in the same vicinity, rapid interaction may be facilitated, possibly even as soon as they are produced (Montero Llopis et al., 2010).

However, this may not be the case for all bacterial mRNAs, some of which may be targeted to specific sites, around the cell membrane, at the cell poles, or in a helix-like pattern in the cytoplasm (Figure 10b). In *E. coli*, Nevo-Dinur *et al.* observed that the specific subcellular localization of some mRNAs, such as *nifH* for example, correlated with the position where their future protein product is required (Govindarajan et al., 2012; Nevo-Dinur et al., 2011, 2012).

However, the molecular mechanism that localizes these mRNAs is still not clear. Given, the short half-life of bacterial mRNAs and the short generation time of bacteria, active mechanisms may be involved in the localization of the mRNA (Govindarajan et al., 2012). The Nevo-Dinur study will have to be confirmed, but it suggests that bacteria can spatially organize mRNA processes essential for the transfer of genetic information, in absence of a nucleus or other internal organelles.

2.1.3. Bacterial Proteins Can Localize to Specific Subcellular Regions

Protein localization is also a part of bacterial organization. Indeed, by using a high throughput method for analysis of protein localization in *C. crescentus*, Werner *et al.* were able to show that over 10 % of predicted encoded proteins exhibited specific and reproducible subcellular localization (Werner et al., 2009).

Other studies showed that protein localization in bacteria is critical for growth, cell cycle, chemotactic behaviors, and differentiation. For example, the position of the septal FtsZ-ring dictates where the division takes place (Margolin, 2005). Moreover, the clustering of chemotaxis proteins at either one or both poles and along the cell body plays a key role in the rapid responsiveness of the cell to small changes in attractants or repellents (Ames and Parkinson, 2006). It is also known that the localization of sporulation proteins governs spore morphogenesis (Errington, 2003; Higgins and Dworkin, 2012). These examples, described more precisely below, show the importance of subcellular localization for cellular activities and raise the question of how these proteins are correctly localized. Indeed, it is quite remarkable that many proteins are localized at specific areas such as cell poles, mid cell, or even in cytoplasmic clusters because these different regions are not separated from the rest of the cytoplasm by physical dividers such as specific membranes. Therefore, bacteria must exploit intrinsic localization factors such as the nucleoid, membrane cues, or the bacterial cytoskeleton to organize their cytoplasm.

2.2. Bacterial Localization Factors

2.2.1. The Bacterial Chromosome Acts as a Template for Protein Localization

The bacterial chromosome can serve as a scaffold for the localization of protein complexes. Some protein complexes have been shown to localize within the cytoplasm at fixed locations,

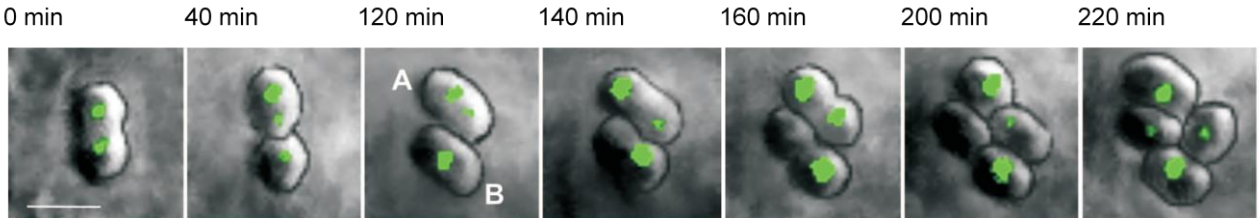

Figure 11. Time-lapse images of the cytoplasmic chemotaxis protein cluster in *R. sphaeroides*. One cell containing two clusters divides into cells A and B (120 min). The single A cluster becomes two clusters early in cell growth (40 min), and each cluster migrates rapidly to positions at one-fourth and three-fourths of the cell length (140 min), where they remain until the cell divides. This positioning results in each daughter cell inheriting a cluster at about mid-cell (200 min). The B cell contains a single cluster throughout most of the cell cycle. This cluster is inherited by one of the daughter cells, and a new cluster is observed in the other daughter cell soon after septation. Contour lines showing the outlines of the cells are superimposed. Scale bar = 2 μm (modified from Thompson et al., 2006).

while lacking any obvious membrane attachment. Moreover, this cytoplasmic organization is maintained over successive cycles of division. How is this specific localization achieved?

One well studied example is the positioning of cytoplasmic clusters of chemotaxis proteins in *Rhodobacter sphaeroides*. These proteins form a single cluster, early and stably localized at the center of cells, which divides into two daughter clusters (Figure 11). The daughter clusters are located at the one-fourth and three-fourths positions of the cell, a pattern reminiscent of that seen for certain low-copy number plasmids. After cell division, these two clusters are partitioned between the two daughter cells and each one of them shows one cluster at mid cell (Figure 11). This mechanism ensures the capability of each daughter cell to perform chemotaxis immediately after division. The separation in two daughter clusters and their segregation in daughter cells are dependent on a homologue of a bacterial type I DNA partitional factor (ParA), PpfA (Thompson et al., 2006). PpfA uses the chromosome as a scaffold to ensure that each daughter cell inherits a cytoplasmic cluster: on one hand, PpfA binds nonspecifically to the chromosome, and on the other hand, PpfA interacts with one component of the chemotaxis cluster, TlpT (ParB homologue). Thus, the segregation of the chemotaxis cytoplasmic cluster depends upon dynamic localization to the chromosome: (Roberts et al., 2012; Thompson et al., 2006). Orphan *parA*-like genes have been identified in several chemotaxis operons of different bacterial species, suggesting that the chemotaxis cytoplasmic clusters segregation mechanism in *R. sphaeroides* might be widespread in bacteria (Roberts et al., 2012).

The chromosome can also guide the positioning of protein complex negatively, such as the main division protein FtsZ. As we will show below, FtsZ plays a major role in the positioning of division proteins at the septum. Hence, it must be correctly localized to ensure that cell division starts at the right time and at the right place in the cell. It has been demonstrated that the nucleoid itself inhibits FtsZ polymerization and thus acts as a spatial regulatory system. Indeed, nucleoid occlusion prevents the assembly of the Z-ring on top of unreplicated chromosomal DNA, and thus prevents the "guillotining" of the chromosomal DNA by forming septa when chromosome replication or segregation is perturbed (Bernhardt and de Boer, 2005). As a result, the Z-ring does not form at the cell midpoint until most of the chromosome has been duplicated and partitioned in each daughter cell (Govindarajan et al., 2012; Margolin, 2005; Shapiro et al., 2009). Nucleoid occlusion in *B. subtilis* and *E. coli* involves respectively the Noc and SlmA proteins that do not share sequence similarities. Both of them bind to DNA and inhibit Z-ring assembly over the chromosome. Noc and SlmA bind to specific DNA sequences that are

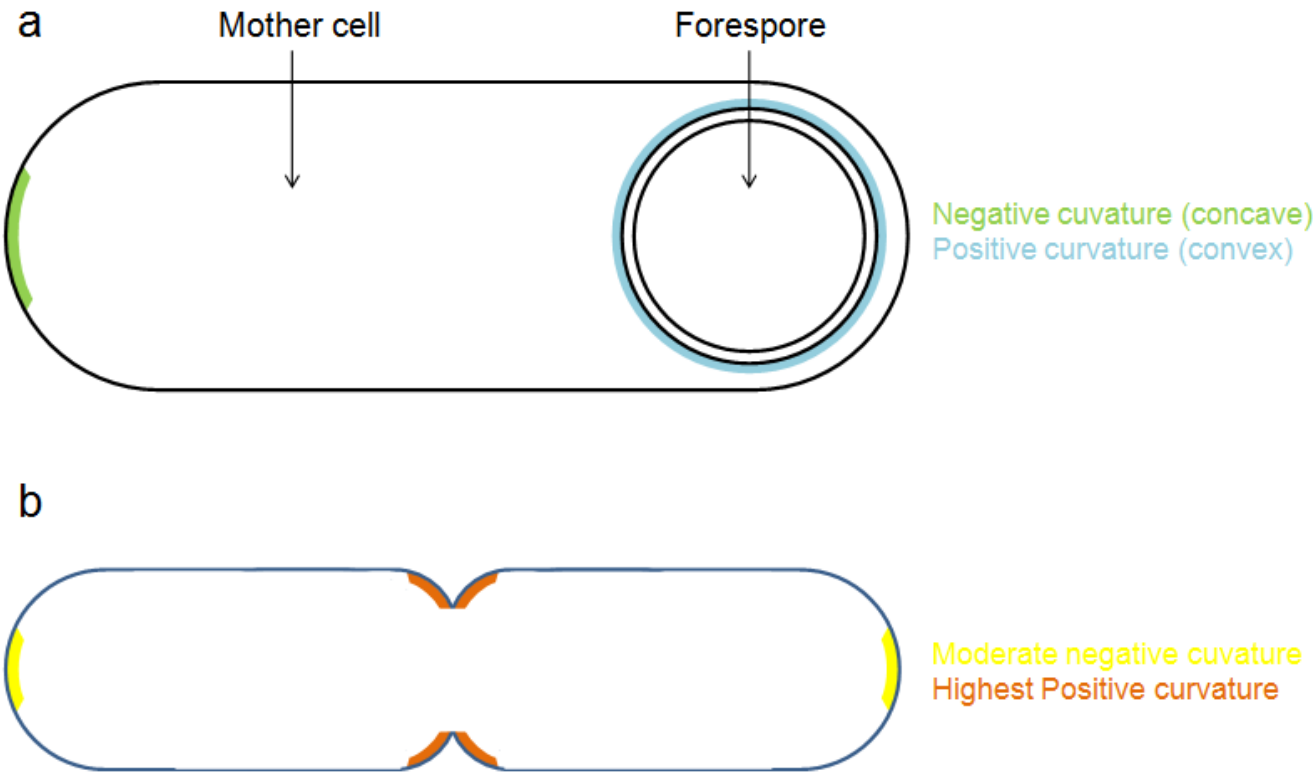

Figure 12. Difference in membrane curvatures. a. Representation of the engulfment of the forespore by the mother cell. In a sporulating *B. subtilis* cell, the outer surface of the forespore (blue) is the only positively curved surface (convex). b. In a rod-shaped dividing *B. subtilis* cell, the highest negative curvature is near the forming septum (orange), whereas the hemisphere poles are characterized by moderate negative curvature (yellow) (adapted from Govindarajan et al., 2012; Ramamurthi et al., 2009).

particularly sparse near the terminus region of the chromosome. It has been shown that SlmA is able to interact directly with FtsZ, whereas for Noc, no such interaction has as yet been shown. For *B. subtilis* and *E. coli*, the terminus region occupies the midcell region when replication is almost complete. SlmA and Noc are therefore kept away from midcell due to chromosome segregation, allowing FtsZ to polymerize at mid-cell (Bernard et al., 2010; Bernhardt and de Boer, 2005; Margolin, 2005; Rodrigues and Harry, 2012; Tonthat et al., 2011, 2013; Wu et al., 2009).

In conclusion, these two selected examples show that the nucleoid can exert both positive and negative roles to localize proteins at subcellular sites.

2.2.2. Geometric Cues can Lead to Protein Localization

Recent studies identified that the geometry of the bacterial membrane could act as a physical cue for protein localization. Both concave (negative curvature) and convex (positive curvature) shapes can act as targets for protein localization (Figure 12a). An example of this mechanism is given by the study of two *Bacillus subtilis* proteins: SpoVM and DivIVA.

SpoVM, a protein essential for the assembly of the *B. subtilis* spore coat, was the first protein whose localization was shown to be determined by membrane curvature in bacteria. SpoVM is expressed exclusively in the mother cell during sporulation but localizes specifically to the outer membrane surface of the forespore rather than the cytoplasmic membrane that surrounds the mother cell (Figure 12a). Ramamurthi *et al.* found that SpoVM can discriminate between the positive curvature of the membrane surrounding the forespore and the negative curvature of the cytoplasmic membrane of the mother cell, and thus binds preferentially to the positive forespore-surrounding membrane (Figure 12a). Recognition seems to involve cooperative interactions between SpoVM subunits, so that a curved membrane of 500 nm radius can be sensed and bound by a protein of 40 Ångström (Å) (Ramamurthi et al., 2009).
The discovery that positive membrane curvature is a localization factor raised the possibility that negative membrane curvature might also be exploited for protein localization in bacteria. This question was addressed by the study of the subcellular localization of DivIVA. DivIVA localizes principally as a ring at the nascent septa and secondarily, to the less negatively curved polar regions (Figure 12b) (Eswaramoorthy et al., 2011; Lenarcic et al., 2009; Ramamurthi and Losick, 2009). Thus, DivIVA localizes in cellular regions that show high negative curvature: division septa and poles, suggesting that DivIVA is able to discriminate among degrees of concavity

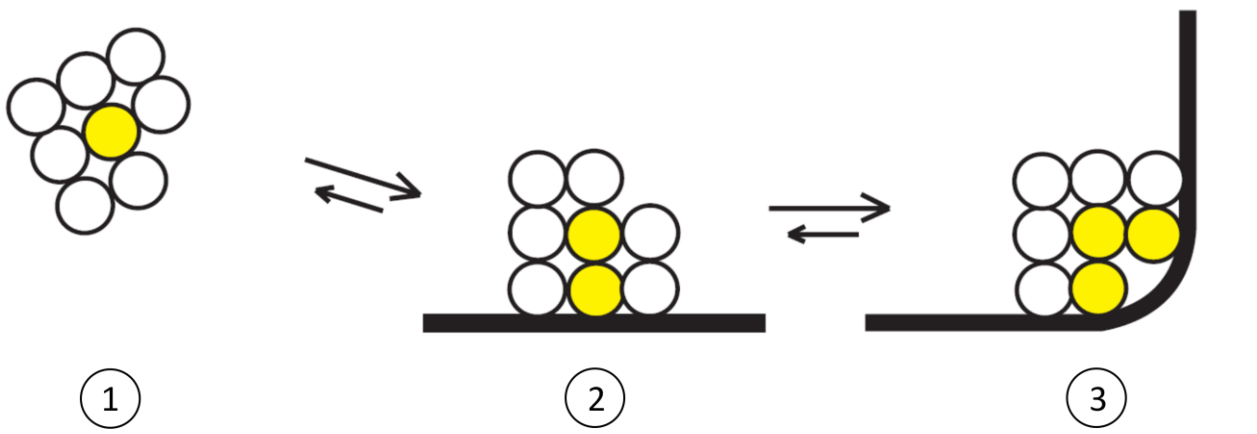

Figure 13. Schematic representation of the "Molecular Bridging" principle. DivIVA monomers are represented by spheres. These spheres are able to interact with each other and with the cell membrane. A cluster of eight DivIVA freely floats in the cytoplasm (step 1). Spheres at the periphery of this cluster (transparent spheres) have fewer interactions and are more prone to detach and diffuse away, whereas spheres that are enclosed are more stable (yellow spheres). Binding of this cluster to the lateral flat cytoplasmic membrane (step 2) decreases the exposed surface and stabilizes the cluster. This effect is reinforced when the membrane is strongly curved (step 3) (modified from Strahl and Hamoen, 2012).

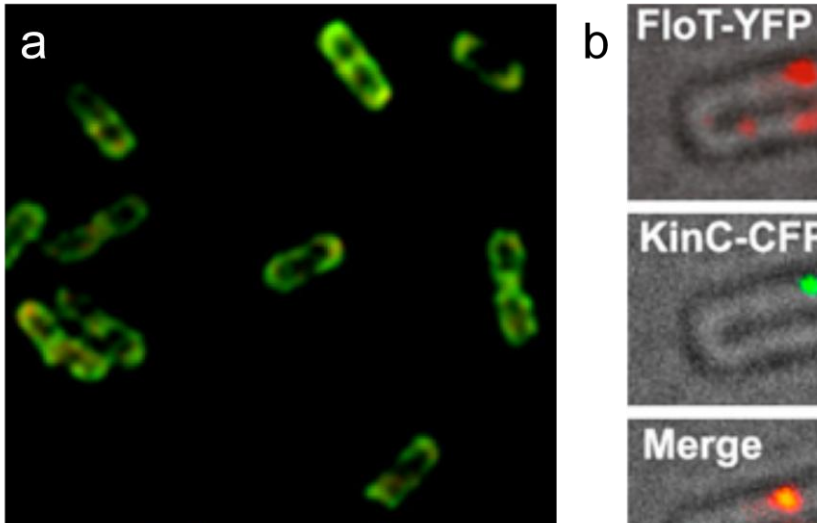

Figure 14. Lipids form distinct microdomain in bacterial membrane. a. Staining of *E. coli* cells with fluorescent dye NAO, which revealed the localization of cardiolipin-enriched membrane domains (Mileykovskaya and Dowhan, 2009). b. Colocalization of the flotillin FloT and the histidine kinase KinC in a double-labeled *B. subtilis* strain expressing the translational fusions FloT-YFP (false colored red, upper panel) and KinC-CFP (false colored green, middle). Regions where the two signals overlapped appear yellow in the merge panel (lower panel). Scale bar = 1 mm (López and Kolter, 2010).

(Ramamurthi and Losick, 2009). Lenarcic *et al.* proposed a model, called the "molecular bridging model", explaining how DivIVA might recognize negative curvature (Figure 13) (Lenarcic et al., 2009; Strahl and Hamoen, 2012). This model, shown in Figure 13, is based on the characteristics of DivIVA which has affinity for membranes and is able to form oligomers (4-8 monomers). When clusters of DivIVA are free in the cytoplasm, peripherical monomers have fewer interactions and are more prone to detach and diffuse away. Thus, they proposed that clusters of DivIVA are more stable when they bind strongly curved membranes because their exposed surface to the cytoplasm is decreased (Figure 13).

These findings raise the possibility that membrane curvature is exploited widely as a beacon for protein localization in bacteria. However, we do not know if all the proteins that recognize membrane curvature use the "Molecular Bridging" mechanism or if bacteria evolved other mechanism to sense the curvature.

2.2.3. Membrane Lipid Composition

Recently, it has been suggested that the bacterial membrane is composed of lipid microdomains, which are made of different phospholipids with different properties. Indeed, analysis of the subcellular localization of phospholipids revealed that they are not uniformly distributed. Some of them were observed as microdomains within the membrane, which can be compared to the so-called lipid rafts in eukaryotes. Two lipids that form distinct microdomain in bacterial membranes are well characterized: the cardiolipins, that localize at the polar and septal regions (Figure 14a) (Mileykovskaya and Dowhan, 2009) and the polyisoprenoids which are components of the newly discovered bacterial "lipid rafts" (Figure 14b) (López and Kolter, 2010). This lateral heterogeneity of lipids in the bacterial membranes could act as a localization cue for lipid binding proteins, and thus could be employed to create specific environments for the structural organization of membrane protein complexes.

For example, Romantsov *et al.* demonstrated that the subcellular localization of the osmosensory transporter ProP and the mechanosensitive channels protein McsS in *E. coli* depends on their ability to bind cardiolipins at the poles and at the septa of dividing *E. coli* cells (Romantsov et al., 2010). Furthermore, in *B. subtilis*, lipid microdomains may organize signal transduction proteins. Indeed, a homologue of eukaryotic flotillin, a protein that organizes the eukaryotic lipid rafts, FloT, forms discrete foci along the bacterial membrane (Figure 14b). López and Kolter suggest

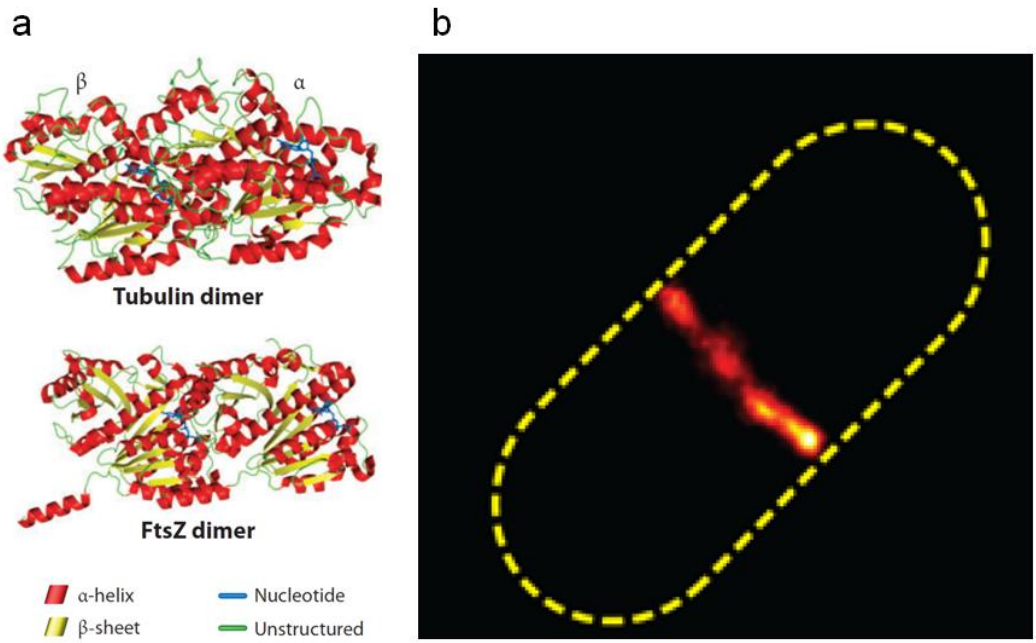

Figure 15. The tubulin-like FtsZ. a. Tubulin and FtsZ are structurally homologs. Crystal structures of the αβ tubulin dimer (α with GTP and β with GDP) (upper panel); FtsZ dimer (both subunits GTP-bound) (lower panel). Images were made with PyMol (from Cabeen and Jacobs-Wagner, 2010). b. Live-cell PALM imaging of ring-like FtsZ structures. Image of live wild type cells expressing FtsZ-mEos2. The dotted yellow line is a general indicator of the cell outline (from Buss et al., 2013).

that FloT associates with polyisoprenoid lipids and thus organizes microdomains containing the membrane histidine kinase KinC, which is an essential component of the signal transduction pathway that controls biofilm formation (Figure 14b). Thus, these microdomains may allow the compartmentalization of proteins and also proteins involved in the same pathway, in tightly packed membrane areas, facilitating their activities (in the case of KinC, by facilitating its dimerization essential to its activity) and their coordination respectively (López and Kolter, 2010).

2.2.4. The Role of the Bacterial Cytoskeleton

For a long time, bacteria were thought to be devoid of cytoskeletal elements because no close homologues of eukaryotic cytoskeleton such as actin, tubulin or intermediate filament were found to be encoded in their genome. However, the recent discovery of cytoskeletal proteins with structural homologies to actin, tubulin and even intermediate filaments changed this preconception. The existence of bacterial cytoskeleton has raised the question of their involvement in molecules localization, like the cytoskeleton of eukaryotic cells.

Bacteria possess among others (Bactofilins and CTP-synthase, not described in this manuscript; Ingerson-Mahar et al., 2010; Kühn et al., 2010) three well-described cytoskeletal elements: the tubulin-like protein FtsZ, the actin-like protein MreB, and the intermediate filament-like protein crescentin. These cytoskeletal proteins are capable of self-assembly into filaments. Below, I discuss how these filaments might control the localization of molecules in the cell.

2.2.4.1. The Tubulin-Like Protein FtsZ

FtsZ was the first bacterial cytoskeletal protein to be discovered. It is a homologue of tubulin (Figure 15a) and it is found in almost all bacteria. Like eukaryotic tubulin, FtsZ polymerizes in a GTP-dependent manner. During cell division, FtsZ self assembles into a ring-like complex at midcell, called the Z-ring (Figure 15b), which is an essential scaffold to recruit the proteins of the divisome, a complex machinery that that performs cell division (Barry and Gitai, 2011; Cabeen and Jacobs-Wagner, 2010; Margolin, 2005). Construction of the divisome is a two-step process: early, at the future division site, the Z-ring recruits ZipA and FtsA (which stabilizes the Z-ring), ZapA, ZapB, ZapC, ZapD, and FtsEX proteins. Then, immediately before constriction, the divisome matures by incorporating FtsK, FtsQ, FtsL, FtsB, FtsW, PBP3, PBP1B and FtsN. How

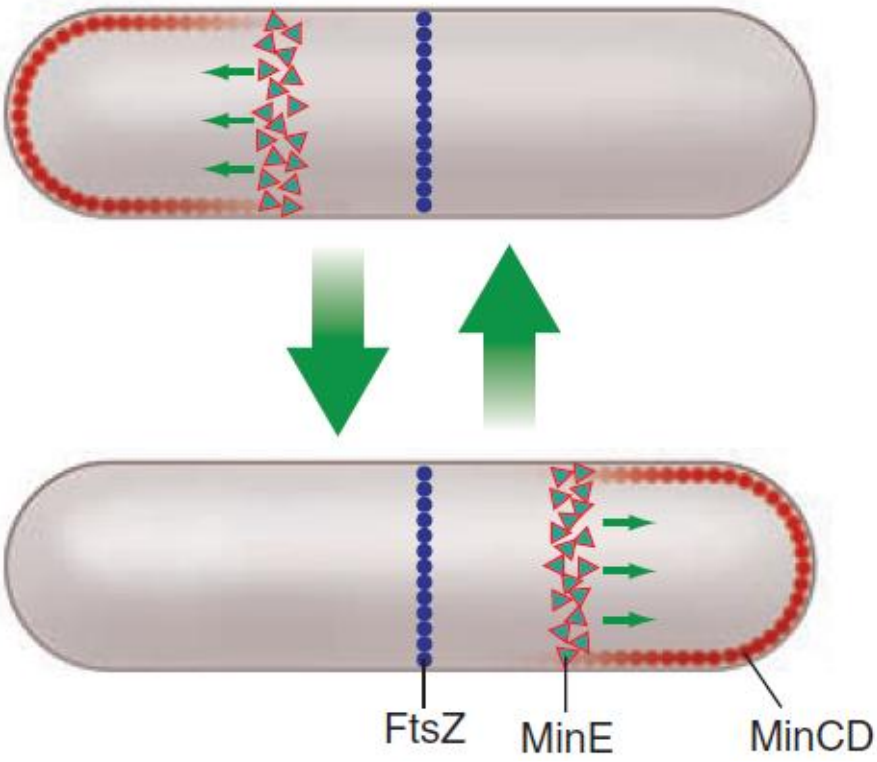

Figure 16. Repression of FtsZ polymerization by oscillation of the Min inhibitory system in *E. coli* (Shapiro et al., 2009).

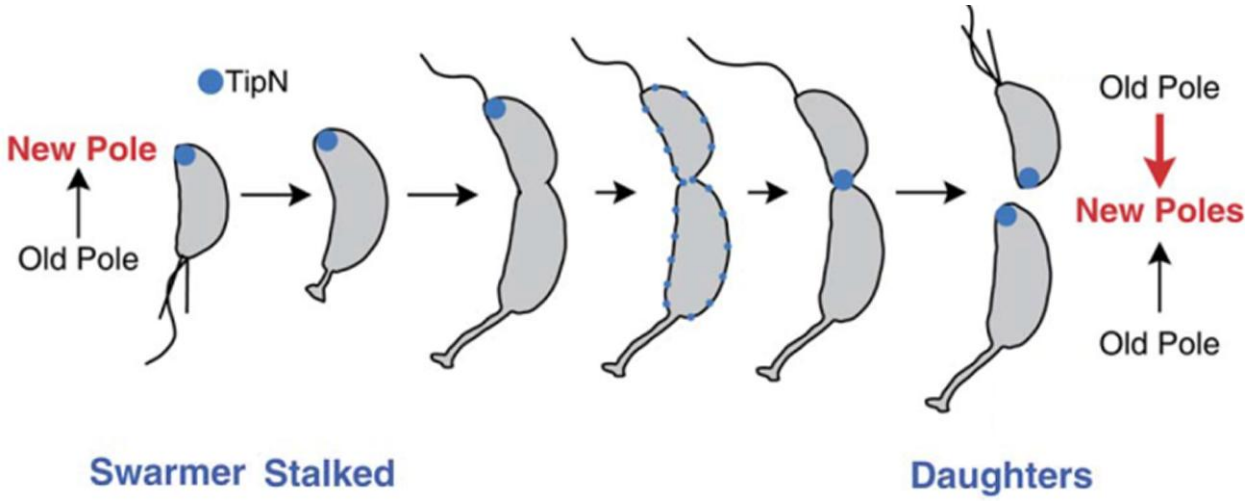

Figure 17. Model for TipN-dependant regulation of cell polarity of *C. crescentus*. In wild-type cells, TipN at the pole provides a positional cue to orient and maintain the correct polarity axis (from Lam et al., 2006).

divisome assembly is controlled temporally is unknown but likely involves multiple protein–protein interactions between its components (Egan and Vollmer, 2013).

Since FtsZ plays a major role in the positioning of division proteins, it must be correctly localized to ensure that the cell division starts at the right time and at the right place along the cell length. As discussed above, nucleoid occlusion participates in Z-ring formation but it is not the sole mechanism. In many rod shaped bacteria, assembly of the cell division FtsZ-ring is driven to the center of the cell by the spatial action of inhibitors of FtsZ polymerization. These inhibitors (Min) are dynamically localized to the cell poles to create an inhibitor-free zone at midcell. In *E. coli*, this system consists of the FtsZ assembly inhibitor MinC, and the MinD and MinE proteins, which oscillate from one cell pole to the other (Figure 16). MinD is an ATPase that binds to the membrane in its ATP form and is released from the membrane after its ATP hydrolysis. MinE drives MinD off the membrane by binding to MinD and stimulating its ATP hydrolysis. Subsequent diffusion of MinD–ADP and nucleotide exchange causes MinD–ATP to rebind to the membrane; this new binding occurs far away from the original site because of the transient presence of MinE at the original site and the kinetics of nucleotide exchange. Because MinC associates with the oscillating MinD protein, FtsZ assembly is inhibited most at the cell poles and least at midcell (Figure 16) (Margolin, 2005; Shapiro et al., 2009). Hence, the Min proteins and the nucleoid occlusion mechanism also ensure the high precision by which *E. coli* and *B. subtilis* cells define its mid-cell position.

Since in most rod-shaped bacteria the new septum ultimately becomes the new pole, FtsZ can be used to localize polar proteins. For example, Lam *et al.* and Huitema *et al.* showed that the protein TipN localizes at the division septum in a FtsZ-dependant manner. And subsequently, TipN localizes to the newborn pole after cell division in *C. crescentus* (Figure 17). The cell uses this positional information as a source of intracellular asymmetry to establish and maintain the orientation of the polarity axis, which is crucial for polar morphogenesis and division. Indeed, in *tipN* mutant cells, new pole markers, such as for example the flagellum and signaling proteins, are often incorrectly targeted to the old pole (Huitema et al., 2006; Lam et al., 2006). This example shows that cell division can leave positional marks, called "birth scars", to direct the positioning of polar complexes(Huitema et al., 2006).

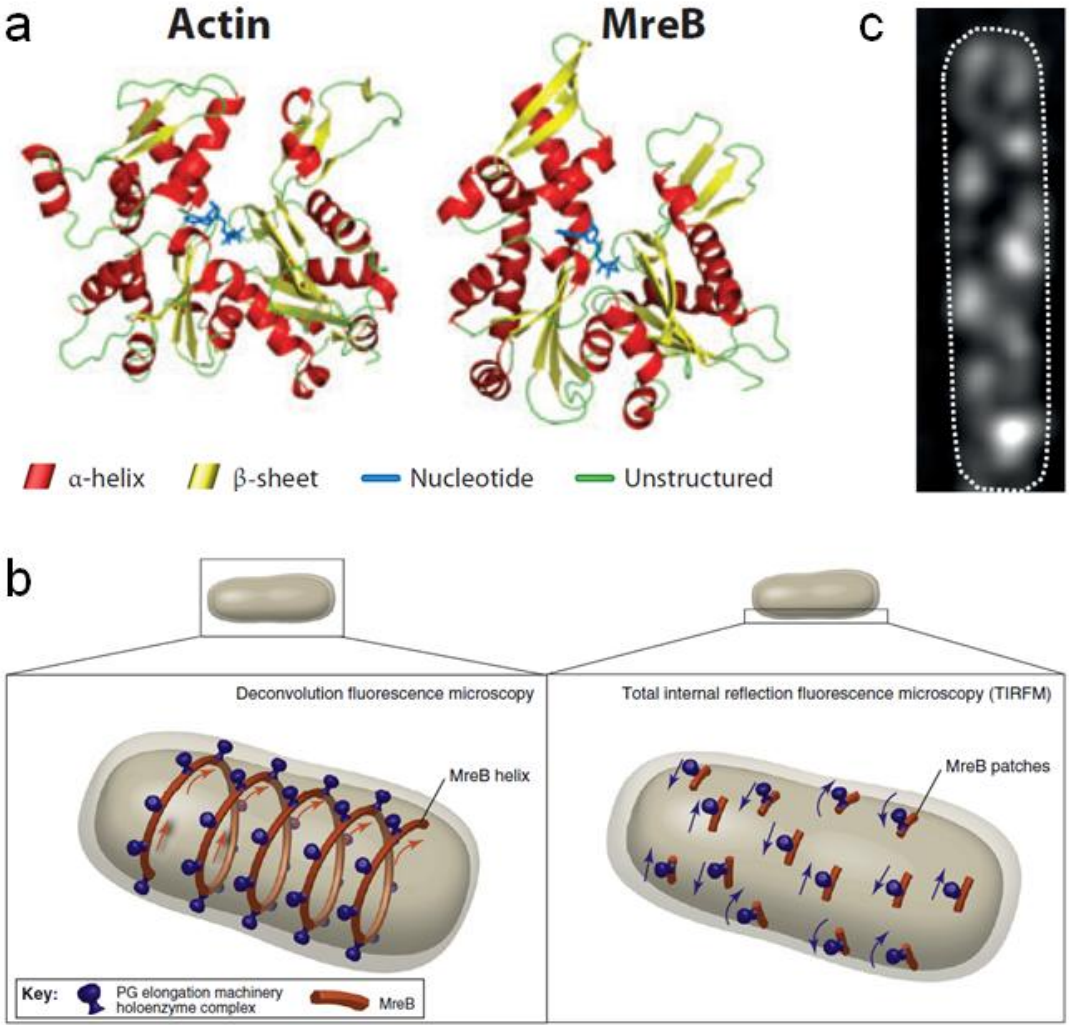

Figure 18. The actin-like protein MreB. a. Actin and MreB are structurally homologues. Crystal structures of eukaryotic actin-ATP (left panel) and prokaryotic MreB (right panel). Images were made with PyMol (from Cabeen and Jacobs-Wagner, 2010). b. Cartoon depicting a simplified comparison of two separate microscopic techniques used to visualize MreB ultra-structure and movement (from White and Gober, 2012). c. GFP-MreB imaged by TIRF microscopy (from Domínguez-Escobar et al., 2011).

2.2.4.2. The Actin-Like Protein MreB

MreB was initially described to be involved in the determination of cell shape in rod bacteria (Doi et al., 1988; Levin et al., 1992; Wachi et al., 1987). Indeed, the *mreB* gene is absent in spherical bacterial species (Cabeen and Jacobs-Wagner, 2010). In the early 2000's, it was discovered that MreB is a structural homologue of actin (Figure 18a) (van den Ent et al., 2001) and forms cytoskeletal filamentous helical structures lying close to the cytoplasmic membrane in bacterial cells (Figure 18b) (Jones et al., 2001).

MreB was firstly described to form dynamic helical structures spanning the length of the cell (Figure 18b) (Jones et al., 2001; Mauriello et al., 2010). However, recent studies that use total internal reflection fluorescence (TIRF) and confocal microscopy showed that contrary to the first observations, MreB forms small patches or filaments that move around the cell circumference perpendicularly to its long axis (Figure 18bc) (Domínguez-Escobar et al., 2011; Garner et al., 2011; van Teeffelen et al., 2011). It was shown that MreB movement is not due to its own polymerization, but rather to peptidoglycan synthesis. Indeed, direct and indirect interaction was shown between MreB and peptidoglycan synthesis enzymes and cell morphogenesis proteins (MreC, MreD, Pbp2, RodA, RodZ and MurG) and the depletion of three proteins of the peptidoglycan synthesis enzymes (RodA, RodZ and Pbp2) resulted in a gradual slowing of MreB movement. It was concluded that MreB positions the initial sites of new cell wall synthesis by recruiting and/or positioning and/or stabilizing peptidoglycan biosynthesis machineries, while coupling MreB rotation to the process of cell wall assembly ensures a uniform distribution of initiation sites, a necessary condition to maintain rod shape during growth (Ingerson-Mahar and Gitai, 2012; Shaevitz and Gitai, 2010; van Teeffelen et al., 2011; Typas et al., 2012). The cell-wall synthesis machinery may thus constitute a novel type of extracellular motor that exerts force on cytoplasmic MreB. Therefore, it could be envisaged that bacteria harness the energy of cell-wall assembly to power intracellular protein motion, for example to move some intracellular proteins around the cell circumference (van Teeffelen et al., 2011).

Additionally to its role in the organization of cell wall synthesis machineries, MreB has also been suggested to be involved in many cellular processes such as chromosome segregation in several bacteria (Cabeen and Jacobs-Wagner, 2010; Shaevitz and Gitai, 2010) and in the subcellular organization of bacterial proteins such as the gliding and twitching motility proteins in *Myxococcus xanthus* and *Pseudomonas aeruginosa* (Cowles and Gitai, 2010; Mauriello et al., 2010), the chemotaxis

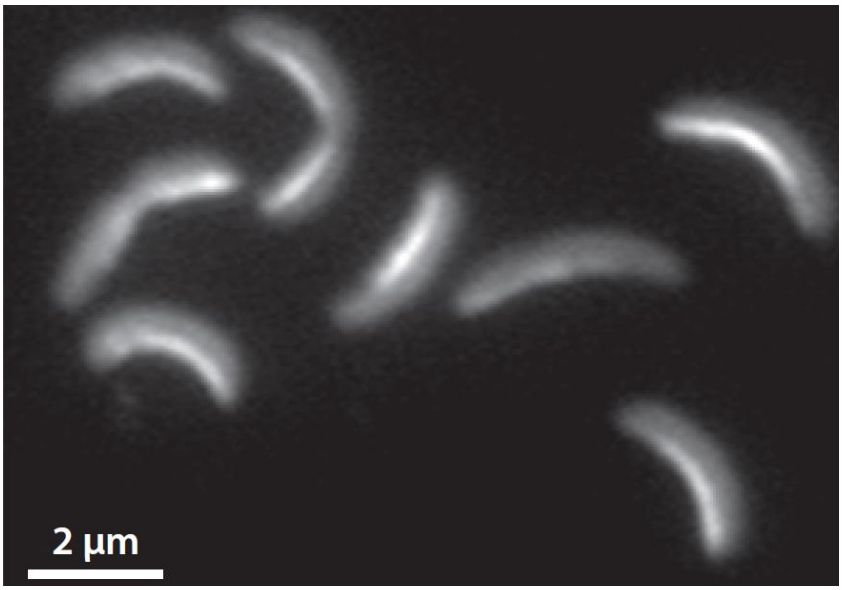

Figure 19. Fluorescence micrograph of FlAsH-stained crescentin in *C. crescentus* (Cabeen and Jacobs-Wagner, 2010).

receptors in *E. coli* (Shih et al., 2005), polar markers in *C. crescentus* (Gitai et al., 2004), or larger protein complexes or organelles such as the stalk in *C. crescentus* (Divakaruni et al., 2007). However, one issue with studying the role of MreB relies in its pleiotropic functions. Today, the role of MreB in chromosome segregation remains controversial and in all cases, it remains unclear whether MreB directly or indirectly affects proteins localization. Therefore, the current challenge is to understand the mechanism by which MreB impacts these cellular processes and distinguish the direct effects of MreB on subcellular localization from indirect effects caused by decreased growth or disrupted morphology.

2.2.4.3. The Intermediate Filament Protein Crescentin

Crescentin is a member of a large family of intermediate filaments-like proteins in bacteria and was discovered in the Alpha-proteobacterium *C. crescentus* as a mediator of the curved morphology of this organism. Crescentin possesses intermediate filament-like domain organization and as the other cytoskeletal elements presented above, crescentin is able to polymerize, thus forming intermediate filament-like structures (Charbon et al., 2009).

Crescentin is responsible for the crescent shape of *C. crescentus*: in its absence, cells lose their curvature and adopt straight-rod morphology. In cells, crescentin localizes along the positive curvature surface (the crescentin side) of the crescent-shaped *C. crescentus* cell (Figure 19). It has been proposed that the crescentin filamentous structure is held at the cytoplasmic membrane in a stretched configuration that must be maintained through a connection with the cell wall *via* unknown factors. This structure would counteract cell wall expansion during growth, generating a compressive force that biases new cell wall insertion to the opposite side, such that in total less material is added on the crescentin side of the cell, leading to cell curvature during growth (Cabeen and Jacobs-Wagner, 2010; Cabeen et al., 2009; Charbon et al., 2009).

Like FtsZ and MreB, crescentin is also required for the right positioning of proteins. In *C. crescentus*, crescentin recruits the metabolic enzyme CtpS to the inner cell curvature. CtpS was previously characterized as the enzyme responsible for the synthesis of CTP from UTP, ATP, and glutamine. CtpS is conserved in all organisms and in *C. crescentus* and *E. coli*, CtpS forms a linear structure. Importantly, CtpS colocalizes with crescentin to the inner cell positive curvature and its interaction with crescentin is essential for its functionality (Ingerson-Mahar and Gitai, 2012; Ingerson-Mahar et al., 2010).

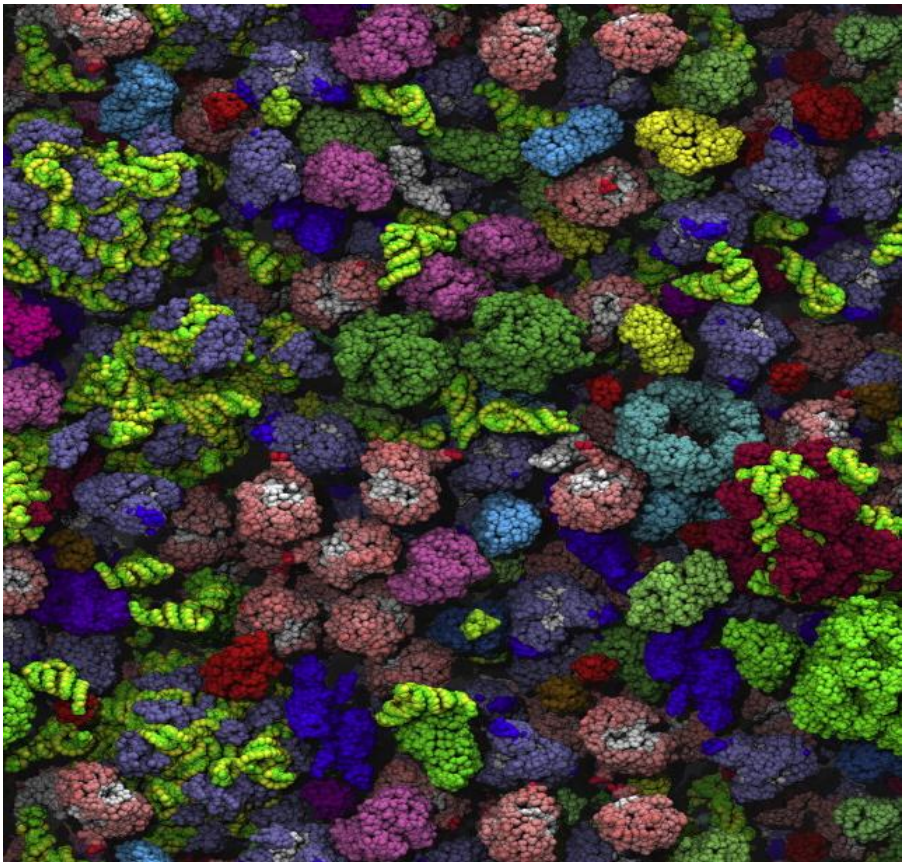

Figure 20. Crowded cytoplasm of bacteria. Picture representing the *E. coli* cytoplasm in *in vivo* conditions (with a macromolecule concentration of 275 g/L) (from McGuffee and Elcock, 2010; Mika and Poolman, 2011).

In summary, cytoskeletal protein filaments can organize the bacterial cell by acting as a scaffold on which proteins are assembled to regulate their action temporally and spatially. Cytoskeletal filaments can also contribute mechanically to cellular organization potentially by exerting forces on targets such as membrane, which is the case with FtsZ for the constriction and crescentin for cell curvature.

2.3. Protein Localization Mechanisms

We showed previously that bacteria possess several intrinsic localization factors. This raises the questions of how bacterial macromolecules reach their final destination. I will discuss that both passive and active mechanisms exist. But first of all, I will present the bacterial cytoplasm wherein the transport of molecules will happen.

2.3.1. The Bacterial Cytoplasm is Highly Crowded

It is generally thought that most of the bacterial enzymatic reactions occur through passive diffusion even though the bacterial cytoplasm is even more crowded than the eukaryotic cytoplasm. In such a crowded environment, how can passive diffusion be achieved?
In bacterial cells, all cellular functions needed are concentrated in a small compartment. Indeed, the volume of *E. coli* is 3-5 orders of magnitude smaller than that of the mammalian cells (Mika and Poolman, 2011). It has been determined that the concentration of macromolecules (proteins, RNA, DNA) in *E. coli* during exponential growth phase is around 300 g/L (≈ 200 g/L of proteins, 75 g/L of RNA and 20 g/L of DNA) (Mika and Poolman, 2011; Zimmerman and Trach, 1991) (Figure 20). This is 3 to 6 fold higher than in eukaryotic cells where proteins concentrations range between 50-100 g/L (Mika and Poolman, 2011).
The fact that the bacterial cytoplasm is highly crowded has therefore consequences on the mobility of cytoplasmic molecules: in the *E. coli* cytoplasm, the diffusion coefficient of green fluorescent protein (GFP) is around 5-8 $\mu m^2/s$, which is lower than in eukaryotic cells (24 $\mu m^2/s$). A decrease of molecule mobility is also observed when the size of the molecules increase (Mika and Poolman, 2011; Potma et al., 2001). Yet, although diffusion in the crowded bacterial cytoplasm is slow compared to the eukaryote cytoplasm, it is still fast at the level of most cellular processes: for example, for a low diffusion coefficient of 0,02 $\mu m^2/s$, large macromolecules such as ribosomes, will take 75 seconds to travel from one end of an *E. coli* cell to another (about 3 μm). Thus, since the doubling time of *E. coli* is about 30 min in rich media, even large complexes

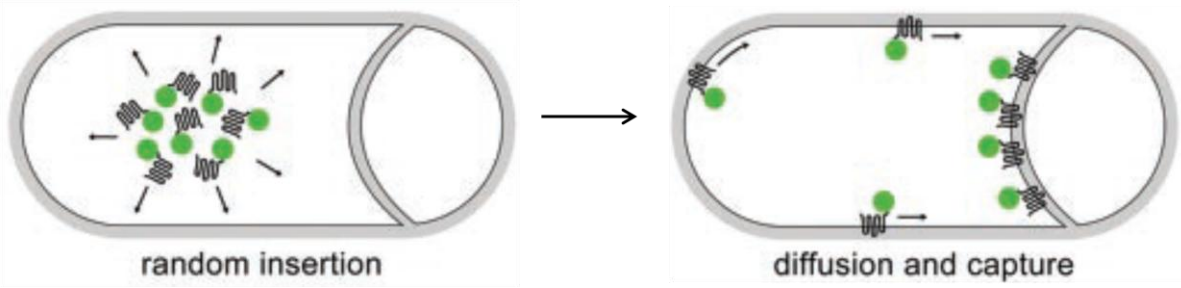

Figure 21. Model explaining how SpoIVFB achieves proper localization to the engulfing septal membrane. SpoIVFB-GFP is randomly inserted into all mother-cell membranes. The protein then achieves proper localization by diffusing in the cytoplasmic membrane until it is captured in the engulfing septal membrane (modified from Rudner et al., 2002).

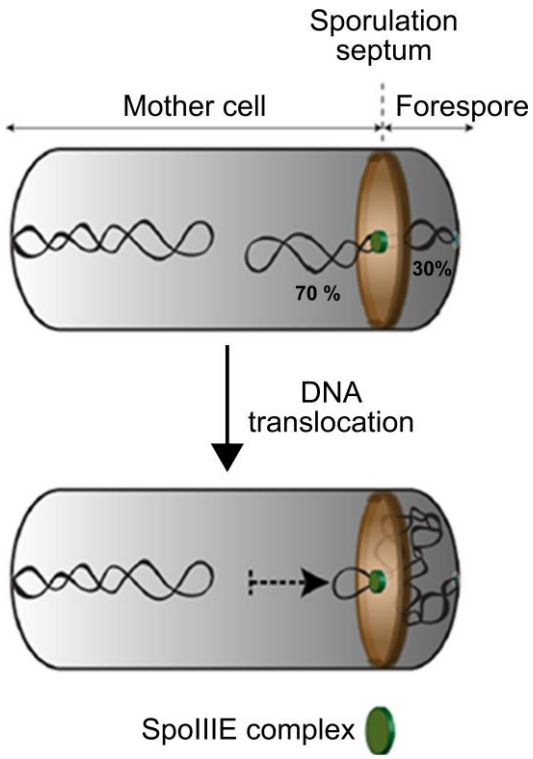

Figure 22. Role of SpoIIIE in chromosome segregation during sporulation in *B. subtilis*. Formation of the asymmetric sporulation septum (brown disc) divides the cell into mother cell and forespore compartments, and traps 30 % of the forespore chromosome (black ribbon) inside the forespore (upper panel). Packaging of the remaining 70 % of the forespore chromosome into the nascent spore (lower panel) is achieved by SpoIIIE (green disc), a septal-bound double-stranded DNA motor of the FtsK family (modified from Fiche et al., 2013).

can travel forward and backward several times during the life-span of the cell (Mignot and Shaevitz, 2008; Mika and Poolman, 2011). These estimates suggest that passive diffusion may be sufficient to drive most biochemical reactions and localization processes in the bacterial cell.

2.3.2. Protein Localization by Diffusion and Capture

One mechanism that seems to govern the subcellular localization of proteins is the so-called "diffusion and capture" mechanism, whereby proteins find their target by diffusion, in a one dimensional space as in the case of DNA binding proteins, in a two dimensional space as in the case of membrane proteins or in a three dimensional space as in the case for a soluble protein (Rudner and Losick, 2010).

The Lac repressor bound to DNA is an example of one dimensional diffusion and capture. When bound to DNA, LacI slides randomly along DNA segments until it finds its *lacO* operator sequence. If LacI does not find its target sequence rapidly, it dissociates and binds another DNA segment non-specifically and scans it again, until it becomes tethered to the *lacO* operator sequence (Elf et al., 2007; Mika and Poolman, 2011).

Diffusion and capture also drives the localization of the integral membrane protein SpoIVFB to the outer forespore membrane, which is essential for *B. subtilis* sporulation. Rudner *et al.* demonstrated that SpoIVFB is inserted randomly into the cytoplasmic membrane from which it diffuses and becomes captured into the membrane that surrounds the forespore (Figure 21). SpoIVFB is specifically retained in the forespore membrane because its interacts with another protein, SpoIVFA, at this site (Rudner et al., 2002).

2.3.3. Active Transport Mechanism

Although passive modes of localization like diffusion capture may suffice to drive most subcellular processes, active modes of intracellular transport may be required for larger macromolecular complexes/macromolecules. For example, following their replication bacterial chromosomes and plasmids must be actively transported / separated to ensure their proper segregation in each daughter cell at each division cycle.

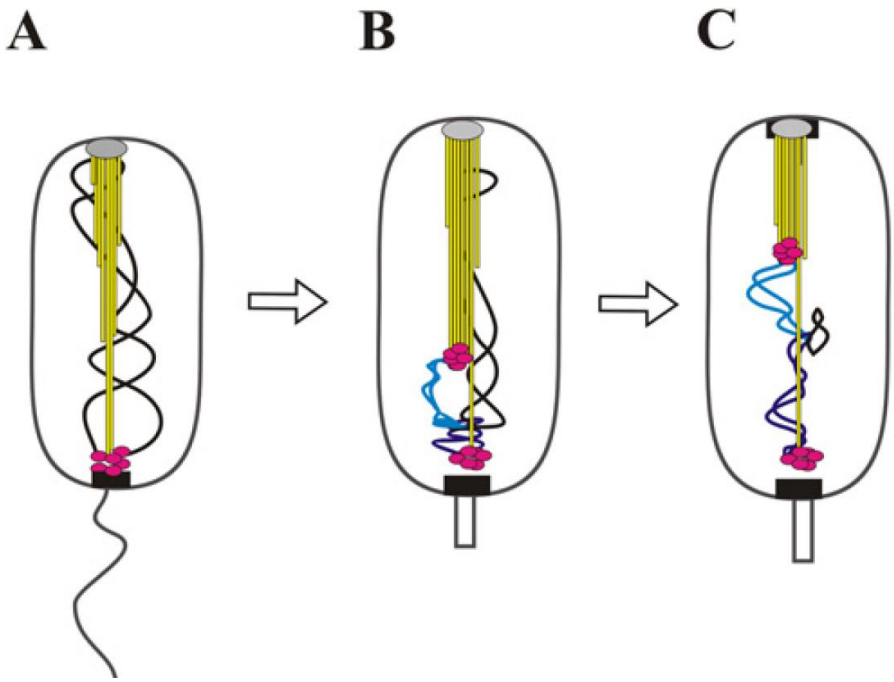

Figure 23. ParA and ParB localization during cell cycle of *C. crescentus*. A. In a *C. crescentus* cell, a single partitioning nucleoprotein complex ParB/*parS* (purple circles) close to the *oriC* is initially attached by PopZ (black bar) to the older cell pole. While a small fraction of ParA (yellow sticks) in the cell interact with the partitioning complex, most ParA is distributed throughout the cell (like a comet tail) with a higher concentration at the opposite pole, where it is tethered by TipN polymers (grey circle). B and C. Before initiation of replication, nucleoprotein ParB/*parS* complex is released from PopZ polymers. Replication of the origin region results in duplication of ParB foci. One nucleoprotein ParB/*parS* complex remains at the older pole, whereas the other advances into the vicinity of the ParA "comet tail" and moves to the new pole. Retracting ParA pulls the ParB/*parS* complex towards the opposite pole (modified from Mierzejewska and Jagura-Burdzy, 2012).

2.3.3.1. Chromosomes Segregation

One of the largest objects in the bacterial cell is the chromosome and during the cell cycle, it needs to be replicated, transcribed and segregated in each daughter cell. Passive diffusion is not sufficient to separate the sister chromosomes through the crowded cytoplasm. Moreover, cells need to segregate their chromosomes quickly into the daughter compartments, before the constricting ring closes. To date, several machineries have been described to be implicated in the process of chromosome segregation.

One characterized example comes from the study of the FtsK/SpoIIIE family of ATP-dependant DNA transporters. These proteins are membrane-anchored, ATP-fuelled, and are directional motors driving chromosomal segregation in bacteria. SpoIIIE drive chromosome segregation during sporulation in *B. subtilis* (Figure 22), and FtsK is involved during cell division in *E. coli* (Burton et al., 2007; Sherratt et al., 2010). Because the mechanism of chromosome segregation is similar for both of these proteins, I will only present SpoIIIE. Because the asymmetric division during sporulation naturally traps approximately 30 % of the forespore chromosome in the forespore, this leaves 70 % of the forespore chromosome in the mother cell (Figure 22). SpoIIIE is thus required to actively translocate the remaining 70 % of the chromosome into the forespore. SpoIIIE possesses a transmembrane domain which allows its anchoring in the membrane at the cell division septum. It also contains an ATPase motif and the directionality γ-domain. SpoIIIE translocates the double stranded DNA in the forespore in an ATP-dependant manner. A remarkable feature of these chromosome transporters is their ability to move the DNA in the appropriate direction thanks to the presence of short sequence motifs (8 nucleotides) in the chromosomal DNA, known at SRS sequences for SpoIIIE. SRS sequences are overrepresented on the plus-strand of the chromosome and are recognized by the γ-domain which uses them as a guide to accurately move the chromosome into the forespore (Ptacin et al., 2008).

Another example of active chromosome transport comes from the study of *C. crescentus* cells, where a copy of the duplicated origin region moves rapidly and directionally to the opposite pole in what is thought to be an active process (Viollier et al., 2004). The replication origin of the circular chromosome is localized to the older pole (Figure 23) of the cell and one of the newly replicated chromosome is directed to the opposite pole. The ParAB-*parS* system is essential for the chromosome segregation in *C. crescentus*. This system is composed by the ParA protein, which is an ATPase; the ParB protein which is able to recognize and bind parS sequences; and the parS

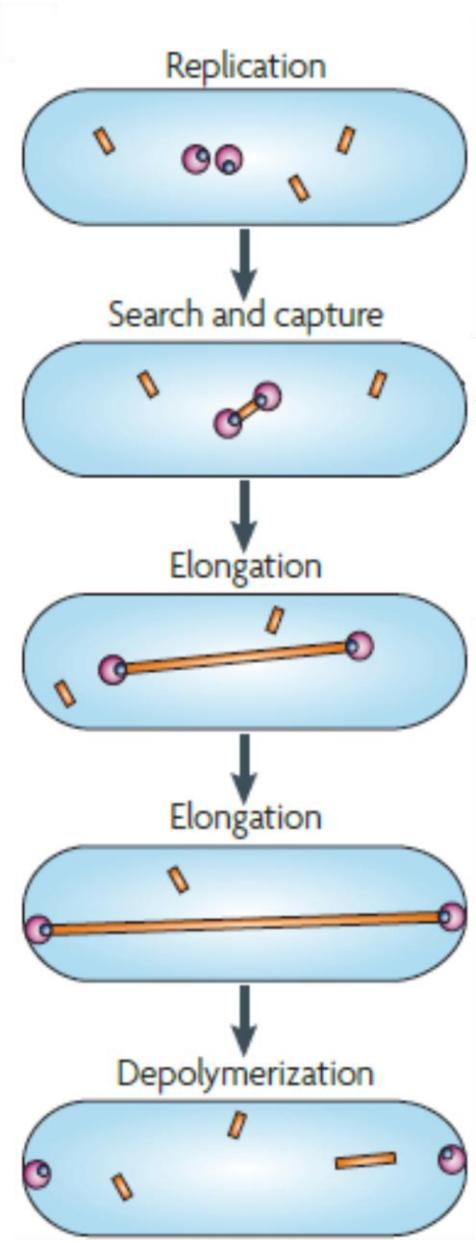

Figure 24. Schematic representation of plasmid segregation by the ParMR-*parC* system. Plasmids are shown in pink, ParR in blue and ParM in orange (modified from Salje et al., 2010).

sequences, most of them located close to the oriC region. In addition, two polar localization factors are important for chromosome segregation: PopZ at the stalked pole and TipN at the swarmer cell pole (see above). During chromosome segregation, PopZ binds ParB and the replication origin at the stalked pole. At the other pole, the ParA ATPase is trapped by TipN (described above) and extends towards the stalked pole by ATP-dependant polymerization. Upon association with the ParB-*parS* nucleoprotein complex, ParA pulls one copy of the chromosome across the cell by retraction (Mierzejewska and Jagura-Burdzy, 2012). Indeed, ParB interaction stimulates ParA ATP hydrolysis, promoting ParA depolymerization, which provides the putative motive force for DNA transport (Figure 23) (Ingerson-Mahar and Gitai, 2012; Mierzejewska and Jagura-Burdzy, 2012). Thus, the ParAB complex moves the replicated chromosome unidirectionally from the old pole to the new pole, in contrast to the bidirectional movement observed for plasmid segregation (described below).

2.3.3.2. Plasmids Partitioning

During bacterial cell division, an equal distribution of replicated plasmids to daughter cells ensures their stable inheritance. Low-copy-number plasmids, such as the *E. coli* plasmid R1, encode the simplest known DNA segregation machine to perform this task: the ParMR-*parC* plasmid partionning apparatus. It comprises: ParM, an actin-like protein, which forms filaments; ParR, a DNA-binding adaptor protein which binds specifically to nucleotidic *parC* plasmidic sequences. The ParM filaments are dynamically unstable unless they are capped by the plasmid-bound ParR/*parC* nucleoprotein complex (analogous to the ParB/*parC* complex), and thus ParM filament grows and shrinks constantly, searching the cellular space for plasmids (search and capture mechanism). Once ParM filaments are bound by a ParR/*parC* complex at both ends, the filaments become stabilized and bidirectional elongation by insertional polymerization ensures that the filaments-bound sister-plasmids move to opposite cellular poles, ensuring their vertical transfer to the daughter cells (Figure 24).

2.4. Conclusions

In this chapter, I used selected examples to demonstrate that the bacterial cell is highly organized. Bacteria have evolved several mechanisms to localize macromolecules to specific subcellular sites, most of them involving simple diffusion. Aside from secretion systems (not discussed in this thesis), active transport mechanisms seem restricted to DNA transport and protein-directed

intracellular transport systems, such as those described in eukaryotic cells, allowing the trafficking of proteins or RNA, have not been found. The discovery of bacterial cytoskeletal proteins with structural homologies to actin, tubulin and even intermediate filaments raised the possibility that dedicated motors akin to myosin, kinesins and dynein could transport proteins throughout the cytoplasm. But despite extensive search, no such bacterial motors have been identified so far.

In this thesis, starting with the study of a motility system in *M. xanthus*, we have discovered a new class of processive transport systems that move protein complexes directionally in the cell envelope. While these systems drive gliding motility, they can also promote the assembly of a spore coat, a form of bacterial capsule. These machineries are broadly distributed in bacteria and their structure is highly versatile, suggesting that they may have a large functional repertoire. At the end of this manuscript, I will discuss how this class of proteins may generally participate in the organization of the bacterial cell.

3. Bacterial Gliding Motility

In the previous chapter, I discussed the high level of organization in bacteria raising the question of the existence of active transport mechanisms to target proteins to specific sites in the cell. Recently, it has been suggested by electron and fluorescence microscopy approaches, that the gliding motility of certain bacteria, such as *Flavobacterium johnsoniae* and *Myxococcus xanthus*, could be powered by the directional movement of cell-surface adhesins along the cell body. This active and directional transport of adhesins would translate into motility when these adhesins come in contact and adhere to the substratum.

Many bacteria are capable of moving over solid surfaces without the aid of pili, flagella or any obvious organelles, and without observable changes in cell morphology by a phenomenon called gliding motility. This phenomenon is observed in very diverse phylogenetically unrelated bacterial groups among which and only to name a few studied examples are the cyanobacteria, the mollicutes, the *Cytophaga/Flabobacterium* group and the myxobacteria. In each case, it appears that the proteins required for cell movement are species-specific, suggesting that gliding motility may have evolved independently in different bacterial groups and that more than one motility mechanism is involved in the gliding of these bacteria (Jarrell and McBride, 2008; McBride, 2001).

The initial aim of my thesis was to characterize the gliding machinery, and especially the gliding motor of *M. xanthus*. To understand the scientific context of the beginning of my thesis, I will present state-of-the-art knowledge of the gliding motility mechanism in *F. johnsoniae* and *M. xanthus* at the time when I started my thesis project. Importantly, *F. johnsoniae* and *M. xanthus* are the only bacteria where gliding has been studied at the molecular/genetic level (with the exception of the mollicutes, but these bacteria have a very particular cell structure, Miyata, 2010).

3.1. *Flavobacterium johnsoniae*

Flavobacterium johnsoniae belongs to the Bacteroidetes phylum, and many members of this phylum are characterized by their rapid gliding motility (1-3 μm/s) (Jarrell and McBride, 2008). This bacterium is capable of gliding over various solid surface such as agar, glass, polystyrene and Teflon (Shrivastava et al., 2012).

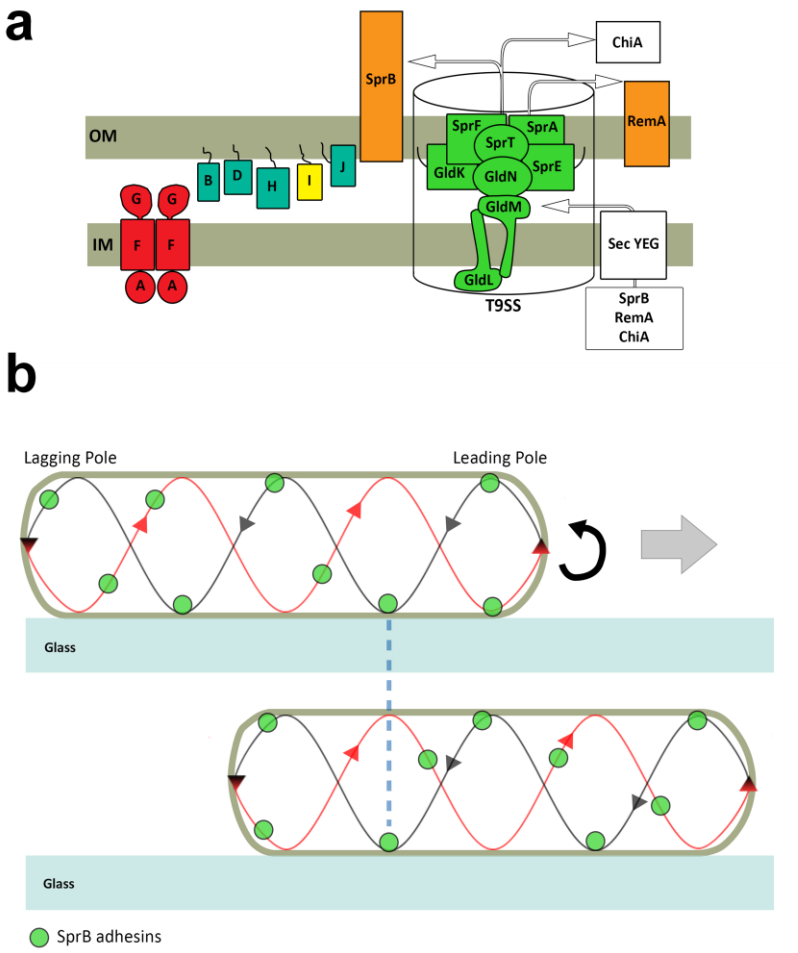

Figure 25. Gliding mechanism of *F. johnsoniae*. a. Proteins involved in *F. johnsoniae* gliding motility and protein secretion. SprB and RemA (orange) are thought to function as adhesins that are propelled along the cell surface by the some of the other proteins shown. GldA, GldF, and GldG (red) comprise an ATP-binding cassette transporter whose exact role in gliding is not known. GldI (yellow) is a peptidylprolyl isomerase involved in protein folding. Proteins in green (GldK, GldL, GldM, GldN, SprA, SprE, SprF, SprT) constitute the PorSS and are required for secretion of SprB and RemA and for motility. They also secrete the chitinase ChiA (white), which is not involved in motility. Proteins secreted by the PorSS have a predicted type 1 signal peptides and are predicted to be exported across the cytoplasmic membrane by the Sec system before being secreted across the outer membrane by the PorSS. Proteins in blue (GldB, GldD, GldH, and GldJ) are also required for gliding. Black lines indicate lipid tails on lipoproteins. b. *Flavobacterium* gliding is thought to be powered by motors composed of Gld proteins in the cell envelope that propel adhesins, such as SprB, along the cell surface. Adhesin SprB moves along the left-handed helical loop and has two different states: SprB moving toward the front of the cell and SprB moving toward the rear of the cell. In a translocating cell, SprB moving toward the rear of the cell adheres to the surface, generating left-handed rotation and right-directed translocation of the cell (adapted from Jarrell and McBride, 2008; McBride and Zhu, 2013; Nakane et al., 2013; Shrivastava et al., 2012, 2013).

3.1.1. Gliding Model

Based on recent data (McBride and Zhu, 2013; Nakane et al., 2013; Nelson et al., 2008; Shrivastava et al., 2012), a model explaining the gliding motility of *F. johnsoniae* was proposed. First, the gliding machinery appears to comprise a secretion system (the PorSS which is described below; McBride and Zhu, 2013), which transports adhesins (SprB and RemA which are also described below; Nelson et al., 2008; Shrivastava et al., 2012) to the cell surface. At the surface, the adhesins interact with an as yet unknown machinery and move rapidly from pole to pole in a left-handed helical manner along the length of the cell. Once the adhesins reach the back of the cell, they appear to be transported back along the same helical structure (Nakane et al., 2013). Adhesin movements are rapid, processive, and directional, strongly suggesting that a transport machinery is required to propel the adhesins at the cell surface. When cells are on a solid surface, the adhesins attach to the substratum and create friction forces propelling the cell body forward. Due to the helical arrangement of the adhesins, the cell body is thought to rotate. Upon reaching the rear of the cell, attached adhesins are released from the substratum, and recycled to the front of the cell. How adhesions are released is unknown but adhesins that move back to the front pole are unable to attach the substrate and thus only the adhesins that move toward the rear of the cell exert force on the substrate (Figure 25b) (Nakane et al., 2013).

Although, it appears clear that the surface transport of adhesins attached to the substratum results in cell movement, many questions remain unsolved with regards to the mechanism of *Flavobacterium* gliding. The identity of the rigid helical closed loop and of the motor that propels the adhesins remains unknown. However, forward genetic screens have identified several gliding proteins which I discuss below.

3.1.2. Gliding Proteins

The search for genes that are required for *Flavobacterium* gliding motility led to the identification of several genes, namely the *gld*, *spr* and *rem* genes (Figure 25a) (Braun and McBride, 2005; Braun et al., 2005). Many of these genes are unique to members of the Bacteroidetes phylum, suggesting that gliding of *F. johnsoniae* and their relatives has evolved independently from other forms of bacterial gliding (McBride and Zhu, 2013). Although many gliding genes were identified, the identity of the gliding machinery is unclear. However, some functions have been assigned to certain gliding genes.

For example, a subset of the gliding proteins (Gld and Spr proteins) constitutes a trans-envelope Bacteroidetes-specific protein secretion system (Figure 25a): the Porphyromonas secretion system (PorSS), thus called because it was originally identified in the non-motile pathogen *Porphyromonas gingivalis*, which, like *F. johnsoniae*, belongs to the phylum Bacteroidetes. Recently, the PorSS has been referred to as the type IX secretion system (T9SS) (Nakane et al., 2013; Shrivastava et al., 2013). It has been shown that the PorSS is responsible for the secretion of several proteins, including chitinase, and the SprB and RemA adhesins, both of which are required for gliding (Figure 25a and described below) (McBride and Zhu, 2013; Rhodes et al., 2011; Shrivastava et al., 2013). It is still unclear if the PorSS is only required for the assembly of the gliding machinery by secreting some of its components to the cell surface or if it is also an integral component of the motility machinery like the type III secretion system (T3SS) part of the flagellar apparatus (Erhardt et al., 2010).

The PorSS secretes SprB and RemA, two major adhesins of the motility apparatus (Figure 25a). SprB, a huge protein (669 kDa), likely plays redundant functions in the motility machinery because although an *sprB* mutant cell fails to glide on agar, it still exhibits some limited movement on glass (Nelson et al., 2008). SprB is thus required for movement on specific substrates, for example, agar. As described in the gliding model, SprB is a mobile component of the motility machinery and rapid lateral movements of SprB along the cell surface were observed by two studies. First, 500 nm protein G-coated polystyrene spheres carrying antibodies against SprB, were rapidly propelled at 2 μm/s at the cell surface, similar to the speed at which cells glide on glass. These spheres often moved continuously along the length of the cell, around the pole and back down the opposite side of the cell (Nelson et al., 2008). Secondly, SprB antibodies were also observed moving rapidly along the cell axis with an approximately speed of 2 μm/s. In this study, SprB appeared to migrate around the pole and continue at the same speed toward the opposite pole along an apparent left handed helical closed loop (Nakane et al., 2013). Importantly, the motility model is mostly inferred from studies of SprB dynamics.

The partial motility defect of *sprB* mutant raised the possibility that additional mobile adhesins might function to allow movement over some surfaces. By a genetic approach, Shrivastava *et al.* identified one *sprB* paralog, *remA*. Cells with mutation in *remA* exhibited motility defects that were only apparent when *sprB* was also defective (Shrivastava et al., 2012). Shrivastava *et al.* also showed that RemA moves rapidly along the cell surface with similar pattern and speed as those observed for SprB (Shrivastava et al., 2012). RemA likely functions in adhesion because wild type *F. johnsoniae* cells are able to form aggregates in liquid cultures whereas *remA* mutant cells are

deficient in aggregate formation. Furthermore, the over-expression of RemA resulted in the formation of larger aggregates. The presence of a predicted lectin-like domain in RemA suggests that RemA binds to polysaccharides on the surface of neighboring cells. Consistent with this, the addition of galactose, rhamnose or lactose results in the rapid dispersion of the aggregates, suggesting that RemA recognize sugar moieties. Moreover, the same genetic screen that searched motility mutants in *sprB* mutant cells and resulted in the identification of *remA*, also identified three additional genes, *remC*, *wza* and *wzc* (Shrivastava et al., 2012). Remarkably, the *remC* gene encodes a putative glycosyl transferase, *wza and wzc* encode critical parts of a capsular polysaccharide secretion system Wza, a so-called outer membrane auxiliary (OMA) that forms an octameric secretion pore in the outer membrane, and an inner membrane tyrosine autokinase that is critical for transport. Mutant cells of each of these three genes failed to form large cell aggregates. Thus both RemA and secreted polysaccharides are required for aggregate formation suggesting that RemA interacts with a capsular-type polysaccharide synthesized and secreted by RemC, Wza and Wzc. Shrivastava *et al.* suggested that this interaction could facilitate gliding of one cell over another cell resulting in collective motion. Also, by producing and secreting polysaccharides that interact with RemA or other cell surface motility proteins, the cells may produce their own substrate and allow productive contact with a large variety of surfaces. Cells could reuse such substrate, resulting in the multicellular patterns that are characteristic of *F. johnsoniae* (Shrivastava et al., 2012). A similar model was also proposed for *M. xanthus* gliding and will be discussed in the section Discussion (Sections 1.1. and 1.2., Discussion).
It is possible that *F. johnsoniae* also uses many other uncharacterized adhesins because its genome is predicted to encode several other lectin-like proteins, which could explain how this bacterium attaches to and glides over such diverse surfaces.

F. johnsoniae gliding motility machinery is thus the result of the coordination of different subparts. The PorSS transports adhesins to the cell surface and then, these adhesins are propelled along the cell body by a motor, resulting in cell movement. Although the cell surface adhesins involved in motility are known, the motor propelling these adhesins has not been yet identified.

3.1.3. The Gliding Motor

Although the motility motor has not been identified, several studies indicate that the proton motive force (PMF) could directly power the gliding of *F. johnsoniae* (Dzink-Fox et al., 1997; Nakane et al., 2013). Indeed, Dzink-Fox *et al.* showed that acetate, a protonophore known to

dissipate the PMF, inhibits cell movements and bead movements at the cell surface (Dzink-Fox et al., 1997). More recently, Nakayama *et al.* showed that the movement of SprB and gliding cells, was rapidly and reversibly blocked by the addition of carbonyl cyanide *m*-chlorophenylhydrazone (CCCP), which also dissipates the PMF across the cytoplasmic membrane (Nakane et al., 2013). The CCCP effect is very rapid and reversible (3 seconds for stopping the gliding movement and 6 seconds for the reversibility effect) suggesting that the PMF and not ATP is the fuel of the motility engine.

These data support the hypothesis that PMF drives the gliding motility of *F. johnsoniae*, suggesting that the gliding molecular motor is a proton channel localized in the inner membrane. Therefore, it was suggested that *F. johnsoniae* requires inner membrane proteins to convert chemical energy into cell movement. Of the proteins essential for *F. johnsoniae* gliding, only GldF, GldG, GldL, and GldM are thought to span the cytoplasmic membrane (Figure 25a). GldF and GldG are components of an ATP-binding cassette transporter and thus are likely to rely on ATP rather than the PMF to perform their functions. However, GldF and GldG, which are required for *F. johnsoniae* gliding, are not essential for the gliding motility of other members of the Bacteroidetes phylum, suggesting that these proteins are not core components of the gliding motility machinery (Shrivastava et al., 2013). Thus, GldL and GldM are the only candidates left for the motor proteins, however, these proteins are not similar in sequence to proteins of known function, and they are components of the PorSS secretion system (Shrivastava et al., 2013). Alternatively, some unidentified inner membrane proteins may perform this motor function. Jarrell and McBride proposed that the motor is not localized in the inner membrane but anchored to the peptidoglycan and oriented towards the outer membrane (Jarrell and McBride, 2008). While this is plausible, it is not clear how such motor would derive its energy source as ATP is not present in the periplasmic space and the PMF is exerted at the inner membrane.

In conclusion, many mysteries remain concerning the mechanism of gliding motility, the identity of the rigid helical track and the identity of the motor. Further understanding could come from the study of *M. xanthus* gliding, whose gliding appears to share similarities with the gliding of *F. johnsoniae* (discussed below in the Section 2.2., Discussion).

3.2. *Myxococcus xanthus*

M. xanthus is a Delta-proteobacterium, which displays a complex life cycle. When facing starvation, *M. xanthus* is able to organize the movements of thousand cells to build a fruiting body

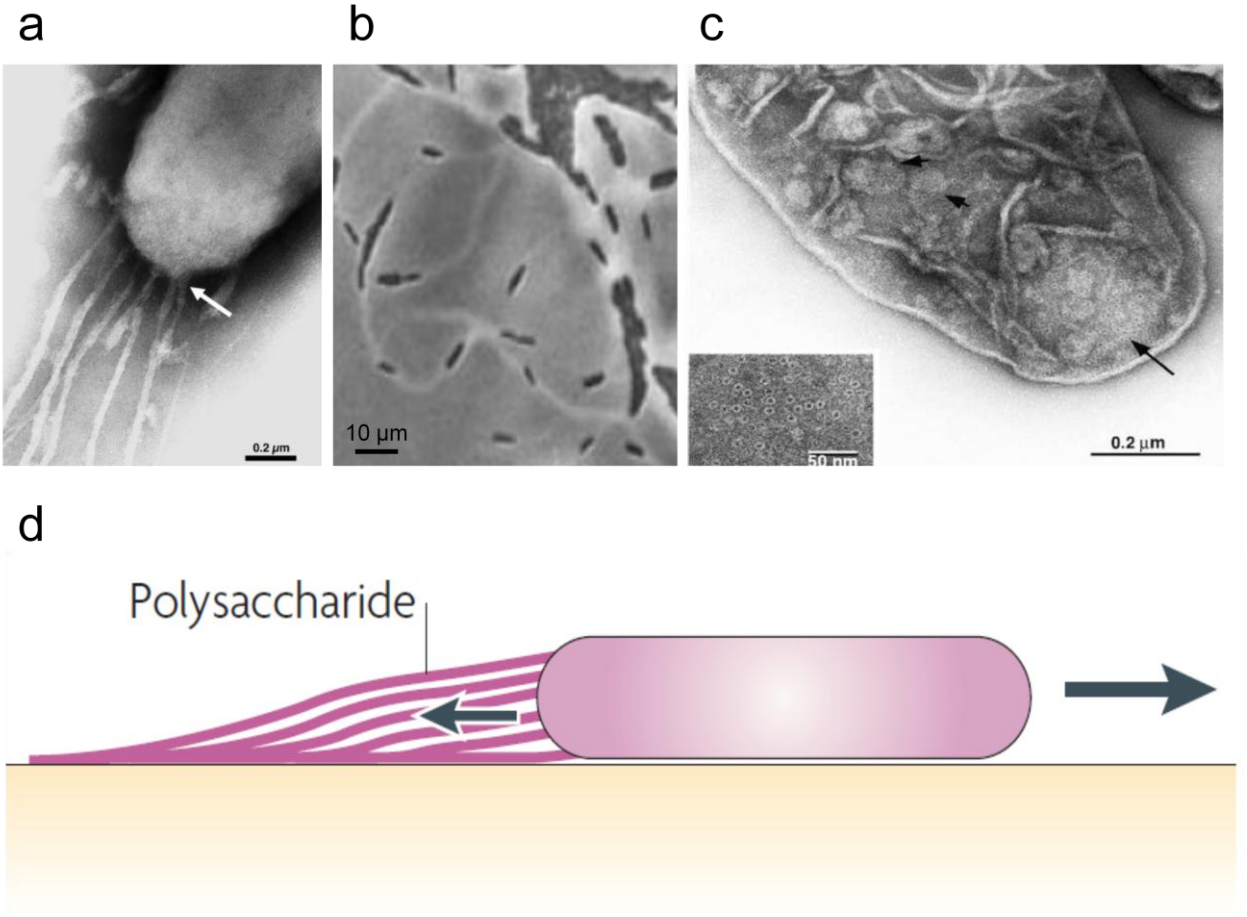

Figure 26. Slime secretion model. a. Electron micrograph of the cell pole of a gliding *M. xanthus* cell. Slime trails are composed of several slime bands, which are thought to be secreted at the cell pole, where potential pores are located (large arrow) (Wolgemuth et al., 2002). b. Phase contrast micrographs of slime trails deposition by *M. xanthus* as it glides on agar (Wolgemuth et al., 2002). c. Electron micrograph of a negatively stained cell-envelope of *M. xanthus*. The pore-like structures are visible as ring-shaped structures, which are located at the cell pole (long arrow). Along the rest of the cell surface, the density of the pore-like structures is much smaller (short arrow). The inset shows a higher magnification of the pore-like structures array at the cell pole (Wolgemuth et al., 2002). d. Polysaccharide secretion model which involves a polar secretion and hydration of a polysaccharide to propels the cell forward (Jarrell and McBride, 2008).

wherein many of the cells differentiate into environmentally-resistant spores. *M. xanthus* is also noted for other complex multicellular behaviors such as swarming, rippling and predation (Mignot, 2007; Nan and Zusman, 2011).

To realize its life cycle, *M. xanthus* requires two motility systems that are genetically distinct (Hodgkin and Kaiser, 1979). One set of genes is required for the so-called "social motility" (S-motility), which involves the movement of cells in group; whereas the other set of genes controls "adventurous motility" (A-motility), characterized by the movement of individual cells. S-motility in *M. xanthus* is an adapted form of twitching motility and is driven by the cooperation of a retractile bacterial type IV pilus (T4P) and surface exopolysaccharides (EPS) (Li et al., 2003; Wu and Kaiser, 1995). Most of the S-motility genes are therefore similar to the twitching motility genes of *Pseudomonas* and *Neisseria* and mostly encode a type IV pilus super-complex (Mattick, 2002). *M. xanthus* twitching motility is not the focus of this thesis and thus it will not be discussed below. On the contrary, the A-motility mechanism, a slow movement (2-4 μm/min) of *M. xanthus* cells along their axis in absence of visible extracellular organelles (Burchard, 1981), is a form of bacterial gliding motility and its mechanism has been a mystery for a long time.

3.2.1. Gliding Models

When I started my PhD in Tâm Mignot's group in 2009, two conflicting models were proposed to explain gliding motility in *M. xanthus*. These models were based on the putative function of certain gliding genes, on electron microscopy (EM) of *M. xanthus* cells, and on the localization of some gliding proteins. Both of these models are presented below.

3.2.1.1 The Slime Secretion Model

In the early 40's the observation that *M. xanthus* deposits a mucus when it glides, suggested that *M. xanthus* gliding motility results from the asymmetric secretion of a substance, likely a polysaccharide, loosely called slime. In this process, slime would act as a propulsive element, producing more pressure on one end of the cell than on the other end (Beebe, 1941). Several decades later, Wolgemuth *et al.* used electron microscopy and observed pore-like structures enriched at the cell poles (Figure 26). Ribbons of slime appeared to be exiting from these structures (Figure 26abc) suggesting that they are a surface component of a slime secretion apparatus. Assuming that slime is a polysaccharide, the authors computed theoretically that secretion through the pores could generate sufficient thrust to account for the gliding velocity of

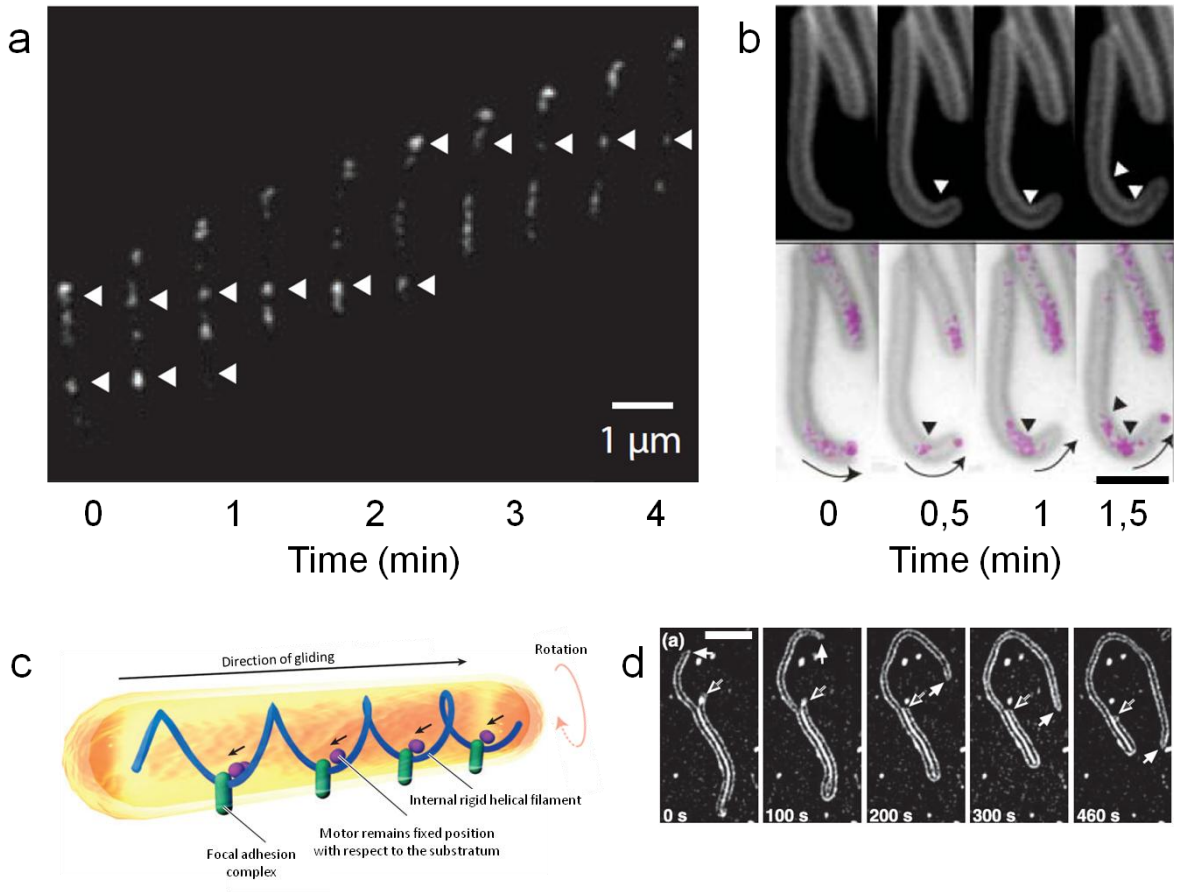

Figure 27. The focal adhesion complexes model. a. AglZ-YFP localizes to periodic sites that remain fixed relative to the substratum in a cell moving at constant velocity. Numbered arrowheads highlight selected bright fluorescence clusters. Scale bar = 1 µm (from Mignot et al., 2007). b. AglZYFP fluorescence clusters in a cell that bends while in motion. (Top) Cells stained with the membrane dye FM4-64 are shown. (Bottom) An overlay of the membrane signal (gray) and the AglZ-YFP signal (magenta), which is artificially colored for better clarity, are shown. White and black arrowheads point to regions of cell-body curvature and localization of the YFP signal, respectively. Arrows indicate the direction of movement. Scale bar = 1 µm (Mignot et al., 2007). c. In this model, large focal adhesion complexes penetrate the cell envelope, stick to the substratum at one end and connect to cytoskeletal filaments at the other end. Motor proteins push backward (small arrows) against the focal adhesion complexes, pushing the cell forward (from Nan and Zusman, 2011). d. Time-lapse series of cephalexin-treated cells stained with FM4-64. Empty arrows indicate the rear ends of the cells; solid white arrows indicate the front ends. Scale bar = 3 µm (Sliusarenko et al., 2007).

M. xanthus cells (Figure 26d) (Wolgemuth et al., 2002). The selective activation of the pores at the back of the cell would account for directionality of the cell.

Consistent with a role for polysaccharides in gliding motility, Youderian *et al.* identified several genes essential for gliding motility in *M. xanthus*. Among these genes, the authors identified several genes encoding enzymes for polysaccharide biosynthesis, sugar polymerases and carbohydrate kinases (Youderian et al., 2003). Accordingly, Yu and Kaiser also identified genes encoding putative polysaccharide production proteins that are involved in gliding motility (Yu and Kaiser, 2007). However, none of the mutation in these genes resulted in a slime-free phenotype. Thus, if slime contains polysaccharides, it is either essential or consists of more than one type.

3.2.1.2 The Focal Adhesion Complexes Model (FAC)

A couple of years before I joined the laboratory, the slime secretion model had been challenged by an alternative model (Mignot et al., 2007). This model was based on studies of the dynamic localization of a gliding protein, AglZ, in moving cells. Mignot *et al.* showed that during cell movement, AglZ localized in clusters, which are distributed with regular intervals along the cell body (Figure 27a). Remarkably, time-lapse experiments revealed that these clusters were initially assembled at the leading pole and retained a fixed position with respect of the substratum as the cell moved forward. The stationary position of the clusters relative to the substratum revealed that they are in fact moving in the opposite direction to that of the cell at the same velocity. These clusters eventually became dispersed when they reached the rear of the cell (Figure 27a) (Mignot et al., 2007). The dynamics of AglZ suggested that a complex connecting surface adhesion to an internal cellular structure could power cellular movement (Figure 27ab).

The so-called "focal adhesion" model proposes that gliding machinery units are assembled at the leading cell pole and travel along a rigid structure until they become disassembled at the lagging cell pole. Adhesion of the complex to the underlying substratum would create friction and thrust, analogous to adhesins of the *Flavobacterium* motility apparatus. According to this hypothesis the gliding machinery would be composed of a rigid "cytoskeletal" structure, a molecular motor and an associated trans-envelope complex to transduce its activity to adhesions at the cell exterior. The AglZ clusters are periodically assembled along the cell body, suggesting their anchoring to a periodic structure, possibly a helix that spans the length of the cell (Figure 27c). Thus the action of the motor may also induce the cell body to rotate as it pulls the cell forward (Mignot et al., 2007).

The rigid helical structure could be the MreB cytoskeleton because MreB may form helical scaffolds in the cell (although this is a current debate; see Dye et al., 2005; Jones et al., 2001; Kruse et al., 2003 versus Domínguez-Escobar et al., 2011; Garner et al., 2011; van Teeffelen et al., 2011). Indeed, a direct role of MreB is suggested by micro-fluidic experiments using the MreB-specific perturbing compound A22, which interferes with the dynamic polymerization of MreB. In these experiments A22 blocked gliding motility rapidly and reversibly and disrupted the localization of AglZ (Mauriello et al., 2010). Mauriello *et al.* also performed *in vitro* cross-linking experiments and showed that MreB interacts with AglZ (Mauriello et al., 2010). These experiments suggested that the MreB cytoskeleton has a direct role in the localization of the regulator protein AglZ, which could conduct to the assembly of the gliding machinery (Mauriello et al., 2010). However, the recent data showing that MreB does not form a helix, but rather forms small patches or filaments (Domínguez-Escobar et al., 2011; Garner et al., 2011; van Teeffelen et al., 2011), questions the exact role of MreB as a rigid track for the motility machinery (see discussion).

The focal adhesion model is compatible with several indirect lines of evidence. Using cephalexin, it has been shown that the velocity of gliding motility was not affected when cells are artificially elongated up to ten times their natural length (Sun et al., 1999). This is most easily explained by a distributed molecular engine because the number of such engines would increase proportionally as a function of cell length. On the contrary, a polar engine (*i.e.* the putative slime secretion apparatus) would be spatially limited and expected to stall when the cells become too long. According, twitching motility, which is powered by a type-IV pilus polar engine, proportionally decreased when the cell body became elongated (Sun et al., 1999). In addition, in some elongated cells, it has been observed that the leading pole of the elongated cells moved forward, whereas the lagging pole remained stationary (Figure 27d) (Sliusarenko et al., 2007). These experiments are in favor of a distributed motor rather than a motor localized at the lagging pole. However, the *Myxococcus* motility machinery must be identified to determine which model is correct, if any, which was one of the major aims of this thesis.

3.2.2. Gliding Proteins

To understand gliding motility, several genetic screens were realized to map motility genes and identify the implicated machinery. Thanks to these studies, approximately 40 genes were identified as being required for gliding motility. Unfortunately, these types of screens are negative screens creating many false positive because the inactivation of house-keeping genes is also likely

to impair motility. In addition, transposons were found in many genes of unknown function, which also rendered the identification of a gliding machinery difficult (Hodgkin and Kaiser, 1977, 1979; Youderian et al., 2003).

In conclusion, prior to my arrival in the laboratory, the genetic approach had failed to provide evidence to discriminate between the "slime secretion" and the "focal adhesion complexes" models, both of them largely relying on indirect evidences. To solve the debate between these two models, we decided to focus on the identification of the gliding motor, one of the essential parts of the gliding machinery. Indeed, the characterization and localization of this gliding motor provided a direct proof in favor of the "focal adhesion" model. Moreover, in the course of this study, we also made the discovery that this gliding motor was essential not only for motility but also for sporulation, a cellular process during which the cells become surrounded by a thick polysaccharide. Our results on both gliding and sporulation systems demonstrated the existence of a novel class of bacterial motors involved in intracellular transport of sugar-associated complex. These modular motors could be adapted to specific functions based which output complex they interact with. Therefore, it is conceivable that other motor associations could promote processive transport of proteins, lipids or other molecules in bacteria and thus could participate in the general organization of the bacterial cell.

RESULTS

Article I

Motor-Driven Intracellular Transport Powers Bacterial Gliding Motility.

Mingzhai Sun[1, a], Morgane Wartel[1, b, c], Eric Cascales[d], Joshua W. Shaevitz[a, e], Tâm Mignot[b, c].

[1] M.S. and M.W. contributed equally to this work.

[a] Lewis-Sigler Institute for Integrative Genomics

[b] Laboratoire de Chimie Bactérienne, Centre National de la Recherche Scientifique, Unité Propre de Recherche 9043

[c] Institut de Microbiologie de la Méditerranée, Université Aix-Marseille, Marseille Cedex 13402, France

[d] Laboratoire Ingénierie des Systèmes Macromoléculaires, Centre National de la Recherche Scientifique, Unité Propre de Recherche 9027, Institut de Microbiologie de la Méditerranée, Université Aix-Marseille, Marseille Cedex 13402, France

[e] Department of Physics, Princeton University, Princeton, NJ 08540

Published in PNAS, May 2011.

By localizing the gliding protein AglZ in moving cells, Mignot *et al.* found an indirect evidence for the FAC model. In gliding cells, they showed that the cytoplasmic AglZ-YFP (yellow fluorescent protein) protein forms distributed clusters that remain fixed relative to the substratum when cell moves (Mignot et al., 2007). The stationary position of these clusters relative to the substratum revealed that they are in fact moving in the opposite direction to that of the cell at the same velocity. These observations led us to hypothesize that intracellular motors moving on cytoplasmic cytoskeletal filaments transmit force through the cell envelope to transport adhesion complexes attached to the substratum, causing the forward translocation of the cell body. Therefore, we decided to identify this gliding molecular motor to confirm or infirm this model of cell movement.

According to the "focal adhesion" hypothesis, the AglZ-YFP clusters are only apparently stationary because they are bound to the substratum. Thus, in a surface immobilized cell, which still possesses a functional gliding machinery, these adhesion complexes should move from one pole to the other. Thus, if AglZ-YFP is linked to the gliding motor, we should observe its unidirectional movement from one pole to the other, in immobilized cells. Indeed, in cells immobilized on a chemically treated glass cover-slip, we observed the processive and directional transport of AglZ-YFP, along the cell body from the leading pole to the lagging pole. Using this assay to test if traction forces are generated along the cell body, we added polystyrene beads directly to the outer surface of immobilized cells with an optical trap in an approach inspired by experiments conducted on *F. johnsoniae* (Section 3.1., Introduction). Beads were propelled directionally along the cell body and linked to AglZ-YFP, suggesting that these traction forces are indeed produced by the gliding machinery. We then decided to identify the gliding machinery responsible of the directional transport of AglZ and beads along the cell body.

Thanks to previous genetic screens, approximately 50 genes were identified to be essential for gliding motility (Youderian et al., 2003). However, because functions could not be predicted for a majority of the gene products, the gliding motor could not be identified. To guide the research of gliding motor genes, we sought to identify the energy source of gliding motility by using a chemical approach. In living cells, ATP and the PMF are common energy sources for molecular motors and each can be targeted with metabolic inhibitors such as CCCP, nigericin, or valinomycin that inhibit the PMF or its components and arsenate which depletes the ATP pools. Using these drugs in a micro-fluidic chamber, we demonstrated that it is likely the PMF, and more precisely its proton gradient component that fuels *M. xanthus* gliding motility. These results suggested that a proton channel, akin to the flagellar stator (MotAB) or the TolQR/ExbBD

proteins, energized the motility apparatus. Proton channels operate by harnessing the proton gradient across the inner membrane to generate mechanical force. Thus, we searched in the collection of *M. xanthus* gliding mutants for genes encoding homologues of *motAB* or *tolQR*. Among several potential candidates (eight gene loci), we identified the *aglRQS* locus that encodes one MotA/TolQ homologue (AglR), and two MotB/TolR homologues (AglQ and AglS) and had been previously identified by Youderian *et al.* (Youderian et al., 2003). We thus constructed in-frame deletions of the *aglR*, *aglQ* and *aglS* genes and showed that these mutations abolished gliding motility as well as the trafficking of AglZ-YFP, showing that each of the three *aglR, aglQ* and *aglS* genes are essential for gliding in *M. xanthus*.

To understand how the AglRQS complex might power gliding motility, we localized the AglQ protein by constructing a C-terminal fluorescent fusion of AglQ to mCherry. We found that the localization of AglQ-mCherry overlapped with that of AglZ-YFP at the FACs. In a time-lapse experiment, AglQ-mCherry also formed a bright polar cluster at the leading pole and periodic clusters along the cell body that remain fixed relative to the substratum during cell movement. Finally, consistent with the notion that bead transport reflects the activity of the motility machinery, we showed that bead transport was dependent on the proton gradient. Additionally, in *agl* motor mutants, bead transport was abolished.

Based on these results, we concluded that the gliding motility motor was identified and its localization strongly favored the notion that the gliding machinery localizes to the FACs. This work was done in collaboration with the biophysicists Joshua Shaevitz and Mingzhai Sun from the Department of Physics at Princeton University. Specifically, the Shaevitz Lab developed the traction force assay, applying polystyrene beads to immobilized cells with an optical trap. I was involved in the identification of the energy source and the molecular and cell biology characterization of the AglRQS complex.

Directional intracellular trafficking in bacteria

Lotte Søgaard-Andersen[1]
Max Planck Institute for Terrestrial Microbiology, 35043 Marburg, Germany

In their natural environments, bacteria often colonize biotic and abiotic surfaces, and the intimate association with biotic surfaces can be a prerequisite for pathogenesis. Once on a surface, cells may remain sessile and simply grow and divide. Alternatively, cells may display active cell movements and translocate across the surface by one of three different mechanisms: swarming, twitching, or gliding (1, 2). Swarming depends on rotating flagella that are randomly distributed on the cell surface and form a bundle that pushes a cell forward (2, 3). Twitching depends on type IV pili, which extend from the cell surface, attach to the surface on which a cell resides, and then retract with a retraction event, pulling a cell forward (1, 4). Whereas swarming and twitching each depend on a cell surface organelle, gliding occurs in the absence of any eye-catching structures, and the molecular mechanism has remained puzzling for years. In PNAS, an important part of the puzzle is solved by the identification of the molecular motor that powers gliding in *Myxococcus xanthus* (5). Moreover, the finding that this motor moves in a directed manner between subcellular regions has major implications for our understanding of how bacterial cells become spatially organized.

The story begins in 2007 with the astonishing observation that the AglZ protein, which is required for gliding motility in the Gram-negative, rod-shaped bacterium *M. xanthus* (6), localizes to the leading cell pole as well as to focal adhesion complexes (FACs) that are distributed regularly along the cell body (7). In a moving cell, the FACs remain stationary with respect to the surface on which the cell is translocating and thus indirectly move from the leading to the lagging cell pole. If a cell is immobilized on a surface, the FACs visibly move from one pole to the other. So, in both scenarios, the FACs move in a directed manner from one pole to the other.

Sun et al. (5) build on these observations and find that tiny beads attached to the surface of immobilized cells also move from the leading to the lagging cell pole. Moreover, the beads colocalize with AglZ-YFP in the FACs, providing evidence that traction force is generated at the sites of the FACs. Using chemical biology, Sun et al. (5) identify the energy source that powers the FACs motor as the H^+-gradient over the cytoplasmic membrane. In addition to ATP synthase, three homologous bacterial motors are known to harness the energy of this gradient to generate mechanical force: MotA/MotB (8), ExbB/ExbD (9), and TolQ/TolR (10) (Fig. 1). Armed with this information, Sun et al. (5) searched a collection of *M. xanthus* gliding mutants (11) and identified the *aglQRS* locus that encodes one MotA/TolQ/ExbB homolog (AglR) and two MotB/TolR/ExbD homologs (AglQ and AglS) as their candidate for the motor. All three AglQ/AglR/AglS proteins are required for gliding, and according to pull-down assays they interact to form a complex. Turning to live-cell imaging, it is shown that AglQ-mCherry localization matches that of AglZ: in moving cells, AglQ-mCherry localizes in a cluster at the leading pole as well as to FACs; and in immobilized cells, AglQ moves from the leading to the lagging cell pole. Genetic inactivation of the H^+-channel in the AglQ/AglR/AglS complex blocked gliding as well as trafficking of FACs to the lagging pole but did not interfere with formation of the FACs. Thus, the AglQ/AglR/AglS complex seems to be the component of the FACs that is involved in force generation, and force generation leads to trafficking of the FACs in a directed manner from the leading to the lagging cell pole.

The findings of Sun et al. have implications well beyond gliding motility.

M. xanthus cells occasionally undergo reversals during which cells stop and then resume gliding in the opposite direction, with the old leading pole becoming the new lagging cell pole. During reversals gliding motility proteins relocate between the poles, and the FACs disappear (7, 12). After a reversal, the FACs reappear and now track in the opposite direction, suggesting that they can generate force in at least two directions, depending on the overall leading/lagging pole polarity of a cell.

The findings of Sun et al. (5) have implications well beyond gliding motility. Over the last decade it has become clear that bacterial cells are spatially highly organized (13). In eukaryotic cells, the spatial organization depends on cargo transport by molecular motors that track directionally on filaments, with kinesins and dynein tracking in opposite directions on microtubules and myosins tracking on actin (14). The findings of Sun et al. (5) identify AglQ/AglR/AglS as the first bacterial motor able to move in a directed manner between subcellular regions. Therefore, in a larger perspective, the findings by Sun et al. (5) open up the possibility that similar motors could be involved in organizing bacterial cells spatially by bringing cargo such as proteins, DNA, or mRNA to their individual subcellular addresses.

A challenge for the future will be to understand how the H^+-flux through AglQ/AglR/AglS is converted to mechanical force. A comparison with homologous systems is instructive (Fig. 1). The MotA/MotB proteins form an H^+-channel in the cytoplasmic membrane, make up the stator part of the flagellar rotary motor, and interact with the FliG protein in the rotor part of the flagellar motor to generate torque, thereby setting up the flagellar rotations (8). MotB contains a domain that fixes MotA/MotB to the peptidoglycan, in that way allowing the complex to function as a stator. Many flagella can rotate both clockwise and counterclockwise, and in both directions rotations depend on the interaction between MotA and FliG. ExbB and ExbD interact with TonB to form a complex in the cytoplasmic membrane (9). H^+-flux through ExbB/ExbD induces conformational changes in TonB that are converted to conformational changes in TonB-dependent receptors in the outer membrane, such as FhuA, to energize transport over this membrane. TolQ and TolR together with TolA form a complex in the cytoplasmic membrane that is important for outer membrane integrity and cell division (10). Here, H^+-flux through the TolQ/TolR H^+-channel induces conformational changes in TolA, which ultimately changes the interaction between TolA and the outer membrane protein Pal (10). Thus, in all three systems the energy from H^+-flux is converted to changes in protein conformation that regulate membrane processes. Moreover, in all three systems, the H^+-channels MotAB, TolQR, and ExbBD are the motors that harvest the energy from the H^+-flux, and this energy is converted to a mechanical output because the motors are hooked up to a partner

Author contributions: L.S.-A. wrote the paper.
The author declares no conflict of interest.
See companion article on page 7559.
[1]E-mail: sogaard@mpi-marburg.mpg.de.

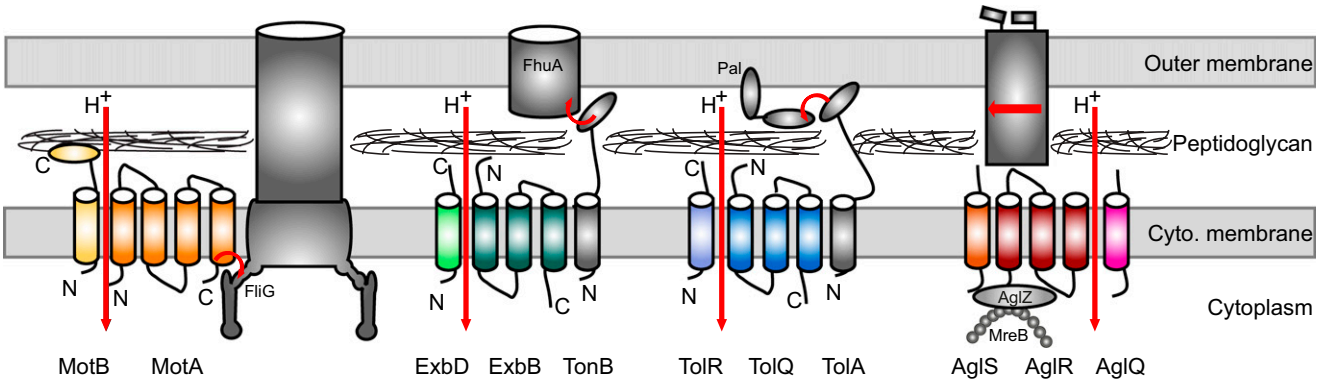

Fig. 1. Schematics of the MotA/MotB, ExbB/ExbD, TolQ/TolR, and AglQ/AglR/AglS proton channels. The membrane topology of the involved proteins is shown in the context of the cell envelope. System specific components are indicated in gray. H^+-flux (vertical red arrows) induced interactions that determine the system specific outputs are indicated by red arrows. For simplicity, the H^+-flux in the AglQRS system is only shown to involve AglR and AglQ. For simplicity, the interactions between AglQRS and AglZ and between AglZ and MreB are shown as direct. For simplicity, all complexes are shown with 1:1 stoichiometries. The stoichiometry of MotAB is 4:2, with 11 to 12 complexes making up the full stator ring, of ExbBDTonB 7:2:1, of TolQRA 4–6:2:1, and of AglQRS it is not known.

protein, such as FliG, TolA, or TonB. The AglQ/AglR/AglS system presumably works by a similar mechanism, and the partner protein(s) likely extend from the cytoplasmic membrane to the cell surface, for the proton-flux to be converted to traction force (Fig. 1).

Sun et al.'s article (5) raises many fascinating questions for the future. A critical question is how the FACs move given the presence of peptidoglycan in the periplasm (i.e., does movement of the FACs involve breaking and resealing of peptidoglycan?). FACs are suggested to assemble at the leading pole and disassemble at the lagging pole (7). How does this happen? It was previously suggested the FACs move or even track along the cytoskeletal element formed by the actin-like MreB protein in the cytoplasm (7, 15). An open question is the function of this interaction. Recently, several proteins required for gliding were suggested to be part of FACs (16), and the AgmU protein was proposed to form a helical filament in the periplasm (17). Resolving the function of these proteins in gliding is a formidable challenge. In total, the *M. xanthus* genome contains eight gene clusters for MotA/TolQ/ExbB and MotB/TolR/ExbD homologs. In addition to *aglQRS*, the *aglXV* cluster has been implicated in gliding motility (11, 17). It will be interesting to determine how many different gliding motors *M. xanthus* contains.

Gliding motility systems in different bacteria are very different (1). For instance, the gliding proteins in *Flavobacterium johnsoniae* are not present in *M. xanthus*, suggesting that mechanisms for gliding evolved independently several times (1). In the case of *M. xanthus*, the identification of AglQ/AglR/AglS as the gliding motor suggests that this gliding machinery evolved by tinkering with spare parts from an existing motor.

ACKNOWLEDGMENTS. Our work on motility is supported by The Max Planck Society, the graduate program "Intra- and intercellular transport and communication" funded by the German Research Foundation, and the Landes-Offensive zur Entwicklung Wissenschaftlich-ökonomischer Exzellenz (LOEWE) Research Center for Synthetic Microbiology.

1. Jarrell KF, McBride MJ (2008) The surprisingly diverse ways that prokaryotes move. *Nat Rev Microbiol* 6: 466–476.
2. Harshey RM (2003) Bacterial motility on a surface: Many ways to a common goal. *Annu Rev Microbiol* 57: 249–273.
3. Kearns DB (2010) A field guide to bacterial swarming motility. *Nat Rev Microbiol* 8:634–644.
4. Craig L, Li J (2008) Type IV pili: Paradoxes in form and function. *Curr Opin Struct Biol* 18:267–277.
5. Sun M, Wartel M, Cascales E, Shaevitz JW, Mignot T (2011) Motor-driven intracellular transport powers bacterial gliding motility. *Proc Natl Acad Sci USA* 108: 7559–7564.
6. Yang R, et al. (2004) AglZ is a filament-forming coiled-coil protein required for adventurous gliding motility of *Myxococcus xanthus*. *J Bacteriol* 186:6168–6178.
7. Mignot T, Shaevitz JW, Hartzell PL, Zusman DR (2007) Evidence that focal adhesion complexes power bacterial gliding motility. *Science* 315:853–856.
8. Minamino T, Imada K, Namba K (2008) Molecular motors of the bacterial flagella. *Curr Opin Struct Biol* 18: 693–701.
9. Postle K, Kadner RJ (2003) Touch and go: Tying TonB to transport. *Mol Microbiol* 49:869–882.
10. Zhang XY-Z, et al. (2009) Mapping the interactions between *Escherichia coli* tol subunits: Rotation of the TolR transmembrane helix. *J Biol Chem* 284:4275–4282.
11. Youderian P, Burke N, White DJ, Hartzell PL (2003) Identification of genes required for adventurous gliding motility in *Myxococcus xanthus* with the transposable element *mariner*. *Mol Microbiol* 49:555–570.
12. Leonardy S, Freymark G, Hebener S, Ellehauge E, Søgaard-Andersen L (2007) Coupling of protein localization and cell movements by a dynamically localized response regulator in *Myxococcus xanthus*. *EMBO J* 26: 4433–4444.
13. Shapiro L, McAdams HH, Losick R (2009) Why and how bacteria localize proteins. *Science* 326:1225–1228.
14. Ross JL, Ali MY, Warshaw DM (2008) Cargo transport: Molecular motors navigate a complex cytoskeleton. *Curr Opin Cell Biol* 20:41–47.
15. Mauriello EMF, et al. (2010) Bacterial motility complexes require the actin-like protein, MreB and the Ras homologue, MglA. *EMBO J* 29:315–326.
16. Nan B, Mauriello EMF, Sun IH, Wong A, Zusman DR (2010) A multi-protein complex from *Myxococcus xanthus* required for bacterial gliding motility. *Mol Microbiol* 76:1539–1554.
17. Nan B, et al. (2011) Myxobacteria gliding motility requires cytoskeleton rotation powered by proton motive force. *Proc Natl Acad Sci USA* 108:2498–2503.

Nature Reviews Microbiology | AOP, published online 9 May 2011; doi:10.1038/nrmicro2579

BACTERIAL PHYSIOLOGY

Motor helps gliders to gain traction

Myxococcus xanthus cells move across a surface by one of two mechanisms: twitching motility and gliding motility. Whereas the pilus-driven mechanism of twitching motility is relatively well characterized, far less is known about the manner in which force is generated to propel the cell across the substrate surface during gliding motility. Now Sun *et al.* show that gliding is driven by membrane-bound motor complexes that are transported along the axis of the cell.

> “the AglRQS motor sits in the cytoplasmic membrane, coupled to both the MreB cytoskeleton and to the substratum, and uses the PMF to power gliding motility.”

The authors had previously shown that a yellow fluorescent protein (YFP)-tagged version of adventurous-gliding motility protein Z (AglZ), a gliding regulatory factor, formed spatially periodic foci that remained in a fixed position relative to the substrate over which the cell was gliding. To further investigate the potential role of these foci during gliding, the authors immobilized *M. xanthus* cells expressing AglZ–YFP and observed processive and unidirectional transport of fluorescent foci from one end of the cell to the other. When the authors bound polystyrene beads to the surface of the immobilized cells, AglZ–YFP levels increased in the vicinity of the beads, and the beads were transported along the cell surface. Treating the immobilized cells with the drugs A22 (which depolymerizes rod shape-determining MreB filaments) or nigericin (which reduces the proton gradient across the cytoplasmic membrane) disrupted the AglZ–YFP foci and blocked bead movement, suggesting that AglZ foci have a role in connecting the cell surface with the intracellular cytoskeleton and driving gliding motility in a manner that depends on the proton-motive force (PMF).

To identify those components of the AglZ foci that might be involved in generating PMF-dependent movement, Sun *et al.* searched the *M. xanthus* genome for putative proton-channel-type motors based on homology to known motors such as the MotAB motility proteins, which drive flagellar rotation. They identified the three-gene *aglRQS* locus as encoding putative orthologues of MotA (AglR) and MotB (AglQ and AglS) and found that deletion of each of these genes eliminated gliding but not twitching motility. Co-immunoprecipitation experiments and fluorescent labelling revealed that AglR, AglQ and AglS form a complex that colocalizes to the same foci as AglZ. Importantly, in immobilized cells from an *aglQ* deletion strain, the AglZ–YFP foci remained located in fixed positions in the cells.

The authors propose a model in which the AglRQS motor sits in the cytoplasmic membrane, coupled to both the MreB cytoskeleton and to the substratum, and uses the PMF to power gliding motility. However, the factors that are important for making these connections and the mechanics of force generation during gliding remain to be determined.

Andrew Jermy

ORIGINAL RESEARCH PAPER Sun, M. *et al.* Motor-driven intracellular transport powers bacterial gliding motility. *Proc. Natl Acad. Sci. USA* **108**, 7559–7564 (2011)
FURTHER READING Zusman, D. R. *et al.* Chemosensory pathways, motility and development in *Myxococcus xanthus*. *Nature Rev. Microbiol.* **5**, 862–872 (2007) | Nan, B. *et al.* Myxobacteria gliding motility requires cytoskeleton rotation powered by proton motive force. *Proc. Natl Acad. Sci USA* **108**, 2498–2503 (2011)

Motor-driven intracellular transport powers bacterial gliding motility

Mingzhai Sun[a,1], Morgane Wartel[b,c,1], Eric Cascales[d], Joshua W. Shaevitz[a,e,2], and Tâm Mignot[b,c,2]

[a]Lewis-Sigler Institute for Integrative Genomics and [e]Department of Physics, Princeton University, Princeton, NJ 08540; [b]Laboratoire de Chimie Bactérienne, Centre National de la Recherche Scientifique, Unité Propre de Recherche 9043, [c]Institut de Microbiologie de la Méditerranée, Université Aix-Marseille, Marseille Cédex 13402, France; and [d]Laboratoire Ingénierie des Systèmes Macromoléculaires, Centre National de la Recherche Scientifique, Unité Propre de Recherche 9027, Institut de Microbiologie de la Méditerranée, Université Aix-Marseille, Marseille Cédex 13402, France

Edited by Thomas J. Silhavy, Princeton University, Princeton, NJ, and approved March 14, 2011 (received for review January 21, 2011)

Protein-directed intracellular transport has not been observed in bacteria despite the existence of dynamic protein localization and a complex cytoskeleton. However, protein trafficking has clear potential uses for important cellular processes such as growth, development, chromosome segregation, and motility. Conflicting models have been proposed to explain *Myxococcus xanthus* motility on solid surfaces, some favoring secretion engines at the rear of cells and others evoking an unknown class of molecular motors distributed along the cell body. Through a combination of fluorescence imaging, force microscopy, and genetic manipulation, we show that membrane-bound cytoplasmic complexes consisting of motor and regulatory proteins are directionally transported down the axis of a cell at constant velocity. This intracellular motion is transmitted to the exterior of the cell and converted to traction forces on the substrate. Thus, this study demonstrates the existence of a conserved class of processive intracellular motors in bacteria and shows how these motors have been adapted to produce cell motility.

murein cluster B | proton motive force

Because of its small size, the bacterial cell was long thought to be a disordered compartment where random collisions and diffusion drive enzymatic reactions and cellular processes (1). However, recent advances in light microscopy have shown that, akin to eukaryotic cells, bacteria are spatially organized by a complex cytoskeleton, potentially allowing directed sorting of proteins to specific subcellular sites (1). Despite the characterization of bacterial actins and tubulins, processive transport motors akin to myosins or kinesins have not been found. Because eukaryotic cell motility is driven, in part, by processive intracellular motors, studying how bacteria glide over solid surfaces may lead to the identification of similar types of motors.

Directed motility is a vital feature of the behavior of many organisms and often is essential for biofilm formation and virulence (2). *Myxococcus xanthus*, a rod-shaped, Gram-negative, soil-dwelling bacterium, uses a combination of gliding motility, termed "adventurous" (A), and pilus-driven twitching motility, termed "social" (S), to form organized multicellular structures (3). Directional control in *M. xanthus* is achieved by modulating the period of cellular reversals, wherein the leading and lagging poles exchange roles (3). Recent work has shown that a set of motility-regulatory proteins is localized at the two distinct poles in moving cells. Frizzy protein S (FrzS) and Adventurous gliding protein Z (AglZ) are found at the leading pole (4, 5), and RomR is located at the lagging pole (6). Every 6 min, on average, gliding direction is reversed, and the protein-localization pattern is switched. The frequency of these oscillations is regulated by the Frz chemosensory system that acts upstream of the Ras-like protein Mutual function for gliding protein A (MglA) to produce a dynamic and controlled cell polarity (7, 8).

Despite several decades of research, the physical mechanism driving gliding motility has remained difficult to define. Two general classes of models for force production in gliding bacteria have been proposed. The first class invokes the motion of substrate-bound motors on tracks inside the cell (5, 9, 10). The second class proposes that hydration of an extruded polyelectrolyte "slime" gel from the rear of the cell propels the cell forward (11). One key difference between these two models is the location of force generation at the cell surface: A distributed motor-based mechanism requires traction to be generated along the cell cylinder, whereas in the slime-extrusion model force is generated only at the rear of the cell (12).

We recently found indirect evidence for a distributed, motor-based mechanism of gliding motility by observing the subcellular localization of the gliding motility regulatory factor AglZ in moving *M. xanthus* cells (13). In gliding cells, cytoplasmic AglZ-YFP formed spatially periodic foci that remained fixed relative to the surface even as the cell moved by a distance of several microns. Based on this and other observations, we hypothesized that intracellular motors moving on cytoskeletal filaments in the cytoplasm transmit force through the cell wall to dynamic adhesion complexes attached to the substrate, causing the cell to move forward. The identification of such molecular motors is a critical step toward confirming this model of this cell locomotion.

Results and Discussion

Intracellular Transport Generates Traction Force During Cell Gliding. If AglZ-YFP is linked to intracellular motor-driven motion, this protein should exhibit unidirectional flow from the leading cell pole in the cell frame of reference. In cells immobilized on a chemically treated glass coverslip (*SI Materials and Methods*), AglZ-YFP does not distribute uniformly or form fixed foci. Instead, as expected, we observed the processive, unidirectional transport of AglZ clusters from the front of the cell, defined by the brightest pole, toward the back (Movie S1). This flow is observed most easily in kymographs of AglZ-YFP fluorescence from single cells (Fig. 1*A*). Moving clusters of AglZ appear as diagonal lines in the kymograph corresponding to unidirectional motion at a constant velocity. Line fits to trajectories from multiple cells yielded an average velocity of 6.0 ± 2.1 μm/min (91 trajectories from 35 cells). Almost all the trajectories, 94 ± 2%, were oriented away from the leading pole, the same relative motion between the cluster and cell pole as observed in gliding cells with fixed AglZ clusters (Fig. 1*A*). Multiple clusters could be found moving at the same time in a single cell, and, surprisingly, in a few instances we observed two clusters in the same cell moving in opposite directions at the same time (Fig. 1*A*). Further analysis of the ratio of forward- and reverse-moving foci in different genetic backgrounds

Author contributions: M.S., M.W., J.W.S., and T.M. designed research; M.S., M.W., and E.C. performed research; M.S., M.W., J.W.S., and T.M. analyzed data; and M.S., M.W., J.W.S., and T.M. wrote the paper.

The authors declare no conflict of interest.

This article is a PNAS Direct Submission.

Freely available online through the PNAS open access option.

See Commentary on page 7283.

[1]M.S. and M.W. contributed equally to this work.

[2]To whom correspondence may be addressed. E-mail: shaevitz@princeton.edu or tmignot@ifr88.cnrs-mrs.fr.

This article contains supporting information online at www.pnas.org/lookup/suppl/doi:10.1073/pnas.1101101108/-/DCSupplemental.

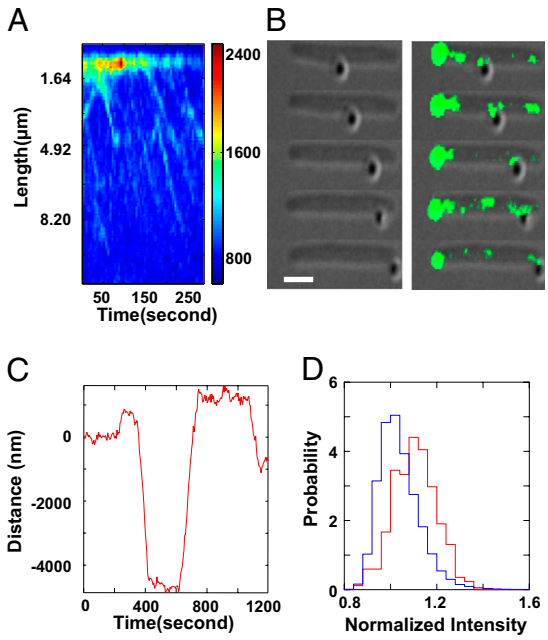

Fig. 1. Intracellular transport drives extracellular membrane-bound motion. (*A*) Kymograph of AglZ-YFP fluorescence in an immobilized cell. Moving clusters of AglZ appear as diagonal lines in the kymograph corresponding to unidirectional motion at a constant velocity. (*B*) Colocalization of AglZ-YFP clusters with a gliding bead. A bead moves along an immobilized cell (DIC image, *Left*). An overlay of the DIC image and an AglZ-YFP fluorescence image (green) shows the colocalization of the gliding bead with a cluster of AglZ-YFP fluorescence (*Right*) (Scale bar, 2 μm.) (*C*) A position record of a bead moving on the side of an immobilized cell. (*D*) Histograms of AglZ-YFP fluorescence intensity in immobilized cells. The blue histogram is derived from the intensity of all pixels within a cell except those belonging to the bright leading pole. The red histogram is derived from a subset of these pixels, those that are within 1 pixel from the center of a moving bead. All the intensity values are normalized by the mean intensity of pixels within a cell, excluding the bright leading pole. The higher mean value represented by the peak of the red histogram is the result of a significant enhancement of AglZ-YFP fluorescence near moving beads.

may uncover details about how bidirectionality and control is achieved by motor complexes.

We next probed whether traction forces are generated along the sides of cells, as predicted by the distributed motor-based model, using polystyrene beads bound to the outer surface of immobilized cells in a technique inspired by work on other gliding bacteria, particularly members of the bacteroides phylum (2, 9, 14). Similar to these previous observations, beads often were transported along the sides of the cell (Fig. 1*B* and Movie S2). Beads exhibited saltatory motion wherein motionless periods were interrupted by long runs (1.8 ± 1.2 μm) of unidirectional motion along the side of the cell (Fig. 1 *B* and *C*). During periods of fast motion, the bead velocity was 3.3 ± 1.8 μm/min. The speeds of AglZ-YFP clusters in immobilized cells, traveling beads on cell surfaces, and cells moving on agar (1.3 ± 1.8 μm/min) all have similar magnitudes, consistent with the notion that they reflect the activity of a common machinery. Subtle discrepancies in the exact magnitude of these speeds probably are caused by differences in the substrata and different applied loads experienced by the motility engine in each case. To examine the relative motion of multiple beads on a single cell, we artificially elongated cells by inhibiting the division-associated protein Penicillin-Binding Protein 3 (PBP3) with the drug cephalexin (15). Most of the beads on these cells, 93 ± 4%, moved in the same direction, away from the leading pole labeled with a bright AglZ focus, whereas 7% of the beads moved in the opposite direction, consistent with the behavior of AglZ-YFP cluster motion observed in immobilized cells. These results show that traction force is generated along the side of a cell and are consistent with the distributed motor-based model but are inconsistent with the slime-extrusion model of Wolgemuth et al. (11).

We performed several measurements that confirm that beads are powered by the cell-gliding machinery. First, we sought to connect the motion of the beads with the transport of AglZ along the axis of stationary cells by simultaneously measuring bead position and AglZ-YFP localization. Colocalizing AglZ-YFP and moving beads is challenging. Photobleaching of the AglZ-YFP foci occurs relatively quickly, whereas bead motion occurs sporadically, presumably because the unfunctionalized beads interact with the motor system only transiently. The difference in these time scales makes coincident measurement of AglZ-YFP fluorescence and bead velocity difficult. Nevertheless, whenever bead movement occurred rapidly after illumination, beads colocalized with AglZ-YFP (Fig. 1*B*). If AglZ-associated complexes of proteins drive extracellular motion, AglZ-YFP fluorescence intensity should be enhanced in the vicinity of moving beads. We compared the fluorescence intensity of regions of a cell that were within 82 nm (1 camera pixel) of the center of a moving bead with the overall fluorescence in the cell. Histograms of these two distributions show that AglZ-YFP fluorescence is enhanced near moving beads (Fig. 1*D*). Second, we added A22 to the medium and measured the effect on bead motion. A22 is a drug that has recently been shown to induce the depolymerization of the actin homolog MreB and reversibly to destabilize the AglZ-YFP complexes and inhibit gliding motility (16). After A22 treatment, processive bead motion was disrupted dramatically (Fig. S1*C*). Taken together, these data strongly suggest that gliding motility is driven by processive intracellular motors that interact with the MreB cytoskeleton.

Protein Transport and Motility Require the Proton Gradient. To guide the search for candidate motor genes, we sought to find the source of energy for gliding motility. ATP and the proton motive force (PMF) are common energy sources for molecular motors such as kinesin, myosin, and the bacterial flagellar motor. We used carbonyl cyanide-m-chlorophenylhydrazone (CCCP) to probe the dependence of gliding on the PMF. In our hands, CCCP at a concentration of 10 μM destroys the PMF in *M. xanthus* (Table S4) and rapidly abolishes cell movement (Fig. 2 *A* and *B*). This effect is reversible. When CCCP is washed out, cells regain their ability to glide. CCCP has the same reversible effect on bead movement using immobilized cells. To quantify the effect of drugs on bead motion, we calculated histograms of the speed of beads moving along immobilized cells (*Materials and Methods*). Upon the injection of CCCP, beads immediately stop moving (Fig. 2*E*). These results suggest that the PMF supplies the energy for gliding motors.

The PMF arises from gradients in both the chemical potential energy, in the form of a pH difference across the cell membrane, and electrical potential energy, caused by a voltage difference across the membrane. We used two drugs, nigericin and valinomycin, to uncover the relative roles that these two potential energies play in gliding motility. In *M. xanthus* cells, nigericin reduces the pH gradient without changing membrane potential, whereas valinomycin destroys the membrane potential with no change in the magnitude of the pH gradient (Table S4 and Fig S2*D*). When we added nigericin to gliding cells, motility was abolished, much as it was in the presence of CCCP. Cell and bead motion were stopped, and AglZ-YFP foci disappeared (Fig. 2 *A*, *C*, and *E* and Figs. S1*A* and S2*A*). As with CCCP, the effect of nigericin was reversible. In contrast, valinomycin has no effect on either cell or bead movement (Fig. 2 *A* and *D*). From these results, we conclude that gliding and bead motion are energized directly by the proton gradient. We further confirmed that CCCP and nigericin treatment did not affect the intracellular ATP pools during the short timescales relevant for gliding motility experiments (Fig S2*C* and *Materials and Methods*). Additionally, nigericin treatment had no significant effect on twitching motility, which uses the hydrolysis of

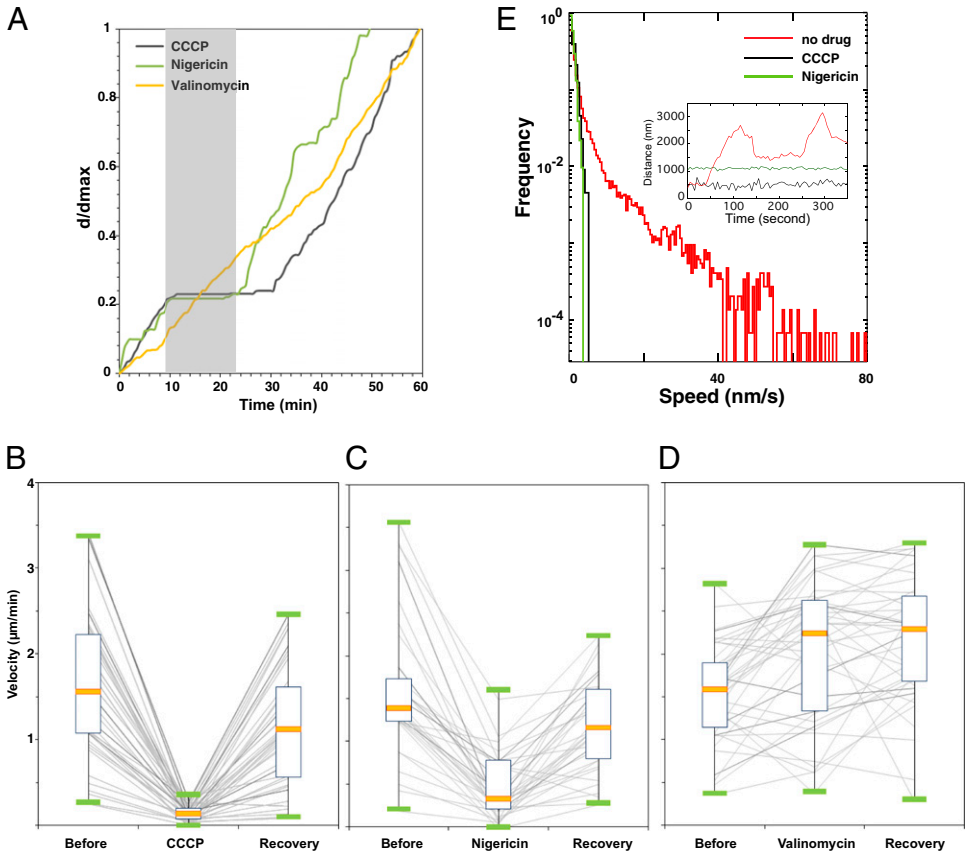

Fig. 2. Gliding motility in *M. xanthus* is driven by the proton gradient. (*A*) Reversible effects of metabolic PMF-uncoupling drugs on single cell motility. The relative cumulated distances corresponding to the distance traveled by a cell at any given time over the maximum traveled distance by that cell at the end of the time lapse (d/dmax) are plotted over time. The gray rectangle indicates the time interval when the cells were in the presence of drugs. (*B–D*) Box plots of wild-type cell (n = 50) velocities before, during, and after treatment by CCCP (*B*), nigericin (*C*), and valinomycin (*D*). The solid orange bars represent the average velocity of the population during each condition. Each line represents a single cell before, during, and after treatment. (*E*) Histograms of bead gliding speeds. (*Inset*) Trajectories of gliding beads along nontreated (red), CCCP-treated (black), and nigericin-treated (green) cells. The absolute value of the first derivative of the trajectories is used to form speed histograms. Both CCCP and nigericin completely stop bead movement.

ATP as an energy source, showing that this drug does not affect motility systems that are powered by ATP (Fig. S2*B*).

A Proton Channel Powers Force Generation. Taken together, the above data show that gliding motility in *M. xanthus* is driven by a proton gradient, suggesting that the mechanism underlying bacterial gliding and swimming may be linked to a common form of molecular motor, a proton channel. Bacterial motors that make use of a proton gradient are widespread and power flagellar rotation [Motility proteins AB (MotAB)], ATP synthesis (F_1F_O), and macromolecular transport across the cell envelope [Tolerant proteins QR (TolQR), Excretion of an inhibitor of Colicin B proteins BD (ExbBD)]. We searched the *Myxococcus* genome for homologs of MotAB and TolQR/ExbBD (Fig S3*A*) and found one particular locus, *aglRQS* (MXAN6862-60), which fulfilled all the expected criteria for a gliding motor candidate. Transposon insertions in *aglR* (MXAN6862) and *aglS* (MXAN6860) have been described as specifically inactivating gliding and not twitching motility (17). Sequence analysis indicates that AglR is a TolQ/ExbB/MotA homolog, whereas AglQ (previously MXAN6861) and AglS are TolR/ExbD/MotB homologs (Fig. 3*A* and Fig. S3 *B–D*). AglR, AglQ, and AglS all contain the key residues in the predicted lumen of the channel that enable proton conduction, and theoretically both AglRQ and AglRS can form functioning channels (Fig. 3*A* and Fig. S3 *B–D*) (18).

Other TolQR homolog pairs are found in the *Myxococcus* genome but are less likely to be the true gliding motor (Fig S3*A*). Nan et al. (10) identified AglX and AglV as necessary for gliding motility. However, these genes are found in a putative operon upstream from TolA, TolB, and Peptidoglycan-associated lipoprotein (Pal) homologs and thus probably are involved in global maintenance of the cell envelope (19). Therefore we favor the idea that deletion of these proteins inhibits gliding through pleiotropic effects on the cell exterior, e.g., by the maintenance of external adhesion structures within the motor complex. AglRQS homologs also are found in a third cluster on the *Myxococcus* genome (MXAN3005-3003; Fig S3*A*). However, in-frame deletion of the MXAN3004 gene did not abolish gliding motility (Fig S4), suggesting that these genes are cryptic or perform a distinct, nongliding function.

To test the role of the AglRQS system directly, we characterized motility in strains containing in-frame deletions in *aglR*, *aglQ*, and *aglS*. All three deletions eliminate gliding motility but do not affect pilus-based twitching motility when assayed by colony morphology or single-cell analysis (Fig. 3*C* and Fig. S4). Cells containing a double deletion *of aglR*, *-Q*, or *-S* in combination with *pilA* do not exhibit any motility in either assay (Fig. 3*C* and Fig. S4). All *agl* deletions were fully complemented when *aglR*, *-Q*, and *-S* were expressed ectopically, showing that all three *agl* genes are essential for gliding motility (Fig. 3*C* and Fig. S4). A point mutation in a conserved residue of AglQ (D28N), predicted to abolish H^+ binding within the lumen of the proton channel (20), does not affect protein stability but completely abolishes cell gliding, indicating that proton transport is required for gliding motility (Fig. 3 *B* and *C*). Finally, to test whether AglR, -Q, and -S form a complex, we searched for proteins that may associate with AglQ in vivo by conducting immunoprecipitation experiments using HA-tag fusion constructs of the wild-type and D28N mutant forms of AglQ as bait. Matching the spectra obtained from liquid chromatography-tandem mass spectrometry (LC-MS/MS) of the eluted trypsin-digested peptides against the *Myxococcus* sp. proteome resulted in the unambiguous identification of AglR and AglS in these samples but not in control samples derived from cells lacking the fusion proteins (Fig. S5). Thus, we expect that both AglR and AglS associate physically with AglQ-containing motility complexes.

The AglRQS motor proteins exhibit the same intracellular localization dynamics as AglZ. To examine the localization of this motor system, we constructed a C-terminal fluorescent fusion of AglQ to mCherry (Fig. S6*A*). Cells expressing this fusion move with reduced velocity, 0.1 ± 0.1 μm/min compared with 1.3 ± 1.8 μm/min in wild-type cells, demonstrating that the fusion is partially de-

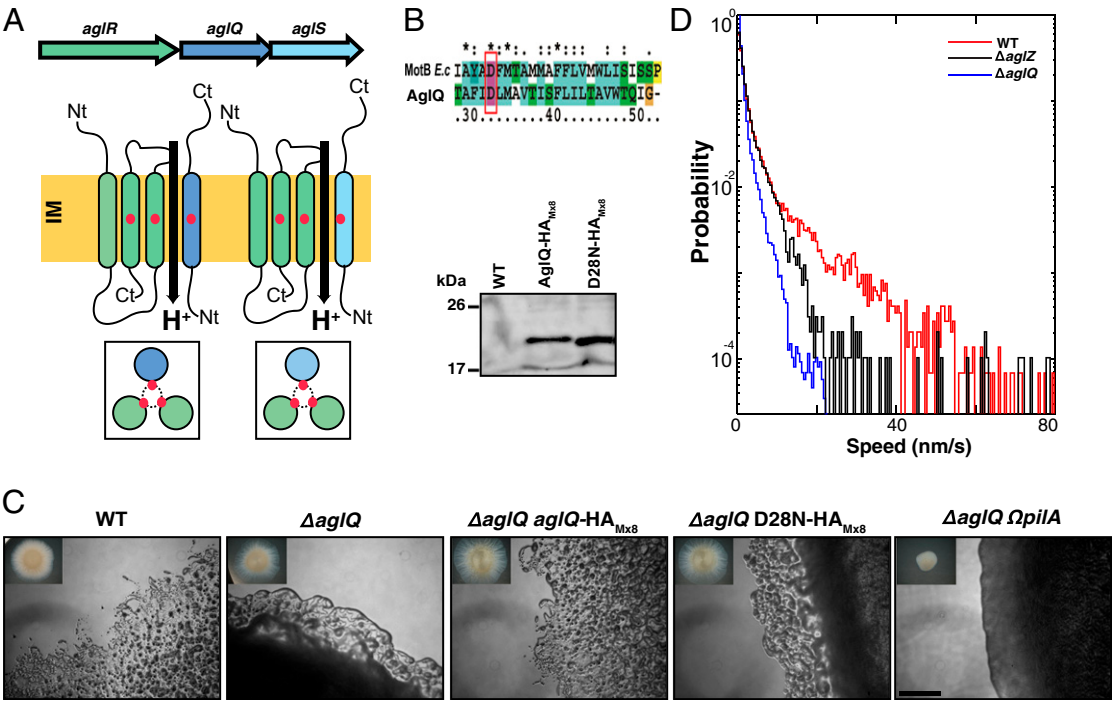

Fig. 3. The *aglRQS* locus encodes a proton-conducting channel essential for gliding motility. (*A*) Proton-conducting channels encoded by the AglRQS proteins. The proposed membrane topologies of the proteins are inspired by work with *Escherichia coli* TolQR. Proton-conducting residues are systematically conserved in AglR, -Q, and -S (red dots). (*Insets*) Top view of the potential heterotrimeric channels. (*B*) Conserved aspartate in the AglQ and *E. coli* MotB channel-forming transmembrane helix. The D28N substitution does not affect the stability of a functional AglQ-HA protein. (*C*) The channel function of AglQ is strictly required for gliding motility. Single-cell gliding motility of *aglQ* mutants cannot be detected at the edges of colonies on hard (1.5%) agar, but motility on soft (0.5%) agar, which detects only S-motility, is intact. As expected a Δ*aglQ* ΩpilA is nonmotile on both substrata. (Scale bar, 1 mm.) (*D*) Histograms of bead gliding speeds on wild-type (red), Δ*aglZ* (black), and Δ*aglQ* (blue) cells. Compared with wild-type cells, gliding motility is perturbed in ΔaglZ cells. However, speeds faster than 30 nm/s are still observed. In contrast, gliding motility in *ΔaglQ* cells is disrupted more severely, with a narrower speed histogram and no events showing speeds faster than 30 nm/s.

fective but still proficient for motility. As does AglZ-YFP, this construct forms a bright polar spot at the leading pole and fixed periodic adhesion complexes that colocalize with AglZ-YFP in gliding cells (Fig. 4 *A* and *C*). The bright spot switches to the new leading pole when cells reverse direction (Fig. 4*B*). In stationary cells, AglQ-mcherry traffics away from the head in dynamic foci that colocalize with AglZ-YFP (Fig. 4*D*). Transport also occurred at a reduced speed compared with the speed measured for AglZ-YFP spots in a wild-type background (1.0 ± 0.5 μm/min vs. 6.0 ± 2.1 μm/min in wild type). Consistent with this interpretation, the velocity of bead trafficking also was reduced in these cells (0.8 ± 0.4 μm/min). The observation that this construct exhibits reduced velocity for both gliding and cytoplasmic transport lends further support to the conclusion that intracellular motion is connected to cell motility. In cells treated with nigericin, AglQ-mCherry foci dispersed rapidly and condensed at the cell pole, similar to the pattern of localization seen in nigericin-treated AglZ-YFP cells (Fig. S1*B*). Finally, an AglQ (D28N)-mCherry fusion also assembled bright fluorescent clusters that remained stationary because of the lack of channel activity (Fig. 4*E* and Fig. S6*B*), confirming that the mutant protein assembles paralyzed motor complexes. Thus, cluster formation and/or maintenance requires an intact pH gradient, whereas cluster motion requires an active AglRQS complex.

To examine further the role of this proton channel in gliding motility, we examined the dynamics of AglZ-YFP in an *aglQ*-deletion strain. On agar, these cells contain a single bright polar spot and several observable periodic foci across the length of the cell. However, the periodic foci are not dynamic and remain fixed, slowly losing fluorescence intensity via photobleaching (Fig. S7). In addition, kymographs do not show any evidence of transport of AglZ in these cells (Fig. 4*F*). That AglZ-YFP still forms midcell clusters in an *aglQ* mutant suggests that the AglRQS system is required for the movement but not for the connection of cytoplasmic proteins such as AglZ and MreB to the substrate. Most interestingly, although the periodic foci remained fixed, the bright polar spot did exhibit reversal dynamics (Fig. 4*F* and Fig. S7). After an average of 6.4 ± 1.4 min ($n = 20$ cells), the bright polar spot switched poles even though cells and the periodic foci remained stationary. This observation strongly suggests that the periodic relocation of polarly localized proteins from one pole to the other, which generates directional reversal, does not require cell motion or a functioning gliding apparatus.

The distributed motor-based model of gliding motility supported by the data presented here requires the global coordination of a number of individual moving proteins to produce directional force and gliding. It is highly likely, therefore, that gliding motility mutants might exhibit a complex set of phenotypes relating to defects in directionality, coordination, and/or core motor function. The role that specific genes play in these different functions can be found by using a combination of the motility assays described here. Moving-bead experiments provide information on the motion of single motor complexes, whereas cell gliding presumably requires a sufficient level of coordination between multiple motor units to produce motion. For example, many previously studied gliding motility genes, such as *aglZ*, can be thought of as purely regulatory, because their disruption can be rescued by deletion of genes upstream in the control pathway, such as *frzCD* (21). Consistent with this concept, the motion of beads bound to the side of *aglZ*-deleted cells is severely perturbed but not completely abolished. In multiple instances in time, *ΔaglZ* cells powered the motion of beads with speeds faster than 30 nm/s, as seen in speed histograms (Fig. 3*D*). However, gliding motility in a *ΔaglQ* background is not restored by a second-site *frz* mutation, and beads on *ΔaglQ* cells show a much more dramatic reduction in the level of movement (Fig. 3*D*).

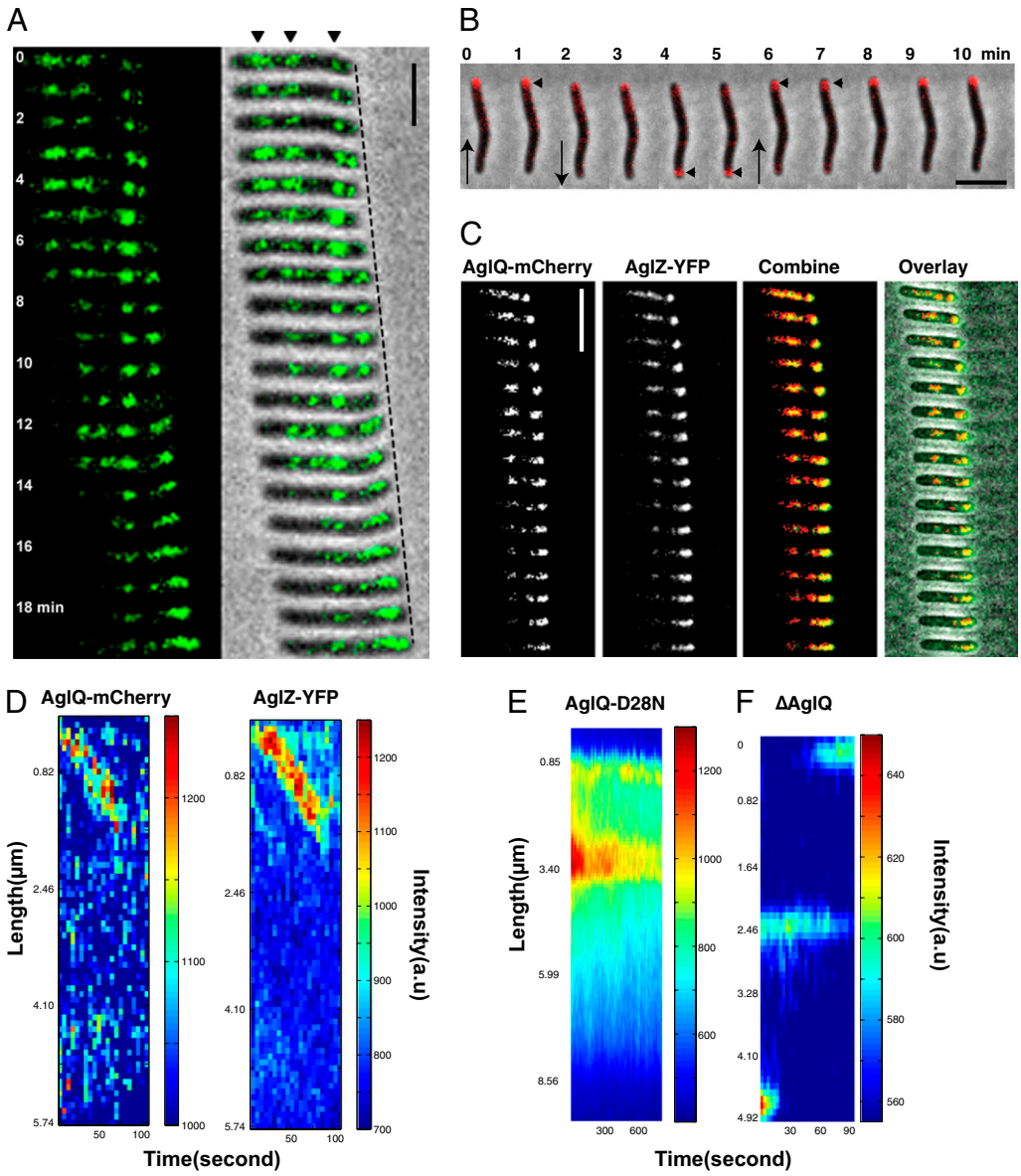

Fig. 4. AglQ is a component of the gliding motility engine. (*A*) AglQ-mCherry localizes to fixed internal clusters in moving cells (black arrowheads). (*B*) AglQ-mCherry oscillates from pole to pole when moving cells reverse. (Scale bar, 2 μm.) (*C*) AglQ-mCherry colocalizes with AglZ-YFP in moving cells. (*D*) Kymographs of AglQ-mCherry (*Left*) and AglZ-YFP (*Right*) fluorescence in an immobilized cell. AglQ-mCherry and AglZ-YFP colocalize and are transported together along the cell from head to tail. (*E*) Kymograph of AglQ(D28N)-mCherry fluorescence in an immobilized cell. (*F*) Kymograph of AglZ-YFP fluorescence in an immobilized cell. The AglZ-YFP clusters retain a fixed position at all times, but directional pole-to-pole oscillation still is observed.

To transmit mechanical forces from the cytoplasmic membrane, where the AglRQS motors lie, to the cell exterior, a mechanical linkage must be established between the inner and outer membranes. In a recent publication, Nan et al. (10) reported observations of MreB-dependant, PMF-driven rotation of the periplasmic protein Adventurous gliding motility protein U (AgmU). The authors also used theoretical modeling to show that PMF-driven motor proteins running along helical tracks might produce gliding motility through a viscous interaction with the substrate that is mediated by AgmU. Our data strongly indicate that the AglRQS complex is the gliding-associated, PMF-driven motor, although a number of important avenues remain to be explored experimentally: How is traction force transduced from AglRQS to the substrate, and does it link directly through AgmU? What are the molecular components of the full transducing complex, and how is force transmitted through the structural cell wall? Are viscous or elastic contributions dominant in the interaction with the substrate?

Here, we show that a widely conserved class of bacterial motors, which includes both the flagellar motor and the gliding motor, can drive intracellular protein transport in bacteria and suggest that gliding motility emerged through the recruitment of these motors. This type of motor-based locomotion is likely to be quite widespread, because externally bound beads also are propelled along the sides of members of the Bacteroidetes phylum, although in those systems the molecular engine remains to be characterized (2). In addition, the existence of intracellular trafficking in bacteria opens up the exciting possibility that transport might be widely used to localize proteins for many other bacterial processes.

Materials and Methods

Bacterial Strains, Plasmids, and Growth. Plasmids were introduced into *M. xanthus* by electroporation. Mutants and transformants were obtained by homologous recombination. Detailed construction schemes of the strains and plasmids and the sequences of all primers are shown in Tables S1–S3.

Measurement of the Effect of Drugs on Cell Gliding. Drug-injection experiments with gliding cells were performed as previously described (22) on A^+S^- cells (Δ*pilA*) to ascertain that the drugs specifically affected gliding motility. Briefly, the injection experiments were conducted in a custom diffusion chamber where cells were immobilized on a thin layer of TPM agar and chemicals reached the cells by diffusion through the agar (22). Injections were performed by a coupled computerized injector system at a flow rate of 10 μL/s. Typically, CCCP (10 μM), valinomycin (40 μM), and nigericin (100 μM) were injected in TPM medium [10 mM Tris (pH 7.6), 8 mM $MgSO_4$, 100 mM KH_2PO_4) containing 10 mM glucose. When effects were detected, reversibility was checked after the diffusion chamber was flushed with TPM-glucose.

Measurement of Membrane Potential, Intracellular ATP Level, and pH. The effect of CCCP, valinomycin, and nigericin on membrane potential was measured with the standard lipophilic cation tetraphenylphosphonium (TPP^+) as described previously (23). Details about the procedure are given in *SI Materials and Methods*.

Intracellular ATP levels were measured at different times after drug addition [100 μM nigericin, 10 μM CCCP, or 50 mM arsenate (47.5 mM sodium arsenate; 2.5 mM potassium arsenate, pH 8.0)] to 10^6 exponentially growing cells with a standard luminescence assay using luciferase ATP-dependent light emission and the ATP Bioluminescence Assay Kit HS II as described by the manufacturer (Roche Applied Bioscience). Bioluminescence expressed in arbitrary units was measured with an Infinite M200 microplate reader from Tecan.

The effects of metabolic poisons on intracellular pH were measured with the dye BCECF-AM (Molecular Probes), a standard pH fluorescent reporter probe (*SI Materials and Methods*).

Coimmunoprecipitation of the AglRQS Complex. Procedures for the preparation of solubilized AglRQS complex, coimmunoprecipitation, and mass spectrometry analysis are provided in *SI Materials and Methods*.

Western Blotting. Western blotting was performed as described previously (13) with 1/1,000 dilutions of anti-HA (Roche) or anti-mCherry (kind gift from V. Géli, Université d'Aix-Marseille, Marseille, France) antisera.

Imaging of Cell Gliding. Time-lapse experiments of gliding motility were performed over TPM agar using an automated and inverted TE2000-E-PFS epifluorescence microscope (Nikon). Details can be found in *SI Materials and Methods*.

Optical Trap. Our optical trap is built on a modified Nikon TE2000 inverted microscope with both differential interference contrast (DIC) and epifluorescence modules. A Nd:YVO4 laser (1,064 nm; Spectra Physics) is used to generate the trapping potential. For position detection, the scattering of an 855-nm diode laser (Bluesky Research) is detected by a position-sensitive detector (Newfocus). The trap and sample are steered using a closed-loop piezo-driven tip-tilt mirror and stage, respectively (Mad City Labs).

Surface Coating for Cell Immobilization. A fluid tunnel slide was formed with a microscope slide and a clean glass coverslip separated by two layers of double-sided tape, and 20 μL agarose DMSO (Sigma Aldrich) solution (0.75% wt/vol) was injected into the fluid tunnel. Ten minutes later the tunnel was washed with 400 μL distilled water, and 20 μL of the overnight cell culture was injected into the tunnel. After 30 min, floating cells were flushed out with 400 μL TPM solution containing 10 mM glucose. For drug treatments, the corresponding drug solution was injected into the tunnel during an experiment.

Bead Preparation. For all bead experiments, we used polystyrene beads 0.5 μm in diameter (Bangs Labs) diluted in TPM solution (0.01% wt/vol). To study the motion of beads on a cell surface, freely floating beads were trapped in solution and then were stuck gently on the top of immobilized cells.

Kymograph Analysis and Bead Tracking. For kymograph analysis and bead tracking, images were taken every 10 s using the modified Nikon TE2000 inverted microscope with a 100×/1.49 oil immersion objective lens (Nikon) and a CCD camera (Andor Technology). A laser-based, 3D feedback method was used to overcome drift of the microscope focus during time-lapse imaging by monitoring the forward scattered light pattern of the 855-nm detection laser sent through a coverslip-bound polystyrene bead 0.5 μm in diameter (Bangs Labs). The output of the position-sensitive detector (PSD) was held constant by adjusting the position of the 3D closed-loop piezo-driven stage (Mad City Labs) using a modified proportional–integral–derivative (PID) algorithm. Custom software written in Matlab was used to construct the kymograph and to track bead motion (*SI Materials and Methods*).

Construction of the Speed and Fluorescence Intensity Histograms. The time-dependent position of a bead was smoothed with a second-order Savitzky–Golay filter with a fixed window size of 25 s and differentiated to obtain the instantaneous velocity. The absolute value of the instantaneous velocity was used to construct the speed histogram. For fluorescence intensity histograms, fluorescence intensity was normalized by the average intensity from each cell. The area under the curve was normalized to 1 to create a normalized histogram.

All errors are SDs unless otherwise specified. For measured fractions, f, the SD is calculated using the binomial distribution $SD = \sqrt{\frac{f(1-f)}{N}}$.

ACKNOWLEDGMENTS. We thank Vincent Géli for the gift of the α-mCherry antiserum and Zhaomin Yang for pBJΔpilA. We also thank Thierry Doan, Romé Voulhoux, and Gérard Michel for advice on detergents and membrane preparations; Adrien Ducret for help with pH measurements; Adrien Ducret, Yi Deng, and Gordon Berman provided help with data processing and valuable discussions, and Adèle Sanràn-Cune for critical reading of the manuscript. We acknowledge the assistance of David H. Perlman in the Princeton Mass Spectrometry Center, which is supported by National Institutes of Health Grant P50GM071508. This work was funded by a joint Human Frontier Science Program Young Investigators Award (RGY0075/2008) (to T.M. and J.W.S.). M.W. is supported by a Ministere de l'Education Nationale de la Recherche et de Technologie thesis fellowship.

1. Mignot T, Shaevitz JW (2008) Active and passive mechanisms of intracellular transport and localization in bacteria. *Curr Opin Microbiol* 11:580–585.
2. Jarrell KF, McBride MJ (2008) The surprisingly diverse ways that prokaryotes move. *Nat Rev Microbiol* 6:466–476.
3. Mignot T, Kirby JR (2008) Genetic circuitry controlling motility behaviors of *Myxococcus xanthus*. *Bioessays* 30:733–743.
4. Mignot T, Merlie JP, Jr., Zusman DR (2005) Regulated pole-to-pole oscillations of a bacterial gliding motility protein. *Science* 310:855–857.
5. Mignot T (2007) The elusive engine in *Myxococcus xanthus* gliding motility. *Cell Mol Life Sci* 64:2733–2745.
6. Leonardy S, Freymark G, Hebener S, Ellehauge E, Søgaard-Andersen L (2007) Coupling of protein localization and cell movements by a dynamically localized response regulator in *Myxococcus xanthus*. *EMBO J* 26:4433–4444.
7. Zhang Y, Franco M, Ducret A, Mignot T (2010) A bacterial Ras-like small GTP-binding protein and its cognate GAP establish a dynamic spatial polarity axis to control directed motility. *PLoS Biol* 8:e1000430.
8. Leonardy S, et al. (2010) Regulation of dynamic polarity switching in bacteria by a Ras-like G-protein and its cognate GAP. *EMBO J* 29:2276–2289.
9. Lapidus IR, Berg HC (1982) Gliding motility of *Cytophaga* sp. strain U67. *J Bacteriol* 151:384–398.
10. Nan B, et al. (2011) Myxobacteria gliding motility requires cytoskeleton rotation powered by proton motive force. *Proc Natl Acad Sci USA* 108:2498–2503.
11. Wolgemuth C, Hoiczyk E, Kaiser D, Oster G (2002) How myxobacteria glide. *Curr Biol* 12:369–377.
12. Kaiser D (2009) Are there lateral as well as polar engines for A-motile gliding in myxobacteria? *J Bacteriol* 191:5336–5341.
13. Mignot T, Shaevitz JW, Hartzell PL, Zusman DR (2007) Evidence that focal adhesion complexes power bacterial gliding motility. *Science* 315:853–856.
14. Pate JL, Chang L-YE (1979) Evidence that gliding motility in procaryotic cells is driven by rotary assemblies in the cell envelopes. *Curr Microbiol* 2:59–64.
15. Pogliano J, Pogliano K, Weiss DS, Losick R, Beckwith J (1997) Inactivation of FtsI inhibits constriction of the FtsZ cytokinetic ring and delays the assembly of FtsZ rings at potential division sites. *Proc Natl Acad Sci USA* 94:559–564.
16. Mauriello EM, et al. (2010) Bacterial motility complexes require the actin-like protein, MreB and the Ras homologue, MglA. *EMBO J* 29:315–326.
17. Youderian P, Burke N, White DJ, Hartzell PL (2003) Identification of genes required for adventurous gliding motility in *Myxococcus xanthus* with the transposable element mariner. *Mol Microbiol* 49:555–570.
18. Zhou J, et al. (1998) Function of protonatable residues in the flagellar motor of *Escherichia coli*: A critical role for Asp 32 of MotB. *J Bacteriol* 180:2729–2735.
19. Nan BY, Mauriello EMF, Sun IH, Wong A, Zusman DR (2010) A multi-protein complex from *Myxococcus xanthus* required for bacterial gliding motility. *Mol Microbiol* 76:1539–1554.
20. Goemaere EL, Cascales E, Lloubès R (2007) Mutational analyses define helix organization and key residues of a bacterial membrane energy-transducing complex. *J Mol Biol* 366: 1424–1436.
21. Mauriello EM, Nan B, Zusman DR (2009) AglZ regulates adventurous (A-) motility in *Myxococcus xanthus* through its interaction with the cytoplasmic receptor, FrzCD. *Mol Microbiol* 72:964–977.
22. Ducret A, et al. (2009) A microscope automated fluidic system to study bacterial processes in real time. *PLoS ONE* 4:e7282.
23. Cascales E, Christie PJ (2004) Agrobacterium VirB10, an ATP energy sensor required for type IV secretion. *Proc Natl Acad Sci USA* 101:17228–17233.

Supporting Information

Sun et al. 10.1073/pnas.1101101108

SI Materials and Methods

Bacterial Strains, Plasmids, and Growth. Plasmids were introduced into *Myxococcus xanthus* by electroporation. Mutants and transformants were obtained by homologous recombination. Complementation, expression of the fusion, and mutant proteins were all obtained after ectopic integration of the genes of interest at the Mx8-phage attachment site in appropriate deletion backgrounds (1). Integration at $Mx8_{att}$ has no effect on cell motility (1, 2).

For phenotypic assays, cells (10 μL) at a concentration of 4×10^9 cfu/mL were spotted on charcoal yeast extract (CYE) plates containing an agar concentration of either 0.5% [favoring twitching (S) motility] or 1.5% [supporting both gliding (A) and twitching motility], incubated at 32 °C, and photographed after 48 h with an Olympus SZ61 binocular or a Nikon Eclipse (model TE2000E) microscope.

Preparation of Solubilized AglRQS Complex. A midexponential phase, a culture of wild type or the AglQ-HA–expressing strain grown in 1L CYE medium was harvested, washed, resuspended in 25 mL lysis buffer [50 mM NaCl, 1 mM EDTA, 200 μg/mL lysozyme, 20 mM Tris-HCl (pH 7.5), 500 U Benzonase, and 10 mM PMSF) and lysed using a French pressure cell press. Cell debris was removed by slow-speed centrifugation. Ultracentrifugation (1 h at 10,0000 × *g*) then was used to pellet the cell membrane containing the AglRQS proteins, and the supernatant corresponding to the soluble fraction was discarded. The membrane pellet was resuspended in 2 mL lysis buffer (without lysozyme) and homogenized with a Potter–Elvehjem homogenizer. Membranes then were solubilized gently with 1% dodecyl maltoside (DDM) for 1 h at 4 °C. Solubilized membranes were ultracentrifuged again, and the soluble fraction containing the solubilized protein complex was subjected to the coimmunoprecipitation procedure.

Coimmunoprecipitation of the AglRQS Complex. Solubilized membranes were mixed with 100 μL anti-HA affinity matrix (Roche) and incubated at 4 °C for 1 h. The beads were washed repeatedly in Y-Buffer [50 mM NaCl, 1 mM EDTA, 20 mM Tris-HCl (pH 7.5)] containing decreasing amounts of DDM (1–0.1%). After washing, the beads were resuspended directly in 100 μL of Laemmli buffer and boiled at 100 °C for 10 min. Eluates were analyzed by SDS/PAGE and stained with Sypro-Ruby (Bio-Rad). As a control, protein lysates from the nontransformed *M. xanthus* wild-type strain were prepared following the same procedure (membrane solubilization and coimmunoprecipitation).

Mass Spectrometry and Data Analysis. After SDS-PAGE and staining of protein lysates from the AglQ-HA fusion protein constructs (wild type or D28N mutant) and nontransformed control, lanes were excised and subjected to antigen retrieval by heating, disulfide reduction, and alkylation with iodoacetamide, in-gel trypsin digestion, and peptide elution (3). Peptides were desalted using microscale reversed-phase chromatography and then were subjected to reversed-phase nano-liquid chromatography (LC)-MS and MS/MS performed on a 2D nano-flow capillary HPLCy system (Eksigent) coupled to an LTQ-Orbitrap hybrid mass spectrometer (ThermoFisher Scientific). Sample concentration and desalting were performed online using a trapping column (180 μm × *ca*. 20 mm) packed with 5 μm 100 Å Magic AQ C18 material (Michrom) at a flow rate of 7 μL/min for 2 min. Separation was achieved using an analytical capillary column (100 μm × *ca*. 100 mm) packed with 3 μm 100 Å Magic AQ C18 material (Michrom) terminating in a pulled sprayer tip, under a linear gradient of buffers A [3% acetonitrile (ACN)/0.1% formic acid (FA)] and B [97% ACN/ 0.1% FA] over 70 min at a flow rate of ~0.5 μL/min. Electrospray ionization was carried out at 2.5 kV, with the LTQ heated capillary set to 200 °C. Full-scan mass spectra were acquired in the Orbitrap in the positive-ion mode over the range *m*/*z* 300–2000 at a resolution of 60,000. Mass accuracy after internal calibration typically was within 2–3 ppm. Simultaneously, MS/MS was acquired using the LTQ for the seven most abundant, multiply charged species in the mass spectrum with signal intensities of >1,000 nL. MS/MS collision energies were set at 35%. Dynamic exclusion was set so that MS/MS for each species was acquired a maximum of once over a period of 120 s. All spectra were recorded in profile mode for further processing and analysis. Xcalibur software (ThermoFisher Scientific) was used for MS and MS/MS data analysis. Peptide and protein assignments were conducted using Mascot (Matrix Science) to search against the *M. xanthus* species subset of the Trembl database, using a error window of 8 ppm on the precursor ions and 1.2 Da on the fragment ions. Fixed modifications were set to include carbamidomethylation of cysteine; variable modifications were set to include oxidation of methionine. Scaffold software (Proteome Software) was used to collate and coalesce database search results.

Kymograph Analysis and Bead Tracking. We used custom software written in Matlab to construct the kymograph. The user selected a region of interest (ROI) that included only one cell image. A 2D matrix then was formed from the intensity profiles along the middle line (axial direction) of the cell image from a time-sequence stack. The 2D matrix was displayed as a pseudocolored image to form the kymograph.

For bead tracking, the original image (ROI) was preprocessed to get uniform background. Next, the mean intensity of the image was subtracted from the image. Then, the image was inverted, and the mean intensity of the inverted image was subtracted. The two subtracted images were added together to form the final image. In this way, the contour and contrast of the cell were greatly enhanced. The final image was segmented with a clustering (*k*-means) algorithm by assuming three clusters, which correspond to the bead (brightest cluster), the cell (second-brightest cluster), and the background (darkest cluster). The areas of the bead and cell were used as secondary criteria to eliminate false segments. The centroids of the segmented cell and bead then were calculated. The movement of the bead relative to the cell was recorded to compensate for any drift of the cell relative to the imaging optics.

Measurement of the Membrane Potential, Intracellular ATP Level, and pH. Typically, *M. xanthus* cells were grown in CYE to $OD_{0.5}$, and each drug was added at the appropriate concentration for 15 min at 32 °C. Then 1 mL of each suspension was centrifuged, and the cell pellets were concentrated 50-fold in 100 mM Tris HCl (pH 7.8) and 1 mM EDTA. After 3-min incubation at 32 °C, each suspension was diluted 20-fold in 100 mM NaPi (pH 7.5), 1 mM KCl, and 0.4% glycerol and was equilibrated at 32 °C for 15 min. ^{3}H-TPP$^+$ was added to the suspension at 10 μM (70,000 cpm) and incubated for 1 h at 32 °C. Incorporated radioactivity in 100 μL of the cell suspension was measured directly on filters after three washes in 100 mM NaPi (pH 7.8) with a Beckman Coulter scintillation counter. Under these conditions (pH 7.8), we determined that $\Delta pH = 0$; thus the proton motive force (PMF) equals the membrane potential (PMF = $\Delta\psi$). The membrane

potential then was calculated using the Nernst equation as previously described (4).

To measure changes in intracellular pH, cells were grown to midexponential phase and mixed with BCEF-AM (0.5 mM, Molecular Probes) before they were transferred to a standard TPM-agar pad (pH 6) on a microscope slide. Nigericin, valinomycin, and carbonyl cyanide-m-chlorophenylhydrazone (CCCP) were injected at appropriate concentrations directly on the microscope. All fluorescence images were captured with a 480-nm excitation filter but with two different emission filters (535 and 610 nm) to monitor changes in intracellular pH. Intracellular pH variations were quantified by calculating R = fluorescence λ535 nm/fluorescence λ610 nm. Emission of BCECF (Molecular Probes) at λ535 nm decreases with intracellular pH; thus any drug that collapses the pH gradient is expected to decrease R, because the pH of the surrounding medium is acidic (pH 6) and the initial intracellular pH is 7.8.

Imaging of Cell Gliding. The microscope was equipped with a "Perfect Focus System" (PFS) that automatically maintains focus so that the point of interest within a specimen is in sharp focus at all times, despite any mechanical or thermal perturbations. Images were recorded with a CoolSNAP HQ 2 (Roper Scientific,) and a 40×/0.75 DLL Plan-Apochromat or a 100×/1.4 DLL objective. All fluorescence images were acquired with a minimal exposure time to minimize bleaching and phototoxicity effects. Before any image processing, phase-contrast or fluorescent gray-scale images used for segmentation were equalized to reduce fluctuations in background noise. Cell tracking was performed automatically. When appropriate to correct tracking errors, manual measurements also were performed with tools built into the software. Images were processed under both ImageJ 1.40g (National Institutes of Health) and MetaMorph.

1. Leonardy S, Freymark G, Hebener S, Ellehauge E, Søgaard-Andersen L (2007) Coupling of protein localization and cell movements by a dynamically localized response regulator in *Myxococcus xanthus*. *EMBO J* 26:4433–4444.
2. Mignot T, Shaevitz JW, Hartzell PL, Zusman DR (2007) Evidence that focal adhesion complexes power bacterial gliding motility. *Science* 315:853–856.
3. Shevchenko A, Tomas H, Havlis J, Olsen JV, Mann M (2006) In-gel digestion for mass spectrometric characterization of proteins and proteomes. *Nat Protoc* 1:2856–2860.
4. Cascales E, Christie PJ (2004) Agrobacterium VirB10, an ATP energy sensor required for type IV secretion. *Proc Natl Acad Sci USA* 101:17228–17233.

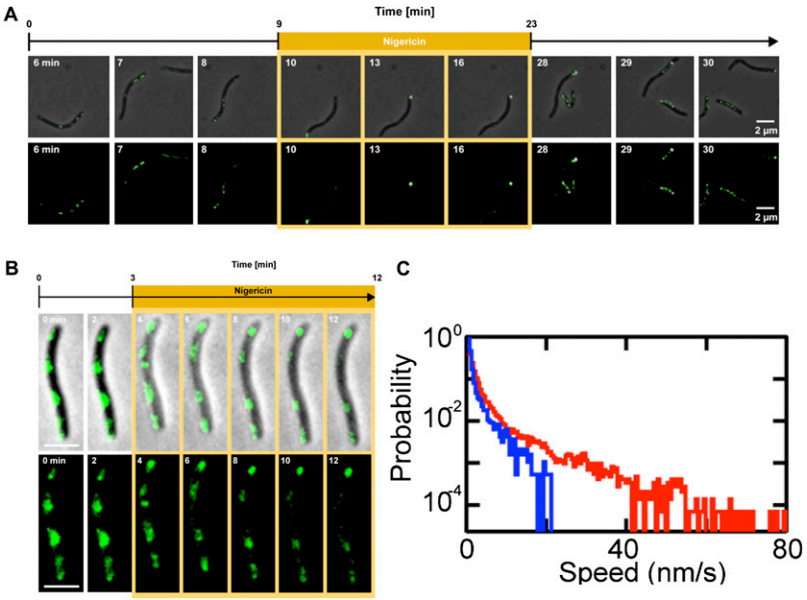

Fig. S1. (*A*) Addition of nigericin (100 μM) rapidly blocks movement and disperses the AglZ-YFP clusters. After washing, movement is resumed coincidently with the reappearance of AglZ-YFP internal clusters. (*B*) Nigericin disperses the AglQ-mCherry clusters. Note the condensation of a polar cluster upon nigericin treatment. (Scale bar, 2 μm.) (*C*) Addition of A22 (50 μg/mL) significantly decreases bead gliding speed (blue) as compared with the speed on nontreated cells (red).

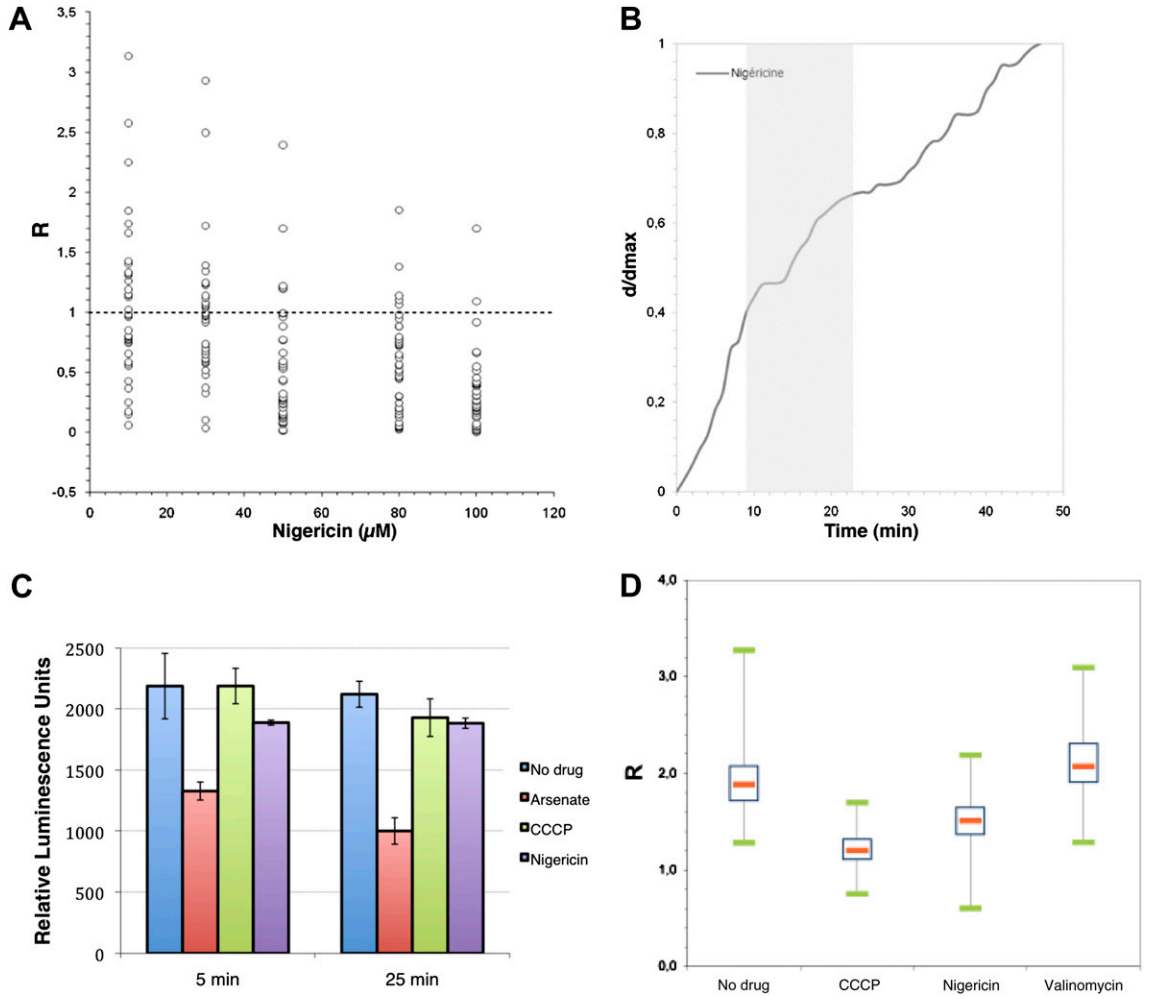

Fig. S2. (*A*) Nigericin affects A motility in a dose-dependent manner. The ratios of the velocity of the cells after treatment with various concentrations of nigericin to the velocity of the cells before treatment (*R*) were calculated (n = 40 cells). (*B*) Nigericin does not affect type IV pilus-dependent S motility. To measure S motility, GFP-labeled cells were mixed at a 1:10 ratio with an A^-S^+ mutant (*aglQ*), and fluorescent cells were tracked within the nonfluorescent population. The d/dmax ratio of a representative cell is shown over time and during nigericin (100 μM) injection. (*C*) Effects of nigericin (100 μM) and CCCP (10 μM) on the intracellular ATP pools. The intracellular ATP levels remain high even after 25 min of nigericin or CCCP treatment. In contrast, arsenate, known to inhibit ATP recycling (1), rapidly affects the ATP intracellular pools. (*D*) After injection of CCCP, nigericin, and valinomycin, changes in intracellular pH were monitored using BCEF. Shown are boxplots of *R* values for calculated for 200 cells in each condition (*Materials and Methods*).

1. Jaffe JD, Miyata M, Berg HC (2004) Energetics of gliding motility in *Mycoplasma mobile*. *J Bacteriol* 186:4254–4261.

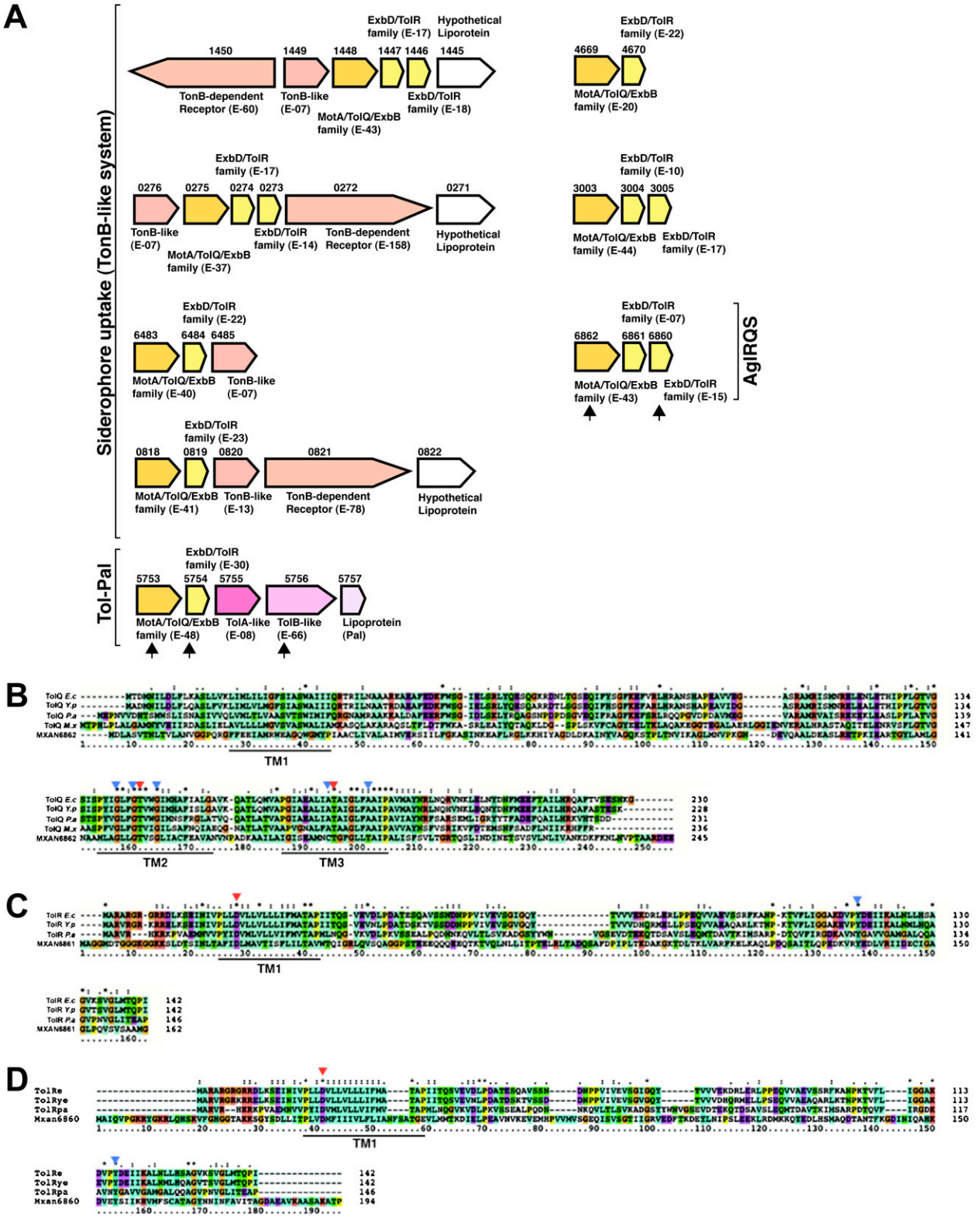

Fig. S3. (*A*) The *Myxococcus* genome contains eight loci carrying genes encoding Tol/Exb/Mot. Four clusters encode TonB-like systems involved in iron siderophore transport (1) and thus were discarded for this analysis. Transposon insertions known to disrupt A motility are shown (black arrows). Three insertions were found in a cluster encoding a complete Tol-Pal system. However, Tol-Pal also is required for S motility (2). In fact, Tol-Pal is involved in membrane integrity, cell division, and protein localization in all systems studied so far (3–5); thus the effects on motility probably are indirect. Blast E values are shown for each predicted gene. (*B–D*) Multiple sequence alignment of AglR, AglQ,. and AglS with TolQ (*B*) and TolR (*C* and *D*) from canonical Tol-Pal systems (Ec: *Escherichia coli*; Yp: *Yersinia pseudotuberculosis*; Ye: *Yersinia enteroccolitica*; Pa: *Pseudomonas aeruginosa*). The critical transmembrane helices are conserved

Legend continued on following page

in all AglRQS proteins. Blue arrows indicate critical residues for channel assembly in *E. coli* TolQ. Note that some of these residues are missing in AglR. Red arrows indicate residues that are essential for proton conductance in *E. coli* TolQR. All these residues are systematically conserved in AglR, -Q, and -S.

1. Postle K, Kadner RJ (2003) Touch and go: tying TonB to transport. *Mol Microbiol* 49:869–882.
2. Youderian P, Burke N, White DJ, Hartzell PL (2003) Identification of genes required for adventurous gliding motility in *Myxococcus xanthus* with the transposable element mariner. *Mol Microbiol* 49:555–570.
3. Lloubès R, et al. (2001) The Tol-Pal proteins of the *Escherichia coli* cell envelope: An energized system required for outer membrane integrity? *Res Microbiol* 152:523–529.
4. Gerding MA, Ogata Y, Pecora ND, Niki H, de Boer PA (2007) The trans-envelope Tol-Pal complex is part of the cell division machinery and required for proper outer-membrane invagination during cell constriction in *E. coli*. *Mol Microbiol* 63:1008–1025.
5. Yeh YC, Comolli LR, Downing KH, Shapiro L, McAdams HH (2010) The caulobacter Tol-Pal complex is essential for outer membrane integrity and the positioning of a polar localization factor. *J Bacteriol* 192:4847–4858.

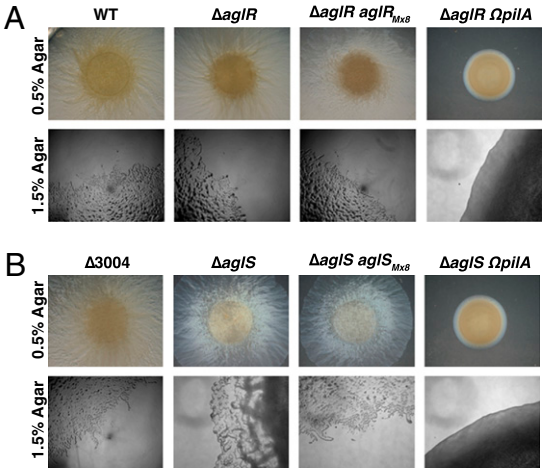

Fig. S4. Both *aglR* and *aglS* are essential for gliding motility. Hard and soft agar motility assays showing motility defects of the *aglR* (*A*) and *aglS* (*B*) deletion mutants. For both mutants, single motile cells are not detected at the colony edges, and combined *pilA* disruption results in complete loss of motility. Both *aglR and aglS* defects are fully complemented when *aglR and aglS* are expressed ectopically from the Mx8 phage attachment site, confirming their respective roles in gliding motility.

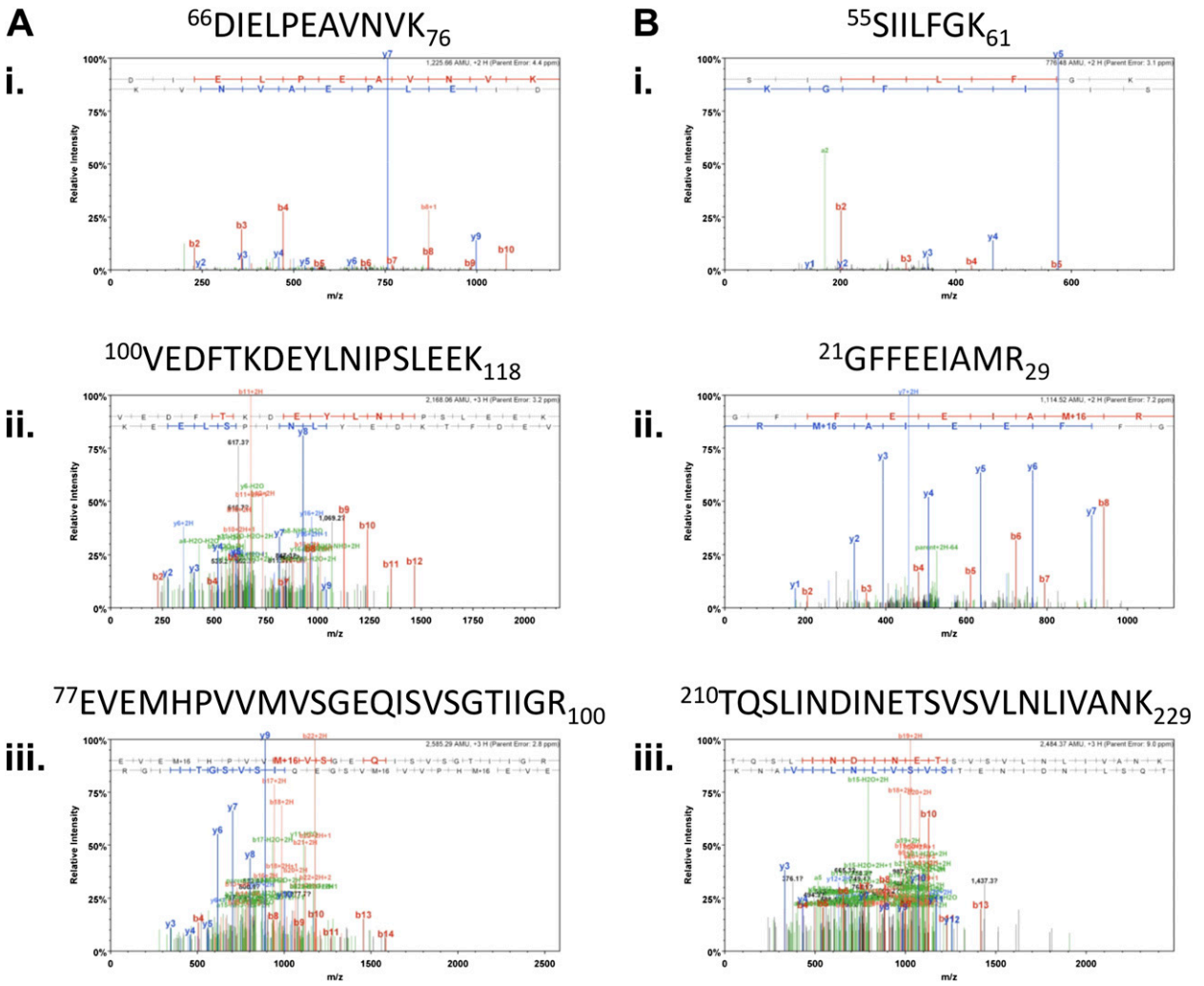

Fig. S5. AglR, -Q, and -S form a complex. Mass spectra from LC-MS of peptides derived from SDS/PAGE analysis of proteins associated with immunoprecipitated AglQ-HA fusion proteins. Prominent detected ions in the spectra are annotated with the theoretical fragment ions of the peptides to which they were assigned by Mascot. Peptide sequences are shown above the spectra. (*A*) Peptides assigned to AglR are (*i*) 66–76, detected as an $[M+2H]^{2+}$ ion at *m/z* 613.8378; (*ii*)100–118, detected as an $[M+^{3}H]^{3+}$ ion at *m/z* 723.6939; and (*iii*) 77–100, detected as an $[M+^{3}H]^{3+}$ ion at *m/z* 862.7707; Mascot scores are 38, 31, and 41, respectively. (*B*) Peptides assigned to AglR are (*i*) 55–61, detected as an $[M+2H]^{2+}$ ion at *m/z* 389.2484; (*ii*) 21–29, detected as an $[M+2H]^{2+}$ ion at *m/z* 558.2672; and (*iii*) 210–229, detected as an $[M+^{3}H]^{3+}$ ion at *m/z* 829.1293; Mascot scores are 19, 53, and 36, respectively. Peptide scores correspond to expectation values <0.05. Consequently, both proteins were assigned a Scaffold confidence score of 100% with no grouping ambiguity.

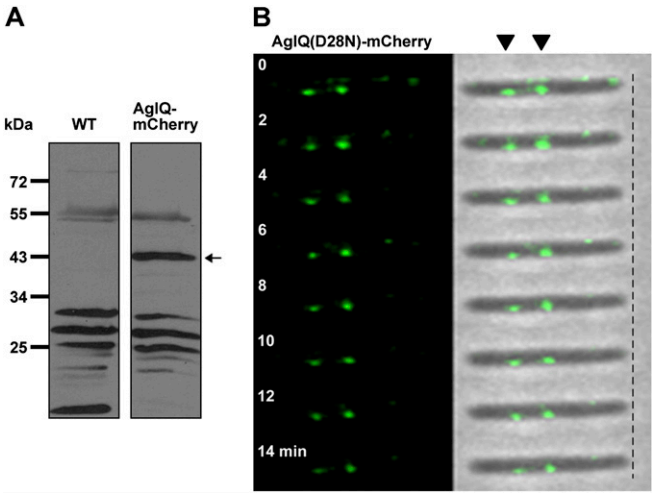

Fig. S6. (*A*) AglQ-mCherry was expressed from its natural promoter at the Mx8 phage attachment site in the AglQ mutant. The chimeric protein promotes motility, albeit at reduced velocities. Western immunoblot using an anti-mCherry antiserum show stable expression of a specific species of expected size. (*B*) AglQ(D28N)-mCherry assembles clusters that are not dynamic.

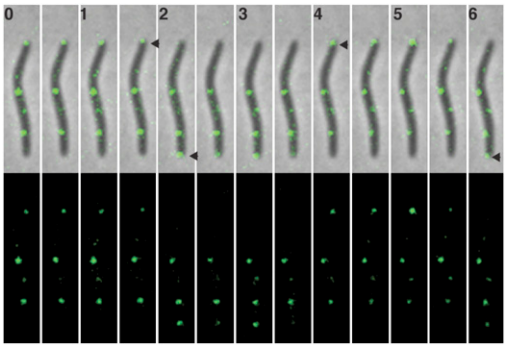

Fig. S7. Localization of AglZ-YFP in an *aglQ* mutant. The AglZ-YFP clusters retain a fixed position at all times, but directional pole-to-pole oscillation still is observed (black arrows). Time is indicated in minutes.

Table S1. Plasmids and strains used in this study

Plasmid or strain	Description	Source
Plasmid		
pBJ114	Used to create deletions, *galK*, KmR	Laboratory collection
pSWU19	KmR used to integrate genes ectopically at mx8att	Laboratory collection
pSWU30	TetR used to integrate genes ectopically at mx8att	Laboratory collection
pBJΔpilA	pBJ114 allowing deletion of *pilA*	Z. Yang
pBJΔaglQ	pBJ114 allowing deletion of *aglQ*	This work
pBJAglZY	pBJ114 with a cassette allowing construction of the *aglZ-YFP* chimeric gene	Laboratory collection
pSWU19aglQHA	pSWU19 allowing expression of *aglQ-HA* from it own promoter at $mx8_{att}$	This work
pSWU19D28NHA	pSWU19 allowing expression of *aglQD28N-HA* from it own promoter at $mx8_{att}$	This work
pSWU19aglQCh	pSWU19 allowing expression of *aglQ-mCherry* from it own promoter at $mx8_{att}$	This work
pSWU30aglQCh	pSWU30 allowing expression of *aglQ-mCherry* from it own promoter at $mx8_{att}$	This work
pSWU19D28NC	pSWU19 allowing expression of $aglQ_{D28N}$-*mCherry* from it own promoter at $mx8_{att}$	This work
pBJΔaglR	pBJ114 allowing deletion of *aglR*	This work
pBJΔaglS	pBJ114 allowing deletion of *aglS*	This work
pSWU30aglR	pSWU30 allowing expression of *aglR* from it own promoter at $mx8_{att}$	This work
pSWU30aglS	pSWU30 allowing expression of *aglS* from it own promoter at $mx8_{att}$	This work
pBJΔ3004	pBJ114 allowing deletion of MXAN3004	This work
Strain	Construction and genotype	
DZ2	Wild type	Laboratory collection
TM9	DZ2 *aglZYFP; aglZ-YFP*	Laboratory collection
TM146	DZ2 Δ*aglQ* (pBJΔaglQ); Δ*aglQ*	This work
TM156	DZ2 *pilA::tet;* Ω*pilA*	This work
TM163	TM146 *aglZYFP* (pBJAglZY); Δ*aglQ aglZ-YFP*	This work
TM251	TM146 *mx8att::aglQHA* (pSWU19aglQHA); Δ*aglQ aglQ-HA*	This work
TM255	TM146 *pilA::tet;* Δ*aglQ* Ω*pilA*	This work
TM295	TM146 *frzE::tn5Ω226;* Δ*aglQ* Ω*frzE*	This work
TM312	TM146 *mx8att::aglQD28NHA* (pSWU19D28NHA); Δ*aglQ aglQD28N-HA*	This work
TM333	TM146 *mx8att::aglQmCherry* (pSWU19aglQCh); Δ*aglQ aglQ-mCherry*	This work
TM348	TM146 *mx8att::aglQmCherry* (pSWU30aglQCh); Δ*aglQ aglQ-mCherry*	This work
TM337	TM255 *mx8att::aglQmCherry* (pSWU19aglQCh); Ω*pilA* Δ*aglQ aglQ-mCherry*	This work
TM340	TM163 *mx8att::aglQmCherry* (pSWU30aglQCh); *aglZYFP* Δ*aglQ aglQ-mCherry*	This work
TM364	TM255 *mx8att::*$aglQ_{D28N}$*mCherry* (pSWU19D28NCh); Δ*aglQ* $aglQ_{D28N}$-*mCherry* Ω*pilA*	This work
TM384	DZ2 Δ*aglR* (pBJΔaglR); Δ*aglR*	This work
TM449	TM384 Δ*pilA* (pBJΔpilA); Δ*aglR* Δ*pilA*	This work
TM452	DZ2 Δ*aglS* (pBJΔaglS); Δ*aglS*	This work
TM450	TM384 *mx8att::aglR* (pSWU30aglR); Δ*aglR aglR*	This work
TM455	TM452 *mx8att::aglS* (pSWU30aglS); Δ*aglS aglS*	This work
TM454	TM452 *pilA::tet;* Δ*aglS* Ω*pilA*	This work
TM363	DZ2 ΔMXAN3004 (pBJΔ3004); ΔMXAN3004	This work

Table S2. Primers

Name	Sequences of primers (5′–3′)
Δ6861–1	AAAGAATTCAATTCCTGTGAGATTTCAGCACTTAAC
Δ6861–2	AAAGGATCCGGCGTTCTTCTCCTTCGGC
Δ6861–3	AAAGGATCCCCGCCCAAGGAGCTCACG
Δ6861–4	TTTAAGCTTCCGCCAGCTTCGTGCC
AglR-3	CGGGATCCGAAGTCCTTCGGGAACCCG
AglR-7	CCCAAGCTTTTAAGCGTAGTCTGGGACGTCGTATGGGTAGCCCATCGCCGCGGACA
AglR-5	GATGAATGCCGTGAGGTTGATGG
AglR-9	CTCACGGCATTCATCAACCTGATGGCGGTGACCATCAG
6861-mCherry-1	GCCCATCGCCGCGGACAC
6861-mCherry-2	GTCCGCGGCGATGGGCGTGAGCAAGGGCGAGGAG
6861-mCherry-3	CCCAAGCTTTTACTTGTACAGCTCGTCCATG
D6862-5	GGAATTCAATCAGCTCCGCCAGGGAC
D6862-6	CGGGATCCCGAGTGTTGCCTCCACAG
D6862-7	CGGGATCCGAAGTCCTTCGGGAACCC
D6862-8	CCCAAGCTTGAGCTTCTCCTCCAGCGACG
D6860-5	GGAATTCAGACGCCGAAGATCGAGGC
D6860-6	CGGGATCCGACGTGTCGTGAGCTCCTTG
D6860-7	CGGGATCCCTTCCAGGTGATTGGGCCTTG
D6860-8	CCCAAGCTTATGAAGGGCTCGCGCTCC
D3004-1	CCGAATTCGCGAAATCACCGAGCAGC
D3004-2	CCGGGAGTAGTGGAACGCC
D3004-3	TTCCACTACTCCCGGACCCTGGGAGCCATCTGAG
D3004-4	CCAAGCTTGATCCTCAGCGCCAACGAG
CgmoA-1	CGGGATCCGAATCCGGCCTTAACACGCG
CgmoA-2	CCCAAGCTTGGCGTTCTTCTCCTTCGGC
CgmoC-1	GAGCTCCTTGGGCGGCGAGTGTTGCCTCCACAGGC
CgmoC-2	CCGCCCAAGGAGCTCAC
CgmoC-3	CCCAAGCTTTCCATCGAGGTCGAAGATG

Table S3. Plasmid construction schemes

Plasmid	Construction scheme*
pBJΔaglQ	Primer pairs Δ6861–1/Δ6861–2 and Δ6861–3/Δ6861–4 were used to amplify a 1-kb fragment upstream and downstream of the *aglQ* ORF. First the upstream fragment was cloned at the EcoRI and BamHI sites of pBJ114. Then the downstream fragment was ligated at the BamHI and HindIII sites of the pBJ114-upstream fragment.
pSWU19aglQHA	A fragment encompassing *aglQ* and the *aglQ* promoter region was amplified from the DZ2 chromosome with primers AglR-3/AglR-7 and cloned at the BamHI and *Hin*dIIII sites of pSWU19.
pSWU19D28NHA	A *aglQ(D28N)HA* allele was generated by splicing by overlapping extension (SOE) PCR fusing a fragment amplified from primers AglR-3/AglR-5 to a fragment amplified from AglR-9/AglR-7 using the DZ2 chromosome as a template. The resulting fragment then was ligated to the BamHI and *Hind*IIII sites of pSWU19.
pSWU19aglQCh	Primers AglR-3/6861-mCherry-1 were used to amplify a *aglQ* fragment and its promoter region from the DZ2 chromosome. Primers 6861-mCherry-2/6861-mCherry-3 were used to amplify the *mcherry* fragment from a plasmid containing the *mcherry* gene. Both fragments were fused by SOE-PCR and cloned at the BamHI and HindIII sites of pSWU19.
pSWU30aglQCh	Primers AglR-3/6861-mCherry-1 were used to amplify the *aglQ* fragment and its promoter from the DZ2 chromosome. Primers 6861-mCherry-2/6861-mCherry-3 were used to amplify the fragment *mcherry* from a plasmid containing the *mcherry* gene. Both fragments were fused by SOE-PCR and cloned at the BamHI and *Hind*III sites of pSWU30.
pSWU19D28NC	A *aglQ-D28N-mCherry* allele was generated by SOE PCR fusing a fragment amplified from primers AglR-3/AglR-5 to a fragment amplified from AglR-9/6861-mCherry-1 using the DZ2 chromosome as a template. The resulting fragment then was fused to a third fragment amplified from primers 6861-mCherry-2/6861-mCherry-3 using a plasmid containing the *mcherry* gene as a template. The resulting fragment then was ligated to the BamHI and *Hin*dIIII sites of pSWU19.
pBJΔaglR	Primer pairs D6862-5/D6862-6 and D6862-7/D6862-8 were used to amplify a 1-kb fragment upstream and downstream from the *aglR* ORF. First the upstream fragment was cloned at the EcoRI and BamHI sites of pBJ114. Then the downstream fragment was ligated at the BamHI and HindIII sites of the pBJ114-upstream fragment.
pBJΔaglS	Primer pairs D6860-5/D6860-6 and D6860-7/D6860-8 were used to amplify a 1-kb fragment upstream and downstream from the *aglS* ORF. First the upstream fragment was cloned at the EcoRI and BamHI sites of pBJ114. Then the downstream fragment was ligated at the BamHI and HindIII sites of the pBJ114-upstream fragment
pSWU30aglR	A fragment encompassing *aglR* and the *aglR* promoter region was amplified from the DZ2 chromosome with primers CgmoA-1/CgmoA-2 and cloned at the BamHI and HindIII sites of pSWU30.
pSWU30aglS	Primers CgmoA-1/CgmoC-1 were used to amplify the promoter of *aglS* from the DZ2 chromosome. Primers CgmoC-2/CgmoC-3 were used to amplify *aglS* from the DZ2 chromosome. Both fragments were fused by SOE-PCR and cloned at the BamHI and EcoRI sites of pSWU30.
pBJΔ3004A	Primer pairs D3004-1/D3004-2 and D3004-3/D3004-4 were used to amplify a 1-kb fragment upstream and downstream from the MXAN_3004 ORF. Both fragments were fused by SOE-PCR and cloned at the EcoRI sites and HindIII sites of pBJ114.

*All plasmid inserts were sequenced to ensure the absence of PCR-introduced mutations.

Table S4. Effects of CCCP, valinomycin, and nigericin on the membrane potential

Drug treatment	Effect on membrane potential Δψ (mV)
No treatment	154
CCCP (10 μM)	0
Valinomycin (40 μM)	0
Nigericin (100 μM)	158

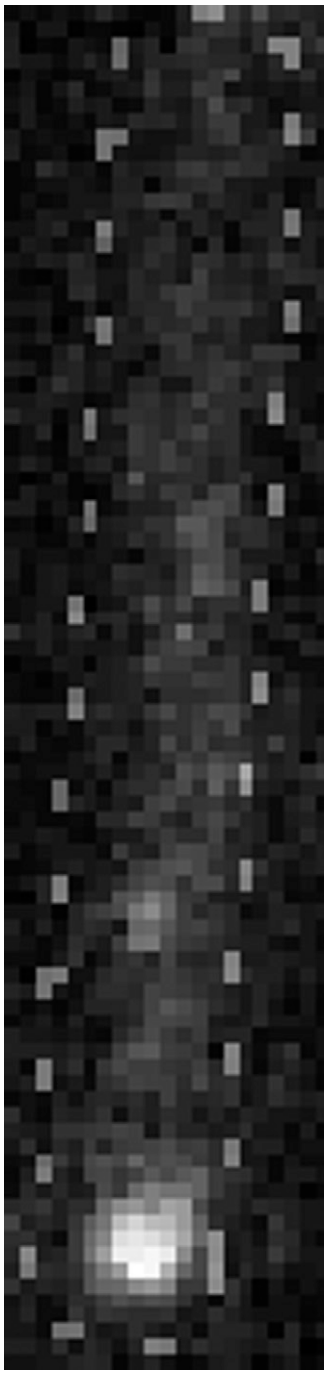

Movie S1. Intracellular transport of AglZ-YFP clusters. Most AglZ-YFP clusters move from the cell head, defined as the brightest pole, toward the back. Some clusters move opposite this direction, and the cell can support both directions of motion at the same time.

Movie S1

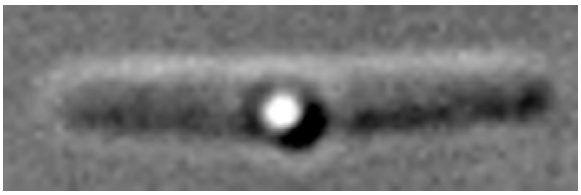

Movie S2. A bead moves along the side of an immobilized cell. Long, unidirectional runs are interrupted by periods of motionless pausing.

Movie S2

Article II

Emergence and Modular Evolution of a Novel Motility Machinery in Bacteria.

Jennifer Luciano[T, 1, 2], Rym Agrebi[T, 1, 2], Anne-Valérie Le Gall[1, 2], Morgane Wartel[1, 2], Francesca Fiegna[1, 2], Adrien Ducret[1, 2], Céline Brochier-Armanet[1, 2], Tâm Mignot[1, 2].

[T] These authors contributed equally to this work.

[1] Institut de Microbiologie de la Méditerranée (IFR88) - Laboratoire de Chimie Bactérienne, CNRS UPR 9043, Marseille, France

[2] Aix-Marseille University, Marseille, France

Published in PLoS Genetics, September 2011.

Since the AglRQS motor is localized to the bacterial inner membrane, it must interact with other proteins in the cell envelope to power motility. In *Myxococcus*, the *aglRQS* motor genes are organized in an operon but their immediate genetic environment is not indicative of the genes that encode the transducer complex. Thus, to identify the transducer proteins we re-investigated the 51 genes previously identified by transposon-based genetic screens and looked for genes encoding proteins with certain characteristics. We hypothesized that (i), the transducer complex proteins must have coevolved with the gliding motor proteins; (ii), the gliding genes must encode predicted membrane proteins, exported proteins and proteins containing protein-protein interaction motifs [tetratricopeptide repeat (TPR) or coiled-coil domains for example]. This analysis led us to identify three functionally related genetic clusters containing in total 14 genes: a seven gene operon (later named *gltD-J*), a four gene operon (*gltA*, *gltB*, *gltC* and *gltK*) and the *aglRQS* motor cluster itself.

The taxonomic distribution of the *glt* genes revealed that seven of the fourteen genes were clustered together (*gltC*, *gltD*, *gltE*, *gltG*, *agl*R, *aglQ*, and *aglS*), encoding a putative standalone machinery in many Delta-proteobacteria, Gamma-proteobacteria, and some representatives of Fibrobacter and Beta-proteobacteria. Thus, the seven genes could form a functional gene core encoding a machinery of yet unknown function. Remarkably, this core set of genes contained genes of each of the three separate loci identified in *Myxococcus*. The seven other genes (*gltA*, *gltB*, *gltF*, *gltH*, *gltI*, *gltJ*, and *gltK*) were found only in the Delta-proteobacteria (where *M. xanthus* belongs) and thus must have been acquired only recently during the evolution of the Delta-proteobacteria. These data suggest that the *Myxococcus* motility machinery is encoded by genes that derived from the modular expansion of an ancestral machinery (the core machinery). The putative function of the core machinery will be discussed further in the third article and in the Discussion section.

To test whether the *glt* genes indeed encode components of the gliding machinery, we made in-frame deletions in all of the *glt* genes and showed that these genes are essential for gliding motility. We then determined the subcellular localization of several *glt* genes (i), by cell fractionation experiments that showed that the Glt proteins are present in the cell envelope, inner membrane, periplasmic space and outer membrane; (ii), by fluorescent gene fusions to the GltD and GltF proteins which were found to colocalize with AglZ-YFP at FACs. Finally, we could further show that the AglRQS motor interacts with the Glt complex by a direct interaction between the GltG and AglR proteins.

Based on these results, we concluded that the AglRQS-Glt proteins assemble as a dynamic envelope spanning motility machinery at the FACs. Mechanical work from the AglRQS motor is therefore predicted to be transduced to the cell exterior by the cognate Glt protein assemblage to give rise to cell motion. However, how this force is transduced remains to be elucidated. During this work, my specific contribution was to show the direct interaction between the Agl motor and the Glt complex using a bacterial two-hybrid assay.

OPEN ACCESS Freely available online

PLoS GENETICS

Emergence and Modular Evolution of a Novel Motility Machinery in Bacteria

Jennifer Luciano[1,2☯], Rym Agrebi[1,2☯], Anne Valérie Le Gall[1,2], Morgane Wartel[1,2], Francesca Fiegna[1,2], Adrien Ducret[1,2], Céline Brochier-Armanet[1,2*], Tâm Mignot[1,2*]

1 Institut de Microbiologie de la Méditerranée (IFR88)–Laboratoire de Chimie Bactérienne, CNRS UPR 9043, Marseille, France, **2** Aix-Marseille University, Marseille, France

Abstract

Bacteria glide across solid surfaces by mechanisms that have remained largely mysterious despite decades of research. In the deltaproteobacterium *Myxococcus xanthus*, this locomotion allows the formation stress-resistant fruiting bodies where sporulation takes place. However, despite the large number of genes identified as important for gliding, no specific machinery has been identified so far, hampering in-depth investigations. Based on the premise that components of the gliding machinery must have co-evolved and encode both envelope-spanning proteins and a molecular motor, we re-annotated known gliding motility genes and examined their taxonomic distribution, genomic localization, and phylogeny. We successfully delineated three functionally related genetic clusters, which we proved experimentally carry genes encoding the basal gliding machinery in *M. xanthus*, using genetic and localization techniques. For the first time, this study identifies structural gliding motility genes in the Myxobacteria and opens new perspectives to study the motility mechanism. Furthermore, phylogenomics provide insight into how this machinery emerged from an ancestral conserved core of genes of unknown function that evolved to gliding by the recruitment of functional modules in Myxococcales. Surprisingly, this motility machinery appears to be highly related to a sporulation system, underscoring unsuspected common mechanisms in these apparently distinct morphogenic phenomena.

Citation: Luciano J, Agrebi R, Le Gall AV, Wartel M, Fiegna F, et al. (2011) Emergence and Modular Evolution of a Novel Motility Machinery in Bacteria. PLoS Genet 7(9): e1002268. doi:10.1371/journal.pgen.1002268

Editor: Josep Casadesús, Universidad de Sevilla, Spain

Received February 3, 2011; **Accepted** July 14, 2011; **Published** September 8, 2011

Funding: JL is the recipient of an FRM "projet innovants" fellowship (ING20080914223). FF is the recipient of an EMBO long-term postdoctoral fellowship. RA is supported by an ERC starting grant (ERC-2010-StG_20091118) to TM. MW is supported by a thesis fellowship from MENRT. AD is supported by the Human Frontier Science Program (RGY75/2008). This work was supported by an ERC starting grant (ERC-2010-StG_20091118) to TM and an Action Thématique et Incitative sur Programme (ATIP) of the French Centre National de la Recherche Scientifique (CNRS) to CB-A. The funders had no role in study design, data collection and analysis, decision to publish, or preparation of the manuscript.

Competing Interests: The authors have declared that no competing interests exist.

* E-mail: cbrochier@ifr88.cnrs-mrs.fr (CB-A); tmignot@ifr88.cnrs-mrs.fr (TM)

☯ These authors contributed equally to this work.

Introduction

In Gram-negative bacteria, envelope machineries connecting the cell interior to the extracellular milieu must span all envelope layers, including the inner membrane, peptidoglycan and outer membrane. Despite these constraints, gram-negative bacteria have evolved sophisticated envelope nano-machines to interact with their environment. Conspicuous examples are bacterial organelles such as flagella, pili, and transport and secretion systems [1,2]. In general, the structural genes encoding these systems are clustered within large transcriptional units allowing co-regulation of their expression. However, assembly also relies on additional complexity and must involve "just-in time" transcriptional regulations, specific targeting and protein self-assembly properties [3]. This raises the question of the evolutionary processes that led to the emergence of these macromolecular systems [4].

Non-homologous envelope macro-molecular structures mediate motility in bacteria. For example, bacteria swim in extremely viscous environments by means of a rotary flagellum, one of the most sophisticated known biological nano-machines [3]. Bacteria can also crawl across surfaces, for example, polymerization and de-polymerization of pilin fibers from the bacterial cell pole pull the cell forward, a "twitching" motility mechanism which also involves the coordinated assembly of many envelope proteins [5–7]. However, gram-negative rod-shaped bacteria are also able to move on surfaces by other means. For example, many bacteria move smoothly along their long axis in the absence of obvious extra-cellular organelles [8]. This gliding motility is associated with unusual flexibility of the cell body and can be found in very diverse bacterial phyla, such as, Bacteroidetes, Cyanobacteria and Deltaproteobacteria [8,9]. In most species, the mechanism that drives gliding motility remains speculative. For example, in *Flavobacterium johnsoniae* (Bacteroidetes) gliding motility may be associated with a novel secretion apparatus. However, it is unclear whether this system is involved in assembly of the gliding machinery or constitutes the machinery itself [10]. Finally, gliding may be propelled differently in various species [8].

Despite decades of research, dedicated gliding motility machineries have not been identified unambiguously in any bacterial species, hampering detailed mechanistic studies and asking the question of the emergence of this process in bacteria. In *Myxococcus xanthus*, a gram negative deltaproteobacterium, surface motility allows the directed aggregation of thousands of cells into mounds that mature into fruiting bodies where the bacteria differentiate into spores [11]. *Myxococcus* cells can move by twitching motility, but in the absence of pili, the cells are still able to move,

Author Summary

Motility over solid surfaces (gliding) is an important bacterial mechanism that allows complex social behaviours and pathogenesis. Conflicting models have been suggested to explain this locomotion in the deltaproteobacterium *Myxococcus xanthus*: propulsion by polymer secretion at the rear of the cells as opposed to energized nano-machines distributed along the cell body. However, in absence of characterized molecular machinery, the exact mechanism of gliding could not be resolved despite several decades of research. In this study, using a combination of experimental and computational approaches, we showed for the first time that the motility machinery is composed of large macromolecular assemblies periodically distributed along the cell envelope. Furthermore, the data suggest that the motility machinery derived from an ancient gene cluster also found in several non-gliding bacterial lineages. Intriguingly, we find that most of the components of the gliding machinery are closely related to a sporulation system, suggesting unsuspected links between these two apparently distinct biological processes. Our findings now pave the way for the first molecular studies of a long mysterious motility mechanism.

unmasking the activity of the gliding engine [11]. Recent cytological work suggested that motility is driven by protein complexes (Focal Adhesion Complexes, FAC) that push against the substratum as they accumulate periodically on the ventral side of the cell [12–14]. In a live cell assay, FACs can be observed as bright fluorescent fixed spots in cells expressing a fluorescent gliding motility protein (AglZ-YFP, [12]). The formation of AglZ-YFP foci requires the bacterial MreB-actin cytoskeleton [15] and a FACs-localized proton motive force-driven motor (AglRQS) was recently identified [13]. These observations suggest that AglRQS powers motility in concert with the MreB-cytoskeleton; however, how work from AglRQS is tranduced to the cell surface remains unknown and requires the identification of a motor-associated complex that spans the cell envelope.

In the past, 51 genes associated to defects in gliding motility were identified by transposon-based genetic screens, but the functional role of these genes in motility was not established [16,17]. Recent work by Nan et al. [18] uncovered a new motility complex (AgmU, AglZ, AglT, AgmK, AgmX, AglW and CglB) and suggested that AgmU may be actively transported by PMF-utilizing motors [14]. However, the function of this complex and its direct link with the AglRQS motor remains to be established.

In this work, we aimed to identify the motility machinery conclusively. We re-investigated the 51 known *M. xanthus* gliding genes with the premise that the gliding machinery must have co-evolved with the AglRQS motor. This approach allowed us to identify a novel energy-driven protein complex, which we prove to be the basal gliding machinery. The results reveal the architecture of the gliding machinery and suggest a scenario of its emergence (and evolution) in bacteria.

Results/Discussion

Identification of candidate genes encoding the gliding machinery

Two independent transposon-based genetic screen studies [16,17] identified 35 and 23 potential gliding motility genes, respectively (Table S1). Only seven genes overlapped in the two genetic studies, suggesting that the screens are not saturated and thus, the complete set of genes involved in gliding motility has likely not been identified. Nevertheless, these data constituted a good starting point and could indeed contain genes that encode the motility machinery. Irrespective of the exact motility mechanism, a number of cell envelope proteins should be part of the motility machinery. Therefore, we re-visited gene annotations specifically looking for genes encoding predicted membrane proteins, exported proteins and proteins containing motifs mediating protein-protein interaction, such as Tetratricopeptide repeat (TPR) and Coiled-coil domains (Table S1). A total of 28 genes were thus highlighted.

A careful survey of these 28 genes revealed that 13 gene hits were in fact clustered into four chromosomal regions of the *M. xanthus* DK 1622 genome. One region containing three hits, *aglW* (MXAN_5756, *tolB*), *aglX* (MXAN_5753, *tolQ*) and *aglV* (MXAN_5754, *tolR*), encoded together with MXAN_5755 (*tolA*) and MXAN_5757 (pal), *bona fide* components of a complete Tol-Pal system. Tol-Pal maintains envelope integrity and supports cell division in all bacteria where it has been studied [19,20]. Thus, it is unlikely that Tol-Pal constitutes the motility machinery. Consistent with a general envelope function of the Myxococcus Tol-Pal, the *aglV* (*tolR*) mutant was also severely impaired in twitching motility [16]. We then focussed our analysis on the remaining three gene clusters (hereafter referred as Gliding1 (G1), Gliding 2 (G2) and Motor 1 (M1), Figure 1A). The G1 cluster contains eight genes, MXAN_4870-62, six of which have been hit by transposons: *agmU* (MXAN_4870), *aglT* (MXAN_4869), *pglI* (MXAN_4867), *agmV* (MXAN_4864/65, see below), *agmK* (MXAN_4863) and *agmX* (MXAN_4862) (Figure 1A). The G2 cluster contains four genes, MXAN_2538-41, two of them inactivated by transposons: *agmO* (MXAN_2538) and *agnA* (MXAN_2541). Finally, M1 contains the *aglRQS* genes themselves (MXAN_6862-60) and two hits by transposon insertions in *aglR* (MXAN_6862) and *aglS* (MXAN_6860). So overall, the G1, G2 and M1 clusters involve 15 genes, 10 of which have been previously hit by the transposon screens (Table 1).

The M1 cluster encodes the component of a TolQR-like proton conducting motor, which has been characterized elsewhere [13]. The G1 and G2 cluster genes were analysed using public sequences and domain databases. The predicted MXAN_4866 (G1 region) and MXAN_2540 (G2 region) proteins are probably secreted and inserted in the outer membrane because they contain an Autotransporter ß-domain and adopt an OmpA-like fold, respectively (Table 1). AgmO may also be located in the outer-membrane because it carries a typical Outer-membrane Type-II signal sequence. TPR-repeats typically involved in multiprotein assemblies [21] are encoded by four G1 and G2 region genes: *agmU, aglT, agmK,* and *agnA* (Table 1). Among them, AgmU, AglT, and AgnA also carry signal peptides, suggesting that they are exported beyond the inner membrane. PglI (G1 region) is a predicted bi-topic transmembrane protein with a cytosolic Fork-Head-Associated domain (FHA, [22]) and a periplasmic domain of unknown function. AgmX (G1 region) is also a potential integral membrane protein. MXAN_4868 and MXAN_2539 both carry N-terminal signal peptides but do not contain any conserved functional domains (Table 1). Finally, MXAN_4864 and MXAN_4865 are probably not actual genes and were discarded from this study (see Text S1 for justification) In the rest of this work, we tested if the G1 and G2 genes encode the AglRQS motor-associated gliding machinery. For clarity and to homogenize the nomenclature, we renamed all the G1 and G2 genes *glt* (**gl**iding **t**ransducer, see below), with *gltD, E, F, G, H, I* and *J* corresponding respectively to *agmU*, *aglT*, MXAN_4868, *pglI*,

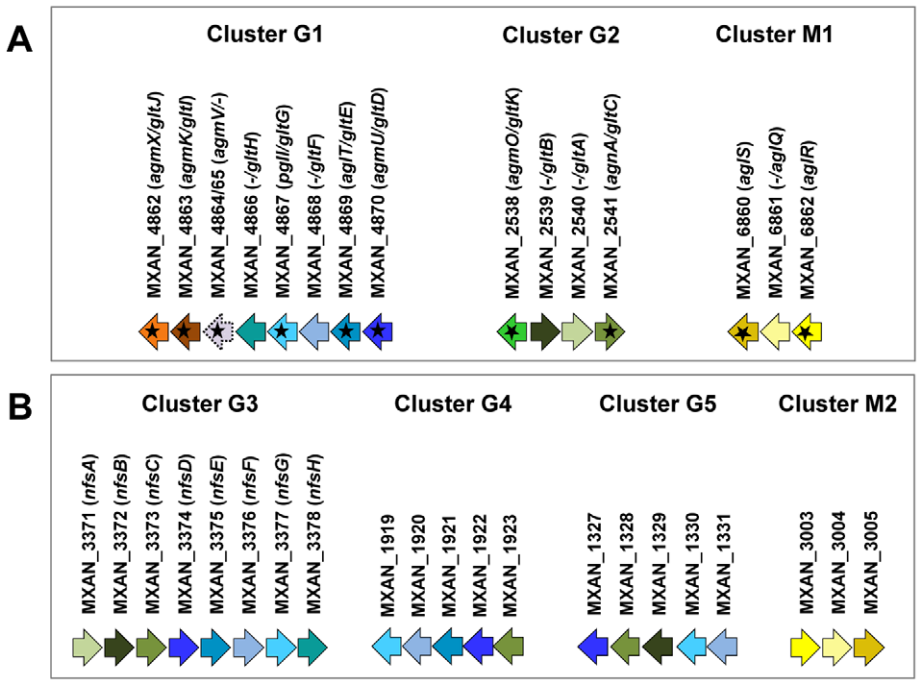

Figure 1. Genetic clusters carrying gliding motility genes in *M. xanthus*. (A) Genetic organisation of the 15 genes composing the G1, G2 and M1 clusters encoding the putative components of the gliding machinery in *Myxococcus xanthus* DK 1622. Predicted genes are indicated with their locus_tag, and their former and new names. The arrow that represents the putative MXAN_4864 and MXAN_4865 genes is a dotted line because they are likely pseudogenes (see text for more details). Stars indicate genes that were hit by the transposon screens [16,17]. (B) Genetic organization of the G3, G4, G5 and M2 homologue clusters in *M. xanthus* DK 1622. The colour code indicates homologous genes and will be used throughout the study.
doi:10.1371/journal.pgen.1002268.g001

MXAN_4866, *agmK* and *agmX* (G1) and *gltC*, *A*, *B* and *K* corresponding to *agnA*, MXAN_2540, MXAN_ 2539 and *agmO* (G2, see below and Text S2 for justification).

The G1, G2, and M1 clusters may encode components of a single macro-molecular machinery

The G1, G2 and M1 clusters encode a majority of potential envelope proteins and a motor complex (see above). A tempting hypothesis would be therefore that all these components constitute the gliding machinery. We systematically investigated the taxonomic distribution of the 14 genes defining the G1, G2 and M1 clusters in the 1180 complete prokaryotic proteomes available at the beginning of this study (see methods). The 14 genes could be separated in two distinct groups based on taxonomic distribution: A first group (Group A) contained seven genes (*gltF*, *gltH*, *gltI*, *gltJ*, *gltK*, *gltB* and *gltA*) that were only present (and sometimes in several copies) in Myxococcales (i.e. *Sorangium cellulosum*, *Plesiocystis pacifica*, *Haliangium ochraceum*, *Stigmatella aurantiaca*, *Myxococcus xanthus and the* four *Anaeromyxobacter sp.*) and in Bdellovibrionales (*Bdellovibrio bacteriovorus*) (Figure 2A). Such restricted taxonomic distribution suggested that these genes appeared only recently during the evolution of the Deltaproteobacteria. By contrast, a second group (Group B) contains seven genes with a much broader taxonomic distribution (Figure 2A). Specifically, blastp and PSI-BLAST queries identified 142 GltD, 2545 GltE, 313 GltG, 83 GltC, 2677 AglR, 2348 AglQ and 2385 AglS homologues. The taxonomic distributions of all these homologues are very different, suggesting that the corresponding genes have undergone different evolutionary histories, which was confirmed by preliminary phylogenetic analyses (not shown). However, in all these phylogenetic trees, the *M. xanthus* sequences emerge within a monophyletic clade containing homologues from other Deltaproteobacteria but also from a set of unrelated bacteria (i.e. one Betaproteobacteria, several Gammaproteobacteria and one member of Fibrobacteres, Figure S4). This strongly suggests that, although these genes belong to large gene families of distinct evolutionary histories, the *M. xanthus gltD*, *gltE*, *gltG*, *gltC*, *aglR*, *aglQ* and *aglS* genes and their closest homologues share a similar evolutionary history. The presence of Group B genes (sometime in several copies per genomes) in a few distantly related bacteria (Figure S1) suggests a complex evolutionary history punctuated with horizontal gene transfer (HGT) and gene duplication events (see below). In all non-Deltaproteobacteria and in *Geobacter*, Group B genes clustered in a single genomic region, possibly an operon, arguing strongly that they encode a single functional unit (i.e. core complex, Figure 2B and Figure S1, Tables S2 and S3). In all these bacteria, the core complex contains an additional gene that has no homologues in Myxococcales and Bdellovibrionales (Figure S1). Remarkably, group B genes (and thus the core complex) group genes from the G1 (*gltD*, *gltE* and *gltG*), G2 (*gltC*) and M1 (*aglQ*, *R and S*) clusters (Figure 2A-2B). This suggests an evolutionary link between the G1, G2 and M1 gene clusters. Strengthening this prediction, homologues of G1 and G2 clusters are grouped on the chromosome of the four *Anaeromyxobacter* relatives (Figure S1). Then, we proceeded to test the functional relationships between the G1, G2 and M1 genes.

Genetic characterization of G1 and G2 gene clusters

In *M. xanthus*, many of the genes composing the G1 and G2 clusters were previously hit by genetic screens [16,17]; however, the genes were only partially characterized, and it was not determined how they might be functionally related. More recently, Nan et al. [18] showed that individual deletions of the G1 genes *gltD-J* impair motility, but their analysis did not test whether these genes

Table 1. Bioinformatic analysis of G1, G2, and M1 cluster genes.

Cluster	Former name	New name	Locus-tag	Ref-seq	Length	Functional domain (Pfam)				Signal peptide	Transmembrane domain
						Name	Accession number	E-value	Position		
Cluster G1	*agmU*	*gltD*	MXAN_4870	YP_633028	1191	Tetratricopeptide repeat	PF07719	0.002	280-306	+	-
	aglT	*gltE*	MXAN_4869	YP_633027	471	Tetratricopeptide repeat	PF07719	5.7e-06	298–330	+	-
	-	*gltF*	MXAN_4868	YP_633026	89	-	-	-	-	+	-
	pglI	*gltG*	MXAN_4867	YP_633025	640	FHA domain Gram-negative bacterial tonB protein	PF00498 PF03544	5.3e-13 1.8e-05	26–90 570–637	-	+
	-	*gltH*	MXAN_4866	YP_633024	209	Autotransporter beta-domain	PF03797	0.084	73–153	+	+
	agmK	*gltI*	MXAN_4863	YP_633022	4132	Tetratricopeptide repeat Tetratricopeptide repeat	PF07719	8.7e-06 9.7e-05	3186–3218 3114–3142	-	-
	agmX	*gltJ*	MXAN_4862	YP_633021	674	-	-	-	-	-	+
Cluster G2	*agmO*	*gltK*	MXAN_2538	YP_630757	170	-	-	-	-	+	-
	-	*gltB*	MXAN_2539	YP_630758	275	-	-	-	-	+	-
	-	*gltA*	MXAN_2540	YP_630759	256	OmpA-like transmembrane domain	PF01389	0.011	168–255	+	-
	agnA	*gltC*	MXAN_2541	YP_630760	673	Tetratricopeptide repeat	PF07719	0.27*	260-289	+	-
Cluster M1	*aglR*	-	MXAN_6862	YP_634979	245	MotA/TolQ/ExbB proton channel family	PF01618	4.4e-18	112–217	-	+
	-	*aglQ*	MXAN_6861	YP_634978	162	Biopolymer transport protein ExbD/TolR	PF02472	6.7e-18	15–158	-	+
	aglS	-	MXAN_6860	YP_634977	194	Biopolymer transport protein ExbD/TolR	PF02472	3.1e-15	28–176	-	+

doi:10.1371/journal.pgen.1002268.t001

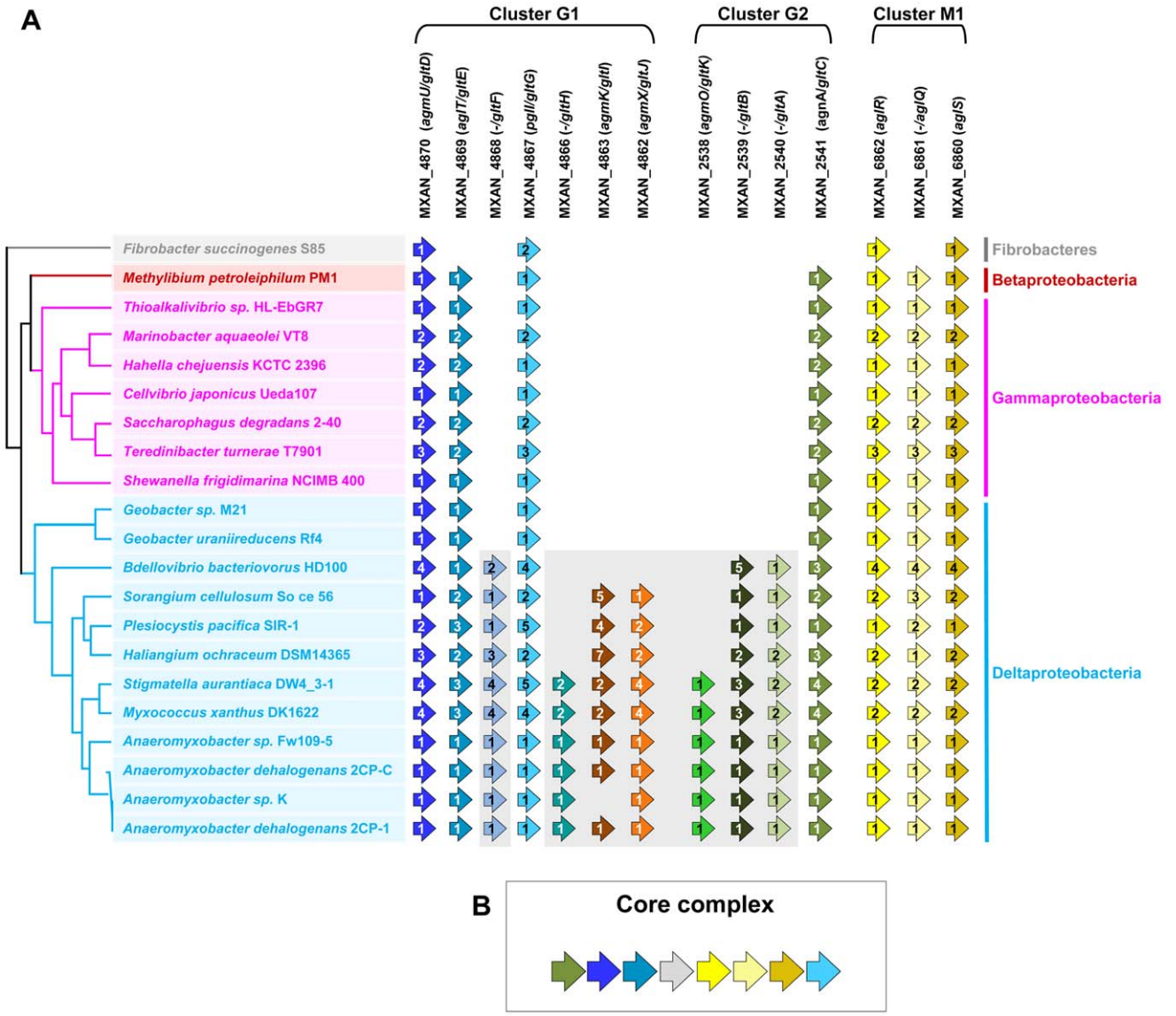

Figure 2. Taxonomic distribution of the closest homologues of the 14 genes composing the G1, G2, and M1 clusters, and genetic organization of the core complex. (A) For a given gene, the number of homologues in the corresponding genome is indicated by the numbers within arrows. The relationships between the species carrying the different homologues of the genes are indicated by the phylogeny on the left. Based on their taxonomic distribution, the 14 genes can be divided into Group A (grey background) and Group B (white background). (B) In all non Deltaproteobacteria and in *Geobacter*, the Group B genes clustered in a single genomic region.
doi:10.1371/journal.pgen.1002268.g002

are structural. In fact, structural motility components cannot be simply discriminated from regulatory motility components solely based on mutational analysis and colony agar plate assays. First, the absence of motility at colony edges does not necessarily indicate that single cells are completely unable to move: for example, a class of directional mutants (FrzCD^{c}, hyper active Frz-receptor mutants,[23]) forms smooth colony edges, yet, when observed under the microscope, individual cells glide but move back and forth at very high frequencies and thus show no net translocation (hyper-reversing cells, [23]). Thus, motility mutants must also be probed in single cell motility assays. Second, some mutations leading to complete motility defects can be suppressed by second-side mutations, showing that the mutated genes are not structural but regulatory. For example, the motility defect of the *aglZ* mutant is suppressed when *frz*, encoding a signal transduction system regulating the directionality of motility, is disrupted [24].

Thus, structural machinery genes must minimally meet the following criteria: (i) gene deletion should result in complete loss of motility in mutants that also lack twitching motility both at colony and single cell scales and (ii), the motility defect should not be suppressed by a *frz* mutation [24]. Consequently, in this study, we systematically combined the deletions to *pilA*- or *frzE*-null mutation (encoding the major pilin sub-unit and the essential FrzE kinase, respectively). It is still possible that regulatory genes may work independently from Frz, but, altogether, the genetic, localization and interaction evidence strongly supports that the Glt proteins are structural (see below).

We therefore made markerless in frame deletions in all the G1 and G2 genes (except *gltI* and *gltJ*) and showed that the deletions

Table 2. *glt* mRNA expression in cluster G1 deletion strains.

Strain	Relevant genotype	Relative gene expression determined by q-RT-PCR				
		gltD	*gltE*	*gltF*	*gltG*	*gltH*
DZ2	Wild type	1	1	1	1	1
TM142	Δ*gltA*	ND[a]	0.63	0.40	0.77	0.65
TM148	Δ*gltB*	1.82	ND	1.89	1.24	1.15
TM136	Δ*gltC*	1.29	0.87	ND	1.24	0.72
TM135	Δ*gltD*	0.85	1.06	0.79	ND	4.66
TM149	Δ*gltE*	1.77	1.85	1.88	1.28	ND

[a]ND = Not Detected. The relative expression of the *gltD*, *gltE*, *gltF*, *gltG* and *gltH* genes in the wild-type strain and in deletion mutant strains was determined by q-RT-PCR. All the values are representative values from several independent experiments.
doi:10.1371/journal.pgen.1002268.t002

did not create polar effects by quantitative RT-PCR (Table 2 and Table 3). Of note, the expression of *gltH* was up-regulated 4-5 folds when *gltG* was deleted, which may point to a regulatory function of GltG (Table 2).

On agar plate assays, the *gltA-H and gltK* mutants retained intact twitching motility but were completely deficient in single cell motility at the colony edges (Figure 3A). *gltA-H* and *gltK pilA* double mutants were all completely non-motile both at the colony and single cell levels (Figure 3A and data not shown), showing that the *glt* genes are specific and essential to gliding motility. In one exception, the *gltH pilA* mutant showed small scales "jerky" displacements on occasions, but the motility defect was still very severe (Figure 3A and Video S1).

In a second step, we observed that *gltA-H* and *gltK frzE* double mutants were also completely non-motile in the colony and single cell assays (Figure 3B and data not shown). As a control, we also tested the simultaneous deletion of *frzE* and *aglZ* and observed that colony and single motility were both restored, as previously described (Figure 3B, [24]). Interestingly, group swarming appeared enhanced on hard agar plates in all cases, suggesting that the *frzE* mutation enhanced twitching in those mutants (Figure S2). Nan et al. [18] reported that motility of a *gltD* mutant allele was restored when a *frz* mutation was introduced, however this conclusion was based on observation of colony edges. In fact, enhanced twitching motility in the double mutant may have been mis-interpreted for restored gliding motility. To test this, we further introduced a *pilA* mutation in the double *gltD frzE* mutant. Motility was completely abolished in the resulting triple mutant. In contrast, the triple *aglZ frzE pilA* mutant was motile under similar conditions, as expected (Figure 3B, compare middle and right panels). The enhanced twitching in the *glt frzE* double mutants points to intriguing couplings between gliding and twitching motility, which will need further investigation.

In conclusion, the *glt* genes are genetically separable from *aglZ*, and may thus encode structural components of the motility machinery. A comparable genetic analysis also suggested that *aglR*, *Q* and *S* are structural [13]. Thus, the genetic results are consistent with a functional link between *aglRQS* and the *glt* G1 and G2 group genes.

G1 cluster proteins localize to the cell envelope

We next aimed to determine the subcellular localization of the suspected Glt protein complex. In absence of specific antibodies to detect all proteins, we only tested some proteins of the G1 cluster: GltD, E, F, G and H, all predicted to localize within the cell envelope (Table 1). We also tested the localization of a functional GltF-mCherry fusion with specific anti-mCherry antibodies. Cell fractionation experiments showed unambiguously that all five proteins localize in the cell envelopes (Figure 4). GltD was also present in the soluble fraction but to minor extents (Figure 4). GltF-mCherry was equally distributed in the soluble and membrane extracts (Figure 4). The GltF-mCherry fusion was functional (Figure S3 and data not shown), however it also seemed to be processed to some extent during the fractionation procedure (Figure 4), thus it cannot be excluded that its presence in the soluble fraction results from improper secretion.

We next wanted to discriminate inner- and outer-membrane proteins. Separating the inner membrane from the outer membrane was difficult using standard sucrose density gradients or detergent-based methods (see Methods). We therefore decided

Table 3. *glt* mRNA expression in the cluster G2 deletion strains.

Strain	Relevant genotype	Relative gene expression determined by q-RT-PCR			
		gltK	*gltB*	*gltA*	*gltC*
DZ2	Wild type	1	1	1	1
TM142	Δ*gltK*	ND[a]	0,89	1,37	1,2
TM148	Δ*gltB*	1	ND	0,76	0,70
TM136	Δ*gltA*	0,99	0,54	ND	1,13
TM135	Δ*gltC*	0,59	0,70	0,61	ND

[a]ND = Not Detected. The relative expression of the *gltK*, *gltB*, *gltA* and *gltC* genes in the wild-type strain and in deletion mutant strains was determined by q-RT-PCR. All the values are representative values from several independent experiments.
doi:10.1371/journal.pgen.1002268.t003

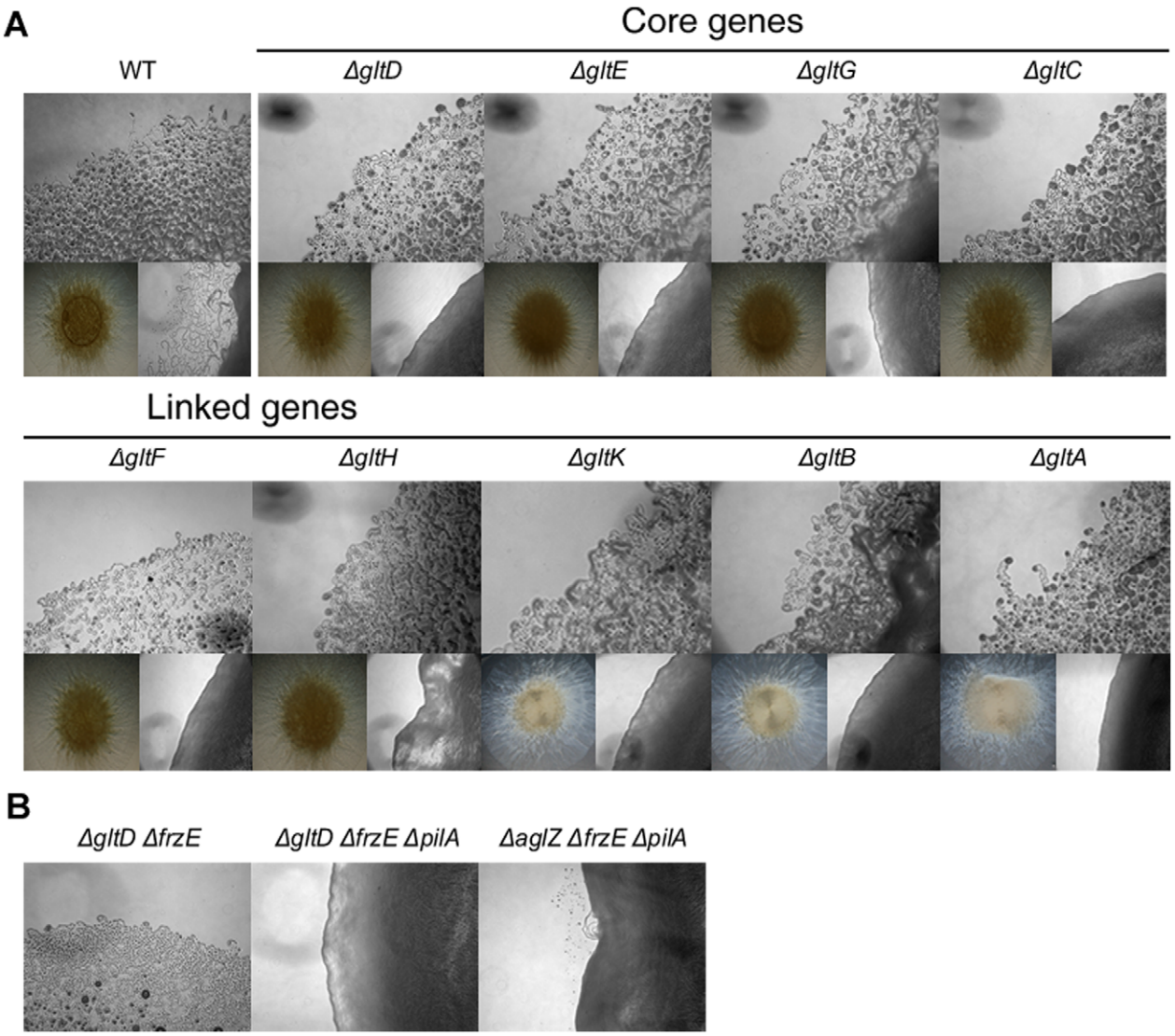

Figure 3. Group B genes encode structural components of the motility machinery. (A) Motility at the *gltA-H*and *gltK* deletion mutants colony edges after 48h incubation at 32°C on hard (1.5%) (upper panel). Lower left panel: twitching motility is unaffected in the *gltA-H* and *gltK* deletion mutants and observed in the form of expanded colony swarms on soft (0.5%). Lower right panel: motility of double *pilA gltA-H* and *pilA gltK* deletion mutants showing the complete absence of motility in these mutants. (B) Hard agar colony edges of the *gltD frzE, gltD frzE pilA* and *aglZ frzE pilA* mutants showing the lack of motility restoration in the *gltD* mutant. Note that single cells are clearly visible in the *aglZ frzE pilA* mutant, consistent with previous literature [24].
doi:10.1371/journal.pgen.1002268.g003

to harvest outer-membrane-derived vesicles (see Methods). Extracted vesicles contained PilQ, the pilus Secretin but not PilC, localizing at the inner membrane, confirming that the vesicles were derived from the outer membrane. Only GltH was detected in the vesicle preparation, which is consistent with the presence of an auto-transporter ß-domain in this protein (Figure 4, Table 1). All together these results suggest that GltD-G form an inner membrane localized complex that extends through the periplasm and connect the cell surface via the outer-membrane protein GltH.

The Glt proteins form an AglRQS-associated dynamic motility complex

In a parallel study, we have demonstrated that the M1 cluster (*aglRQS*) encodes a proton-motive force-driven channel that produces motility traction forces at FACs [13]. The present study suggests that AglRQS and Glt proteins are functionally related, which needed to be proven experimentally. If the Glt proteins interact with the AglZ-AglRQS system, it would be expected that the Glt proteins also localize at FACs. A fluorescent functional GltD-mCherry fusion was already available [18]. We additionally obtained another functional fusion to GltF. In two other studies, GltD-mCherry was found to localize both in fixed clusters [18] and along a dynamic helix-like structure [14]. To rationalize this apparent dual localization pattern, it was proposed that GltD-mCherry molecules traffic along a helix and accumulate at FACs when they become engaged in propulsion [14]. In our hands, the pattern of GltD-, GltF-mCherry fluorescence in live cells was similar: fluorescence was mostly evident around the cell periphery; however, when we collected z-stacks of unprocessed images, fluorescent clusters became clearly apparent when the focal plane was focussed closer to the substratum (Figure 5A, 5B and Video S2). In moving cells, these clusters were fixed and largely co-

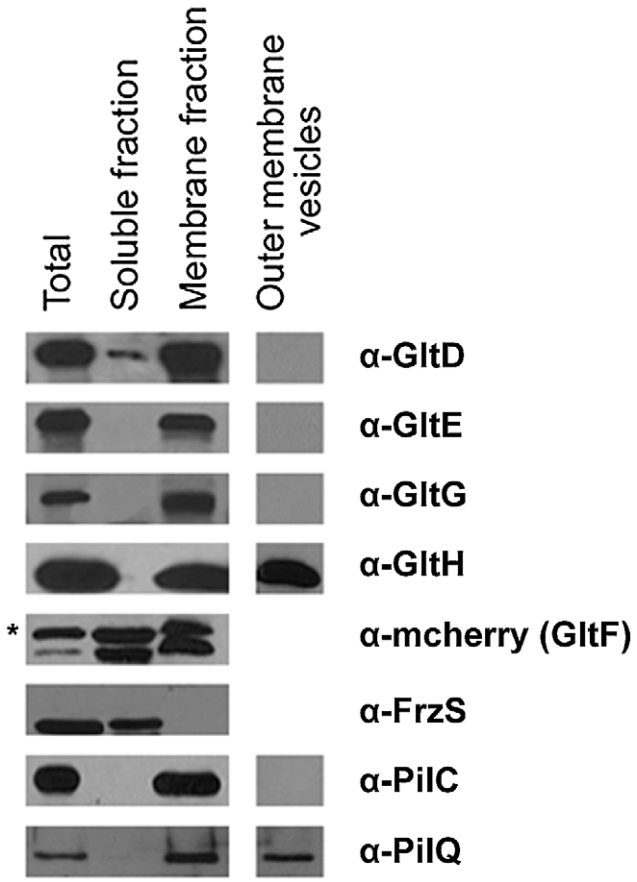

Figure 4. Envelope localization of the Glt proteins. Envelope localization of the Glt proteins. GltF localization is determined by western detection of the GltF-mCherry fusion (as indicated by the asterisk). FrzS, PilC and PilQ were used as control markers of the soluble, inner membrane and outer membrane fractions, respectively.
doi:10.1371/journal.pgen.1002268.g004

localized with AglZ-YFP (Figure 5B and 5C). We were not able to resolve a helical pattern of GltD-mCherry around the cell periphery, but observing this structure may require mathematical image-deconvolution processing [14], which would explain this discrepancy. Nevertheless, these results show that GltD and GltF are recruited at FACs, and may be parts of a complex mediating contact between the exterior and the cell interior.

GltD-mCherry dynamics are dependent on the PMF [14], suggesting that they result from the activity of a motor, possibly the AglRQS complex (M1). Indeed, in an *aglQ* mutant, GltD- and GltF-mCherry failed to accumulate at FACs and were only localized around the cell periphery and at the cell poles (Figure 5A. and data not shown). To prove that AglRQS directly fuels trafficking of the Glt proteins, we searched which Glt protein may interact with the motor. By analogy to the Tol/Exb system, the AglR protein would deliver motor work to an output protein through an H^+-driven conformational change in its N-terminal transmembrane helix [25]. Thus, the best candidate for direct interaction with AglR is the GltG protein. Indeed, this predicted transmembrane protein has a proline-rich TonB-like motif, typically found in TolA and TonB, the effector transducers in the Tol/Exb systems [20]. Moreover, GltG is the only predicted transmembrane protein that belongs to the core complex together with AglRQS (Figure 2B). We tested a potential interaction between AglR and GltG in a bacterial two-hybrid assay [26] (Figure 6). Highly significant β-galactosidase activity was only obtained when AglR and GltG were expressed together, showing that these proteins interact specifically (Figure 6). Finally, GltD-mCherry cluster localization was also abolished in mutants lacking *gltF, G* and *H*, further suggesting that these proteins are parts of one motility complex within the focal adhesion clusters (Figure 5A). All together, the results suggest that the AglRQS-Glt proteins assemble a dynamic envelope spanning motility machinery at the focal adhesion sites.

Emergence and evolutionary history of the gliding machinery

Taken together, the computational and experimental results strongly suggest that the G1, G2 and M1 clusters contain genes encoding the major components of the gliding motility machinery. The most striking result of our *in silico* analysis is the discovery of a conserved core of genes (Group B) coding for several homologues of the gliding machinery components in non-gliding bacteria. To obtain further insights on the evolutionary mechanisms underlying the emergence of the gliding apparatus, we conducted an in-depth phylogenomic analysis (see Text S3). The phylogenies of the closest homologues of the seven genes defining the conserved core of genes (i.e. Group B) showed similar topologies (Figure S4). However, these analyses were based on a fairly small number of unambiguously aligned positions and as a result most of the nodes of the inferred trees were weakly supported (Bootstrap Values (BV) $<90\%$ and Posterior Probabilities (PP) <0.95, Figure S4). This caveat precluded the precise elucidation of the evolutionary histories of the components. To improve the resolution of the phylogenetic trees, we combined the group B genes *gltD, E , G* and *AglR,Q,S* in two distinct supermatrices (See Methods).

As expected, the trees based on each supermatrix showed better resolutions than the individual gene trees (compare PP and BV in Figure 6 and Figure S4). Consistent with the single phylogenies (Figure S4), two separate clades (at odds with the species phylogeny) were observed in the resulting phylogenetic trees (PP = 1.00 and BV = 100%, Figure 7): More precisely, the three *Geobacter* representatives (Deltaproteobacteria) emerged within the Gammaproteobacteria, whereas *F. succinogenes* and the other Deltaproteobacteria, belonging to distinct phyla [27], emerged together in the *glt* and *agl* phylogenetic trees (Figure 7). Moreover, the relationships among the gammaproteobacterial sequences were mostly incongruent with the species phylogeny (Figure 2 and Figure 7). The discrepancy between the organism and gene trees precluded the clear identification of the precise bacterial lineage where the core complex originated, possibly the Gamma- or Deltaproteobacteria (Figure 8A). Nevertheless, HGT of the core complex is apparent: first, between Gammaproteobacteria and Deltaproteobacteria, then among Gammaproteobacteria and from Deltaproteobacteria to *Fibrobacter*, and last, from Gammaproteobacteria or Betaproteobacteria to *Geobacter* (Figure 8A, circles 1 to 4). In contrast, the restricted taxonomic distribution of the Group A genes indicates that they appeared and were recruited more recently during differentiation of the Deltaproteobacteria. An evolutionary scenario may thus be suggested: *gltA, B* and *F* likely appeared in the common ancestor of the Myxococcales and Bdellovibrionales, whereas *gltI* and *gltJ* (MXAN_4863-62) probably appeared in the ancestor of the Myxococcales, while *gltK and H* may have been acquired more recently (Figure 8A).

The evolutionary history of the genes involved in the gliding machinery is complicated by multiple duplication events, sometime followed by gene losses, which occurred in Myxococcales and

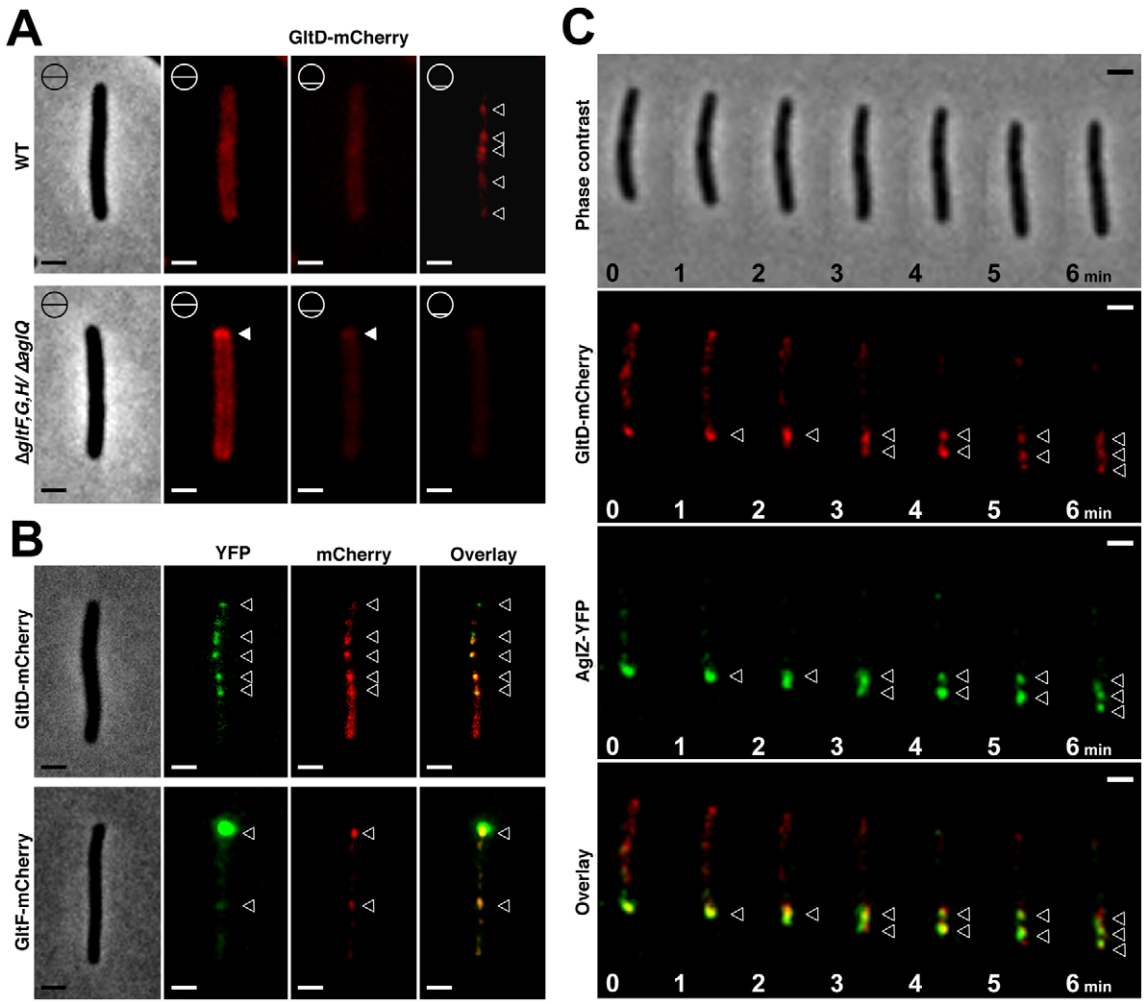

Figure 5. The Glt proteins localize dynamically to the AglZ-YFP clusters in a AglQ-dependent manner. (A) Localization of GltD-mCherry in different *z* sections in WT (upper panel) and mutant backgrounds (lower panel). Shown are unprocessed fluorescent micrographs of the different sections (position of the section along the *z* axis is indicated by a barred circle). Open triangles indicate GltD clusters. Scale bar = 1 μm. (B) Co-localization of GltD- and GltF-mCherry with AglZ-YFP. Open triangles indicate clusters were the chimeric proteins co-localize. Scale bar = 1 μm. (C) dynamic localization of GltD-mCherry and AglZ-YFP during movement. Scale bar = 1 μm.
doi:10.1371/journal.pgen.1002268.g005

Bdellovibrionales but also in Gammaproteobacteria (e.g. two *Marinobacter*, *Teredinibacter turnerae* and *Saccharophagus degradans*) and Fibrobacteres (Figure 8A and Figure S1). As a result, the gene clusters are sometimes present in several copies in the genomes of some species (*i.e.* the G3, G4, G5 and M2 clusters in *M. xanthus*, Figure 1B). Interestingly, none of these copies can substitute for the motility functions of the G1, G2 and M1 genes suggesting that duplications were associated with the emergence of novel functions (see below).

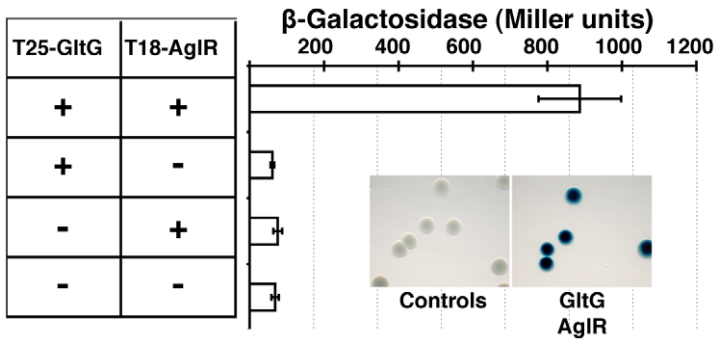

Figure 6. The AglRQS motor interacts directly with the gliding motility machinery. AglR interacts with GltG in a bacterial two-hybrid assay.
doi:10.1371/journal.pgen.1002268.g006

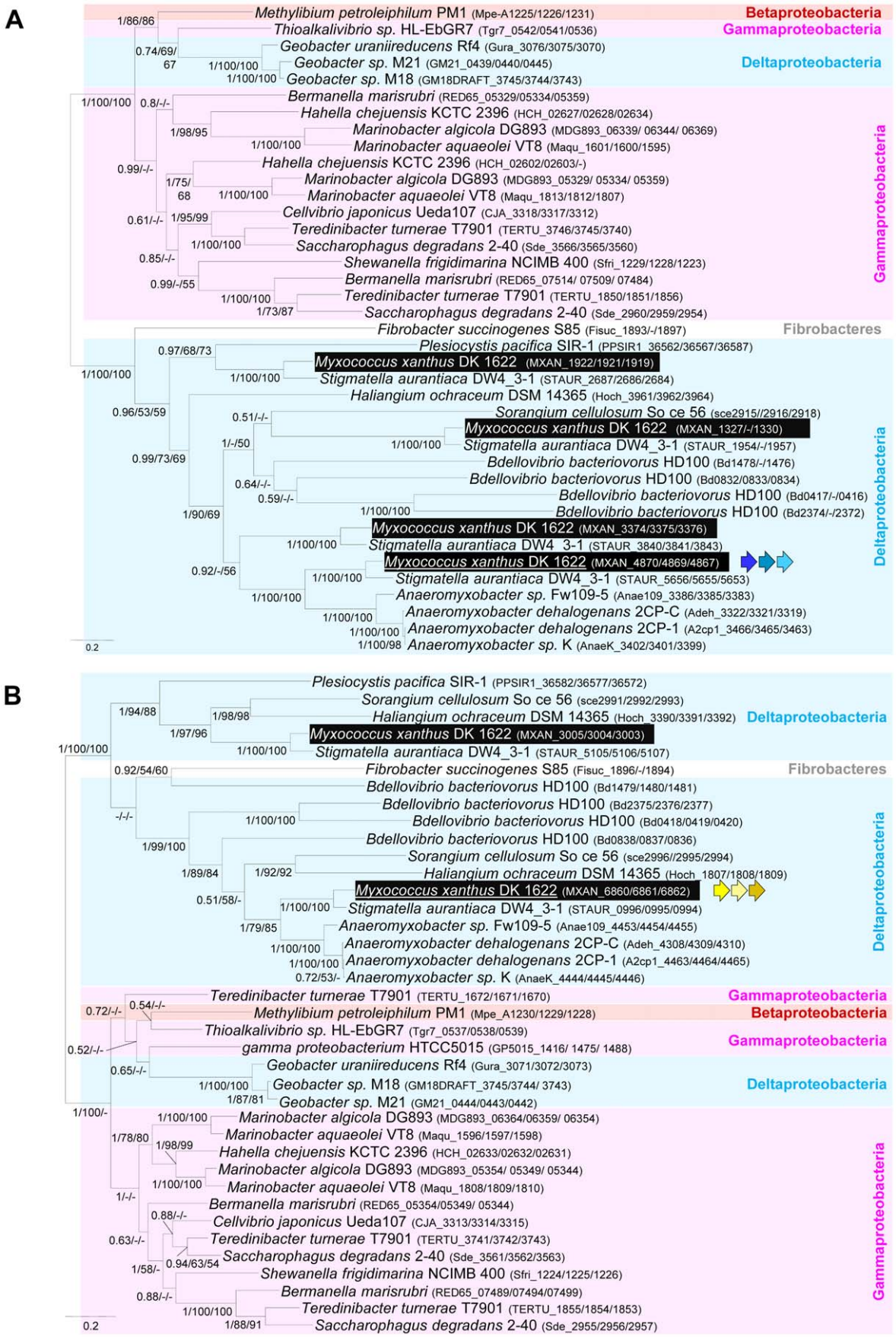
A
Methylibium petroleiphilum PM1 (Mpe-A1225/1226/1231)
Betaproteobacteria
Thioalkalivibrio sp. HL-EbGR7 (Tgr7_0542/0541/0536)
Gammaproteobacteria
Geobacter uraniireducens Rf4 (Gura_3076/3075/3070)
Geobacter sp. M21 (GM21_0439/0440/0445)
Deltaproteobacteria
Geobacter sp. M18 (GM18DRAFT_3745/3744/3743)
Bermanella marisrubri (RED65_05329/05334/05359)
Hahella chejuensis KCTC 2396 (HCH_02627/02628/02634)
Marinobacter algicola DG893 (MDG893_06339/ 06344/ 06369)
Marinobacter aquaeolei VT8 (Maqu_1601/1600/1595)
Hahella chejuensis KCTC 2396 (HCH_02602/02603/-)
Marinobacter algicola DG893 (MDG893_05329/ 05334/ 05359)
Marinobacter aquaeolei VT8 (Maqu_1813/1812/1807)
Cellvibrio japonicus Ueda107 (CJA_3318/3317/3312)
Teredinibacter turnerae T7901 (TERTU_3746/3745/3740)
Saccharophagus degradans 2-40 (Sde_3566/3565/3560)
Shewanella frigidimarina NCIMB 400 (Sfri_1229/1228/1223)
Bermanella marisrubri (RED65_07514/ 07509/ 07484)
Teredinibacter turnerae T7901 (TERTU_1850/1851/1856)
Saccharophagus degradans 2-40 (Sde_2960/2959/2954)
Gammaproteobacteria
Fibrobacter succinogenes S85 (Fisuc_1893/-/1897)
Fibrobacteres
Plesiocystis pacifica SIR-1 (PPSIR1_36562/36567/36587)
Myxococcus xanthus DK 1622 (MXAN_1922/1921/1919)
Stigmatella aurantiaca DW4_3-1 (STAUR_2687/2686/2684)
Haliangium ochraceum DSM 14365 (Hoch_3961/3962/3964)
Sorangium cellulosum So ce 56 (sce2915//2916/2918)
Myxococcus xanthus DK 1622 (MXAN_1327/-/1330)
Stigmatella aurantiaca DW4_3-1 (STAUR_1954/-/1957)
Bdellovibrio bacteriovorus HD100 (Bd1478/-/1476)
Bdellovibrio bacteriovorus HD100 (Bd0832/0833/0834)
Bdellovibrio bacteriovorus HD100 (Bd0417/-/0416)
Bdellovibrio bacteriovorus HD100 (Bd2374/-/2372)
Myxococcus xanthus DK 1622 (MXAN_3374/3375/3376)
Stigmatella aurantiaca DW4_3-1 (STAUR_3840/3841/3843)
Myxococcus xanthus DK 1622 (MXAN_4870/4869/4867)
Stigmatella aurantiaca DW4_3-1 (STAUR_5656/5655/5653)
Anaeromyxobacter sp. Fw109-5 (Anae109_3386/3385/3383)
Anaeromyxobacter dehalogenans 2CP-C (Adeh_3322/3321/3319)
Anaeromyxobacter dehalogenans 2CP-1 (A2cp1_3466/3465/3463)
Anaeromyxobacter sp. K (AnaeK_3402/3401/3399)
Deltaproteobacteria
0.2
B
Plesiocystis pacifica SIR-1 (PPSIR1_36582/36577/36572)
Sorangium cellulosum So ce 56 (sce2991/2992/2993)
Haliangium ochraceum DSM 14365 (Hoch_3390/3391/3392)
Myxococcus xanthus DK 1622 (MXAN_3005/3004/3003)
Stigmatella aurantiaca DW4_3-1 (STAUR_5105/5106/5107)
Deltaproteobacteria
Fibrobacter succinogenes S85 (Fisuc_1896/-/1894)
Fibrobacteres
Bdellovibrio bacteriovorus HD100 (Bd1479/1480/1481)
Bdellovibrio bacteriovorus HD100 (Bd2375/2376/2377)
Bdellovibrio bacteriovorus HD100 (Bd0418/0419/0420)
Bdellovibrio bacteriovorus HD100 (Bd0838/0837/0836)
Sorangium cellulosum So ce 56 (sce2996//2995/2994)
Haliangium ochraceum DSM 14365 (Hoch_1807/1808/1809)
Myxococcus xanthus DK 1622 (MXAN_6860/6861/6862)
Stigmatella aurantiaca DW4_3-1 (STAUR_0996/0995/0994)
Anaeromyxobacter sp. Fw109-5 (Anae109_4453/4454/4455)
Anaeromyxobacter dehalogenans 2CP-C (Adeh_4308/4309/4310)
Anaeromyxobacter dehalogenans 2CP-1 (A2cp1_4463/4464/4465)
Anaeromyxobacter sp. K (AnaeK_4444/4445/4446)
Deltaproteobacteria
Teredinibacter turnerae T7901 (TERTU_1672/1671/1670)
Gammaproteobacteria
Methylibium petroleiphilum PM1 (Mpe_A1230/1229/1228)
Betaproteobacteria
Thioalkalivibrio sp. HL-EbGR7 (Tgr7_0537/0538/0539)
gamma proteobacterium HTCC5015 (GP5015_1416/ 1475/ 1488)
Gammaproteobacteria
Geobacter uraniireducens Rf4 (Gura_3071/3072/3073)
Geobacter sp. M18 (GM18DRAFT_3745/3744/ 3743)
Geobacter sp. M21 (GM21_0444/0443/0442)
Deltaproteobacteria
Marinobacter algicola DG893 (MDG893_06364/06359/ 06354)
Marinobacter aquaeolei VT8 (Maqu_1596/1597/1598)
Hahella chejuensis KCTC 2396 (HCH_02633/02632/02631)
Marinobacter algicola DG893 (MDG893_05354/ 05349/ 05344)
Marinobacter aquaeolei VT8 (Maqu_1808/1809/1810)
Bermanella marisrubri (RED65_05354/05349/ 05344)
Cellvibrio japonicus Ueda107 (CJA_3313/3314/3315)
Teredinibacter turnerae T7901 (TERTU_3741/3742/3743)
Saccharophagus degradans 2-40 (Sde_3561/3562/3563)
Shewanella frigidimarina NCIMB 400 (Sfri_1224/1225/1226)
Bermanella marisrubri (RED65_07489/07494/07499)
Teredinibacter turnerae T7901 (TERTU_1855/1854/1853)
Saccharophagus degradans 2-40 (Sde_2955/2956/2957)
Gammaproteobacteria
0.2

Figure 7. Co-evolution of *gltD-E-G* and *aglR-Q-S*. Rooted Bayesian phylogenetic trees of concatenated alignments of (A) GltD, GltE and GltG (39 sequences, 586 positions) and (B) AglR, AglQ and AglS (38 sequences, 376 positions). The root has been placed according to the phylogenies of the individual proteins. Numbers at nodes indicate posterior probabilities (PP) computed by MrBayes and bootstrap values (BV) computed by Treefinder and PhyML. Only PP and BV above 0.5 and 50% are shown. The scale bars represent the average number of substitutions per site. In each phylogenetic tree the putative *M. xanthus* gliding motility proteins are underlined and are illustrated with colour-coded gene symbols. For each species the individual locus_tags of the concatenated proteins are indicated in brackets. The position of multiple duplications of the concatenated proteins in *M. xanthus* are highlighted by black rectangles.
doi:10.1371/journal.pgen.1002268.g007

The *Myxococcus* gliding machinery and its distribution in bacteria

The data strongly suggest that an ancestral cluster of genes containing GltD, E, G, C and AglR, Q, S (Group B genes) evolved into a motility machinery after sequential recruitment of new components, namely GltF, H, I, J, A B and K (Group A genes). Obviously, ancient genetic linkages were lost during the evolution of the gliding machinery, explaining why it has not been previously identified and precluding the rapid identification of all the motility genes. The Agl/Glt complex is likely the gliding machinery because: (i), individual mutations of all the *aglRQS* [13] and *glt* genes resulted in complete motility defects and were not suppressed by a second-site *frz* mutation. (ii), GltD- and GltF-mCherry fusions showed similar localization patterns and localized to fixed FACs like the AglRQS proteins [13] (iii) GltD localization depended on GltF, G and H and, (iv) AglR interacted with GltG in a bacterial two-hybrid study and the localization of GltD-mCherry depended on AglQ. We thus propose that mechanical work from

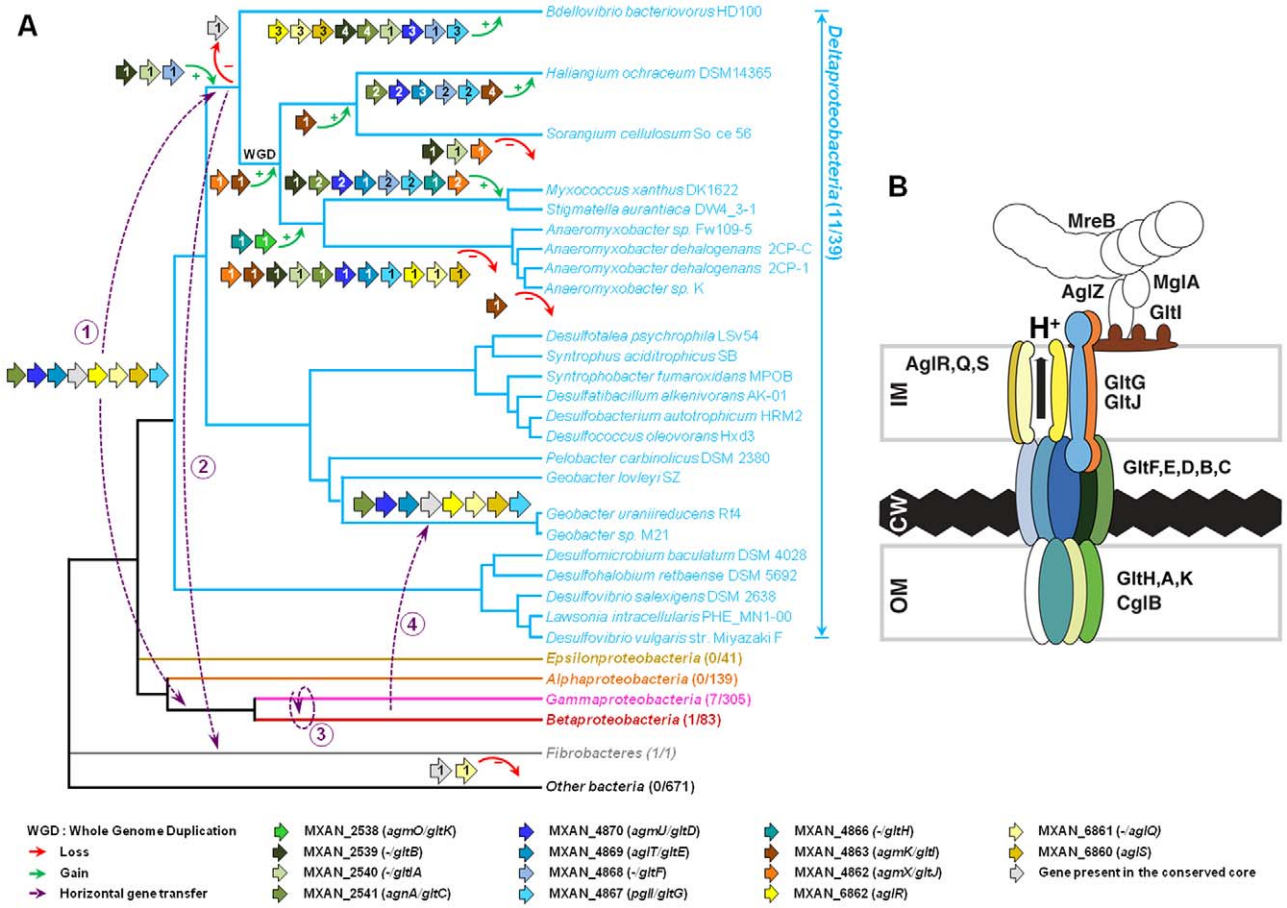

Figure 8. Evolution and structure of the *Myxococcus* gliding motility machinery. (A) Evolutionary scenario describing the emergence and evolution of the gliding motility machinery in *M. xanthus*. The relationships between organisms carrying close homologues of the 14 genes encoding putative components of the gliding machinery in *M. xanthus* are represented by the phylogeny. Green and red arrows respectively indicate gene acquisition and gene loss. The number of gene copies that were acquired or lost is indicated within arrows. The purple dotted arrows represent horizontal gene transfer events of one or several components. WGD marks the putative whole genome duplication event that occurred in the ancestor of Myxococcales. For each gene, locus_tag, former (*agm/agl/agn*) and new (*glt* and *agl*) names are provided. The number of complete genomes that contain homologues of *glt* and *agl* genes compared to the total number of complete genomes available at the beginning of this study are indicated in brackets. (B) The *Myxococcus* gliding machinery. The diagram compiles data from this work and published literature. Components were added based on bioinformatic predictions, mutagenesis, interaction and localization studies. Exhaustive information is not available for all proteins and thus the diagram largely is subject to modifications once more data will be available. Known interactions within the complex from experimental evidence are AglR-GltG, AglZ-MglA and interactions within the AglRQS molecular motor [13,15]. For clarity, the proteins were colour-coded as in the rest of the manuscript.
doi:10.1371/journal.pgen.1002268.g008

the motor is transduced to the cell surface by the Glt complex through a specific interaction with GltG. Here, we have identified a minimal motility machinery gene set, and it cannot be excluded that more Glt proteins may emerge as functional and phylogenomic approaches will be continued. For example, interaction studies identified GltD, E, I, J to be part of a complex also containing CglB and AglW [18]. The functional relevance of these interactions still needs to be demonstrated. CglB is an outer membrane motility lipoprotein [28] that harbours a very restricted taxonomy distribution, being present only in Myxococcales genomes (except the four *Anaeromyxobacter*). CglB may be a surface-exposed components of the complex. However, AglW may not be specifically linked to motility because its genomic localization and its amino acid sequence indicate that it is a *bona fide* structural component of the Tol/Pal system (TolB).

The discovery of the Agl/Glt machinery now provides a new framework to elucidate the gliding motility mechanism (Figure 8B). A low-resolution architecture of the apparatus may be suggested by the genetic/localization/interaction and bioinformatic results (Figure 8B). AglRQS and GltG may constitute an inner membrane platform (this study) linked to the MreB cytoskeleton via proteins such as AglZ and MglA [15] on the cytosolic side and anchored to the substratum by a GltA-K complex in the cell envelope (Figure 8B). Nan et al. [14] proposed that the motility complex does not traverse the peptidoglycan layer but rather deforms it, generating transverse waves propagating down the axis of the cell. While this is plausible, the finding that GltH (and also potentially GltK and GltA based on bioinformatics predictions) is a critical outer-membrane component of the machinery rather argues that the motility complex is continuous through the cell envelope and contacts the cell exterior directly. More work will be required to understand the individual functions of the Glt proteins but the identification of the machinery gene set now opens investigations to understand the motility mechanism as a whole.

Elucidating the motility mechanism may be greatly facilitated by functional studies of the core complex (*aglR, Q, S* and *gltD, E, G, C*). The conservation and genetic linkage of these genes in gammaproteobacterial genomes suggest that they encode a functional protein complex of unknown function in these bacteria. It is unlikely that the core complex drives motility on its own because gliding is not documented in most bacteria where it is found and our study shows that the corresponding genes are not sufficient to drive motility. Based on this later observation, we propose that additional functional blocks (such as Group A genes) have been added sequentially to the original protein complex to convert it into a motility machinery (Figure 8A). What are these building blocks and how many of them remain to be discovered?

A recent study unambiguously showed that *Bdellovibrio bacteriovorus* is a *bona fide* glider [29]. While we cannot definitively rule out the independent emergence of gliding motility in this bacterium, we consider it unlikely: the *Bdellovibrio* genome contains four sets of expanded core complex suggesting that the Bdellovibrionales and Myxococcales gliding apparati are linked evolutionarily. Gliding motility may thus have emerged quite early in the ancestor of the Myxococcales and the Bdellovibrionales. The absence of homologues of GltH, I, J and K, all essential gliding proteins in *Myxococcus*, in the *Bdellovibrio* genome suggests that there are species specific requirements for gliding motility (Figure S1). *Bdellovibrio* cells are unusually small (less than 1 μm in length and 0.5 in diameter *vs* > μm in length and 1 μm in diameter for *Myxococcus*), which could explain some structural differences between gliding apparati. Based on the phylogenetic analysis of the *agl* components, the genes composing the Bd0828-0838 locus appear more closely related to *aglRQS* and may therefore constitute the best candidate to encode the *Bdellovibrio* gliding apparatus (Figure 7B). The Bd0828-0838 cluster also contains many homologues of *M. xanthus* gliding genes (with the exception of *gltH, I, J* and *K*, Figure 7A and Figure S1). Based on the *Bdellovibrio* example, it is tempting to speculate that any bacterium containing AglR,Q,S, GltD, E, F, G, C, A and B is a potential glider. This is for instance the case of *Myxococcus* close relatives, *Stigmatella aurantiaca* and the four *Anaeromyxobacter* species (Figure S1).

Finally, the *M. xanthus* gliding machinery is not conserved in bacteria belonging in other phyla (e.g. Bacteroidetes or Cyanobacteria), confirming that gliding motility evolved several times independently in Bacteria, as suggested by Jarrell and McBride [8].

AglRQS/Glt-like machineries are exquisitely specialized

The presence of multiple copies of the G1, G2 and M1 clusters in Myxococcales (e.g. G3, G4, G5 and M2, in *M. xanthus* Figure 1B) likely results from duplication events. These duplications may be linked to the whole genome duplication event that occurred in the ancestor of the Myxococcales [30] and/or resulted from punctual gene-duplications during differentiation of the terminal branch of the Deltaproteobacteria. Duplications provide the raw material for the evolution of new gene functions [31,32] and, for example, several regulation networks may have emerged this way in *Myxococcus* [30]. This study shows that the G3, G4, G5 and M2 clusters cannot compensate disruptions in the *glt* and *aglRQS* genes, already suggesting that they encode distinct functions. To further test this, we generated polar mutations in all the *gltD* homologues (MXAN_1922, G4; MXAN_1327, G5 and MXAN_3374, G3) and a deletion in MXAN_3004 (M2), the *aglQ* homologue [13]. None of these mutations impacted motility at any appreciable level, (Figure S5 and [13]). If the function of the G4, G5 and M2 regions is unknown, the G3 region was recently shown to be critical for sporulation and named *nfs* (necessary for sporulation, [33]). As expected, our *nfsD* (MXAN_3374) mutant failed to mature spores (data not shown). The *nfsA-H* genes are clustered in a single genomic region containing close homologues of G1 and G2 region genes (with the exception of GltI, J and K). Strikingly, the short evolutionary distances separating the *nfs* and *glt* genes in individual gene trees and in the *glt* supermatrix indicate that the *nfsA*-H genes are in fact the closest homologues of the *glt* genes (Figure 7 and Figure S4). Thus, the Glt and Nfs systems are a clear example of exquisite machinery specialization: in these cases, the ancestral core machinery has terminally differentiated to drive sporulation or gliding motility. In absence of more mechanistic insights, it is not clear which of the two processes is the most recent but this finding points to unsuspected similarities in these two distinct morphological processes. Comparative molecular analysis of the *nsf* and *glt* systems should be powerful to understand how these machineries function and how they can be specialized to enforce sporulation or gliding.

Conclusions

In summary, the mechanism of gliding motility has remained mysterious despite three decades of research. A converging array of evidence now shows that motility is not propelled by slime secretion but results from PMF-energized trans-envelope complexes periodically distributed along the cell body (this study and [12,13,18]). However, how force is transduced from the AglRQS motor to the Glt proteins through the entire cell envelope and ultimately how that translates into motion, remains to be elucidated. The identification of the components of the gliding machinery now paves the way to address these questions. An

immediate goal will be to characterize the motility machinery in an exhaustive manner, which we should be able to resolve combining bioinformatics, genetics and cell biology. In addition, the *M. xanthus* genome contains several gene clusters deriving from the ancestral core complex, but these copies are not functionally redundant and even specify non-motility related functions (*i.e.* the sporulation *nfs* system). Thus, Glt-like systems are remarkably linked to two fundamental processes of the *Myxococcus* life cycle and their acquisition may thus have been critical to the recent diversification of the Deltaproteobacteria. In the future, comparative analysis in *M. xanthus*, but also in the Delta and Gammaproteobacteria should be a powerful approach to elucidate the pathways that led to the evolution and diversification of complex bacterial envelope machineries.

Materials and Methods

Bacterial strains, plasmids, and growth

Primers and plasmids are listed in Tables S4 and S5. See Tables S6 and S7 for strains and their mode of construction. *M. xanthus* strains were grown at 32°C in CYE rich media as previously described [23]. Plasmids were introduced in *M. xanthus* by electroporation. Mutants and transformants were obtained by homologous recombination based on a previously reported method. Complementation of *gltG* and expression of GltF-mCherry were obtained after ectopic integration of the genes of interest at the Mx8-phage attachment site in appropriate deletion backgrounds (Table S6).

For phenotypic assays, cells (10 µl), at a concentration of 4×10^9 cfu ml^{-1}, were spotted on CYE plates containing agar concentrations of 0.5% or 1.5%, incubated at 32°C and photographed after 48 h with an Olympus SZ61 binocular or a Nikon Eclipse (model TE2000E) microscope (4x objective).

mRNA extraction and QT-Reverse Transcription PCR

RNA from appropriate strains was extracted using a standard RNA purification kit (Promega). One microgram of total RNA was reverse-transcribed following the recommendations of the iScript cDNA Synthesis Kit (Bio-Rad). The resulting cDNA was then diluted (1/16), and 5 µl were used for the quantitative reverse transcription-PCR (q-RT-PCR) reaction. This step was performed on a Mastercycler ep realplex instrument (Eppendorf), using the SYBR Premix Ex Taq (Perfect Real Time) PCR kit (Takara Bio Group, Japan) according to manufacturer instructions in a final volume of 20 µl. Specific primers used for the reactions are described in Table S4. Melting curves were systematically analyzed to control for the specificity of the PCR reactions. The relative units were calculated from a standard curve plotting four different dilutions (1/80, 1/400, 1/2,000, and 1/10,000) against the PCR cycle number at which the measured fluorescence intensity reached the threshold (C_T), corresponding to ~10 times the standard deviation and thus significantly above the noise band of the baseline.

Western blotting

Western blotting was performed as previously described [34] with 1/1000-1/5000 dilutions of polyclonal α-GltD, α-GltE, α-GltG, α-GltH (all raised for this study) and α-mCherry[13], α-PilC, α-PilQ [35] and α-FrzS [36].

Preparation of cell membrane fractions and OMVs

Membrane Fractions and OMVs were purified from exponentially-growing cell cultures. Vegetative cells of *M. xanthus* were grown in CYE medium to an $OD_{600\ nm} = 0.7$. For membrane fractions, cells were harvested by centrifugation at 8.000 rpm for 10 min at RT, resuspended in 50 mM Tris-HCl pH 7.6 and lysed by sonication. Cell debris were removed by low speed centrifugation (14000 rpm). The supernatants were then centrifuged at 45,000 *g* for 1 hr at 4°C. The resulting supernatants are enriched in soluble proteins. Pellets containing the crude envelope fractions (Inner and outer membrane) were resuspended in 50 mM Tris-HCl pH 7.6 and homogenized. The quality of the fractionation procedure was tested with antibodies to FrzS (soluble protein [36]) and PilC (inner membrane protein [35]).

Standard procedures to separate the inner membrane from the outer membrane using sucrose density gradients [37] did not successfully separate the two membranes. Detergent-based methods have been used successfully in *Myxococcus*, however in our case we could not prevent rapid degradation of the Glt proteins during the separation process [35]. OMVs are largely derived from the outer membranes, which was recently confirmed by proteomic analysis of the *Myxococcus* outer-membranes [38]. Thus, to test which Glt proteins are in the outer membranes we tested their presence in purified vesicules. For OMVs purification, cells and were discarded by centrifugation (8.000 rpm for 10 min at RT) and the culture supernatant was used for the isolation of vesicles. Culture supernatants (1 L) were passed through a 0.2 µm vacuum filter (Millipore). The resulting filtrate was centrifuged at 125 000× g for 2 h at 4°C to recover membrane vesicles. The supernatant was carefully removed and the vesicle pellet was resuspended in 50 mM Tris-HCl pH 7.6 and centrifuged at 180 000× g for 2 h at 4°C to concentrate and wash vesicles. The quality of the purification procedure was tested by electron microscopy (not shown) and antibodies to PilQ (outer membrane protein [35]) and PilC (inner membrane protein [35]).

Bacterial two-hybrid experiments

Bacterial two-hybrid experiments, plate and ß-Galactosidase assays were performed as previously described [26] and as recommended by the manufacturer (Euromedex).

Time lapse video-microscopy

Time lapse experiments were performed as previously described [39]. Microscopic analysis was performed using an automated and inverted epifluorescence microscope TE2000-E-PFS (Nikon, France). The microscope is equipped with "The Perfect Focus System" (PFS) that automatically maintains focus so that the point of interest within a specimen is always kept in sharp focus at all times, in spite of any mechanical or thermal perturbations. Images were recorded with a CoolSNAP HQ 2 (Roper Scientific, Roper Scientific SARL, France) and a 40x/0.75 DLL "Plan-Apochromat" or a 100x/1.4 DLL objective. All fluorescence images were acquired with appropriate filters with a minimal exposure time to minimize bleaching and phototoxicity effects.

Cell tracking was performed automatically using a previously described macro under the METAMORPH software (Molecular devices), when appropriate, manual measurements were also performed to correct tracking errors with tools built into the software. Typically, the images were equalized, straightened and overlaid under both ImageJ 1.40 g (National Institute of Health, USA) and METAMORPH.

Annotation and mapping of gliding motility genes

The genetic screens of Youderian et al. ([16]) and Yu and Kaiser ([17]) allowed the identification of 35 and 23 potential gliding motility genes, respectively (Table S1). The function of the corresponding proteins was investigated using sequence similarity based approaches against the non-redundant (nr) database at the

National Center for Biotechnology Information (NCBI, http://www.ncbi.nlm.nih.gov/) and Pfam (release 24.0) databases ([40]). The presence and location of signal peptide signal cleavage sites and of transmembrane helix were the predicted using the signalP 3.0 server ([41]) and TMHMM server v.2.0 ([42]). Finally, the location and the neighbourhood of each gene in the chromosome of *M. xanthus* DK 1622 were investigated using the complete genome sequence available at the NCBI ([30]; CP000113).

Datasets construction

Homologues of each *M. xanthus* candidate protein were retrieved from a local database containing all complete prokaryotic proteomes available at the NCBI (April 8, 2010) using blastp with default parameters [43]. We also include in our analyses the genome sequences of *Stigmatella auriantiaca* DW4/3-1 and of *Plesiocystis pacifica* SIR-1 that came out in November 2010 and whose assembly is ongoing, respectively, both genomes being available at the NCBI. Importantly, the distinction between homologous and non-homologous sequences was assessed by visual inspection of each blastp outputs (no arbitrary cut-off on the E-value or score). To ensure the exhaustive sampling of homologues, iterative blastp queries were performed using homologues identified at each step as new seeds. PSI-BLAST queries were also used in order to recover very divergent homologues [43]. The absence of homologue in any complete proteome was systematically verified by tblastn queries against the nucleotide sequence of the corresponding genome. For each candidate protein, the retrieved homologues were gathered in a dataset. The corresponding sequences were aligned using the ClustalW2 program (Default parameters, [44]). Each alignment was visually inspected and manually refined when necessary using the ED program from the MUST package [45]. Regions where the homology between amino acid positions was doubtful were manually removed using NET from the MUST package.

Working on complete genomes may introduce major biases due to the taxonomic sampling of available complete genomes. Accordingly, for each candidate protein a second set of datasets based on homologues retrieved from the non-redundant (nr) protein database (the most exhaustive public database) at the NCBI was assembled. The taxonomic distribution and the phylogeny of homologues retrieved from either the nr database or from complete genomes showed similar patterns (data not shown). Thus, our analyses based on complete genomes are representative and reflect the taxonomic distribution of known homologues. Accordingly, only the results based on complete genomes will be presented in the results section.

The preliminary phylogenetic analyses of the candidate proteins allowed the identification of closest relatives of *M. xanthus* sequences. For each protein these homologues were gathered in a second dataset, the sequences were aligned and the resulting alignment was manually refined and cleaned like previously described. For the phylogenetic analyses of some of these datasets, we were removed some divergent sequences that can bias the phylogenetic reconstruction.

One approach to improve the resolution of the phylogenetic trees is to combine the genes that share a common evolutionary history in a single large alignment (also called supermatrix), [46–48]. Among the seven genes composing the Group B, *gltD, E* and *G* homologues are always clustered together in genomes and their individual phylogenies are very similar. Thus, these genes likely share a similar evolutionary history and can be used to build a supermatrix. For similar reasons, we combined the *aglR*, Q and S alignments in a second supermatrix. In contrast, *gltC* could neither be included in the *glt* nor in the *agl* supermatrix because it does not cluster physically with the corresponding genes in most Deltaproteobacteria. The Glt and Agl supermatrices were manually constructed by combining the cleaned alignments of GltDEG and AglQRS, respectively. When more than one homologue of these genes were present in a given genome, the genes were combined according to their physical linkage on the chromosome. For instance in the case of AglQRS, in *M. xanthus* the genes were combined as following: (i) MXAN_6860, _6861, _6862 and (ii) MXAN_3005, _3004, _3003.

Phylogenetic analyses

For each individual and concatenated alignment, both Maximum likelihood (ML) and Bayesian phylogenetic trees were computed. ML analyses were run using PHYML version 3.0 with the Le and Gascuel (LG) model (amino acid frequencies estimated from the dataset) and a gamma distribution (4 discrete categories of sites and an estimated alpha parameter) to take into account evolutionary rate variations across sites [49]. The robustness of each branch was estimated by the non-parametric bootstrap procedure implemented in PhyML (100 replicates of the original dataset with the same parameters). Additional ML analyses were performed using TreeFinder with the same parameters [50]. Bayesian analyses were performed using MrBayes [51] with a mixed model of amino acid substitution including a gamma distribution (4 discrete categories) and an estimated proportion of invariant sites. MrBayes was run with four chains for 1 million generations and trees were sampled every 100 generations. To construct the consensus tree, the first 1500 trees were discarded as "burnin".

Supporting Information

Figure S1 Genetic organization of G1, G2, and M1 gene homologues in Deltaproteobacteria, Gammaproteobacteria, Betaproteobacteria and Fibrobacteres. The legend reads as in Figure 1. Dotted lines and question marks design putative highly diverging homologues that are proposed on the base of the genomic context surveys. Locus_tags are shown for all genes.
(PDF)

Figure S2 Enhanced twitching motility in the *ΩfrzE glt* mutants. Soft-agar colony assay showing *glt*-dependent de-repression of twitching motility in the *ΩfrzE* mutant. Scale bar = 0.4 cm.
(PDF)

Figure S3 GltD-mCherry and GltF-mCherry are stably expressed. Western immunoblot using an anti-mCherry antiserum show stable expression of specific species of expected size. The arrows point to bands corresponding to the respective mCherry fusions.
(PDF)

Figure S4 Rooted Bayesian phylogenetic trees (A) of AgmU/GltD (MXAN_4870, 43 sequences, 379 positions), (B) of AglT/GltE (MXAN_4869, 37 sequences, 109 positions), (C) of PglI/GltG (MXAN_4867, 47 sequences, 78 positions), (D) of AgnA/GltC (MXAN_2541, 40 sequences, 185 positions), (E) of AglR (MXAN_6862, 38 sequences, 184 positions) and (F) of AglQ-AglS (MXAN_6861-6860, 76 sequences and 86 positions). The root has been placed accordingly to phylogenies based on whole gene families (not shown). Number at nodes indicates posterior probabilities (PP) and bootstrap support (BS) computed by Mrbayes and PhyMl, respectively. Only posterior probabilities and bootstrap values greater, respectively, than 0.5 and 50 % are shown. The scale bars represent the number of substitutions per

site. In each phylogenetic tree proteins putatively involved in gliding in *M. xanthus* are underlined.
(PDF)

Figure S5 Motility phenotypes of the ΩMxan1327, ΩMxan1922 and Ω*nsfD*. Colony edges after 48 h incubation on hard (1,5%) agar show WT gliding motility. Insets: twitching motility on soft (0,5%) agar.
(PDF)

Table S1 List of the 23 and 35 Myxococcus xanthus genes identified by two transposon mutagenesis experiments (Yo = [16]; Yu = [17]). For each gene, the locus tag in the genome of *M. xanthus*, the accession number of the corresponding protein in the ref_seq database and the original functional annotation are provided. For each protein, we indicated the presence of functional conserved domains, of signal peptide and of transmembrane domains. $ signs design false positive genes that have been removed from the current version of the *M. xanthus* genome. Asterisks correspond to the 28 genes fitting our criteria as putative components of the gliding machinery. Among them we showed that nine (in red) co-localize in three small genomic regions.
(PDF)

Table S2 List of complete genomes of Deltaproteobacteria, Gammaproteobacteria, Betaproteobacteria and Fibrobacteres carrying homologues of the 14 candidates genes coding for the gliding machinery in *M. xanthus*. For each genome, the accession number in the nucleic ref_seq and in the GenBank databases, the size (in megabases) and the release date are provided.
(PDF)

Table S3 Exhaustive list of the homologues of the genes of the G1, G2 and M1 clusters found in complete genomes listed in Table S2. For each gene, the locus_tag, and the accession number, the length and the functional annotation of the corresponding proteins according to the ref_seq database are provided.
(PDF)

Table S4 Primers.
(PDF)

Table S5 Plasmids.
(PDF)

Table S6 *Myxococcus* strains.
(PDF)

Table S7 Plasmid constructions.
(PDF)

Text S1 MXAN4864 and MXAN4865 may not be actual motility genes.
(DOCX)

Text S2 Justification for a *glt* nomenclature of the gliding motility machinery genes.
(DOCX)

Text S3 Principle of the phylogenomic analysis.
(DOCX)

Video S1 "Jerky" motility phenotype of *gltH* mutant cells.
(MOV)

Video S2 Localization of GltD-mCherry in differents *z*-planes. Le bar within the circle indicates the positions of the respective focal planes relative to the short axis of the cell.
(AVI)

Acknowledgments

We would like to thank Iryna Bulyha and Lotte Søgaard Andersen for the gift of the anti-PilC and PilQ antibodies as well as for help with the fractionation procedure. We thank Beiyan Nan and David Zusman for the GltD-mCherry-expressing strain. We also thank Véronique Viarre and Romé Voulhoux for help with the sucrose density gradients. Jean Raphaël Fantino is thanked for his help with the QT-PCR. Jennifer Spagnolo is acknowledged for the construction of the ΩMXAN_1922 and Ω*nfsD* mutants. We thank Anne-Lise Ducluzeau for many discussions and preliminary analysis of the *glt* genes. We thank Céline Petitjean, Laura Eme, Mireille Ansaldi, Patrick Morton, and Joshua Shaevitz for discussions and critical reading of the manuscript. We also thank Rémi Planel for his technical assistance.

Author Contributions

Conceived and designed the experiments: JL RA CB-A TM MW. Performed the experiments: JL RA AD AVLG FF MW. Analyzed the data: JL RA AD FF CB-A TM MW. Wrote the paper: JL RA CB-A TM.

References

1. Rego AT, Fronzes R, Waksman G (2010) SnapShot: Bacterial Appendages I. Cell 140: 162–162.e1. doi:10.1016/j.cell.2009.12.047.
2. Rego AT, Fronzes R, Waksman G (2010) SnapShot: Bacterial appendages II. Cell 140: 294–294.e1. doi:10.1016/j.cell.2010.01.006.
3. Erhardt M, Namba K, Hughes KT (2010) Bacterial nanomachines: the flagellum and type III injectisome. Cold Spring Harb Perspect Biol 2: a000299. doi:10.1101/cshperspect.a000299.
4. Pallen MJ, Matzke NJ (2006) From The Origin of Species to the origin of bacterial flagella. Nat. Rev. Microbiol 4: 784–790. doi:10.1038/nrmicro1493.
5. Merz AJ, So M, Sheetz MP (2000) Pilus retraction powers bacterial twitching motility. Nature 407: 98–102. doi:10.1038/35024105.
6. Skerker JM, Prasol MS, Perchuk BS, Biondi EG, Laub MT (2005) Two-component signal transduction pathways regulating growth and cell cycle progression in a bacterium: a system-level analysis. PLoS Biol 3: e334. doi:10.1371/journal.pbio.0030334.
7. Pelicic V (2008) Type IV pili: e pluribus unum? Mol. Microbiol 68: 827–837. doi:10.1111/j.1365-2958.2008.06197.x.
8. Jarrell KF, McBride MJ (2008) The surprisingly diverse ways that prokaryotes move. Nat. Rev. Microbiol 6: 466–476. doi:10.1038/nrmicro1900.
9. Mignot T (2007) The elusive engine in Myxococcus xanthus gliding motility. Cell. Mol. Life Sci 64: 2733–2745. doi:10.1007/s00018-007-7176-x.
10. Sato K, Naito M, Yukitake H, Hirakawa H, Shoji M, et al. (2010) A protein secretion system linked to bacteroidete gliding motility and pathogenesis. Proc. Natl Acad Sci U S A 107: 276–281. doi:10.1073/pnas.0912010107.
11. Mauriello EMF, Mignot T, Yang Z, Zusman DR (2010) Gliding motility revisited: how do the myxobacteria move without flagella? Microbiol. Mol. Biol. Rev 74: 229–249. doi:10.1128/MMBR.00043-09.
12. Mignot T, Shaevitz JW, Hartzell PL, Zusman DR (2007) Evidence that focal adhesion complexes power bacterial gliding motility. Science 315: 853–856. doi:10.1126/science.1137223.
13. Sun M, Wartel M, Cascales E, Shaevitz JW, Mignot T (2011) Motor-driven intracellular transport powers bacterial gliding motility. Proc. Natl Acad Sci. U.S.A, 108: 7559–7564. doi:10.1073/pnas.1101101108.
14. Nan B, Chen J, Neu JC, Berry RM, Oster G, et al. (2011) Myxobacteria gliding motility requires cytoskeleton rotation powered by proton motive force. Proc Natl Acad Sci. U.S.A, 108: 2498–2503. doi:10.1073/pnas.1018556108.
15. Mauriello EMF, Mouhamar F, Nan B, Ducret A, Dai D, et al. (2010) Bacterial motility complexes require the actin-like protein, MreB and the Ras homologue, MglA. EMBO J 29: 315–326. doi:10.1038/emboj.2009.356.
16. Youderian P, Burke N, White DJ, Hartzell PL (2003) Identification of genes required for adventurous gliding motility in Myxococcus xanthus with the transposable element mariner. Mol. Microbiol 49: 555–570.
17. Yu R, Kaiser D (2007) Gliding motility and polarized slime secretion. Mol. Microbiol 63: 454–467. doi:10.1111/j.1365-2958.2006.05536.x.
18. Nan B, Mauriello EMF, Sun I-H, Wong A, Zusman DR (2010) A multi-protein complex from Myxococcus xanthus required for bacterial gliding motility. Mol. Microbiol 76: 1539–1554. doi:10.1111/j.1365-2958.2010.07184.x.
19. Yeh Y-C, Comolli LR, Downing KH, Shapiro L, McAdams HH (2010) The caulobacter Tol-Pal complex is essential for outer membrane integrity and the positioning of a polar localization factor. J Bacteriol 192: 4847–4858. doi:10.1128/JB.00607-10.
20. Lloubès R, Cascales E, Walburger A, Bouveret E, Lazdunski C, et al. (2001) The Tol-Pal proteins of the Escherichia coli cell envelope: an energized system required for outer membrane integrity? Res. Microbiol 152: 523–529.

21. Blatch GL, Lässle M (1999) The tetratricopeptide repeat: a structural motif mediating protein-protein interactions. Bioessays 21: 932–939. doi:10.1002/(SICI)1521-1878(199911)21:11<932::AID-BIES5>3.0.CO;2-N.
22. Hammet A, Pike BL, McNees CJ, Conlan LA, Tenis N, et al. (2003) FHA domains as phospho-threonine binding modules in cell signaling. IUBMB Life 55: 23–27. doi:10.1080/1521654031000070636.
23. Bustamante VH, Martínez-Flores I, Vlamakis HC, Zusman DR (2004) Analysis of the Frz signal transduction system of Myxococcus xanthus shows the importance of the conserved C-terminal region of the cytoplasmic chemoreceptor FrzCD in sensing signals. Mol. Microbiol 53: 1501–1513. doi:10.1111/j.1365-2958.2004.04221.x.
24. Mauriello EMF, Nan B, Zusman DR (2009) AglZ regulates adventurous (A-) motility in Myxococcus xanthus through its interaction with the cytoplasmic receptor, FrzCD. Mol. Microbiol 72: 964–977. doi:10.1111/j.1365-2958.2009.06697.x.
25. Goemaere EL, Cascales E, Lloubès R (2007) Mutational analyses define helix organization and key residues of a bacterial membrane energy-transducing complex. J. Mol. Biol 366: 1424–1436. doi:10.1016/j.jmb.2006.12.020.
26. Karimova G, Pidoux J, Ullmann A, Ladant D (1998) A bacterial two-hybrid system based on a reconstituted signal transduction pathway. Proc Natl Acad Sci. , U.S.A, 95: 5752–5756.
27. Krieg NR, Ludwig W, Whitman WB, Hedlung BP Paster BJ, et al. (2011) Bergey's Manual of Systematic Bacteriology. Dans. 948 p.
28. Nudleman E, Wall D, Kaiser D (2005) Cell-to-cell transfer of bacterial outer membrane lipoproteins. Science 309: 125–127. doi:10.1126/science.1112440.
29. Lambert C, Fenton AK, Hobley L, Sockett RE (2011) Predatory bdellovibrio bacteria use gliding motility to scout for prey on surfaces. J Bacteriol 193: 3139–3141. doi:10.1128/JB.00224-11.
30. Goldman BS, Nierman WC, Kaiser D, Slater SC, Durkin AS, et al. (2006) Evolution of sensory complexity recorded in a myxobacterial genome. Proc Natl Acad Sci. U.S.A, 103: 15200–15205. doi:10.1073/pnas.0607335103.
31. Sémon M, Wolfe KH (2007) Consequences of genome duplication. Curr. Opin. Genet. Dev 17: 505–512. doi:10.1016/j.gde.2007.09.007.
32. Van de Peer Y, Maere S, Meyer A (2009) The evolutionary significance of ancient genome duplications. Nat. Rev. Genet 10: 725–732. doi:10.1038/nrg2600.
33. Müller F-D, Treuner-Lange A, Heider J, Huntley SM, Higgs PI (2010) Global transcriptome analysis of spore formation in Myxococcus xanthus reveals a locus necessary for cell differentiation. BMC Genomics 11: 264. doi:10.1186/1471-2164-11-264.
34. Zhang Y, Franco M, Ducret A, Mignot T (2010) A bacterial Ras-like small GTP-binding protein and its cognate GAP establish a dynamic spatial polarity axis to control directed motility. PLoS Biol 8: e1000430. doi:10.1371/journal.pbio.1000430.
35. Bulyha I, Schmidt C, Lenz P, Jakovljevic V, Höne A, et al. (2009) Regulation of the type IV pili molecular machine by dynamic localization of two motor proteins. Mol. Microbiol 74: 691–706. doi:10.1111/j.1365-2958.2009.06891.x.
36. Mignot T, Merlie JP Jr., Zusman DR (2005) Regulated pole-to-pole oscillations of a bacterial gliding motility protein. Science 310: 855–857. doi:10.1126/science.1119052.
37. Viarre V, Cascales E, Ball G, Michel GPF, Filloux A, et al. (2009) HxcQ liposecretin is self-piloted to the outer membrane by its N-terminal lipid anchor. J. Biol. Chem 284: 33815–33823. doi:10.1074/jbc.M109.065938.
38. Kahnt J, Aguiluz K, Koch J, Treuner-Lange A, Konovalova A, et al. (2010) Profiling the outer membrane proteome during growth and development of the social bacterium Myxococcus xanthus by selective biotinylation and analyses of outer membrane vesicles. J Proteome Res 9: 5197–5208. doi:10.1021/pr1004983.
39. Ducret A, Maisonneuve E, Notareschi P, Grossi A, Mignot T, et al. (2009) A microscope automated fluidic system to study bacterial processes in real time. PLoS ONE 4: e7282. doi:10.1371/journal.pone.0007282.
40. Finn RD, Mistry J, Tate J, Coggill P, Heger A, et al. (2010) The Pfam protein families database. Nucleic Acids Res 38: D211–222. doi:10.1093/nar/gkp985.
41. Bendtsen JD, Nielsen H, von Heijne G, Brunak S (2004) Improved prediction of signal peptides: SignalP 3.0. J. Mol. Biol 340: 783–795. doi:10.1016/j.jmb.2004.05.028.
42. Krogh A, Larsson B, von Heijne G, Sonnhammer EL (2001) Predicting transmembrane protein topology with a hidden Markov model: application to complete genomes. J Mol Biol 305: 567–580. doi:10.1006/jmbi.2000.4315.
43. Altschul SF, Madden TL, Schäffer AA, Zhang J, Zhang Z, et al. (1997) Gapped BLAST and PSI-BLAST: a new generation of protein database search programs. Nucleic Acids Res 25: 3389–3402.
44. Larkin MA, Blackshields G, Brown NP, Chenna R, McGettigan PA, et al. (2007) Clustal W and Clustal X version 2.0. Bioinformatics 23: 2947–2948. doi:10.1093/bioinformatics/btm404.
45. Philippe H (1993) MUST, a computer package of Management Utilities for Sequences and Trees. Nucleic Acids Res 21: 5264–5272.
46. Brown JR, Douady CJ, Italia MJ, Marshall WE, Stanhope MJ (2001) Universal trees based on large combined protein sequence data sets. Nat. Genet 28: 281–285. doi:10.1038/90129.
47. Brochier C, Bapteste E, Moreira D, Philippe H (2002) Eubacterial phylogeny based on translational apparatus proteins. Trends Genet 18: 1–5.
48. Delsuc F, Brinkmann H, Philippe H (2005) Phylogenomics and the reconstruction of the tree of life. Nat. Rev. Genet 6: 361–375. doi:10.1038/nrg1603.
49. Guindon S, Gascuel O (2003) A simple, fast, and accurate algorithm to estimate large phylogenies by maximum likelihood. Syst. Biol 52: 696–704.
50. Jobb G, von Haeseler A, Strimmer K (2004) TREEFINDER: a powerful graphical analysis environment for molecular phylogenetics. BMC Evol. Biol 4: 18. doi:10.1186/1471-2148-4-18.
51. Huelsenbeck JP, Ronquist F (2001) MRBAYES: Bayesian inference of phylogenetic trees. Bioinformatics 17: 754–755.

Figure S1

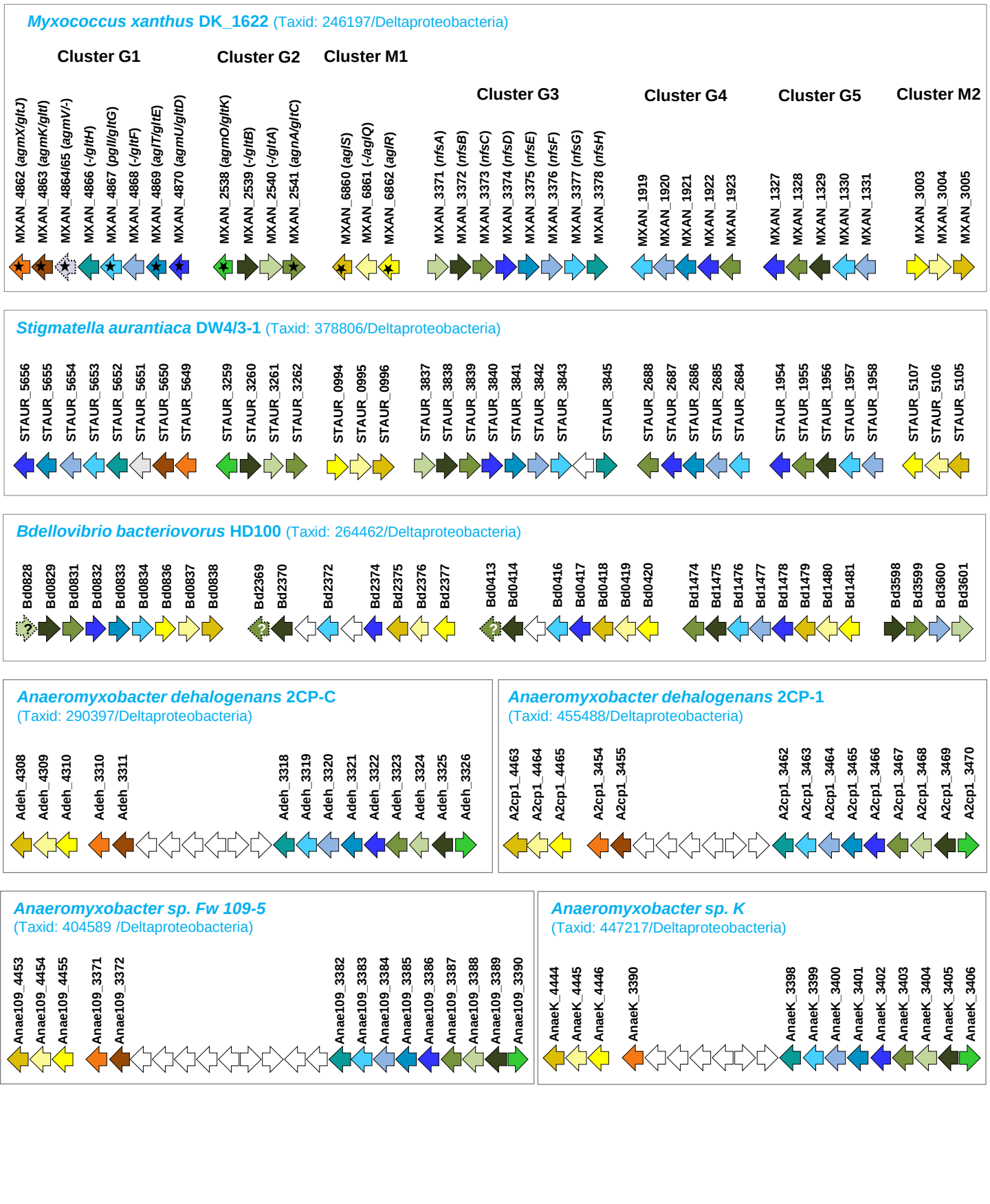
Myxococcus xanthus DK_1622 (Taxid: 246197/Deltaproteobacteria)
Cluster G1
Cluster G2
Cluster M1
Cluster G3
Cluster G4
Cluster G5
Cluster M2
MXAN_4862 (agmX/gltJ)
MXAN_4863 (agmK/gltI)
MXAN_4864/65 (agmV/-)
MXAN_4866 (-/gltH)
MXAN_4867 (pglI/gltG)
MXAN_4868 (-/gltF)
MXAN_4869 (aglT/gltE)
MXAN_4870 (agmU/gltD)
MXAN_2538 (agmO/gltK)
MXAN_2539 (-/gltB)
MXAN_2540 (-/gltA)
MXAN_2541 (agnA/gltC)
MXAN_6860 (aglS)
MXAN_6861 (-/aglQ)
MXAN_6862 (aglR)
MXAN_3371 (nfsA)
MXAN_3372 (nfsB)
MXAN_3373 (nfsC)
MXAN_3374 (nfsD)
MXAN_3375 (nfsE)
MXAN_3376 (nfsF)
MXAN_3377 (nfsG)
MXAN_3378 (nfsH)
MXAN_1919
MXAN_1920
MXAN_1921
MXAN_1922
MXAN_1923
MXAN_1327
MXAN_1328
MXAN_1329
MXAN_1330
MXAN_1331
MXAN_3003
MXAN_3004
MXAN_3005
Stigmatella aurantiaca DW4/3-1 (Taxid: 378806/Deltaproteobacteria)
STAUR_5656
STAUR_5655
STAUR_5654
STAUR_5653
STAUR_5652
STAUR_5651
STAUR_5650
STAUR_5649
STAUR_3259
STAUR_3260
STAUR_3261
STAUR_3262
STAUR_0994
STAUR_0995
STAUR_0996
STAUR_3837
STAUR_3838
STAUR_3839
STAUR_3840
STAUR_3841
STAUR_3842
STAUR_3843
STAUR_3845
STAUR_2688
STAUR_2687
STAUR_2686
STAUR_2685
STAUR_2684
STAUR_1954
STAUR_1955
STAUR_1956
STAUR_1957
STAUR_1958
STAUR_5107
STAUR_5106
STAUR_5105
Bdellovibrio bacteriovorus HD100 (Taxid: 264462/Deltaproteobacteria)
Bd0828
Bd0829
Bd0831
Bd0832
Bd0833
Bd0834
Bd0836
Bd0837
Bd0838
Bd2369
Bd2370
Bd2372
Bd2374
Bd2375
Bd2376
Bd2377
Bd0413
Bd0414
Bd0416
Bd0417
Bd0418
Bd0419
Bd0420
Bd1474
Bd1475
Bd1476
Bd1477
Bd1478
Bd1479
Bd1480
Bd1481
Bd3598
Bd3599
Bd3600
Bd3601
Anaeromyxobacter dehalogenans 2CP-C
(Taxid: 290397/Deltaproteobacteria)
Adeh_4308
Adeh_4309
Adeh_4310
Adeh_3310
Adeh_3311
Adeh_3318
Adeh_3319
Adeh_3320
Adeh_3321
Adeh_3322
Adeh_3323
Adeh_3324
Adeh_3325
Adeh_3326
Anaeromyxobacter dehalogenans 2CP-1
(Taxid: 455488/Deltaproteobacteria)
A2cp1_4463
A2cp1_4464
A2cp1_4465
A2cp1_3454
A2cp1_3455
A2cp1_3462
A2cp1_3463
A2cp1_3464
A2cp1_3465
A2cp1_3466
A2cp1_3467
A2cp1_3468
A2cp1_3469
A2cp1_3470
Anaeromyxobacter sp. Fw 109-5
(Taxid: 404589 /Deltaproteobacteria)
Anae109_4453
Anae109_4454
Anae109_4455
Anae109_3371
Anae109_3372
Anae109_3382
Anae109_3383
Anae109_3384
Anae109_3385
Anae109_3386
Anae109_3387
Anae109_3388
Anae109_3389
Anae109_3390
Anaeromyxobacter sp. K
(Taxid: 447217/Deltaproteobacteria)
AnaeK_4444
AnaeK_4445
AnaeK_4446
AnaeK_3390
AnaeK_3398
AnaeK_3399
AnaeK_3400
AnaeK_3401
AnaeK_3402
AnaeK_3403
AnaeK_3404
AnaeK_3405
AnaeK_3406

***Geobacter uraniireducens* Rf4**
(Taxid: 351605/Deltaproteobacteria)

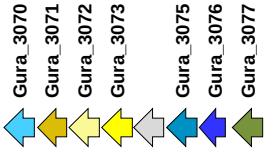

***Geobacter sp.* M21**
(Taxid: 443144/Deltaproteobacteria)

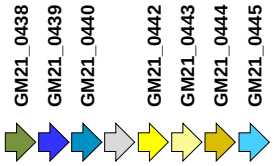

***Fibrobacter succinogenes* S85**
(Taxid:59374/Fibrobacteres)

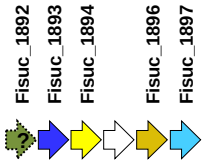

***Haliangium ochraceum* DSM 14365** (Taxid: 502025/Gammaproteobacteria)

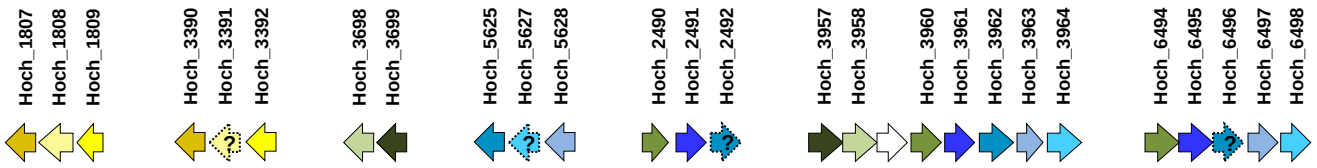

***Sorangium cellulosum* Soce56** (Taxid: 448385/Deltaproteobacteria)

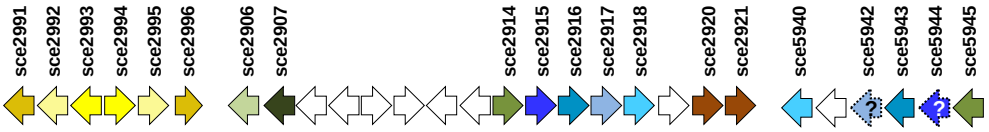

***Thioalkalivibrio sp.* HL-EbGR7**
(Taxid: 396588/Gammaproteobacteria)

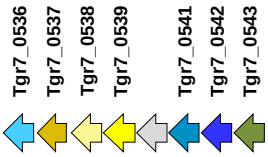

***Teredinibacter turnerae* T7901** (Taxid: 377629/Gammaproteobacteria)

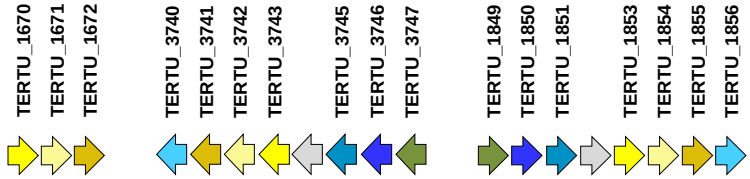

***Sccharophagus degradans* 2-40**
(Taxid: 203122/Gammaproteobacteria)

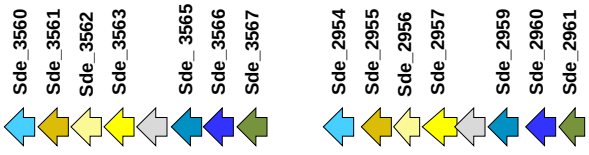

***Hahella chejuensis* KCTC 2396**
(Taxid: 349521/Gammaproteobacteria)

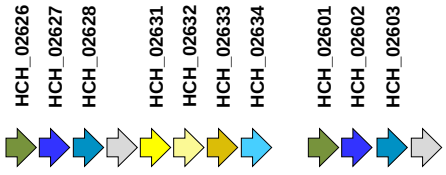

***Cellvibrio japonicus* Ueda107**
(Taxid:498211/Gammaproteobacteria)

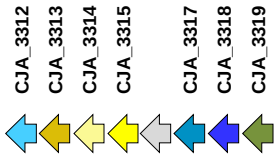

***Shewanella frigidimarina* NCIMB 400**
(Taxid: 318167/Gammaproteobacteria)

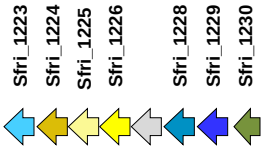

***Marinobacter aquaeolei* VT8** (Taxid: 351348/Gammaproteobacteria)

***Methylibium petroleiphilum* PM1**
(Taxid: 420662/Betaproteobacteria)

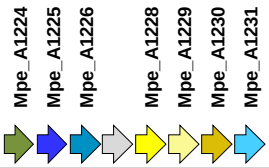

Figure S2

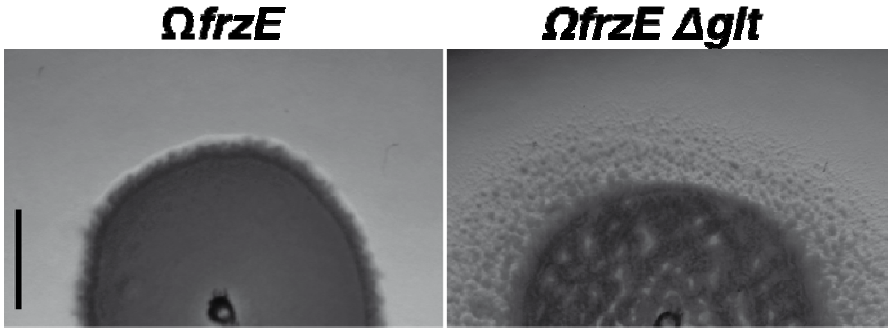

Figure S3

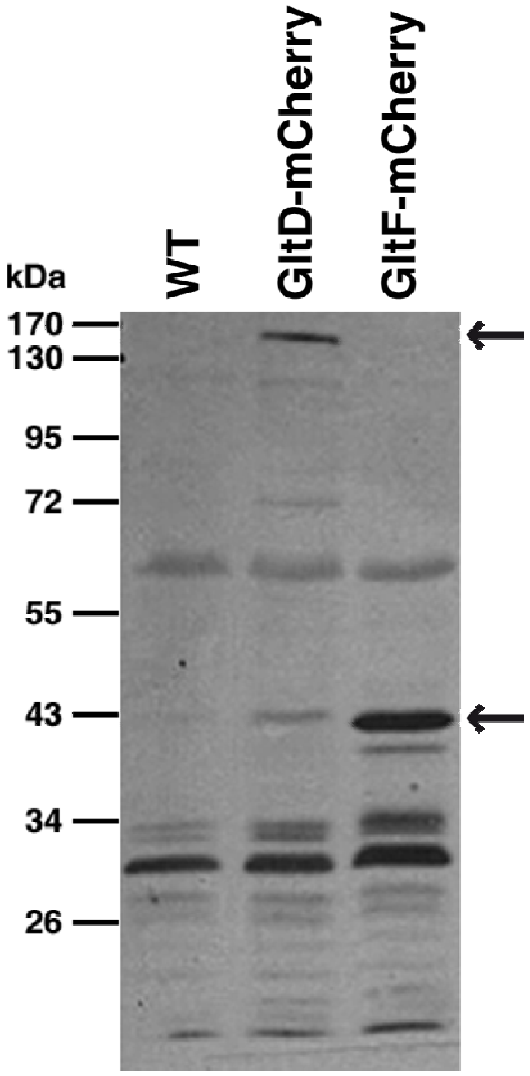

Figure S4

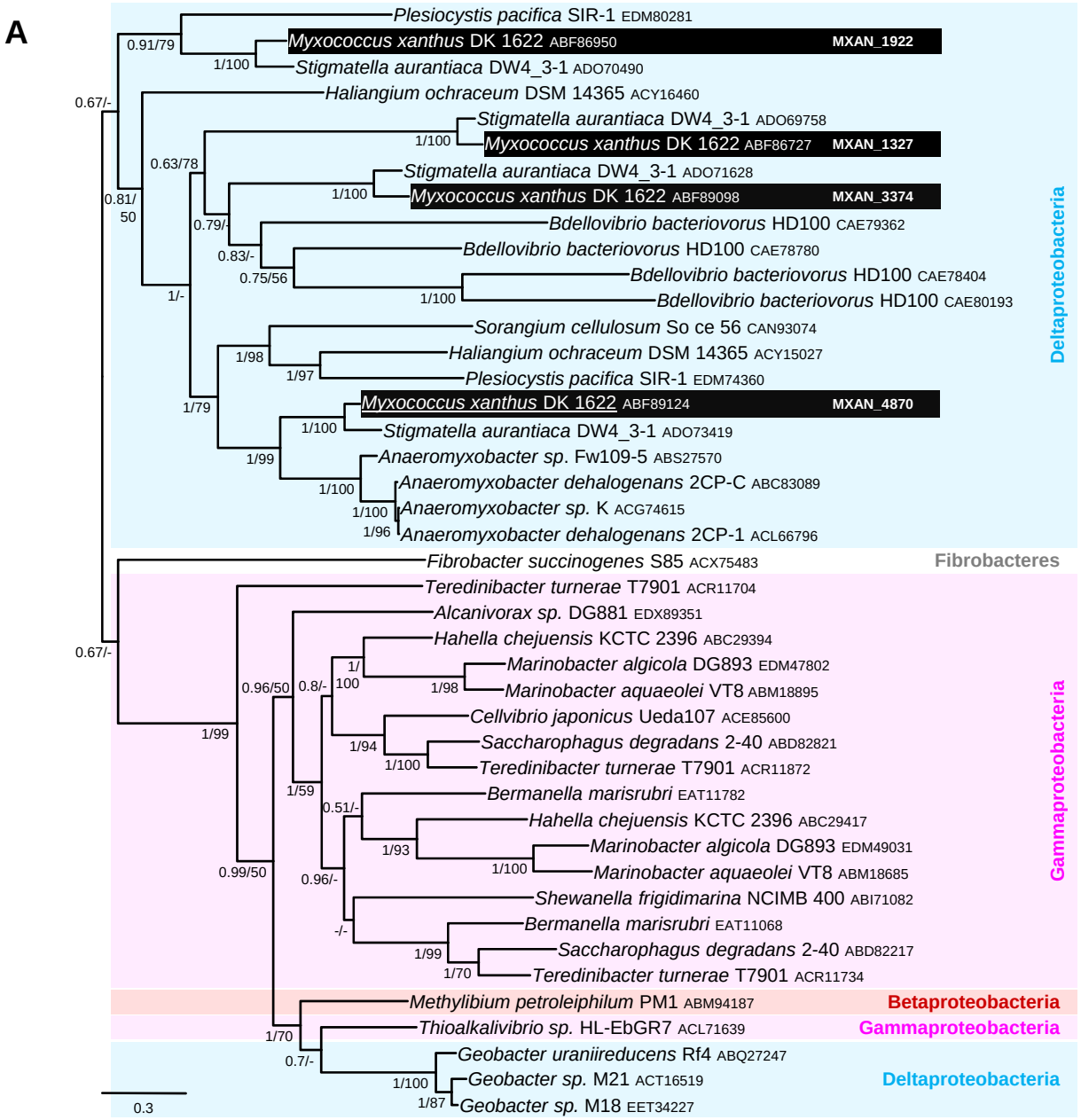
A
Plesiocystis pacifica SIR-1 EDM80281
Myxococcus xanthus DK 1622 ABF86950 MXAN_1922
Stigmatella aurantiaca DW4_3-1 ADO70490
Haliangium ochraceum DSM 14365 ACY16460
Stigmatella aurantiaca DW4_3-1 ADO69758
Myxococcus xanthus DK 1622 ABF86727 MXAN_1327
Stigmatella aurantiaca DW4_3-1 ADO71628
Myxococcus xanthus DK 1622 ABF89098 MXAN_3374
Bdellovibrio bacteriovorus HD100 CAE79362
Bdellovibrio bacteriovorus HD100 CAE78780
Bdellovibrio bacteriovorus HD100 CAE78404
Bdellovibrio bacteriovorus HD100 CAE80193
Sorangium cellulosum So ce 56 CAN93074
Haliangium ochraceum DSM 14365 ACY15027
Plesiocystis pacifica SIR-1 EDM74360
Myxococcus xanthus DK 1622 ABF89124 MXAN_4870
Stigmatella aurantiaca DW4_3-1 ADO73419
Anaeromyxobacter sp. Fw109-5 ABS27570
Anaeromyxobacter dehalogenans 2CP-C ABC83089
Anaeromyxobacter sp. K ACG74615
Anaeromyxobacter dehalogenans 2CP-1 ACL66796
Deltaproteobacteria
Fibrobacter succinogenes S85 ACX75483
Fibrobacteres
Teredinibacter turnerae T7901 ACR11704
Alcanivorax sp. DG881 EDX89351
Hahella chejuensis KCTC 2396 ABC29394
Marinobacter algicola DG893 EDM47802
Marinobacter aquaeolei VT8 ABM18895
Cellvibrio japonicus Ueda107 ACE85600
Saccharophagus degradans 2-40 ABD82821
Teredinibacter turnerae T7901 ACR11872
Bermanella marisrubri EAT11782
Hahella chejuensis KCTC 2396 ABC29417
Marinobacter algicola DG893 EDM49031
Marinobacter aquaeolei VT8 ABM18685
Shewanella frigidimarina NCIMB 400 ABI71082
Bermanella marisrubri EAT11068
Saccharophagus degradans 2-40 ABD82217
Teredinibacter turnerae T7901 ACR11734
Gammaproteobacteria
Methylibium petroleiphilum PM1 ABM94187
Betaproteobacteria
Thioalkalivibrio sp. HL-EbGR7 ACL71639
Gammaproteobacteria
Geobacter uraniireducens Rf4 ABQ27247
Geobacter sp. M21 ACT16519
Geobacter sp. M18 EET34227
Deltaproteobacteria
0.3

B

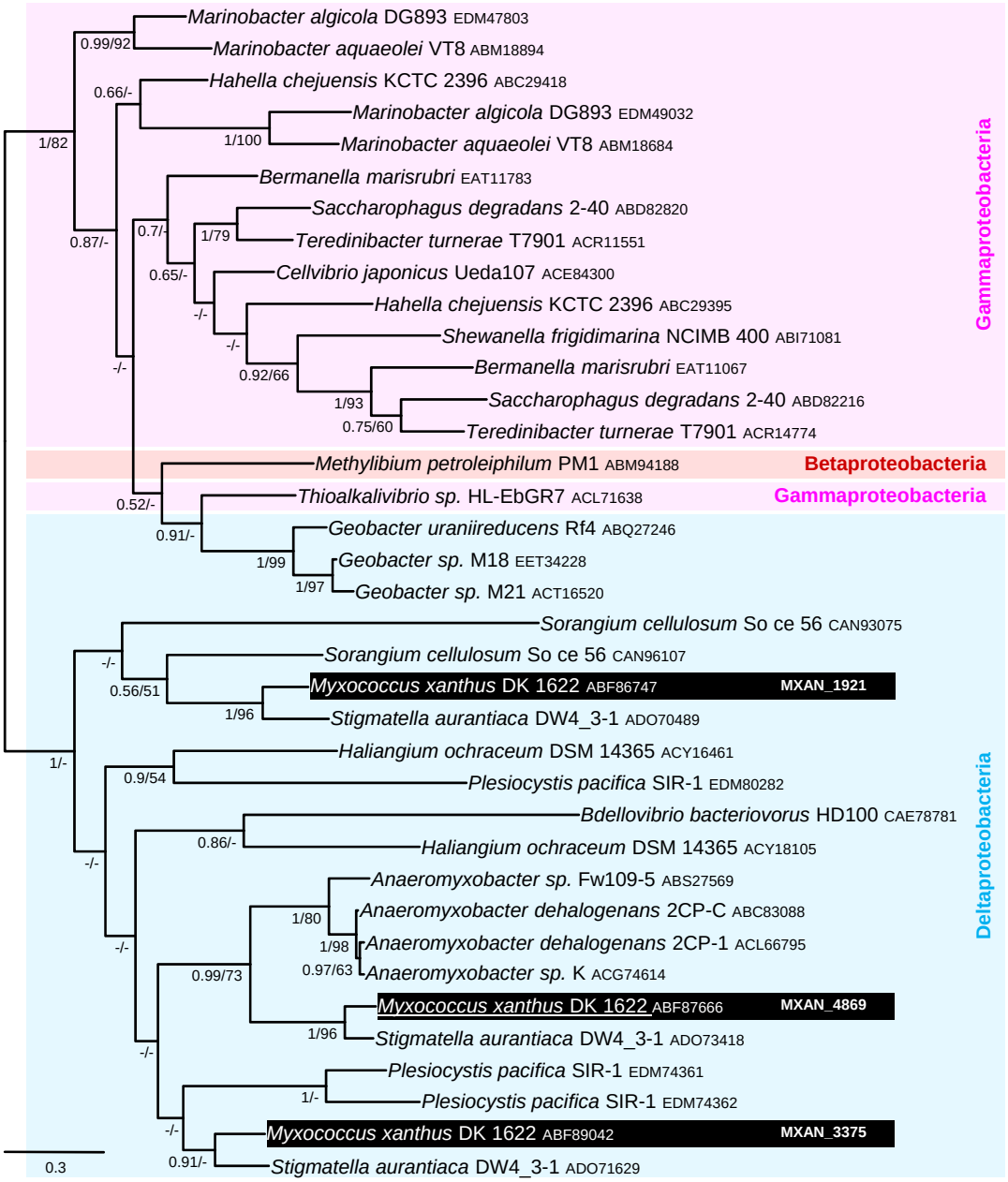
Marinobacter algicola DG893 EDM47803
Marinobacter aquaeolei VT8 ABM18894
Hahella chejuensis KCTC 2396 ABC29418
Marinobacter algicola DG893 EDM49032
Marinobacter aquaeolei VT8 ABM18684
Bermanella marisrubri EAT11783
Saccharophagus degradans 2-40 ABD82820
Teredinibacter turnerae T7901 ACR11551
Cellvibrio japonicus Ueda107 ACE84300
Hahella chejuensis KCTC 2396 ABC29395
Shewanella frigidimarina NCIMB 400 ABI71081
Bermanella marisrubri EAT11067
Saccharophagus degradans 2-40 ABD82216
Teredinibacter turnerae T7901 ACR14774
Gammaproteobacteria
Methylibium petroleiphilum PM1 ABM94188
Betaproteobacteria
Thioalkalivibrio sp. HL-EbGR7 ACL71638
Gammaproteobacteria
Geobacter uraniireducens Rf4 ABQ27246
Geobacter sp. M18 EET34228
Geobacter sp. M21 ACT16520
Sorangium cellulosum So ce 56 CAN93075
Sorangium cellulosum So ce 56 CAN96107
Myxococcus xanthus DK 1622 ABF86747
MXAN_1921
Stigmatella aurantiaca DW4_3-1 ADO70489
Haliangium ochraceum DSM 14365 ACY16461
Plesiocystis pacifica SIR-1 EDM80282
Bdellovibrio bacteriovorus HD100 CAE78781
Haliangium ochraceum DSM 14365 ACY18105
Anaeromyxobacter sp. Fw109-5 ABS27569
Anaeromyxobacter dehalogenans 2CP-C ABC83088
Anaeromyxobacter dehalogenans 2CP-1 ACL66795
Anaeromyxobacter sp. K ACG74614
Myxococcus xanthus DK 1622 ABF87666
MXAN_4869
Stigmatella aurantiaca DW4_3-1 ADO73418
Plesiocystis pacifica SIR-1 EDM74361
Plesiocystis pacifica SIR-1 EDM74362
Myxococcus xanthus DK 1622 ABF89042
MXAN_3375
Stigmatella aurantiaca DW4_3-1 ADO71629
Deltaproteobacteria
0.3

C

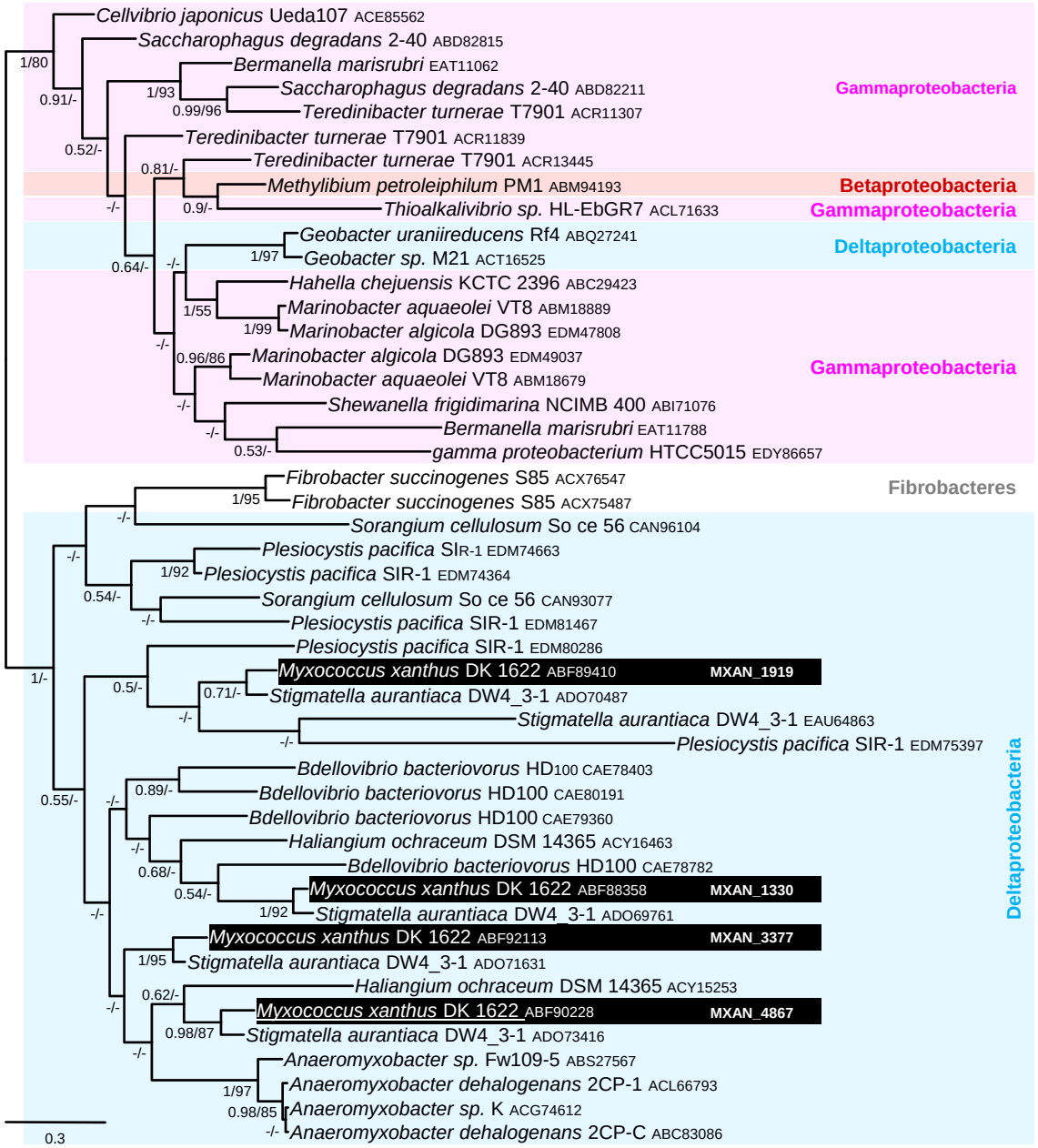
Cellvibrio japonicus Ueda107 ACE85562
Saccharophagus degradans 2-40 ABD82815
Bermanella marisrubri EAT11062
Saccharophagus degradans 2-40 ABD82211
Teredinibacter turnerae T7901 ACR11307
Teredinibacter turnerae T7901 ACR11839
Teredinibacter turnerae T7901 ACR13445
Methylibium petroleiphilum PM1 ABM94193
Thioalkalivibrio sp. HL-EbGR7 ACL71633
Geobacter uraniireducens Rf4 ABQ27241
Geobacter sp. M21 ACT16525
Hahella chejuensis KCTC 2396 ABC29423
Marinobacter aquaeolei VT8 ABM18889
Marinobacter algicola DG893 EDM47808
Marinobacter algicola DG893 EDM49037
Marinobacter aquaeolei VT8 ABM18679
Shewanella frigidimarina NCIMB 400 ABI71076
Bermanella marisrubri EAT11788
gamma proteobacterium HTCC5015 EDY86657
Gammaproteobacteria
Betaproteobacteria
Gammaproteobacteria
Deltaproteobacteria
Gammaproteobacteria
Fibrobacter succinogenes S85 ACX76547
Fibrobacter succinogenes S85 ACX75487
Sorangium cellulosum So ce 56 CAN96104
Plesiocystis pacifica SIR-1 EDM74663
Plesiocystis pacifica SIR-1 EDM74364
Sorangium cellulosum So ce 56 CAN93077
Plesiocystis pacifica SIR-1 EDM81467
Plesiocystis pacifica SIR-1 EDM80286
Myxococcus xanthus DK 1622 ABF89410 MXAN_1919
Stigmatella aurantiaca DW4_3-1 ADO70487
Stigmatella aurantiaca DW4_3-1 EAU64863
Plesiocystis pacifica SIR-1 EDM75397
Bdellovibrio bacteriovorus HD100 CAE78403
Bdellovibrio bacteriovorus HD100 CAE80191
Bdellovibrio bacteriovorus HD100 CAE79360
Haliangium ochraceum DSM 14365 ACY16463
Bdellovibrio bacteriovorus HD100 CAE78782
Myxococcus xanthus DK 1622 ABF88358 MXAN_1330
Stigmatella aurantiaca DW4_3-1 ADO69761
Myxococcus xanthus DK 1622 ABF92113 MXAN_3377
Stigmatella aurantiaca DW4_3-1 ADO71631
Haliangium ochraceum DSM 14365 ACY15253
Myxococcus xanthus DK 1622 ABF90228 MXAN_4867
Stigmatella aurantiaca DW4_3-1 ADO73416
Anaeromyxobacter sp. Fw109-5 ABS27567
Anaeromyxobacter dehalogenans 2CP-1 ACL66793
Anaeromyxobacter sp. K ACG74612
Anaeromyxobacter dehalogenans 2CP-C ABC83086
Fibrobacteres
Deltaproteobacteria
0.3

D

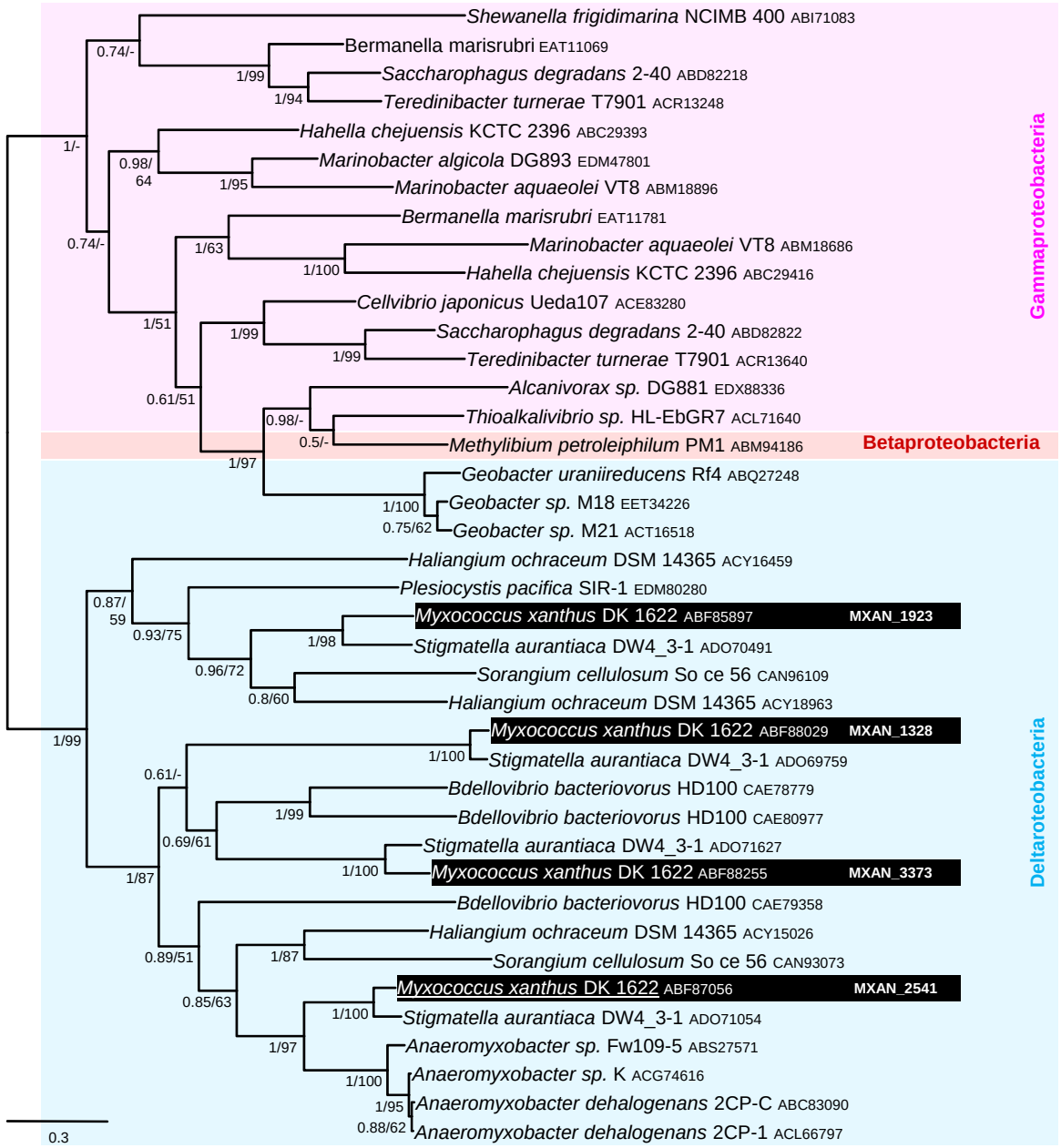
Shewanella frigidimarina NCIMB 400 ABI71083
Bermanella marisrubri EAT11069
Saccharophagus degradans 2-40 ABD82218
Teredinibacter turnerae T7901 ACR13248
Hahella chejuensis KCTC 2396 ABC29393
Marinobacter algicola DG893 EDM47801
Marinobacter aquaeolei VT8 ABM18896
Bermanella marisrubri EAT11781
Marinobacter aquaeolei VT8 ABM18686
Hahella chejuensis KCTC 2396 ABC29416
Cellvibrio japonicus Ueda107 ACE83280
Saccharophagus degradans 2-40 ABD82822
Teredinibacter turnerae T7901 ACR13640
Alcanivorax sp. DG881 EDX88336
Thioalkalivibrio sp. HL-EbGR7 ACL71640
Methylibium petroleiphilum PM1 ABM94186
Geobacter uraniireducens Rf4 ABQ27248
Geobacter sp. M18 EET34226
Geobacter sp. M21 ACT16518
Haliangium ochraceum DSM 14365 ACY16459
Plesiocystis pacifica SIR-1 EDM80280
Myxococcus xanthus DK 1622 ABF85897 MXAN_1923
Stigmatella aurantiaca DW4_3-1 ADO70491
Sorangium cellulosum So ce 56 CAN96109
Haliangium ochraceum DSM 14365 ACY18963
Myxococcus xanthus DK 1622 ABF88029 MXAN_1328
Stigmatella aurantiaca DW4_3-1 ADO69759
Bdellovibrio bacteriovorus HD100 CAE78779
Bdellovibrio bacteriovorus HD100 CAE80977
Stigmatella aurantiaca DW4_3-1 ADO71627
Myxococcus xanthus DK 1622 ABF88255 MXAN_3373
Bdellovibrio bacteriovorus HD100 CAE79358
Haliangium ochraceum DSM 14365 ACY15026
Sorangium cellulosum So ce 56 CAN93073
Myxococcus xanthus DK 1622 ABF87056 MXAN_2541
Stigmatella aurantiaca DW4_3-1 ADO71054
Anaeromyxobacter sp. Fw109-5 ABS27571
Anaeromyxobacter sp. K ACG74616
Anaeromyxobacter dehalogenans 2CP-C ABC83090
Anaeromyxobacter dehalogenans 2CP-1 ACL66797
0.74/-
1/99
1/94
1/-
0.98/64
1/95
0.74/-
1/63
1/100
1/51
1/99
1/99
0.61/51
0.98/-
0.5/-
1/97
1/100
0.75/62
0.87/59
0.93/75
1/98
0.96/72
0.8/60
1/99
1/100
0.61/-
1/99
0.69/61
1/100
1/87
0.89/51
1/87
0.85/63
1/100
1/97
1/100
1/95
0.88/62
0.3
Gammaproteobacteria
Betaproteobacteria
Deltaroteobacteria

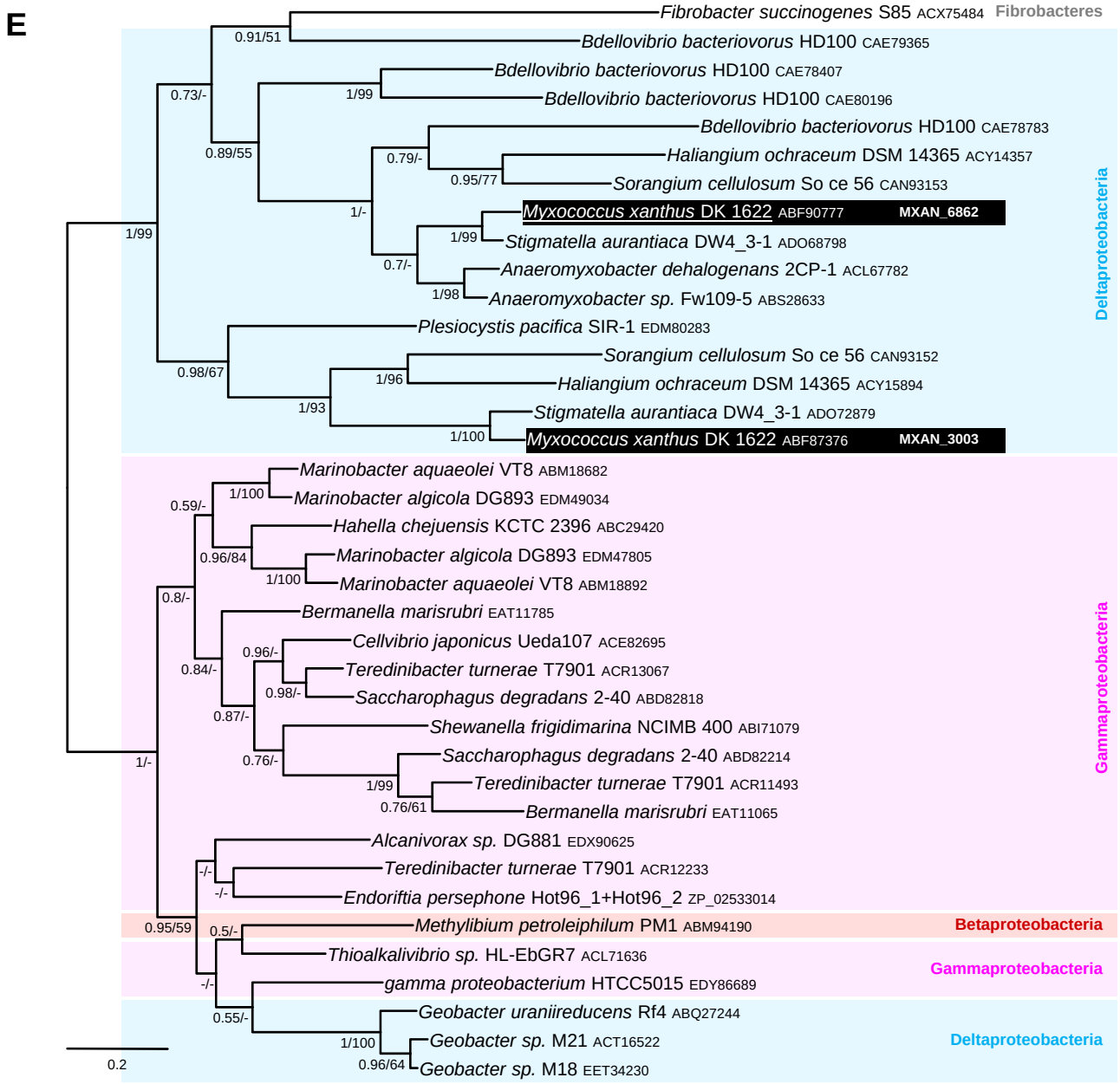
E
Fibrobacter succinogenes S85 ACX75484
Fibrobacteres
Bdellovibrio bacteriovorus HD100 CAE79365
Bdellovibrio bacteriovorus HD100 CAE78407
Bdellovibrio bacteriovorus HD100 CAE80196
Bdellovibrio bacteriovorus HD100 CAE78783
Haliangium ochraceum DSM 14365 ACY14357
Sorangium cellulosum So ce 56 CAN93153
Myxococcus xanthus DK 1622 ABF90777
MXAN_6862
Stigmatella aurantiaca DW4_3-1 ADO68798
Anaeromyxobacter dehalogenans 2CP-1 ACL67782
Anaeromyxobacter sp. Fw109-5 ABS28633
Plesiocystis pacifica SIR-1 EDM80283
Sorangium cellulosum So ce 56 CAN93152
Haliangium ochraceum DSM 14365 ACY15894
Stigmatella aurantiaca DW4_3-1 ADO72879
Myxococcus xanthus DK 1622 ABF87376
MXAN_3003
Deltaproteobacteria
Marinobacter aquaeolei VT8 ABM18682
Marinobacter algicola DG893 EDM49034
Hahella chejuensis KCTC 2396 ABC29420
Marinobacter algicola DG893 EDM47805
Marinobacter aquaeolei VT8 ABM18892
Bermanella marisrubri EAT11785
Cellvibrio japonicus Ueda107 ACE82695
Teredinibacter turnerae T7901 ACR13067
Saccharophagus degradans 2-40 ABD82818
Shewanella frigidimarina NCIMB 400 ABI71079
Saccharophagus degradans 2-40 ABD82214
Teredinibacter turnerae T7901 ACR11493
Bermanella marisrubri EAT11065
Gammaproteobacteria
Alcanivorax sp. DG881 EDX90625
Teredinibacter turnerae T7901 ACR12233
Endoriftia persephone Hot96_1+Hot96_2 ZP_02533014
Methylibium petroleiphilum PM1 ABM94190
Betaproteobacteria
Thioalkalivibrio sp. HL-EbGR7 ACL71636
gamma proteobacterium HTCC5015 EDY86689
Gammaproteobacteria
Geobacter uraniireducens Rf4 ABQ27244
Geobacter sp. M21 ACT16522
Geobacter sp. M18 EET34230
Deltaproteobacteria
0.91/51
0.73/-
1/99
0.89/55
0.79/-
0.95/77
1/-
1/99
0.7/-
1/98
1/99
0.98/67
1/96
1/93
1/100
0.59/-
1/100
0.96/84
1/100
0.8/-
0.96/-
0.84/-
0.98/-
0.87/-
0.76/-
1/-
1/99
0.76/61
-/-
-/-
0.95/59
0.5/-
-/-
0.55/-
1/100
0.96/64
0.2

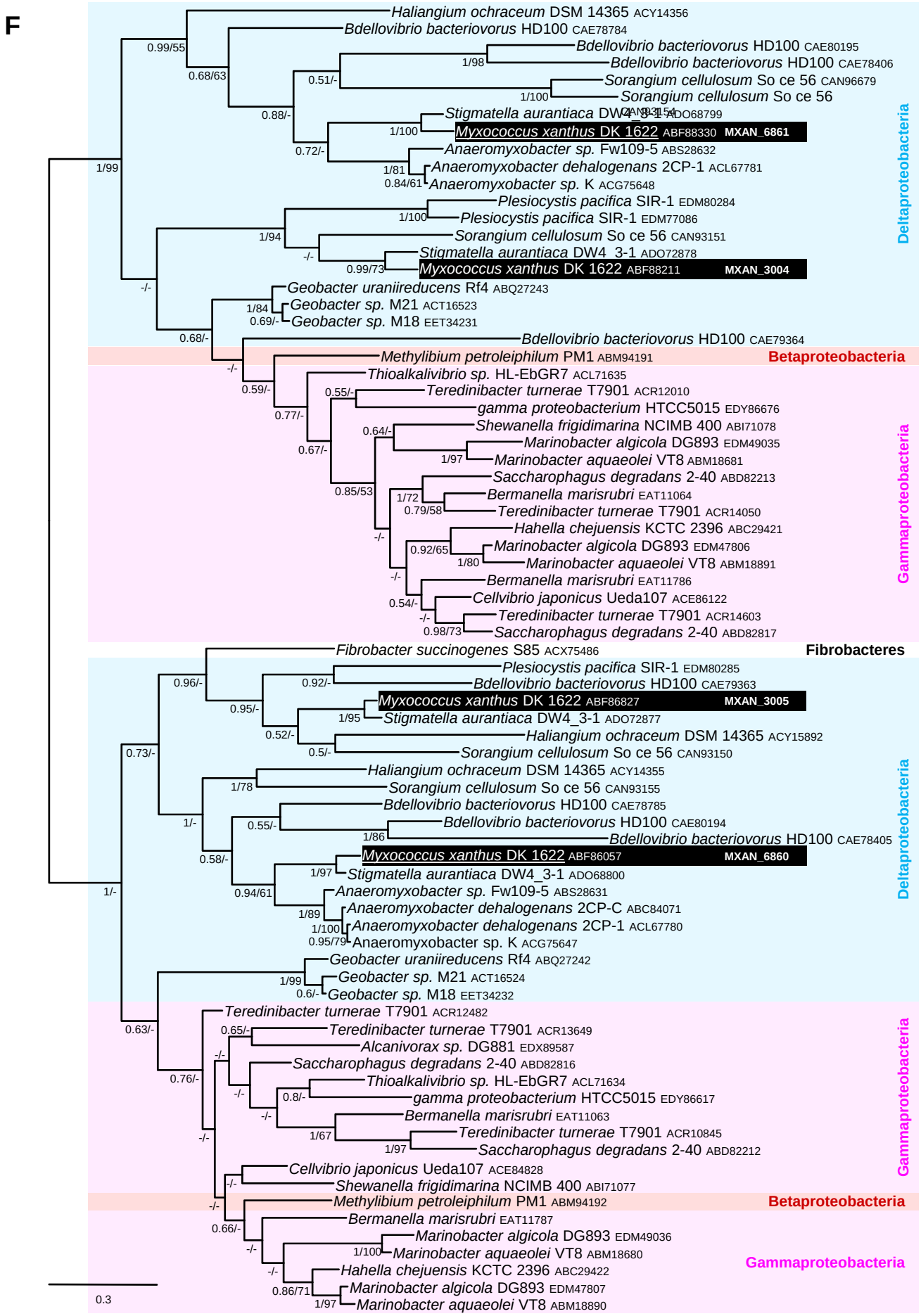
F
Haliangium ochraceum DSM 14365 ACY14356
Bdellovibrio bacteriovorus HD100 CAE78784
Bdellovibrio bacteriovorus HD100 CAE80195
Bdellovibrio bacteriovorus HD100 CAE78406
Sorangium cellulosum So ce 56 CAN96679
Sorangium cellulosum So ce 56
Stigmatella aurantiaca DW4_3-1 ADO68799
Myxococcus xanthus DK 1622 ABF88330 MXAN_6861
Anaeromyxobacter sp. Fw109-5 ABS28632
Anaeromyxobacter dehalogenans 2CP-1 ACL67781
Anaeromyxobacter sp. K ACG75648
Plesiocystis pacifica SIR-1 EDM80284
Plesiocystis pacifica SIR-1 EDM77086
Sorangium cellulosum So ce 56 CAN93151
Stigmatella aurantiaca DW4_3-1 ADO72878
Myxococcus xanthus DK 1622 ABF88211 MXAN_3004
Geobacter uraniireducens Rf4 ABQ27243
Geobacter sp. M21 ACT16523
Geobacter sp. M18 EET34231
Bdellovibrio bacteriovorus HD100 CAE79364
Deltaproteobacteria
Methylibium petroleiphilum PM1 ABM94191
Betaproteobacteria
Thioalkalivibrio sp. HL-EbGR7 ACL71635
Teredinibacter turnerae T7901 ACR12010
gamma proteobacterium HTCC5015 EDY86676
Shewanella frigidimarina NCIMB 400 ABI71078
Marinobacter algicola DG893 EDM49035
Marinobacter aquaeolei VT8 ABM18681
Saccharophagus degradans 2-40 ABD82213
Bermanella marisrubri EAT11064
Teredinibacter turnerae T7901 ACR14050
Hahella chejuensis KCTC 2396 ABC29421
Marinobacter algicola DG893 EDM47806
Marinobacter aquaeolei VT8 ABM18891
Bermanella marisrubri EAT11786
Cellvibrio japonicus Ueda107 ACE86122
Teredinibacter turnerae T7901 ACR14603
Saccharophagus degradans 2-40 ABD82817
Gammaproteobacteria
Fibrobacter succinogenes S85 ACX75486
Fibrobacteres
Plesiocystis pacifica SIR-1 EDM80285
Bdellovibrio bacteriovorus HD100 CAE79363
Myxococcus xanthus DK 1622 ABF86827 MXAN_3005
Stigmatella aurantiaca DW4_3-1 ADO72877
Haliangium ochraceum DSM 14365 ACY15892
Sorangium cellulosum So ce 56 CAN93150
Haliangium ochraceum DSM 14365 ACY14355
Sorangium cellulosum So ce 56 CAN93155
Bdellovibrio bacteriovorus HD100 CAE78785
Bdellovibrio bacteriovorus HD100 CAE80194
Bdellovibrio bacteriovorus HD100 CAE78405
Myxococcus xanthus DK 1622 ABF86057 MXAN_6860
Stigmatella aurantiaca DW4_3-1 ADO68800
Anaeromyxobacter sp. Fw109-5 ABS28631
Anaeromyxobacter dehalogenans 2CP-C ABC84071
Anaeromyxobacter dehalogenans 2CP-1 ACL67780
Anaeromyxobacter sp. K ACG75647
Geobacter uraniireducens Rf4 ABQ27242
Geobacter sp. M21 ACT16524
Geobacter sp. M18 EET34232
Deltaproteobacteria
Teredinibacter turnerae T7901 ACR12482
Teredinibacter turnerae T7901 ACR13649
Alcanivorax sp. DG881 EDX89587
Saccharophagus degradans 2-40 ABD82816
Thioalkalivibrio sp. HL-EbGR7 ACL71634
gamma proteobacterium HTCC5015 EDY86617
Bermanella marisrubri EAT11063
Teredinibacter turnerae T7901 ACR10845
Saccharophagus degradans 2-40 ABD82212
Cellvibrio japonicus Ueda107 ACE84828
Shewanella frigidimarina NCIMB 400 ABI71077
Gammaproteobacteria
Methylibium petroleiphilum PM1 ABM94192
Betaproteobacteria
Bermanella marisrubri EAT11787
Marinobacter algicola DG893 EDM49036
Marinobacter aquaeolei VT8 ABM18680
Hahella chejuensis KCTC 2396 ABC29422
Marinobacter algicola DG893 EDM47807
Marinobacter aquaeolei VT8 ABM18890
Gammaproteobacteria
0.3

Figure S5

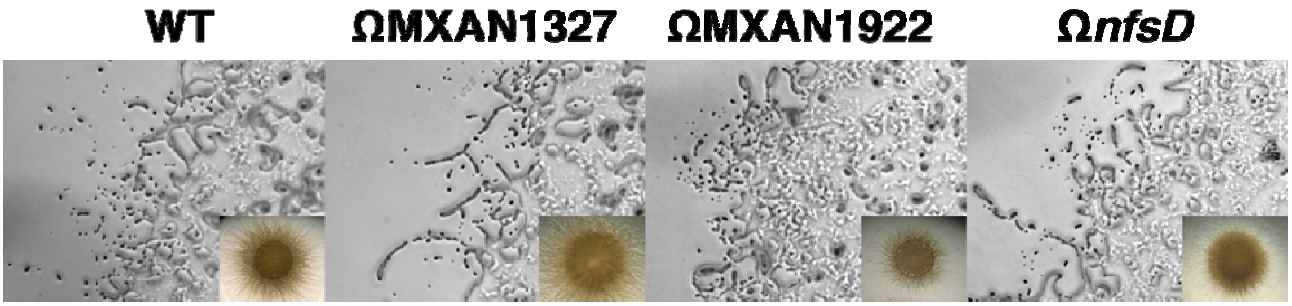

Table S1. List of the 23 and 35 *Myxococcus xanthus* genes identified by two transposon mutagenesis experiments (Yo = [16]; Yu = [17]). For each gene, the locus_tag in the genome of *M. xanthus*, the accession number of the corresponding protein in the ref_seq database and the original functional annotation are provided. For each protein, we indicated the presence of functional conserved domains, of signal peptide and of transmembrane domains. $ signs design false positive genes that have been removed from the current version of the *M. xanthus* genome. Asterisks correspond to the 28 genes fitting our criteria as putative components of the gliding machinery. Among them we showed that nine (in red) co-localize in three small genomic regions.

	Locus_tag/ Ref_seq	Gene	Lengh (aa)	Former annotation	Domain function (pfam)	Signal peptide	Transmembrane domain	
Yo	(**$**)	agmB	-	ATP-dependent RNA helicase NP643917, *Xanthomonas axonopodis*	-	-	-	
Yo	MXAN_0635/ YP_628903	agmE	319	Soj/Par CAB16134, *Bacillus subtilis*	CobQ/CobB/MinD/ParA nucleotide binding domain	no	no	
Yo	MXAN_1673/ YP_629925	agmN	513	Hypothetical protein BAB99656, *Corynebacterium glutamicum*	-	no	no	
Yo	MXAN_2538/ YP_630757	agmO	170	Proto-oncogene tyrosine-protein kinase c-ABL CAA34438, *Homo sapiens*	-	yes	no	*
Yo	MXAN_2542/ YP_630761	agmP	427	Multidrug resistance membrane protein, *Chlorobium tepidum*	Major Facilitator Superfamily	no	10	*
Yo	MXAN_2923/ YP_631134	agmQ	698	Leucine aminopeptidase-rekated protein AAF96710, *Vibrio cholerae*	Bacterial pre-peptidase C-terminal domain	no	no	
Yo	MXAN_3352/ YP_631549	agmF	346	Pseudouridylate synthase AAM24749, *Thermoanaerobacter tengcongensis*	RNA pseudouridylate synthase	no	no	
Yo	MXAN_3502/ YP_631696	agmI	304	Hypothetical protein ZP00079645, *Geobacter metallireducens*	Sporulation related domain	no	1	*
Yo	MXAN_3537/ YP_631730	agmL	432	Isocitrate dehydrogenase BAB06878, *Bacillus halodurans*	socitrate/isopropylmalate dehydrogenase	no	no	
Yo	MXAN_3842/ YP_632024	agmD	347	tRNA synthetase CAB74224, *Campylobacter jejuni*	tRNA synthetases class I (W and Y)	no	no	
Yo	MXAN_3886/ YP_632066	agmA	599	N-acetylmuramoyl L-alanine amidase CAB73523, *Campylobacter jejuni*	N-acetylmuramoyl-L-alanine amidase	yes	no	*
Yo	MXAN_4638/ YP_632804	agmH	279	Lysophospholipase ANN50803, *Leptospira interrogens*	Putative lysophospholipase	no	no	
Yo	MXAN_4798/ YP_632959	agmC	1731	Putative haemagglutinin/haemolysin-related protein CAD18331, *Ralstonia solanacearum*	Protein of unknown function (DUF3607)	no	1	*
Yo	MXAN_4865/ AAO66319 (**$**)	agmV	1151	No significant similarity	-	no	no	
Yo	MXAN_4869/ YP_633027	aglT	478	Predicted N-acetylglucosaminyl tranferase (AGR99) AAH42083, *Homo sapiens*	Tetratricopeptide repeat	yes	no	*
Yo	MXAN_4870/ YP_633028	agmU	1218	TPR-domain containing protein AAM05026, *Methanosarcina acetivorans*	Tetratricopeptide repeat	yes	no	*
Yo	MXAN_5715/ YP_633853	agmZ	399	No significant similarity	Response regulator receiver domain Histidine kinase-, DNA gyrase B-, and HSP90-like ATPase	no	no	
Yo	MXAN_5744/ YP_633881	agmW	458	Carboxy-terminal protease BAC45699, *Bradyrhizobium japonicum*	PDZ domain (Also known as DHR or GLGF) Peptidase family S41	yes	no	*
Yo	MXAN_5753/ YP_633890	aglX	236	TolQ bioploymer transport protein I64064, *Haemophilus influenza*	MotA/TolQ/ExbB proton channel family	no	3	*
Yo	MXAN_5754/ YP_633891	aglV	153	ExbD/TolR AAM71873, *Chlorobium tepidum*	Biopolymer transport protein ExbD/TolR	no	1	*
Yo	MXAN_5756/ YP_633893	aglW	431	TolB AAM71875, *C. tepidum*	TolB amino-terminal domain WD40-like Beta Propeller Repeat	yes	no	*
Yo	MXAN_5818/ YP_633955	agmR	371	Putative ion transporting ATPase CAB45559, *Streptomyces coelicolor*	Anion-transporting ATPase	no	no	
Yo	MXAN_5820/ YP_633957	agmM	360	Putative metalloprotease C69831, *Bacillus subtilis*	Peptidase family M48	no	5	*
Yo	MXAN_6259/ YP_634388	agmJ	636	ABC transporter BAB59028, *Penicillium digitatum*	Protein of unknown function (DUF2629)	no	no	
Yo	MXAN_6519/ YP_634642	agmG	712	Site-specific recombinase CAD14714, *Ralstonia solanacearum*	Site-specific recombinase	no	7	*
Yo	MXAN_6608/ YP_634726	agmS	263	Enoyl-CoA hydratase AE011275, *Leptospira interrogans*	Enoyl-CoA hydratase/isomerase family	no	no	
Yo	MXAN_6860/ YP_634977	aglS	194	ExbD/TolR ACC45288, *Neisseria gonorrhoea*	Biopolymer transport protein ExbD/TolR	no	1	*
Yo	MXAN_6862/ YP_634979	aglR	245	MotA/TolQ/ExbB proton channel AAM72811, *Chlorobium tepidum*	MotA/TolQ/ExbB proton channel family protein	no	3	*
Yo/Yu	MXAN_6607/ YP_634725	agmT	339	Predicted periplasmic solute-binding protein (*Trichodesmium erythraeum*)	YceG-like family	yes	no	*
Yo/Yu	MXAN_1925/ YP_630169	mglA	195	SAR1-like small GTPase / GTPase Sar1p, CAA35978, *Saccharomyces cerevisiae*	ADP-ribosylation factor family	no	no	
Yo/Yu	MXAN_1926/ YP_630170	mglB	159	Guanine nucleotide exchange factor for MglA / Ca2+ binding calreticulin AF340232, *Taenia solium*; roadblock-LC7 domain	Roadblock/LC7 domain	no	no	
Yo/Yu	MXAN_3008/ YP_631217	aglU	547	WD-repeat lipoprotein, acylaminoacyl-peptidase / b-transducin-like protein HET-E2C AAL37299, Podospora anserina; TolB *M.acetivorans*	WD40-like Beta Propeller Repeat	yes	no	*
Yo/Yu	MXAN_3060/ YP_631268	cglB	416	Outer membrane lipoprotein / No significant similarity	-	yes	no	*
Yo/Yu	MXAN_4862/ YP_633021	agmX	674	Outer membrane lipoprotein / Putative DnaJ-domain containing protein AC018929, *Oryza sativa*	-	no	1	*
Yo/Yu	MXAN_4863/ YP_633022	agmK	3822	TPR repeat protein / TPR protein AAF31047, *Leishmania major*	Tetratricopeptide repeat	no	no	*

	Locus_tag/ Ref_seq	Gene	Lengh (aa)	Former annotation	Domain function (pfam)	Signal peptide	Transmembrane domain	
Yu	MXAN_2050/ YP_630279	pglH	927	TPR repeat, CheY-like receiver domain, and a winged-helix DNA-binding domain	Response regulator receiver domain	no	no	
Yu	MXAN_2541/ YP_630760	agnA	673	Unknown	Tetratricopeptide repeat	yes	no	*
Yu	MXAN_2919/ YP_631130	pglJ	441	Integral membrane protein similar to *S. coelicolor* gi:1098142 with local similarity to Wzy_C polymerase	O-Antigen ligase	no	8	*
Yu	MXAN_2921/ YP_631132	pglB	381	Glycosyltranferase similar to YP_000604 of *Leptospira interrogans*	Glycosyl transferases group 1	no	no	
Yu	MXAN_4148/ YP_632323	pglK	302	Predicted transmembrane transcriptional regulator	-	no	1	*
Yu	MXAN_4616/ YP_632784	pglF	750	Glycosyltranferase 1 domain and glycosyltranferase 2 domain	Starch synthase catalytic domain Glycosyl transferases group 1 Glycosyl transferase family 2	no	no	
Yu	MXAN_4710/ YP_632872	pglN	328	ADP-heptose synthase, bifunctional sugar kinase/adenylyltranferase RfaE_like	pfkB family carbohydrate kinase	no	no	
Yu	MXAN_4867/ YP_633025	pglI	640	Hypothetical abductin-like protein	FHA domain Gram-negative bacterial tonB protein	no	1	*
Yu	MXAN_5319/ YP_633470	pglC	841	TPR repeat	Tetratricopeptide repeat	no	no	*
Yu	MXAN_5382/ NC_008095	aspT	77pb	tRNA-Asp	tRNA-Asp			
Yu	MXAN_5585/ YP_633724	pglE	727	Glycosyltransferase of PMT family	Dolichyl-phosphate-mannose-protein mannosyltransferase	yes	17	*
Yu	MXAN_6403/ YP_634527	agnB	408	ABC-type transporter permease protein (*Vibrio fischeri*)	Predicted permease	yes	3	*
Yu	MXAN_6501/ YP_634624	pglD	354	GDP-mannose synthesis	Nucleotidyl transferase Mannose-6-phosphate isomerase	no	no	
Yu	MXAN_7160/ YP_635273	pglM	409	Alanine racemase	Alanine racemase, N-terminal domain Alanine racemase, C-terminal domain	no	no	
Yu	MXAN_7252/ YP_635365	pglA	222	Exopolysaccharide synthesis, ExoD	Exopolysaccharide synthesis, ExoD	no	3	*
Yu	MXAN_7296/ YP_635409	agnC	139	Unknown	Protein of unknown function (DUF3478)	no	1	*

Table S2. List of complete genomes of Deltaproteobacteria, Gammaproteobacteria, Betaproteobacteria and Fibrobacteres carrying homologues of the 14 candidates genes coding for the gliding machinery in *M. xanthus* . For each genome, the accession number in the nucleic ref_seq and in the GenBank databases, the size (in megabases) and the release date are provided.

Genome	Phylum	Size	GenBank	Ref_Seq	Released
***Anaeromyxobacter dehalogenans* 2CP-1**	Deltaproteobacteria	5.02	CP001359.1	NC_011891.1	01/12/2009
***Anaeromyxobacter dehalogenans* 2CP-C**	Deltaproteobacteria	5	CP000251.1	NC_007760.1	01/27/2006
***Anaeromyxobacter sp.* Fw 109-5**	Deltaproteobacteria	5.27	CP000769.1	NC_009675.1	07/17/2007
***Anaeromyxobacter sp.* K**	Deltaproteobacteria	5.06	CP001131.1	NC_011145.1	08/15/2008
***Bdellovibrio bacteriovorus* HD100**	Deltaproteobacteria	3.8	BX842601.2	NC_005363.1	01/31/2004
***Geobacter sp.* M21**	Deltaproteobacteria	4.74	CP001661.1	NC_012918.1	06/20/2008
***Geobacter uraniireducens* Rf4**	Deltaproteobacteria	5.13	CP000698.1	NC_009483.1	05/11/2007
***Haliangium ochraceum* DSM 14365**	Deltaproteobacteria	9.4	CP001804.1	NC_013440.1	04/21/2009
***Myxococcus xanthus* DK 1622**	Deltaproteobacteria	9.13	CP000113.1	NC_008095.1	06/07/2006
***Sorangium cellulosum* Soce56**	Deltaproteobacteria	13.03	AM746676.1	NC_010162.1	11/27/2007
***Stigmatella aurantiaca* DW4/3-1**	Deltaproteobacteria	10	CP002271.1	NC_014623.1	10/21/2010
***Fibrobacter succinogenes* S85**	Fibrobacteres	3.8	CP002158	-	08/06/2010
***Methylibium petroleiphilum* PM1**	Betaproteobacteria	4.64	CP000555.1	NC_008825.1	01/29/2007
***Cellvibrio japonicus* Ueda107**	Gammaproteobacteria	4.57	CP000934.1	NC_010995.1	06/19/2008
Hahella chejuensis KCTC 2396	Gammaproteobacteria	7.2	CP000155.1	NC_007645.1	12/14/2005
***Marinobacter aquaeolei* VT8**	Gammaproteobacteria	4.77	CP000514.1	NC_008740.1	12/28/2006
***Saccharophagus degradans* 2-40**	Gammaproteobacteria	5.05	CP000282.1	NC_007912.1	03/17/2006
***Shewanella frigidimarina* NCIMB 400**	Gammaproteobacteria	4.84	CP000447.1	NC_008345.1	09/14/2006
***Teredinibacter turnerae* T7901**	Gammaproteobacteria	5.2	CP001614.2	NC_012997.1	05/18/2009
***Thioalkalivibrio sp.* HL-EbGR7**	Gammaproteobacteria	3.46	CP001339.1	NC_011901.1	01/13/2009

Table S3. Exhaustive list of the homologues of the genes of the G1, G2 and M1 clusters found in complete genomes listed in Table S2. For each gene, the locus_tag, and the accession number, the length and the functional annotation of the corresponding proteins according to the ref_seq database are provided.

Organism	Locus_tag	Ref_seq	Lengh	Annotation	Homolog to
Anaeromyxobacter dehalogenans 2CP-C	Adeh_3310	YP_466514	605	zinc finger/thioredoxin putative	MXAN_4862
	Adeh_3311	YP_466515	4074	TPR repeat-containing protein	MXAN_4863
	Adeh_3318	YP_466522	205	hypothetical protein Adeh_3318	MXAN_4866
	Adeh_3319	YP_466523	673	FHA domain-containing protein	MXAN_4867
	Adeh_3320	YP_466524	89	hypothetical protein Adeh_3320	MXAN_4868
	Adeh_3321	YP_466525	453	TPR repeat-containing protein	MXAN_4869
	Adeh_3322	YP_466526	1193	TPR repeat-containing protein	MXAN_4870
	Adeh_3323	YP_466527	580	hypothetical protein Adeh_3323	MXAN_2541
	Adeh_3324	YP_466528	261	hypothetical protein Adeh_3324	MXAN_2541
	Adeh_3325	YP_466529	291	hypothetical protein Adeh_3325	MXAN_2539
	Adeh_3326	YP_466530	139	hypothetical protein Adeh_3326	MXAN_2538
	Adeh_4308	YP_467508	194	adventurous gliding motility protein S	MXAN_6860
	Adeh_4309	YP_467509	162	TolR protein	MXAN_6861
	Adeh_4310	YP_467510	224	MotA/TolQ/ExbB proton channel	MXAN_6862
	A2cp1_3454	YP_002493850	588	MJ0042 family finger-like protein	MXAN_4862
	A2cp1_3455	YP_002493851	4104	Tetratricopeptide TPR_2 repeat protein	MXAN_4863
	A2cp1_3462	YP_002493858	205	hypothetical protein A2cp1_3462	MXAN_4866
	A2cp1_3463	YP_002493859	680	FHA domain containing protein	MXAN_4867
	A2cp1_3464	YP_002493860	89	hypothetical protein A2cp1_3464	MXAN_4868
	A2cp1_3465	YP_002493861	451	Tetratricopeptide TPR_2 repeat protein	MXAN_4869

Anaeromyxobacter dehalogenans 2CP-1	A2cp1_3466	YP_002493862	1191	TPR repeat-containing protein	MXAN_4870
	A2cp1_3467	YP_002493863	580	hypothetical protein A2cp1_3467	MXAN_2541
	A2cp1_3468	YP_002493864	261	hypothetical protein A2cp1_3468	MXAN_2541
	A2cp1_3469	YP_002493865	284	hypothetical protein A2cp1_3469	MXAN_2539
	A2cp1_3470	YP_002493866	139	hypothetical protein A2cp1_3470	MXAN_2538
	A2cp1_4463	YP_002494846	194	Biopolymer transport protein ExbD/TolR	MXAN_6860
	A2cp1_4464	YP_002494847	162	Biopolymer transport protein ExbD/TolR	MXAN_6861
	A2cp1_4465	YP_002494848	224	MotA/TolQ/ExbB proton channel	MXAN_6862
Anaeromyxobacter sp. FW 109-5	Anae109_3371	YP_001380539	571	Zinc finger-domain-containing protein	MXAN_4862
	Anae109_3372	YP_001380540	4095	TPR repeat-containing protein	MXAN_4863
	Anae109_3382	YP_001380550	205	hypothetical protein Anae109_3382	MXAN_4866
	Anae109_3383	YP_001380551	667	FHA domain-containing protein	MXAN_4867
	Anae109_3384	YP_001380552	90	hypothetical protein Anae109_3384	MXAN_4868
	Anae109_3385	YP_001380553	427	TPR repeat-containing protein	MXAN_4869
	Anae109_3386	YP_001380554	1162	TPR repeat-containing protein	MXAN_4870
	Anae109_3387	YP_001380555	649	hypothetical protein Anae109_3387	MXAN_2541
	Anae109_3388	YP_001380556	254	hypothetical protein Anae109_3388	MXAN_2541
	Anae109_3389	YP_001380557	285	hypothetical protein Anae109_3389	MXAN_2539
	Anae109_3390	YP_001380558	172	hypothetical protein Anae109_3390	MXAN_2538
	Anae109_4453	YP_001381615	194	adventurous gliding motility protein S	MXAN_6860
	Anae109_4454	YP_001381616	164	TolR protein	MXAN_6861
	Anae109_4455	YP_001381617	226	MotA/TolQ/ExbB proton channel	MXAN_6862
	AnaeK_3390	YP_002135733	610	MJ0042 family finger-like protein	MXAN_4862
	AnaeK_3398	YP_002135740	205	hypothetical protein AnaeK_3398	MXAN_4866
	AnaeK_3399	YP_002135741	682	FHA domain containing protein	MXAN_4867

Anaeromyxobacter sp. K	AnaeK_3400	YP_002135742	89	hypothetical protein AnaeK_3400	MXAN_4868
	AnaeK_3401	YP_002135743	453	Tetratricopeptide TPR_4	MXAN_4869
	AnaeK_3402	YP_002135744	1192	Tetratricopeptide TPR_2 repeat protein	MXAN_4870
	AnaeK_3403	YP_002135745	580	hypothetical protein AnaeK_3403	MXAN_2541
	AnaeK_3404	YP_002135746	261	hypothetical protein AnaeK_3404	MXAN_2541
	AnaeK_3405	YP_002135747	284	hypothetical protein AnaeK_3405	MXAN_2539
	AnaeK_3406	YP_002135748	139	hypothetical protein AnaeK_3406	MXAN_2538
	AnaeK_4444	YP_002136776	194	adventurous gliding motility protein S	MXAN_6860
	AnaeK_4445	YP_002136777	162	TolR protein	MXAN_6861
	AnaeK_4446	YP_002136778	224	MotA/TolQ/ExbB proton channel	MXAN_6862
	Bd0413	NP_967407	355	hypothetical protein Bd0413	MXAN_2541
	Bd0414	NP_967408	246	hypothetical protein Bd0414	MXAN_2539
	Bd0416	NP_967410	408	hypothetical protein Bd0416	MXAN_4867
	Bd0417	NP_967411	987	hypothetical protein Bd0417	MXAN_4870
	Bd0418	NP_967412	165	hypothetical protein Bd0418	MXAN_6860
	Bd0419	NP_967413	149	putative adventurous gliding motility protein V	MXAN_6861
	Bd0420	NP_967414	248	putative adventurous gliding motility protein R	MXAN_6862
	Bd0828	NP_967784	240	hypothetical protein Bd0828	MXAN_2541
	Bd0829	NP_967785	266	hypothetical protein Bd0829	MXAN_2539
	Bd0831	NP_967786	529	hypothetical protein Bd0831	MXAN_2541
	Bd0832	NP_967787	1066	adventurous gliding motility protein U	MXAN_4870
	Bd0833	NP_967788	281	adventurous gliding motility protein T	MXAN_4869
	Bd0834	NP_967789	707	hypothetical protein Bd0834	MXAN_4867
	Bd0836	NP_967790	221	adventurous gliding motility protein R	MXAN_6862
	Bd0837	NP_967791	158	tolR protein	MXAN_6861

Bdellovibrio bacteriovorus HD100	Bd0838	NP_967792	196	adventurous gliding motility protein S	MXAN_6860
	Bd1474	NP_968365	713	hypothetical protein Bd1474	MXAN_2541
	Bd1475	NP_968366	254	hypothetical protein Bd1475	MXAN_2539
	Bd1476	NP_968367	488	hypothetical protein Bd1476	MXAN_4867
	Bd1477	NP_968368	82	hypothetical protein Bd1477	MXAN_4868
	Bd1478	NP_968369	1237	adventurous gliding motility protein U	MXAN_4870
	Bd1479	NP_968370	167	adventurous gliding motility protein S	MXAN_6860
	Bd1480	NP_968371	185	TolR-like protein, putative	MXAN_6861
	Bd1481	NP_968372	236	adventurous gliding motility protein R	MXAN_6862
	Bd2369	NP_969195	531	hypothetical protein Bd2369	MXAN_2541
	Bd2370	NP_969196	235	hypothetical protein Bd2370	MXAN_2539
	Bd2372	NP_969198	376	hypothetical protein Bd2372	MXAN_4867
	Bd2374	NP_969200	996	hypothetical protein Bd2374	MXAN_4870
	Bd2375	NP_969201	175	adventurous gliding motility protein S	MXAN_6860
	Bd2376	NP_969202	151	hypothetical protein Bd2376	MXAN_6861
	Bd2377	NP_969203	244	adventurous gliding motility protein R	MXAN_6862
	Bd3598	NP_970322	278	hypothetical protein Bd3598	MXAN_2539
	Bd3599	NP_970323	513	hypothetical protein Bd3599	MXAN_2541
	Bd3600	NP_970324	52	hypothetical protein Bd3600	MXAN_4868
	Bd3601	NP_970325	239	hypothetical protein Bd3601	MXAN_2541
Geobacter uraniireducens Rf4	Gura_3070	YP_001231814	484	hypothetical protein Gura_3070	MXAN_4867
	Gura_3071	YP_001231815	166	hypothetical protein Gura_3071	MXAN_6860
	Gura_3072	YP_001231816	166	biopolymer transport protein ExbD/TolR	MXAN_6861
	Gura_3073	YP_001231817	211	MotA/TolQ/ExbB proton channel	MXAN_6862
	Gura_3075	YP_001231819	240	TPR repeat-containing protein	MXAN_4869

	Gura_3076	YP_001231820	1108	TPR repeat-containing protein	MXAN_4870
	Gura_3077	YP_001231821	629	hypothetical protein Gura_3077	MXAN_2541
Geobacter sp. M21	GM21_0438	YP_003020276	626	hypothetical protein GM21_0438	MXAN_2541
	GM21_0439	YP_003020277	1090	Tetratricopeptide domain protein	MXAN_4870
	GM21_0440	YP_003020278	272	TPR repeat-containing protein	MXAN_4869
	GM21_0442	YP_003020280	211	MotA/TolQ/ExbB proton channel	MXAN_6862
	GM21_0443	YP_003020281	166	Biopolymer transport protein ExbD/TolR	MXAN_6861
	GM21_0444	YP_003020282	165	Biopolymer transport protein ExbD/TolR	MXAN_6860
	GM21_0445	YP_003020283	505	hypothetical protein GM21_0445	MXAN_4867
Haliangium ochraceum DSM 14365	Hoch_1807	YP_003266248	201	Biopolymer transport protein ExbD/TolR	MXAN_6860
	Hoch_1808	YP_003266249	163	Biopolymer transport protein ExbD/TolR	MXAN_6861
	Hoch_1809	YP_003266250	216	MotA/TolQ/ExbB proton channel	MXAN_6862
	Hoch_2490	YP_003266919	560	Tetratricopeptide repeat protein	MXAN_2541
	Hoch_2491	YP_003266920	1155	Tetratricopeptide repeat protein	MXAN_4870
	Hoch_2492	YP_003266921	441	Tetratricopeptide TPR_2 repeat protein	MXAN_4869
	Hoch_3390	YP_003267785	187	Biopolymer transport protein ExbD/TolR	MXAN_6860
	Hoch_3391	YP_003267786	242	Biopolymer transport protein ExbD/TolR	MXAN_6861
	Hoch_3392	YP_003267787	223	MotA/TolQ/ExbB proton channel	MXAN_6862
	Hoch_3957	YP_003268349	228	hypothetical protein Hoch_3957	MXAN_2539
	Hoch_3958	YP_003268350	268	hypothetical protein Hoch_3958	MXAN_2541
	Hoch_3960	YP_003268352	689	hypothetical protein Hoch_3960	MXAN_2541
	Hoch_3961	YP_003268353	1058	Tetratricopeptide TPR_2 repeat protein	MXAN_4870
	Hoch_3962	YP_003268354	395	Tetratricopeptide TPR_2 repeat protein	MXAN_4869
	Hoch_3963	YP_003268355	185	hypothetical protein Hoch_3963	MXAN_4868
	Hoch_3964	YP_003268356	474	TonB family protein	MXAN_4867

	Hoch_5625	YP_003269998	296	Tetratricopeptide TPR_2 repeat protein	MXAN_4869
	Hoch_5627	YP_003269999	767	FHA domain containing protein	MXAN_4867
	Hoch_5628	YP_003270000	84	hypothetical protein Hoch_5628	MXAN_4868
	Hoch_6494	YP_003270856	823	hypothetical protein Hoch_6494	MXAN_2541
	Hoch_6495	YP_003270857	1202	Tetratricopeptide repeat protein	MXAN_4870
	Hoch_6496	YP_003270858	422	hypothetical protein Hoch_6496	MXAN_4869
	Hoch_6497	YP_003270859	120	hypothetical protein Hoch_6497	MXAN_4868
	Hoch_6498	YP_003270860	490	hypothetical protein Hoch_6498	MXAN_4867
Myxococcus xanthus DK622	MXAN_1327	YP_629584	1089	TPR repeat-containing protein	MXAN_4870
	MXAN_1328	YP_629585	538	hypothetical protein MXAN_1328	MXAN_2541
	MXAN_1329	YP_629586	246	hypothetical protein MXAN_1329	MXAN_2539
	MXAN_1330	YP_629587	749	FHA domain-containing protein	MXAN_4867
	MXAN_1331	YP_629588	162	hypothetical protein MXAN_1331	MXAN_4868
	MXAN_1919	YP_630163	447	hypothetical protein MXAN_1919	MXAN_2541
	MXAN_1920	YP_630164	91	hypothetical protein MXAN_1920	MXAN_4870
	MXAN_1921	YP_630165	490	TPR repeat-containing protein	MXAN_4869
	MXAN_1922	YP_630166	1111	TPR repeat-containing protein	MXAN_4868
	MXAN_1923	YP_630167	809	hypothetical protein MXAN_1923	MXAN_4867
	MXAN_3003	YP_631212	260	MotA/TolQ/ExbB proton channel family protein	MXAN_6862
	MXAN_3004	YP_631213	173	hypothetical protein MXAN_3004	MXAN_6861
	MXAN_3005	YP_631214	193	hypothetical protein MXAN_3005	MXAN_6860
	MXAN_3371	YP_631568	294	hypothetical protein MXAN_3371	MXAN_2541
	MXAN_3372	YP_631569	442	hypothetical protein MXAN_3372	MXAN_2539
	MXAN_3373	YP_631570.1	512	hypothetical protein MXAN_3373	MXAN_2541
	MXAN_3374	YP_631571	1219	TPR repeat-containing protein	MXAN_4870

	MXAN_3375	YP_631572	499	putative adventurous gliding protein T	MXAN_4869
	MXAN_3376	YP_631573	96	hypothetical protein MXAN_3376	MXAN_4868
	MXAN_3377	YP_631574	682	FHA/TonB domain-containing protein	MXAN_4867
	MXAN_3378	YP_631575	200	hypothetical protein MXAN_3378	MXAN_4866
Sorangium cellulosum Soce56	sce2906	YP_001613545	292	hypothetical protein sce2906	MXAN_2541
	sce2907	YP_001613546	308	hypothetical protein sce2907	MXAN_2539
	sce2914	YP_001613553	568	hypothetical protein sce2914	MXAN_2541
	sce2915	YP_001613554	1289	hypothetical protein sce2915	MXAN_4870
	sce2916	YP_001613555	497	hypothetical protein sce2916	MXAN_4869
	sce2917	YP_001613556	90	hypothetical protein sce2917	MXAN_4868
	sce2918	YP_001613557	681	FHA domain-containing protein	MXAN_4867
	sce2920	YP_001613559	1774	TPR repeat-containing protein	MXAN_4863
	sce2921	YP_001613560	2081	TPR repeat-containing protein	MXAN_4863
	sce2991	YP_001613630	202	putative adventurous gliding motility protein	MXAN_6860
	sce2992	YP_001613631	187	TolR-like protein	MXAN_6861
	sce2993	YP_001613632	225	adventurous gliding motility protein R	MXAN_6862
	sce2994	YP_001613633	220	adventurous gliding motility protein R	MXAN_6862
	sce2995	YP_001613634	189	putative biopolymer transport protein	MXAN_6861
	sce2996	YP_001613635	169	putative adventurous gliding motility protein AglS	MXAN_6860
	sce5940	YP_001616584	511	hypothetical protein sce5940	MXAN_4867
	sce5942	YP_001616586	82	hypothetical protein sce5942	MXAN_4868
	sce5943	YP_001616587	449	TPR domain-containing protein	MXAN_4869
	sce5944	YP_001616588	1431	hypothetical protein sce5944	MXAN_4870
	sce5945	YP_001616589	802	hypothetical protein sce5945	MXAN_2541
	STAUR_0994	YP_003950625	246	mota/tolq/exbb proton channel family protein	MXAN_6862

Stigmatella aurantiaca DW4/3-1	STAUR_0995	YP_003950626	160	biopolymer transport protein, exbd/tolr family	MXAN_6861
	STAUR_0996	YP_003950627	195	adventurous gliding motility protein agls	MXAN_6860
	STAUR_1954	YP_003951585	1091	tetratricopeptide repeat protein	MXAN_4870
	STAUR_1955	YP_003951586	520	hypothetical protein STAUR_1955	MXAN_2541
	STAUR_1956	YP_003951587	211	hypothetical protein STAUR_1956	MXAN_2539
	STAUR_1957	YP_003951588	745	fha domain protein	MXAN_4867
	STAUR_1958	YP_003951589	133	hypothetical protein STAUR_1958	MXAN_4868
	STAUR_2684	YP_003952314	450	hypothetical protein STAUR_2684	MXAN_4867
	STAUR_2685	YP_003952315	82	hypothetical protein STAUR_2685	MXAN_4868
	STAUR_2686	YP_003952316	442	tetratricopeptide repeat protein	MXAN_4869
	STAUR_2687	YP_003952317	1109	tetratricopeptide repeat protein	MXAN_4870
	STAUR_2688	YP_003952318	785	hypothetical protein STAUR_2688	MXAN_2541
	STAUR_3259	YP_003952878	176	adventurous gliding motility protein agmo	MXAN_2538
	STAUR_3260	YP_003952879	274	hypothetical protein STAUR_3260	MXAN_2539
	STAUR_3261	YP_003952880	270	hypothetical protein STAUR_3261	MXAN_2541
	STAUR_3262	YP_003952881	674	tetratricopeptide repeat domain protein	MXAN_2541
	STAUR_3837	YP_003953452	273	hypothetical protein STAUR_3837	MXAN_2541
	STAUR_3838	YP_003953453	397	hypothetical protein STAUR_3838	MXAN_2539
	STAUR_3839	YP_003953454	511	hypothetical protein STAUR_3839	MXAN_2541
	STAUR_3840	YP_003953455	1209	tetratricopeptide repeat protein	MXAN_4870
	STAUR_3841	YP_003953456	479	tetratricopeptide repeat family protein	MXAN_4869
	STAUR_3842	YP_003953457	97	hypothetical protein STAUR_3842	MXAN_4868
	STAUR_3843	YP_003953458	641	fha/tonb domain protein	MXAN_4867
	STAUR_3845	YP_003953460	198	hypothetical protein STAUR_3845	MXAN_4866
	STAUR_5105	YP_003954704	175	hypothetical protein STAUR_5105	MXAN_6860

	STAUR_5106	YP_003954705	172	hypothetical protein STAUR_5106	MXAN_6861
	STAUR_5107	YP_003954706	244	mota/tolq/exbb proton channel family protein	MXAN_6862
	STAUR_5649	YP_003955239	653	adventurous gliding motility protein agmx	MXAN_4862
	STAUR_5650	YP_003955240	4089	adventurous gliding motility protein agmk	MXAN_4863
	STAUR_5652	YP_003955242	211	hypothetical protein STAUR_5652	MXAN_4866
	STAUR_5653	YP_003955243	640	fha domain/tonb domain protein	MXAN_4867
	STAUR_5654	YP_003955244	88	hypothetical protein STAUR_5654	MXAN_4868
	STAUR_5655	YP_003955245	474	adventurous gliding protein t	MXAN_4869
	STAUR_5656	YP_003955246	1216	tetratricopeptide repeat protein	MXAN_4870
Fibrobacter succinogenes S85	Fiscuc_1892	YP_003249964	746	TPR repeat-containing protein	MXAN_2541
	Fiscuc_1893	YP_003249965	1292	TPR repeat-containing protein	MXAN_4870
	Fiscuc_1894	YP_003249966	212	MotA/TolQ/ExbB proton channel	MXAN_6862
	Fiscuc_1896	YP_003249968	164	Biopolymer transport protein ExbD/TolR	MXAN_6860
	Fiscuc_1897	YP_003249969	308	TonB family protein	MXAN_4867
Methylibium petroleiphilum PM1	Mpe_A1224	YP_001020421	634	hypothetical protein Mpe_A1224	MXAN_2541
	Mpe_A1225	YP_001020422	941	hypothetical protein Mpe_A1225	MXAN_4870
	Mpe_A1226	YP_001020423	243	hypothetical protein Mpe_A1226	MXAN_4869
	Mpe_A1228	YP_001020425	217	putative adventurous gliding motility protein R	MXAN_6862
	Mpe_A1229	YP_001020426	170	hypothetical protein Mpe_A1229	MXAN_6861
	Mpe_A1230	YP_001020427	163	adventurous gliding motility protein S	MXAN_6860
	Mpe_A1231	YP_001020428	371	hypothetical protein Mpe_A1231	MXAN_4867
Cellvibrio japonicus Ueda107	CJA_3312	YP_001983766	323	TonB family C-terminal domain protein	MXAN_4867
	CJA_3313	YP_001983767	173	putative adventurous gliding motility protein S	MXAN_6860
	CJA_3314	YP_001983768	181	hypothetical protein CJA_3314	MXAN_6861
	CJA_3315	YP_001983769	231	adventurous gliding motility protein R	MXAN_6862

	CJA_3317	YP_001983771	244	putative TPR domain protein	MXAN_4869
	CJA_3318	YP_001983772	964	tetratricopeptide repeat domain protein	MXAN_4870
	CJA_3319	YP_001983773	660	hypothetical protein CJA_3319	MXAN_2541
Hahella chejuensis KCTC 2396	HCH_02601	YP_433818	640	TPR repeat-containing protein	MXAN_4869
	HCH_02602	YP_433819	963	hypothetical protein HCH_02602	MXAN_4870
	HCH_02603	YP_433820	203	TPR repeat-containing protein	MXAN_4869
	HCH_02626	YP_433841	584	TPR repeat-containing protein	MXAN_2541
	HCH_02627	YP_433842	933	hypothetical protein HCH_02627	MXAN_4870
	HCH_02628	YP_433843	197	TPR repeat-containing protein	MXAN_4869
	HCH_02631	YP_433845	221	biopolymer transport protein	MXAN_6862
	HCH_02632	YP_433846	170	hypothetical protein HCH_02632	MXAN_6861
	HCH_02633	YP_433847	165	biopolymer transport protein	MXAN_6860
	HCH_02634	YP_433848	334	hypothetical protein HCH_02634	MXAN_4867
Marinobacter aquaeolei VT8	Maqu_1595	YP_958866	321	hypothetical protein Maqu_1595	MXAN_4867
	Maqu_1596	YP_958867	162	biopolymer transport protein	MXAN_6860
	Maqu_1597	YP_958868	176	biopolymer transport protein ExbD/TolR	MXAN_6861
	Maqu_1598	YP_958869	221	MotA/TolQ/ExbB proton channel	MXAN_6862
	Maqu_1600	YP_958871	162	TPR repeat-containing protein	MXAN_4869
	Maqu_1601	YP_958872	939	TPR repeat-containing protein	MXAN_4870
	Maqu_1602	YP_958873	550	hypothetical protein Maqu_1602	MXAN_2541
	Maqu_1807	YP_959076	324	hypothetical protein Maqu_1807	MXAN_4867
	Maqu_1808	YP_959077	166	biopolymer transport protein ExbD/TolR	MXAN_6860
	Maqu_1809	YP_959078	170	biopolymer transport protein ExbD/TolR	MXAN_6861
	Maqu_1810	YP_959079	235	MotA/TolQ/ExbB proton channel	MXAN_6862
	Maqu_1812	YP_959081	189	TPR repeat-containing protein	MXAN_4869

	Maqu_1813	YP_959082	952	TPR repeat-containing protein	MXAN_4870
	Maqu_1814	YP_959083	648	TPR repeat-containing protein	MXAN_2541
Saccharophagus degradans 2-40	Sde_2954	YP_528423	325	hypothetical protein Sde_2954	MXAN_4867
	Sde_2955	YP_528424	185	hypothetical protein Sde_2955	MXAN_6860
	Sde_2956	YP_528425	169	hypothetical protein Sde_2956	MXAN_6861
	Sde_2957	YP_528426	242	biopolymer transport proteins-like	MXAN_6862
	Sde_2959	YP_528428	230	cellulose binding, type IV	MXAN_4869
	Sde_2960	YP_528429	952	cellulose binding, type IV	MXAN_4870
	Sde_2961	YP_528430	570	hypothetical protein Sde_2961	MXAN_2541
	Sde_3560	YP_529027	325	hypothetical protein Sde_3560	MXAN_4867
	Sde_3561	YP_529028	178	sigma-70 factor	MXAN_6860
	Sde_3562	YP_529029	183	hypothetical protein Sde_3562	MXAN_6861
	Sde_3563	YP_529030	220	ATPase	MXAN_6862
	Sde_3565	YP_529032	222	hypothetical protein Sde_3565	MXAN_4869
	Sde_3566	YP_529033	957	coenzyme A biosynthesis protein	MXAN_4870
	Sde_3567	YP_529034	624	hypothetical protein Sde_3567	MXAN_2541
Shewanella frigidimarina NCIMB 400	Sfri_1223	YP_749914	332	hypothetical protein Sfri_1223	MXAN_4867
	Sfri_1224	YP_749915	177	sigma-70 factor	MXAN_6860
	Sfri_1225	YP_749916	188	hypothetical protein Sfri_1225	MXAN_6861
	Sfri_1226	YP_749917	217	MotA/TolQ/ExbB proton channel	MXAN_6862
	Sfri_1228	YP_749919	263	TPR repeat-containing protein	MXAN_4869
	Sfri_1229	YP_749920	1016	TPR repeat-containing protein	MXAN_4870
	Sfri_1230	YP_749921	692	hypothetical protein Sfri_1230	MXAN_2541
	TERTU_1670	YP_003073195	205	MotA/TolQ/ExbB proton channel	MXAN_6862
	TERTU_1671	YP_003073196	173	transport energizing protein, ExbD/TolR family	MXAN_6861

Teredinibacter turnerae T7901	TERTU_1672	YP_003073197	165	hypothetical protein TERTU_1672	MXAN_6860
	TERTU_1849	YP_003073348	552	hypothetical protein TERTU_1849	MXAN_2541
	TERTU_1850	YP_003073349	947	TPR repeat domain protein	MXAN_4870
	TERTU_1851	YP_003073350	212	tetratricopeptide repeat domain protein	MXAN_4869
	TERTU_1853	YP_003073352	272	transporter, MotA/TolQ/ExbB proton channel family	MXAN_6862
	TERTU_1854	YP_003073353	170	hypothetical protein TERTU_1854	MXAN_6861
	TERTU_1855	YP_003073354	178	hypothetical protein TERTU_1855	MXAN_6860
	TERTU_1856	YP_003073355	321	hypothetical protein TERTU_1856	MXAN_4867
	TERTU_3740	YP_003075049	325	TonB domain protein	MXAN_4867
	TERTU_3741	YP_003075050	176	hypothetical protein TERTU_3741	MXAN_6860
	TERTU_3742	YP_003075051	183	hypothetical protein TERTU_3742	MXAN_6861
	TERTU_3743	YP_003075052	245	ATPase	MXAN_6862
	TERTU_3745	YP_003075054	225	tetratricopeptide repeat protein	MXAN_4869
	TERTU_3746	YP_003075055	964	TPR repeat domain protein	MXAN_4870
	TERTU_3747	YP_003075056	640	tetratricopeptide repeat domain protein	MXAN_2541
Thioalkalivibrio sp. HL-EbGR7	Tgr7_0536	YP_002512620	535	hypothetical protein Tgr7_0536	MXAN_4867
	Tgr7_0537	YP_002512621	170	sigma-70 factor	MXAN_6860
	Tgr7_0538	YP_002512622	168	hypothetical protein Tgr7_0538	MXAN_6861
	Tgr7_0539	YP_002512623	222	MotA/TolQ/ExbB proton channel	MXAN_6862
	Tgr7_0541	YP_002512625	190	TPR repeat-containing protein	MXAN_4869
	Tgr7_0542	YP_002512626	922	hypothetical protein Tgr7_0542	MXAN_4870
	Tgr7_0543	YP_002512627	620	hypothetical protein Tgr7_0543	MXAN_2541

Table S4. Primers	
Name	Sequences of primers (5’---3’)
1922-1	AAAGAATTCCTGGTACGAGAAGAACAAGGGC
1922-2	AAAAAGCTTGTAGATGCGCTCGTACAGCTTC
3374-1	AAAGAATTCCAGTTGGTCCGCAAGGAAATG
3374-2	AAAAAGCTTCTTCTTCGGGTTCTTCTCCTTC
INS1327-1	CCCAAGCTTTGGAGAAGAGCCGCTACG
INS1327-2	CGGGATCCCGTCGTAGAGCTTCTGG
DAGMU7	AAAGAATTCACGCCTCGCCATTCGC
DAGMU8	AAAGGTACCCATGGTCTTCCTAGGAGAGGGGC
DAGMU9	AAAGGTACCAAGACTCAGGTGGACGCC
DAGMU10	AAAAAGCTTCTGGCCCATGCCCTTGTA
DAGLT1	AAGAATTCGAACGAGTACCGGCGCC
DAGLT5	AAAGGATCCTGGCCTTGGAGGACGTAC
DAGLT6	AAAGGATCCCCGACCAGAAGAATGCAGG
DAGLT4	TTAAGCTTCCGTTGACGTACGTGCCC
D4868-1	AAGAATTCCCGGAGCTCCACCACG
D4868-5	AAAGGATCCTCACAGCAGGTCGTCTTCC
D4868-6	AAAGGATCCTAGCCAGCGCCACAACGC
D4868-4	TTAAGCTTCGAAGGCCCCCTTCCTAC
D4867-1	AAGAATTCCGAAGCGCGAGGCCAAG
D4867-5	AAAGGATCCGTCCTTGGAGGCGACCAG
D4867-6	AAAGGATCCCGTGGTGGTCGTCACGTATC
D4867-4	TTAAGCTTACGTCTTTCTCCCGCTAGAAC
D4866-1	AAGAATTCCACCCGAACAAGAAGGACGAG
D4866-2	GCGGTCCTGACGTTGGC
D4866-3	CAACGTCAGGACCGCCGGGAGAAAGACGTGCCTC
D4866-4	TTAAGCTTTCCTCGGCCTCGGGAC
4866-4	AAATCTAGACGCCGGGTGGCCTTTC
4866-5	AAAAAGCTTGAAATCCGTCTTGGAGAGCGC
D4866-4	TTAAGCTTTCCTCGGCCTCGGGAC
D2541-1	GGAATTCCCTCGGCGCTGCCGGGGCGAG
D2541-2	CGGGATCCGGCGACGCGGATGAGCCGGA
D2541-3	CGGGATCCGGACCCGGGACTTCTCCCCC
D2541-4	CCCAAGCTTGCGCCTCGCGCCCTGGCGCG
PROM4868-1	CCCAAGCTTCGACGCCGGCTTCCGGCACGG
4868-SANSSTOP-2	CAGCTCGCCCACGGACTGCATCACCTTG
4868-MCHERRY-3	GTCCGTGGGCGAGCTGGTGAGCAAGGGCGAGGAG
MCHERRY-4	CGGGATCCTTACTTGTACAGCTCGTCCATGCCG
PROM4867-BAMHI	CGCGGATCCATGCAGTCCGTGGG
4867-ECORI-4	CGGAATTCCCGGCGCTATTCGCCG
2539-1	CGGAATTCAACCAGTCGCGCGGAAAGG
2539-2	GCTCTAGACTGGGCGGATGCCAGTGC
2539-3	GCTCTAGAGCAGGCATCTCGCTGTTCC
2539-4	CCCAAGCTTAGGCCCTCGAAGTTCTGC
2540-1	CGGAATTCTTTGAACCGCCCCAAGTTGCTGC
2540-2	GCTCTAGATTCGGTGGTCTGGGCGAAGC
2540-3	GCTCTAGACTGCGCAACCAGCTCCTGTTCG
2540-4	CCCAAGCTTTTGTCGGCTTCCTCGGGCTG
2538-1	CGGAATTCTACTCGGCGAAGGCCTGCATCAGG
2538-2	GCTCTAGACGGACGTTCGGCGAGAACAAC
2538-3	GCTCTAGACATGAGGGCGGTTCGCACGAAC
2538-4	CCCAAGCTTGTAGCCGTCGAAGTGGAGGATGG
AGMU-QT1	CACGAAGATCGTCCAGGAG
AGMU-QT2	GCCATCCTCCATGAGGTAC
AGLT-QT1	CGTCAGGCCTCTGAGAACC
AGLT-QT2	GGAGCACCTCCTGGTACAG
4868-QT1	GAAGACGACCTGCTGTGAAAG

4868-QT2	GAAACACAAGGTTCGCATC
4867-QT1	GCCGTTCCTCTGACACTC
4867-QT2	GAGACGGCCAATCTTGATG
4866-QT1	GTGCGCTTCGTTCGTTCTC
4866-QT2	CGATTTCATCGAACGTGAC
AGMO-QT1	CGCTCCTGTTGGGTGGCT
AGMO-QT2	GGAGTTGTTGTTGGCCGC
2539-QT3	CCTGTGTCTGGTGCCCGC
2539-QT4	GCATCCTGCGATGACTCGG
2540-QT3	CCACCGAAGAGGCGGAAG
2540-QT4	GGAAGACGTGGCCGGAG
2541-QT1	GTGGACGGCCCCCACCTA
2541-QT2	GGTGGGCTTCTTCTTGGG
4867-O1	GCTCTAGACGCCGTTCCTCTGACACTC
4867-O2	GGAATTCCTATTCGCCGGACTGCTTG
GMOA-O1	CCCAAGCTTGGACCTGGCGTCTGTGAC
GMOA-O2	GGAATTCTCCTCCTCGTCGCGAG

Table S5. Plasmids

Name	Description	Source
pBJ114	Used to create deletions, *galK*, Km^R	[23]
pSWU30	Tet^R used to integrate genes ectopically at $Mx8_{att}$	L. Søgaard-Andersen
pBJAglZY	pBJ114 with a cassette allowing construction of the *aglZ-yfp* chimeric gene	[12]
pBJΩMxan_1922	pBJ114 with an insertion cassette for Mxan_1922	This work
pBJΩMxan_3374	pBJ114 with an insertion cassette for Mxan_3374	This work
pBJΩMxan_1327	pBJ114 with an insertion cassette for Mxan_1327	This work
pBJΔgltD	pBJ114 with a deletion cassette for *gltD*	This work
pBJΔgltE	pBJ114 with a deletion cassette for *gltE*	This work
pBJΔgltF	pBJ114 with a deletion cassette for *gltF*	This work
pBJΔgltG	pBJ114 with a deletion cassette for *gltG*	This work
pBJΔgltH	pBJ114 with a deletion cassette for *gltH*	This work
pBJΔgltC	pBJ114 with a deletion cassette for *gltC*	This work
pBJΔgltK	pBJ114 with a deletion cassette for *gltK*	This work
pBJΔgltB	pBJ114 with a deletion cassette for *gltB*	This work
pBJΔgltA	pBJ114 with a deletion cassette for *gltA*	This work
pBJΔpilA	pBJ114 with a deletion cassette for *pilA*	Laboratory stock
pBJΔaglQ	pBJ114 with a deletion cassette for *aglQ*	[13]
pSWU30gltG	pSWU30 allowing expression of *gltG* from its own promoter at $Mx8_{att}$	This work
pSWU30gltFC	pSWU30 allowing expression of *gltF-mCherry* from its own promoter at $Mx8_{att}$	This work
pKT25	Bacterial two-hybrid T25 donor plasmid	Euromedex
pUT18	Bacterial two-hybrid T18 donor plasmid	Euromedex
pUT18AglR	AglR-T18 fusion donor construct	This work
pKT25GltG	GltG-T25 fusion donor construct	This work

Table S6. *Myxococcus* strains

Strain	Construction	Source	Genotype
DZ2	Wild type	Laboratory collection	WT
TM156	DZ2 *pilA: :tet*	Laboratory collection	Ω*pilA*
TM267	DZ2 *frzE::Tn5* Ω*231*	David Zusman	ΩfrzE
DZ4770	DZ2 Δ*aglZ*	[24]	Δ*aglZ*
TM140	DZ2 pBJΩMxan_1922	This work	ΩMxan_1922
TM141	DZ2 pBJΩMxan_3374	This work	ΩMxan_3374
TM643	DZ2 pBJΩMxan_1327	This work	ΩMxan_1327
TM142	DZ2 Δ*gltD* (pBJΔgltD)	This work	Δ*gltD*
TM148	DZ2 Δ*gltE* (pBJΔgltE)	This work	Δ*gltE*
TM136	DZ2 Δ*gltF* (pBJΔgltF)	This work	Δ*gltF*
TM135	DZ2 Δ*gltG* (pBJΔgltG)	This work	Δ*gltG*
TM149	DZ2 Δ*gltH* (pBJΔgltH)	This work	Δ*gltH*
TM456	DZ2 Δ*gltC* (pBJΔgltC)	This work	Δ*gltC*
TM600	DZ2 Δ*gltK* (pBJΔgltK)	This work	Δ*gltK*
TM603	DZ2 Δ*gltB* (pBJΔgltB)	This work	Δ*gltB*
TM606	DZ2 Δ*gltA* (pBJΔgltA)	This work	Δ*gltA*
TM253	TM142 *pilA: :tet*	This work	Δ*gltD* Ω*pilA*
TM297	TM148 *pilA: :tet*	This work	Δ*gltE* Ω*pilA*
TM246	TM136 *pilA: :tet*	This work	Δ*gltF* Ω*pilA*
TM245	TM135 *pilA: :tet*	This work	Δ*gltG* Ω*pilA*
TM244	TM149 *pilA: :tet*	This work	Δ*gltH* Ω*pilA*
TM466	TM456 *pilA: :tet*	This work	Δ*gltC* Ω*pilA*
TM602	TM600 *pilA: :tet*	This work	Δ*gltK* Ω*pilA*
TM605	TM603 *pilA: :tet*	This work	Δ*gltB* Ω*pilA*
TM608	TM606 *pilA: :tet*	This work	Δ*gltA* Ω*pilA*
TM274	TM142 *frzE::Tn5* Ω*231*	This work	Δ*gltD* ΩfrzE
TM275	TM148 *frzE::Tn5* Ω*231*	This work	Δ*gltE* ΩfrzE
TM276	TM136 *frzE::Tn5* Ω*231*	This work	Δ*gltF* ΩfrzE
TM277	TM135 *frzE::Tn5* Ω*231*	This work	Δ*gltG* ΩfrzE
TM293	TM149 *frzE::Tn5* Ω*231*	This work	Δ*gltH* ΩfrzE
TM467	TM456 *frzE::Tn5* Ω*231*	This work	Δ*gltC* ΩfrzE
TM601	TM600 *frzE::Tn5* Ω*231*	This work	Δ*gltK* ΩfrzE
TM604	TM603 *frzE::Tn5* Ω*231*	This work	Δ*gltB* ΩfrzE
TM607	TM606 *frzE::Tn5* Ω*231*	This work	Δ*gltA* ΩfrzE
TM330	DZ4770 *frzE::Tn5* Ω*231*	This work	Δ*aglZ* ΩfrzE
TM392	TM330 ΔpilA (pBJΔpilA)	This work	Δ*aglZ* Δ*pilA* ΩfrzE
TM445	TM274 ΔpilA (pBJΔpilA)	This work	Δ*gltD* Δ*pilA* ΩfrzE
TM248	TM135 *mx8*$_{att}$*::gltG* (pSWU30gltG)	This work	Δ*gltG gltG*
TM273	TM136 *mx8*$_{att}$*::gltF-mCherry* (pSWU30gltFC)	This work	Δ*gltF gltF-mCherry*
TM406	TM273 ΔpilA (pBJΔpilA)	This work	Δ*gltF* Δ*pilA gltC-mCherry*
TM247	*agmU-mcherry*	[18]	*agmU-mcherry*
TM410	TM247 *pilA: :tet*	This work	Ω*pilA agmU-mcherry*
TM472	TM410 *aglZ-yfp* (pBJAglZY)	This work	Ω*pilA agmU-mcherry aglZ-yfp*
TM470	TM410 Δ*aglQ* (pBJΔaglQ)	This work	Δ*aglQ* Ω*pilA agmU-mcherry*
TM471	TM406 Δ*aglQ* (pBJΔaglQ)	This work	Δ*aglQ* Δ*gltF* Δ*pilA gltF-mCherry*

Table S7. Plasmid constructions

Plasmid	Construction scheme[a]
pBJΩ1922	A 1Kb internal fragment of Mxan_1922 was amplified from the DZ2 chromosome with primers 1922-1 / 1922-2 and cloned at the *EcoRI* and *Hind*III sites of pBJ114.
pBJΩ3374	A 1Kb internal fragment of Mxan_3374 was amplified from the DZ2 chromosome with primers 3374-1 / 3374-2 and cloned at the *EcoRI* and *Hind*III sites of pBJ114.
pBJΩ1327	A 750bp internal fragment of Mxan_1327 was amplified from the DZ2 chromosome with primers ins1327-1 / ins1327-2 and cloned at the *HindIII* and *BamHI* sites of pBJ114.
pBJΔgltD	Primer pairs DAgmU7 / DAgmU8 and DAgmU9 / DAgmU10 were used to amplify 1kb fragment upstream and downstream from the *gltD* open-reading frame. The upstream fragment was first cloned at the *EcoRI* and *KpnI* sites of pBJ114. Then, the downstream fragment was ligated at the *KpnI* and *HindIII* sites of the pBJ114-upstream fragment.
pBJΔgltE	Primer pairs DAglT1 / DAglT5 and DAglT6 / DAglT4 were used to amplify 1kb fragment upstream and downstream from the *gltE* open-reading frame. The upstream fragment was first cloned at the *EcoRI* and *BamHI* sites of pBJ114. Then, the downstream fragment was ligated at the *BamHI* and *HindIII* sites of the pBJ114-upstream fragment.
pBJΔgltF	Primer pairs D4868-1 / D4868-5 and D4868-6 / D4868-4 were used to amplify 1kb fragment upstream and downstream from the *gltF* open-reading frame. The upstream fragment was first cloned at the *EcoRI* and *BamHI* sites of pBJ114. Then, the downstream fragment was ligated at the *BamHI* and *HindIII* sites of the pBJ114-upstream fragment.
pBJΔgltG	Primer pairs D4867-1 / D4867-5 and D4867-6 / D4867-4 were used to amplify 1kb fragment upstream and downstream from the *gltG* open-reading frame. The upstream fragment was first cloned at the *EcoRI* and *BamHI* sites of pBJ114. Then, the downstream fragment was ligated at the *BamHI* and *HindIII* sites of the pBJ114-upstream fragment.
pBJΔgltH	Primer pairs D4866-1 / D4866-2 and D4866-3 / D4866-4 were used to amplify 1kb fragment upstream and downstream from the *gltH* open-reading frame. The fragments were then fused by overlap PCR and cloned at the *EcoRI* and *BamHI* sites of pBJ114.
pBJΔgltC	Primer pairs D2541-1 / D2541-2 and D2541-3 / D2541-4 were used to amplify 1kb fragment upstream and downstream from the *gltC* open-reading frame. The upstream fragment was first cloned at the *EcoRI* and *BamHI* sites of pBJ114. Then, the downstream fragment was ligated at the *BamHI* and *HindIII* sites of the pBJ114-upstream fragment.
pSWU30gltG	A fragment encompassing *gltG* and the *glt*G promoter region was amplified from the DZ2 chromosome with primers prom4867-BamHI / 4867EcoRI-4 and cloned at the *BamHI* and *EcoRI* sites of pSWU30.
pSWU30gltFC	Primers prom4868-1 / 4868-sansSTOP-2 were used to amplify the fragment *gltF* and its promoter from the DZ2 chromosome. Primers 4868-mcherry-3 / mcherry-4 were used to amplify the fragment *mCherry* from a plasmid containing the *mcherry* gene. Both fragments were fused by SOE-PCR and cloned at the *BamHI* and *HindIII* sites of pSWU30.
pBJΔgltA	Primer pairs 2540-1 / 2540-2 and 2540-3 / 2540-4 were used to amplify 1kb fragment upstream and downstream from the *gltA* open-reading frame. The upstream (*EcoRI* / *XbaI*) and downstream (*XbaI* / *HindIII*) fragment was cloned in one step at the *EcoRI* and *HindIII* sites of pBJ114.
pBJΔgltB	Primer pairs 2539-1 / 2539-2 and 2539-3 / 2539-4 were used to amplify 1kb fragment upstream and downstream from the *gltB* open-reading frame. The upstream (*EcoRI* / *XbaI*) and downstream (*XbaI* / *HindIII*) fragment was cloned in one step at the *EcoRI* and *HindIII* sites of

	pBJ114.
pBJΔgltK	Primer pairs 2538-1 / 2538-2 and 2538-3 / 2538-4 were used to amplify 1kb fragment upstream and downstream from the *gltK* open-reading frame. The upstream (*EcoRI* / *XbaI*) and downstream (*XbaI* / *HindIII*) fragment was cloned in one step at the *EcoRI* and *HindIII* sites of pBJ114.
pUT18AglR	A fragment encompassing *aglR* was amplified from the DZ2 chromosome with primers GMOA-O1 / GMOA-O2 and cloned at the *HindIII* and *EcoRI* sites of pUT18.
pKT25GltG	A fragment encompassing *gltG* was amplified from the DZ2 chromosome with primers 4867-O1 / 4867-O2 and cloned at the *XbaI* and *EcoRI* sites of pKT25.

[a] All plasmid inserts were sequenced to ensure the absence of PCR-introduced mutations.

Text S1

MXAN4864 and MXAN4865 may not be actual motility genes

The predicted MXAN_4864 and MXAN_4865 overlap and are transcribed in opposite direction (not shown). In fact, the MXAN_4864 and MXAN_4865 ORFs are predicted with equal probability based on third position GC skew (data not shown); however, they both encode hypothetical proteins unique to *M. xanthus* and its very close relative *Stigmatella aurantiaca* DW4/3-1. Thus, these ORFs are likely false positives (MXAN_4865 is no longer annotated in the *M. xanthus* DK1622 genome) and we favour the hypothesis that the *agmV* transposon insertion (inserted in this region) did not disrupt an actual gene but exerted polar effects on the downstream *agmK* [1], potentially by disrupting critical promoter elements.

Text S2

Justification for a *glt* nomenclature of the gliding motility machinery genes.

We propose a new Glt nomenclature for the G1 and G2 genes. The evidence indicates that the G1 and G2 genes encode a trans-envelope complex that interacts with the AglRQS motor and transduces its activity to the cell surface. In consequence we rename those genes **gl**iding **t**ransducer genes (*glt*). This new nomenclature will be helpful for several reasons:

- There is currently no established nomenclature about A-motility genes in *Myxococcus*. Until now names have been given based on genetic screens and authors have used their own nomenclature to name the genes. Early genetic studies named gliding motility genes *agl* and *cgl*, depending on whether the motility defect can be rescued upon cell-cell contact or not [2,3]. More recent genetic screens introduced *agm* (**a**dventurous **g**liding **m**otility), *agn* (**a**dventurous **g**lidi**n**g) and *pgl* (**p**artial **gl**iding) [1,4]. Some genes are even named after two distinct nomenclatures even if they are transcribed in the same operon for example, *agmU*, *aglT* and *pglI* (we rename these genes *gltD*, *gltE* and *gltG*).

-The lack of a clear nomenclature also creates confusion when previously unknown motility genes must be named. For example, this study and also the study by Nan et al. [5] identify new motility functions for open reading frames such as MXAN4868, 4866, 2539 and 2540 that were previously uncharacterized. Many gene letters are already used by the various nomenclatures. The G2 cluster contains AgmO, MXAN2539, MXAN2540 and AgnA. In this example, not only it is not clear which of the *agm* or *agn* nomenclature should be used but *in fine* none is possible because AgmP, AgmQ or AgnB, AgnC are already used for other motility genes [1,4].

- Most of the genes names were given from loss of function transposon-based genetic screens. While clearly some of the genes encode the A-motility machinery, many other genes may encode unrelated functions. Presumably, general cellular defects, for example metabolic or cell division division defects, would also create gliding motility phenotypes. Thus, a Glt nomenclature inspired from flagellar genes (*fla*) or pilus genes (*pil*) would greatly clarify specific gene functions. Such approach has been used recently for the *nfs* system to name the G3 cluster genes with a function in sporulation [6]. For consistency, the *glt* genes were lettered according to their *nfs* homologues. For example *nfsA* is homologous to *gltA*, *nfsB* to *gltB* and so forth.

Text S3

Principle of the phylogenomic analysis

The phylogenomic analysis of a cellular system or complex starts with the comparison of the evolutionary history of its components (i.e. their phylogeny) to the phylogeny of the organisms carrying homologues of the corresponding genes [7,8]. This allows identifying: (i) the evolutionary origins of the components (i.e. in which lineage each of the components appeared), (ii) the events that changed their evolutionary histories (i.e. duplications, losses, transfers, fusions and splits of genes, gains or losses of functional domains, etc.) and (iii), the genomic events that have affected organization of the genes in genomes (i.e. gene cluster formation, disruption, etc.). At this step, working with complete genomic sequences is essential because it allows conclusive inference on the presence/absence of a gene in a given organism. Integrating information on each individual component of a system may thus reveal the evolutionary history of this particular system or complex. In an attempt to do so, we applied such approach to the genes of the G1, G2 and M1 clusters.

Article III

A Versatile Class of Cell Surface Directional Motors Gives Rise to Gliding Motility and Sporulation in *Myxococcus xanthus*.

Morgane Wartel[1], Adrien Ducret[1, 2], Shashi Thutupalli[3], Fabian Czerwinski[3], Anne-Valérie Le Gall[1], Emilia M.F. Mauriello[1], Ptissam Bergam[4], Yves V. Brun[2], Joshua Shaevitz[3], Tâm Mignot[1].

[1] Laboratoire de Chimie Bactérienne, CNRS UMR 7283, Aix-Marseille Université, Institut de Microbiologie de la Méditerranée, 31, Chemin Joseph Aiguier, 13009, Marseille, France

[2] Department of Biology, Indiana University, Bloomington, IN 47405, USA

[3] Department of Physics and the Lewis-Sigler Institute for Integrative Genomics, Princeton University, Princeton, NJ 08540, USA

[4] Plateforme de Microscopie, Institut de Microbiologie de la Méditerranée, 31, Chemin Joseph Aiguier, 13009, Marseille, France

In press in PLoS Biology.

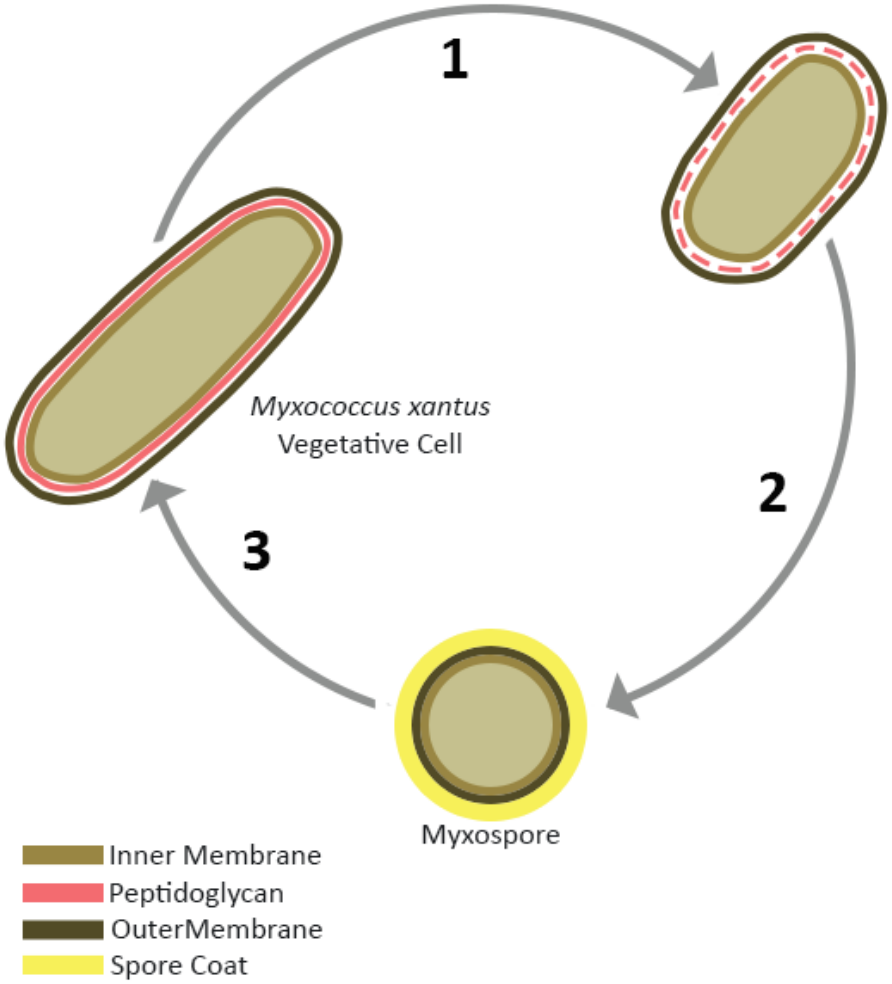

Figure 28. Sporulation of *M. xanthus*. Sporulation is induced by starvation or glycerol addition (step 1). During the sporulation process, the peptidoglycan seems to be degraded. Then, the ExoA-I machinery synthesizes and secretes the spore coat. The Nfs machinery is essential for the formation of dense and compact spore coat around the spore (step 2). Germination happens when nutriments become again available, or when the glycerol inducer is removed (step 3).

The discovery of the Glt proteins revealed that the *Myxococcus* genome contains several other sets of *glt*-like genes (Luciano et al., 2011). Intriguingly, one complex, the so-called *nfs* locus (for necessary for sporulation) was recently shown to be required for spore coat assembly (Müller et al., 2012, 2010). In this study, we investigated the unsuspected link between gliding motility and spore coat assembly.

Sporulation has evolved in many bacterial species to survive under unfavorable conditions. During sporulation, the bacterial genome is encased in a resistant shell, a dormant cell type called a spore. When the environmental conditions improve, the spore germinates and the cell returns to its vegetative state. Spores are more resistant to ultraviolet (UV) radiation, chemicals, extreme heat and other stresses. These resistance properties are mostly due to metabolic dormancy and the dehydrated state of spores.

Sporulation in *M. xanthus* differs from well documented sporulating species, such as endospore formers and actinomycetes. During *M. xanthus* sporulation, the rod-shaped vegetative cell is remodeled into a spherical spore, independently of a septation event (Figure 28) (Kroos, 2007). In *M. xanthus*, sporulation is linked to the formation of multicellular fruiting bodies, a long process that only occurs after 72 hours (Kroos, 2007). *In vitro*, *M. xanthus* sporulation can also be induced by the addition of glycerol to liquid cultures (DWORKIN and GIBSON, 1964). In this latter case, resistant spores are formed in about 8 hours. Therefore, glycerol induction is a useful method to study the sporulation process in laboratories.

Myxospores contain inner and outer membranes, surrounded by a thick carbohydrate-rich spore coat (Kottel et al., 1975). It was recently determined that the peptidoglycan (PG) layer seems to be absent in spores, suggesting that the spore coat itself could replace the PG for the structural preservation of cell shape (Bui et al., 2009). In 2010, Müller *et al.* identified a locus consisting of eight genes, *nfsA-H*, which is essential for producing viable spores (Müller et al., 2010). The *nfs* genes encode close homologues to the GltA-H proteins, involved in gliding motility (Luciano et al., 2011). In their study, Müller *et al.* showed that the Nfs proteins appears to be necessary for the assembly of a dense and compact spore coat on the cell surface (Müller et al., 2012). Specifically, the Nfs proteins seem to function in a pathway involving the *exoA-I* genes, which encodes enzymes that drive spore coat synthesis and secretion. Based on these results, *M. xanthus* sporulation was proposed to be a stepwise process (Figure 28). During the first step of sporulation, the PG layer is seemingly degraded, which leads to cell rounding. Then, the Exo polymer is synthesized and exported by the Exo proteins and deposited around the collapsed

inner and outer membranes. The tight wrapping of the Exo polymer around the spore membranes then requires the Nfs complex by an unknown mechanism.

In this manuscript, we investigated the function of Nfs, reasoning that this study would shed light on the function of Glt-like machineries. Müller *et al.* showed that all *nfs* genes are essential for sporulation and demonstrated that all their products localize to the cell envelope, like their Glt counterparts (Müller et al., 2012, 2010). These results led us to hypothesize that Nfs proteins assemble a Glt-like membrane sporulation complex. Because we previously demonstrated that Glt promoted motility in association with the Agl motor, we supposed that the Nfs system might also require an Agl-like motor to function. By measuring the sporulation efficiency, we showed that the AglRQS motor itself is essential for sporulation. In the gliding machinery, the AglRQS motor contacts the Glt complex through a specific association between AglR and GltG. In the Nfs system, NfsG is the GltG paralogue and as observed for AglR and GltG, we found a direct interaction between AglR and NfsG. These results suggested that the Agl motor interacts with the Nfs complex to promote spore coat assembly.

Müller *et al.* also showed that in absence of Nfs, the spore coat is loosely attached to the spore surface, which results in abortive sporulation. By transmission electron microscopy (TEM), we found that in *nfsD* and *aglQ* mutants, the spore surface was surrounded by hair-like filaments that seemed loosely attached. Because these filaments were absent in an *exoA* mutant, defective for polymer secretion, we concluded that they constitute Exo polymer strands. To further elucidate how the Agl-Nfs machinery drives attachment of Exo polymer to the spore surface, we constructed functional NfsD-mCherry and AglQ-sfGFP (super folder green fluorescent protein) fusions and studied the dynamics of these fusions during sporulation. In contrast to its distributed localization during motility, AglQ-sfGFP accumulated circumferentially all around the spore membrane during the sporulation process. In contrast, NfsD-mCherry covered the cell surface during the initial stage of sporulation, but formed fluorescent bright clusters at the end of the cell-rounding phase. In time-lapse experiments, the NfsD-mCherry clusters were observed to move directionally in orbital trajectories around the spore surface. Nfs rotation is likely energized by the Agl motor because it was abolished by CCCP, or in an *aglQ* mutant.

Since Nfs seems to be linked with spore coat assembly, we hypothesized that the Agl motor may transport Nfs complex and the associated Exo polymer strands to construct a densely packed spore coat around the spore membrane. As previously done to study the gliding motility

machinery, we used micron-sized polystyrene beads assay to test directly whether Agl-Nfs machinery has a surface transport activity. Indeed, beads were transported around the spore surface in an Agl motor dependant manner. In parallel, using a spore coat-specific lectin, we showed that lectin bright clusters are linked with rotating NfsD-mCherry clusters. These results suggest that the Agl-Nfs machinery rotate Exo polymer strands, to construct a densely protective spore coat at surface. We also further demonstrated that the Exo spore coat constitutes itself a directionally factor for Nfs transport: in an *exoA* mutant that does not export the coat polymer, NfsD-mCherry is still able to move, but in an erratic and non-directional manner.

Based on these results, we proposed that following its secretion, the main spore coat polymer is transported at the cell surface by the Agl-Nfs machinery to wrap it around the spore surface. In this system, the AglRQS motor would transport Nfs subunits from one motor to the next, fueled by the PMF and guided by linked Exo-strands. Guidance by Exo polymer strands could occur as they become bound to the spore surface, acting like a molecular ratchet and preventing motor back steps thus restricting Agl-Nfs movement in one direction. In the section Discussion, I will discuss how the study of the Nfs system sheds light on the core function of Agl-Glt/Nfs like machineries.

Myxing It Up

By Mary Hoff

It slices, it dices, it cleans the kitchen sink. We've all heard of—and hailed the ingenious efficiency of—devices that perform more than one function. But humans don't have the corner on that market. A team led by Tâm Mignot and Morgane Wartel recently discovered that when the going gets rough, a common soil-inhabiting bacterium, Myxococcus xanthus, repurposes a molecule that's integral to the mechanism it uses to move around to build a fortress-type coat that protects it from its newly adverse environment.

The story behind the discovery of this remarkable example of making the most of what you have began several years ago, when the team uncovered the mechanism M. xanthus uses to move across a solid surface. They found that a molecular motor, Agl, combines with a second molecular complex, Glt, forming an assembly that the bacterium uses to propel itself with the help of a sugar polymer they call slime. Further analyzing this system, the researchers realized that the genes used as a blueprint to make Glt are similar to—and likely derived from a common ancestor gene with—those used to make another protein complex, Nfs, which must be present in order for the bacterium to use another sugar polymer, Exo, to form a hard, protective coat around itself when it encounters adverse environmental conditions. Considering the similarities between Glt and Nfs and the fact that they both used complex sugars to do their job, the researchers wondered: Might Agl be a multipurpose molecular device, deployed in the Nfs system in a similar manner to the way in which it interacts with Glt, when the cell's task turns from moving around to taking cover within its self-contained defense system?

To answer that question, the researchers took a closer look at how Nfs does its job. By testing the capabilities of mutants lacking the ability to make various proteins, they were able to assess whether genes that code for a different Agl-like molecule are required for spore formation (they aren't) and whether Agl is required for spore coat assembly (it is). Knowing that the Agl complex connects with Glt to create the motility function through the association of a helper molecule, GltG, the researchers then looked for and found a similar helping molecule that is required for proper Nfs system functioning. Based on this evidence, they concluded that the same Agl complex involved in motility does indeed associate with Nfs to provide the spore-forming function.

How exactly does the Agl-Nfs complex create a shell strong enough to protect M. xanthus when times get tough? To answer that question, the researchers used special molecular tools and analysis of the capabilities of various M. xanthus mutants to observe, and in some cases deduce, the movement and activities of Agl, Nfs and Exo as the work together to form a spore coat. The various analytical approaches indicated that the process likely begins when, in the face of adversity, the genes used to make the "gliding" molecular complex Glt turn off and those for the "necessary for sporulation" Nfs molecular complex turn on. As Nfs is formed in the wake of activation of its corresponding gene, it spreads across the outside of the bacterial cell, transported by Agl

and most likely guided by Exo, which is exported from within the cell at a few select locations on the cell surface. As it spreads, the Nfs-Agl complex assembles the protective spore coat by creating a meshwork of Exo strands anchored to the surface of the cell.

The researchers concluded that Agl does indeed play a role in two distinct but remarkably parallel functions within M. xanthus, with the distinction between them dependent on the nature of the accompanying molecular complex, which in turn depends on whether the cell is in move-about or duck-and-cover mode. Reflecting their common genetic heritage, Agl-Glt and Agl-Nfs perform broadly similar functions in transporting materials across the surface of the cell—in the former case, motility-empowering slime, and the latter, the threads that together weave a tight, protective shell. When M. xanthus goes into spore-forming mode, Agl breaks off from Glt and latches onto Nfs, where it serves as a transporter, distributing Nfs around the cell surface in a way that allows it to engage Exo to form the shell.

The authors note in closing that complexes similar to Agl exist in other kinds of bacteria, inviting exciting future studies of potential transport functions in other systems. They also note that the fact this one system, with slight modification, performs two quite different functions, opens the door to a new view of how minor changes at the genetic level can usher in dramatic new capabilities for living systems.

+++

A versatile class of cell surface directional motors gives rise to gliding motility and sporulation in *Myxococcus xanthus*

Morgane Wartel[1], Adrien Ducret[1,2,#], Shashi Thutupalli[3,#], Fabian Czerwinski[3], Anne-Valérie Le Gall[1], Emilia M.F. Mauriello[1], Ptissam Bergam[4], Yves V. Brun[2], Joshua Shaevitz[3], Tâm Mignot[1,*]

[1] Laboratoire de Chimie Bactérienne, CNRS UMR 7283, Aix-Marseille Université, Institut de Microbiologie de la Méditerranée, 31, Chemin Joseph Aiguier, 13009, Marseille, France

[3] Department of Biology, Indiana University, Bloomington, IN 47405

[2] Department of Physics and the Lewis-Sigler Institute for Integrative Genomics, Princeton University, Princeton, NJ 08540, USA

[4] Plateforme de Microscopie, Institut de Microbiologie de la Méditerranée, 31, Chemin Joseph Aiguier, 13009, Marseille, France

[#] denotes equal authorships

[*] Correspondence: tmignot@imm.cnrs.fr

Short title: processive transport in bacteria

Keywords: polysaccharides, active transport, peptidoglycan, cell surface, modular evolution

Abstract

Eukaryotic cells utilize an arsenal of processive transport systems to deliver macromolecules to specific subcellular sites. In prokaryotes, such transport mechanisms have only been shown to mediate gliding motility, a form of microbial surface translocation. Here, we show that the motility function of the *Myxococcus xanthus* Agl-Glt machinery results from the recent specialization of a versatile class of bacterial transporters. Specifically, we demonstrate that the Agl motility motor is modular and dissociates from the rest of the gliding machinery (the Glt complex) to bind the newly expressed Nfs complex, a close Glt paralogue, during sporulation. Following this association, the Agl system transports Nfs proteins directionally around the spore surface. Since the main spore coat polymer is secreted at discrete sites around the spore surface, its transport by Agl-Nfs ensures its distribution around the spore. Thus, the Agl-Glt/Nfs machineries may constitute a novel class of directional bacterial surface transporters that can be diversified to specific tasks depending on the cognate cargo and machinery-specific accessories.

Introduction

In eukaryotic cells, motor-assisted intracellular transport regulates fundamental cellular processes including cell division, macromolecule secretion and cell migration. Because of its small size, the bacterial cell has long been considered to be a disordered compartment where biochemical reactions and cellular processes are governed by diffusion-driven random collisions. However, in recent years, it has become clear that bacteria are highly organized and contain a complex cytoskeleton [1,2]. Despite the identification of bacterial counterparts of actin, tubulin and intermediate filaments, processive cytoskeletal motors akin to myosin, kinesin, or dynein have yet to be found in bacteria [3]. Previously, while studying a mechanism of surface motility in *Myxococcus xanthus*, we have shown that the motility machinery consists of a new type of processive transport system (Agl-Glt, [4,5]). Phylogenomic studies suggested that the motility function of the Agl-Glt machinery emerged from the recent specialization of an older system, predicting that bacterial Agl-Glt-like transporters may be adapted to other functions [5]. Here, we show that in the same bacterium, Agl, the motor component of Agl-Glt machinery, forms a second transport system that propels spore coat assembly proteins during sporulation. This finding suggests that a previously overseen type of bacterial surface transport can be adapted to mediate very different cellular tasks in prokaryotes.

Myxococcus xanthus cells move across solid surfaces by a process termed gliding (A)-motility where surface translocation occurs in the absence of extracellular organelles [6]. In recent years, remarkable progress has been made to elucidate the motility mechanism with the first identification of the motility machinery and the tracking of its localization in live gliding cells [7]. The motility machinery consists of a molecular motor, Agl (AglR, Q and S), a three sub-unit flagellar-type proton channel that assembles in the bacterial inner membrane [4]. During motility, the Agl motor harvests the proton motive force (pmf) to move directionally along a looped continuous path spanning the entire cell length [8]. Helical trafficking of the motor may occur through a connection with the actin-like MreB cytoskeleton on the cytosolic side [8,9]. In the cell envelope, mechanical work from the motor is transduced to the cell surface by the Glt (**Gl**iding **t**ransducer, GltA-K) complex through a direct interaction involving AglR and GltG [5,10]. Transported Glt proteins produce thrust when the machinery comes in contact with the underlying substrate at areas termed focal adhesions (FAs, [4,11]). How exactly the Glt proteins contact the substrate is unknown [7,12], but adhesion is facilitated by slime, a yet undefined sugar polysaccharide specifically bound by the outermost

components of the motility machinery [13]. Thus, the Agl-Glt machinery may be viewed as a modular transport system where an active transport unit (Agl) combines with a specific cargo (Glt) to propel the cells on surfaces.

Remarkably, the *glt* genes are paralogous to the *nfs* (necessary for sporulation, *nfsA-H*, Figure 1) genes involved in assembly of the *Myxococcus* spore coat [5,14]. Bacterial sporulation is a stress-induced differentiation leading to the formation of highly resistant quiescent cell types. In the model bacteria *Bacillus* and *Streptomyces sp*., a spore is formed after elaboration of a complex proteinaceous outer shell, called the spore coat. However, the coat proteins and assembly mechanisms are unrelated (for reviews see [15,16]). *Myxococcus* spores are formed following starvation in multicellular fruiting bodies. During multicellular development, the initiating signals have not been identified but sporulation can be conveniently induced *in vitro* by the addition of glycerol [14]. Glycerol-induced spores display certain morphological differences compared to fruiting body spores (*e.g.* the absence of the outermost protein cuticula, [17]), but they also share many similarities: resistance to heat and sonic disruption as well as germination. Contrary to *Bacillus* and *Streptomyces* spores, the *Myxococcus* spore coat is mostly composed of two carbohydrates, N-acetyl-galactosamine and glucose in a molar ratio of 3:1 [18,19]. The exact structure of the spore coat polymer(s) is unknown, and glucose molecules may form an alpha 1,3-glycan chain independently from the N-acetyl-galactosamine [18,19]. Recently, a locus of nine genes, named *exoA-I* has been shown to be essential for spore coat synthesis [20]. Annotation of *exoA-I* indicates that the main spore coat polymer is likely a capsular-type polysaccharide, exported by an outer membrane Wza-like translocon (the ExoA protein, [20]). For simplicity, the *exo*-dependent spore coat polymer will be named Exo throughout the rest of this manuscript. *Myxococcus* sporulation is a stepwise process. During the first step of sporulation, the peptidoglycan (PG) layer is seemingly degraded, an MreB-dependent process, which leads to cell rounding [20]. Subsequently, the Exo polymer is exported by ExoA and deposited around the collapsed inner and outer membranes [20]. Tight wrapping of Exo around the spore membranes requires the Nfs complex [20]. How exactly the Nfs system promotes spore coat assembly is unknown and is addressed in this manuscript.

The Glt and Nfs proteins are highly similar and seem to associate with extracellular sugar polymers (slime and Exo, respectively). Thus, starting from the premise that both systems share similar operating principles, we investigated the function of Nfs in spore coat assembly. Doing so, we discovered that following the onset of sporulation, the Agl motility

motor dissociates from the Glt complex and becomes recruited to the Nfs complex to transport it around the spore membranes. We further show that following its secretion at discrete sites around the spore surface, the Exo polymer is recruited by mobile Nfs units suggesting that the Agl-Nfs machinery constructs the coat by wrapping Exo strands around the cell surface. We conclude that the Agl-Glt/Nfs machineries constitute a versatile class of active surface transport machineries that may carry out multiple functions in bacterial cell surface organization.

Results

The Nfs and Glt complexes are paralogous complexes

A recent phylogenetic study showed that the *glt* and *nfs* genes likely arose from the recent duplication of a single gene system in one of the terminal branches of the deltaproteobacteria (Figure 1A, [5]). Thus, the Nfs and Glt proteins are paralogues and, when predictable, protein domains are systematically conserved between Nfs and Glt proteins (Table S1). The *nfs* complex consists of eight genes, *nfsA-H* (Figure 1B), respectively homologous to *gltA-H* (Table S1). Nfs is therefore predicted to be a somewhat simpler assemblage, missing paralogues to GltI, J and K. Gene synteny is maintained between the *nfs* and *glt* clusters (Figure 1B). Of note however, *gltA-C* and *gltD-H* form two distinct genomic clusters, but the *nfsA-H* genes are clustered in a single genomic region, possibly forming an operon (Figure 1B, [20]). Consistent with the notion that the *nfs* genes form a complex in the spore membrane, all *nfs* genes are essential for sporulation and their products localize to the cell envelope (tested for NfsA, B, C, D, E, G and predicted for NfsF and H, [20]), like their *glt* counterpart (tested for GltD, E, F, G, H and predicted for GltA, B, C, J and K [5,10]). Therefore, we predict that the Nfs proteins assemble a Glt-like membrane sporulation complex (Figure 1B).

aglRQS and *nfs* are part of a sporulation pathway

Previous works showed that Glt promotes motility in association with the Agl motor [4,5,8]. Therefore, while Nfs might be functional on its own, its function may also require an Agl-like motor. Reasoning that each complex may have its own dedicated motor, we tested whether the *MXAN_3003-5* genes, which encode the only additional complete set of Agl homologues in *M. xanthus* and are dispensable for motility, are required for sporulation like the *nfs* genes [5]. Since *nfs* mutants are defective for sporulation whether they are extracted from fruiting bodies or after glycerol-induction [14], we measured sporulation after glycerol induction throughout this study. Under these conditions, a mutant carrying an in-frame deletion in the *MXAN_3004* gene (the *aglQ* homologue) formed perfectly viable spores indicating that the putative MXAN_3003-5 motor does not play a significant role in sporulation (Figure 2A).

We next tested whether AglRQS itself may be required for sporulation. Strikingly, the *aglR*, *aglQ* and *aglS* mutants all showed a severe sporulation defect, comparable to the sporulation defects of the *nfsD* mutant and the *exoA* mutant lacking the Wza homologue (Figure 2A). An

aglQ$_{D28N}$ point mutant, carrying a substitution in the AglRQS channel previously shown to abolish proton conductance and to paralyze the Agl-Glt motility machinery [4], also failed to sporulate (Figure 2A). Therefore, the AglRQS complex and importantly, its proton-conducting activity are required for both motility and sporulation.

aglRQS are required for spore coat assembly

In the *nfs* mutants, the sporulation program is correctly initiated following glycerol induction: the cells round up and the Exo polymer is produced and exported to the cell surface [20]. However, in absence of Nfs, Exo is loosely attached to the spore surface, which results in loss of cell integrity and abortive sporulation [20]. By Transmission Electron Microscopy (TEM), we also observed a thin and complex electron dense layer around the membranes of WT spores [20], suggesting the presence of a spore coat (Figure 2B). In both the *nfsD* and *aglQ* mutants, this layer was absent and replaced by hair-like filaments that seemed loosely attached to the spore surface at one end (Figure 2B). Since the filaments were completely absent in an *exoA* mutant, they may constitute Exo polymer filaments (Figure 2B, [20]). To confirm that the filaments are not artifacts of TEM sections, we tested a fluorescein-coupled lectin, Griffonia (Bandeiraea) Simplicifolia lectin I (GSL-I) with a selectivity for *N*-acetylgalactosamine, the major sugar component of the spore coat [18,21]. As expected, GSL-I stained the surface of WT spores but not that of spore-coat deficient *exoA* mutants (Figure 2C). On WT spores, GSL-I staining decorated the entire surface with occasional brighter dots (Figure 2C). Moreover, as expected if the spore coat was loosely attached, GSL-I staining of *aglQ* and *nfsD* mutants was not compact around the cell surface (Figures 2C and S1). Taken together, the TEM and lectin-staining experiments suggest that a function of the Agl-Nfs machinery is to promote the formation of a compact spore coat layer around the spore membrane. Additionally, we identified GSL-I staining as a useful tool to detect the spore coat by live fluorescence microscopy (see below).

AglRQS associates with Nfs to form a sporulation-specific machinery

In the gliding machinery, AglRQS contacts the Glt complex through the specific association of AglR and GltG (Figure 2D, [5]). We used a bacterial two-hybrid assay to test whether AglR also contacts the Nfs system through an interaction with NfsG, the GltG paralogue. Consistent with interaction, a significant β-galactosidase activity (>1000 Miller units) was obtained when AglR and NfsG were expressed together (Figure 2D). No significant β-galactosidase activity was measured when each protein was expressed alone or when

MXAN_3003 (the AglR homologue), was co-expressed with NfsG or GltG (Figure 2D). Thus, the AglRQS motor can associate both with the Glt and Nfs complexes.

A genetic switch activates the Agl-Nfs machinery at the onset of sporulation

Myxococcus cells do not complete the sporulation process when spotted directly on an agar pad atop a microscope slide. Thus, to monitor sporulation by live microscopy and elucidate how the Agl-Nfs machinery drives spore coat assembly, we developed a microfluidic chamber assay where cells are immobilized and sporulate in liquid directly on the microscope stage (Figure S2A, S2B and Movie S1). Under these conditions, viable spores were obtained approximately 250-300 minutes after glycerol addition (Figure S2A, S2B). To test the dynamics of the Agl-Nfs machinery during sporulation, we constructed functional NfsD-mCherry and AglQ-sfGFP (super-folder GFP, [22]) fusions, to use as proxies to monitor both Nfs and Agl dynamics (Figure S3). Time-course sporulation experiments showed that NfsD-mCherry is expressed in lieu of GltD-mCherry (the motility NfsD paralogue) during sporulation, suggesting that sporulation depends on a genetic switch that results in the substitution of the Glt complex by the Nfs complex (Figures 3A-B and S4). Consistent with its role in spore coat assembly, expression of AglQ was even increased up to two-fold at the onset of sporulation and maintained at high level throughout the sporulation process (Figure 3A-B).

The AglRQS motor rotates the Nfs complex around the spore surface

In sharp contrast to the focal localization of AglQ during motility [4], AglQ-sfGFP accumulated circumferentially all around the spore membrane throughout the sporulation process (Figure 3B). However, when we analyzed the localization of NfsD-mCherry, we found that this protein covered the entire cell surface during the initial stage of sporulation but later formed fluorescent-bright clusters at the end of the cell-rounding phase, a sporulation stage where the Nfs complex would be expected to become active (Figure 3B). In time-lapse experiments, the NfsD-mCherry foci were observed to move in orbital trajectories around the spore surface (Figure 4A, Movie S2). Orbital trajectories could be captured both when the microscope focal plane was set to the middle or to the top of a sporulating cell, showing that NfsD rotates all around the spore circumference (Figure 4Ai and 4Aii). Rotating NfsD-mCherry clusters could be tracked for distances between 3/4 and up to a full spore circumference, suggesting a high level of directionality (Figures 4Ai and S5). To measure the movement parameters of NfsD-mCherry precisely, we designed a computational method to

measure the distance traveled by NfsD-mCherry foci at subpixel resolution. Moreover, since sporulating cells are spherical the distance that separates two clusters at distinct times is not the euclidian distance but the orthodromic distance (Figure S5). Orthodromic distances traveled by NfsD-mCherry clusters were thus calculated for each time point by projection (see Methods and Figure S5). This analysis revealed that NfsD-mCherry foci moved at instantaneous speeds ranging from 0.1-0.3 µm.min^{-1} (Figure 4B). Movement was clearly directional because, (i) the distance to the origin increased over the time (Figure 4C) and (ii), NfsD-mCherry movements could be described by a Mean Square Displacement (MSD) over time that increased by $4Dt + v^2t^2$ relation (with v the mean velocity, $v=0.12\pm0.05$ µm/min, and D the apparent diffusion coefficient, $D=0.012\pm0.007$ µm²/min, Figure 4D). This directional movement must be linked to the activity of the Agl motor because movement was immediately stopped by addition of Carbonyl Cyanide-m-ChloroPhenylhydrazone (CCCP), a proton motive force uncoupler (Figures 4E, S7C, Movie S3); and paralyzed NfsD-mCherry foci formed both in the *aglQ* mutant and in the *aglQ*$_{D28N}$ mutant (Figure 4B, C, F and data not shown). MSD analysis of NfsD-mCherry clusters in the *aglQ* mutant, showed a typical sub-diffusive behavior, consistent with the absence of significant active movements (Figure 4D).

The Agl-Nfs machinery transports glycan strands across the surface of sporulating cells

During motility, Agl functions to transport Glt proteins and slime along the cell surface [4,11]. Thus, the Agl motor may transport the Nfs complex and associated Exo strands to construct a densely packed spore coat around the spore membrane. We used a micron-sized polystyrene beads assay [4] to test directly whether Agl has a surface transport activity and found that beads were transported along the spore surface with instantaneous speeds matching the dynamics of NfsD-mCherry (0.1-0.3 µm.min^{-1}, Figure 5A-B). Consistent with bead transport by the Agl motor, this transport was undetectable in the *aglQ* mutant and abolished by the addition of CCCP (data not shown and Figure 5B).

To test whether Exo is the terminal cargo of the Agl-Nfs machinery, we stained NsfD-mCherry expressing spores with GSL-I and imaged each fluorophore simultaneously 4 hours after the induction of sporulation. As already mentioned, GSL-I staining covers the entire spore surface but also forms prominent fluorescent clusters (Figure 2C). When these clusters were imaged by time-lapse, they rotated together with NfsD-mCherry clusters (Figure 5C and Movie S4). Co-tracking of NfsD-mCherry and GSL-I foci were occasionally observed to dissociate, which was followed by rapid dispersal of the GSL-I cluster (Figure 5C). Thus,

Exo-linked rotating Agl-Nfs complexes are likely involved in the construction of a densely packed protective mesh at the surface of developing spores.

Nfs transport does not require the MreB cytoskeleton

Mature spores apparently lack PG and the actin-like MreB cytoskeleton [20,23]. Consistent with published data [20], we found that MreB is only required for the initial cell rounding phase of sporulation using A22 a specific MreB-inhibitor (Figure S6A-B [9]). Since the activity of the Agl-Glt motility machinery requires MreB [8,9,11], we tested the effect of A22 on NfsD-mCherry dynamics and found that MreB is dispensable for NfsD-mCherry rotation (Figure S6C). Contrarily to *Bacillus* endospores, myxospores do not contain PG or only trace amounts [23]. The Exo spore coat may provide spore integrity in absence of other rigid cellular scaffolds because *exo*, *nfs* and *agl* mutants all show aberrant cell morphologies after 24 h (Figure S2A, [20]). Thus, during sporulation, both MreB and the PG seem dispensable for the activity of Agl-Nfs.

The Exo polymer is essential for transport directionality

What is the mechanism of Nfs transport? In absence of a rigid scaffold (i.e. MreB filaments and the PG), Agl motor units may distribute circumferentially (Figure 3B) to transport Nfs proteins from one motor unit to the next, similar to actin filaments being moved by immobilized Myosin motors [24]. Alternatively and because the Nfs proteins are terminally associated with the Exo polymer, Exo secretion itself could push Nfs proteins around the spore surface in a mechanism reminiscent of PG glycan strand insertion rotating PG synthetic complexes [25–27]. To discriminate between these two possibilities, we tested NfsD-mCherry dynamics in the *exoA* mutant. In the absence of ExoA, several critical features of Nfs transport emerged: (i), NfsD-mCherry clusters formed foci that appeared smaller in *exoA* mutant than in WT cells, suggesting that Exo polymers organize NfsD-mCherry clustering at the spore surface (compare Figure 4G and A). (ii), NfsD-mCherry movement was erratic and characterized by frequent reversals and saltatory motions, suggesting that directionality is lost in the mutant (Figure 4G). To test this possibility, we computed the MSD of NfsD-mCherry clusters as a function of time in *exoA* mutant cells and found it to be mostly linear, a characteristic of undirected random motion (Figure 4D). In contrast, the MSD of WT cells is characteristic of directed motion (Figure 4D).

In the *exoA* mutant, although NfsD-mCherry clusters appear to move randomly, this movement is unlikely to be driven by diffusion alone because many clusters showed short and

fast movement phases with burst speeds similar to NfsD-mCherry clusters in WT cells (Figure 4B, C and G). These fast movements depend on the activity of the Agl-motor because (i) they were completely abolished by CCCP (Figure S7A) or in an *exoA aglQ* double mutant (Figures 4B, C, D, G and S7B) and (ii), the MSD of NfsD-mCherry was constant over time in the *exoA aglQ* double mutant (Figure 4D). Finally to prove that AglQ-dependent transport can still occur in absence of the Exo polymer, we further tested bead transport in absence in the *exoA* mutant. Similar to the movements of NfsD-mCherry clusters in the *exoA* mutant, bursts of fast bead movements were observed in this strain (Figure 5B). Since movements were completely abolished by the addition of CCCP or in an aglQ mutant background and thus depend on the activity of the Agl motor (Figure 5B). All together, these results show that surface movements at the cell surface (Nfs and beads) result from active Agl-dependent transport and not spore coat polymer secretion, which may instead serve to guide motion (see discussion).

The Exo export system localizes at discrete sites around the spore

Gene homologies suggest that the *exoA-I* genes responsible for spore coat synthesis encode a capsular polysaccharide synthesis and Wza-type export apparatus (Figure 6A, [20]). To further understand the link between Agl-Nfs activity and the export of Exo to the spore surface, we localized structural components of the export apparatus. Fusions to ExoA and ExoC, respectively encoding Wza and transmembrane Wzc-domain homologues were non functional (data not shown). While in general proteobacterial Wzc proteins carry both a transmembrane and a cytosolic BY-kinase domains, in *Myxococcus* the Wzc transmembrane domain and the kinase Wzc domain are carried by two distinct polypeptides (respectively named, ExoC and ExoD/BtkA, [28]), a conformation often found in firmicutes [29]. Nevertheless, BtkA-dependent tyrosine phosphorylation of the Wzc-like transmembrane polypeptide is essential for *Myxococcus* sporulation [28], suggesting that BtkA can be used to localize Exo export sites. We successfully obtained a functional BtkA-sfGFP fusion (Figure S3). Consistent with previous expression studies [28], BtkA-sfGFP was only expressed following sporulation induction. At 4 hours, BtkA-sfGFP formed prominent foci in ≈ 50% of the cells (Figure 6B-C). Each cell contained on average 1.7 ± 1 clusters (counted for 305 cells, with a maximum number of clusters of 6 per cell), all located near the spore membrane suggesting that BtkA-sfGFP is indeed recruited to the export apparatus. Z-sections of 4 hours old spores and 3D reconstructions further revealed that BtkA-sfGFP foci form at discrete sites around the spore periphery (Figure 6D, Movie S5). Importantly, the BtkA-sfGFP foci did not colocalize with NfsD-mCherry and often formed in distinct z-planes around the spore (Figure

6E and S8). In total the BtkA localization data suggests that sporulating cells only assemble a few discrete fixed export sites in the cell envelope, suggesting that rotating Agl-Nfs machineries act downstream from Exo secretion to construct the spore coat (see discussion).

DISCUSSION

Agl-Glt/Nfs machineries are surface transport systems. In this report, we show that the Agl motility motor is modular and interacts with Glt or Nfs proteins, depending on the growth phase. The output of these interactions is remarkably different because Agl-Glt drives gliding motility while Agl-Nfs drives spore coat assembly (Figure 7). Both Agl-Glt and Agl-Nfs interact with extracellular polysaccharides (respectively, slime and the Exo polymer) and the specific function of each system may be linked, at least partially, to the chemical properties of the cognate polymer. For example, motility could be facilitated by the chemical adhesiveness of slime, while the structure of Exo might make it particularly suited to form a coat around the spore membrane (Figure 7).

Since both slime and the Exo polymer are still detected at the cell surface in *agl* mutants, Agl-Glt/Nfs systems are not involved in the synthesis/export of associated sugars. This is particularly clear during sporulation where the synthesis and transport of the Exo polymer is controlled by the *exo* locus. Rather, several lines of evidence suggest that Agl-Glt/Nfs system transport their cognate polymers after export along the cell surface: (i) AglRQS form a flagellar motor-like complex, a predicted pmf-driven motor that interacts both with Glt and Nfs proteins (through a specific interaction between AglR and GltG/NfsG). Accordingly, both the Agl system and the pmf are required for Glt and Nfs movements (this work and [8,11,30]). (ii), Agl exerts transport activity at the surface of motile cells and spores, monitored by addition of polystyrene beads. Transport of slime and Exo was observed directly with fluorescent lectins and in both cases mobile lectin patches were translocated together with mobile AglQ (slime) and NfsD (Exo) complexes (this work and [13]). (iii) During sporulation, secretion of the Exo polymer is not a significant driving force for Nfs movement. Thus, rotation does not result from a pushing action of the Exo polymer, for example like when MreB-associated PG synthetic complexes are moved circumferentially by the incorporation of new glycan strands in the PG meshwork [25–27]. Importantly however, transport directionality was lost in absence of Exo polymer secretion. When Agl-Nfs-linked Exo strands become deposited at the spore surface, they could act like a molecular ratchet, preventing motor back steps and restricting Agl-Nfs movements in one dimension. The rigidity of the growing Exo meshwork may also support Nfs movements, especially since MreB and the PG may not be involved or present. In the motility system, slime could perform analogous functions and explain the mysterious directionality of Agl-Glt complexes.

Unfortunately this could not be tested because the main slime polymer has not been characterized.

While it is still unclear how the Agl-Glt machinery accommodates the rigid PG layer during gliding, the situation may be simpler in spores: circumferential AglQ motors may transport Nfs subunits from one motor to the next, fueled by the pmf and guided by linked Exo strands. Testing this mechanism further will require defining the structure of the Exo polymer and its connection with the Nfs proteins.

Spore coat assembly by Agl-Nfs. The connection between Agl-Nfs and Exo and the severe spore coat assembly defect observed in *nfs* and *agl* mutants suggests that Agl-Nfs mediates spore coat assembly directly. As discussed above Nfs function can be separated from secretion. Using a BtkA-sfGFP fusion, we localized the Exo secretion apparatus and found it to form a limited number of sites around the spore periphery, suggesting that secretion is spatially constricted. This localization is not surprising because immunolocalization of Wza only suggested that the export apparatus forms discrete sites in *E. coli* [31]. Thus, a rotary transport complex may be needed to build a homogenous glycan layer all around the spore. Our experiments and others [20] suggest that the activity of Agl-Nfs is necessary to anchor the spore coat polymer at the surface. In this process, scanning Agl-Nfs complexes may capture newly secreted glycan Exo strands and incorporate/deposit them where necessary in the growing spore coat meshwork. This could occur for example if a glycosyl transferase activity is linked to the Nfs complex. However, other mechanisms are also possible and more work is needed to understand how Agl-Nfs contributes to spore coat assembly at the molecular level.

Agl-Glt/Nfs proteins define a versatile class of transport systems in bacteria. The Agl-Glt/Nfs machineries likely evolved by modular expansion of a conserved system of seven proteins (Figure S9, [5]). This “core” system is found as a standalone machinery in many gammaproteobacteria and some deltaproteobacteria, suggesting that it carries function [5]. Since the core complex consists of an Agl-like motor and a simplified Nfs/Glt-like apparatus (Figure S9), this machinery may constitute a basal transport machinery. A survey of Agl-Glt/Nfs-like machineries in the deltaproteobacteria shows that these machineries adopt many potential conformations and therefore may cover a potentially broad functional repertoire (Figure S9, [5]). Functional specialization of Agl-Glt/Nfs machineries may be linked to the

type of transported cargo and thus expansion of the core system in the deltaproteobacteria may have evolved diverse tasks, sugar polymer transport (Nfs and Glt) but also potentially protein and lipid transport. Even though *glt* and *nfs* paralogues have a rather narrow distribution [5], the Agl motor itself is a member of a ubiquitous family of bacterial motors (Mot/Tol/Exb, [4]). Therefore, it is conceivable that other motor associations also promote processive transport in bacteria.

Many Agl-Glt/Nfs systems are present in bacteria that are not currently genetically tractable. Computational genetic reconstruction of ancestral assemblages is an emerging powerful means to explore both the function of a macromolecular complex and how it evolved [32]. In future works, the reductive genetic study of the Agl-Glt/Nfs machineries in *Myxococcus* should be instrumental to characterize functional intermediates and test the functional repertoire of these systems. Such study would also allow deciphering the evolution of this complex biological machine with high likelihood, an emerging challenge in evolution biology [33]. Finally, critical traits of the *Myxococcus* lifestyle evolved from the diversification of a single molecular system, showing that modifications of a single genetic system can give rise to profound ecological adaptations.

Materials and Methods

Bioinformatics analysis of *glt* and *nfs* genes

Protein sequences were analyzed by BlastP (NCBI), searches of the non-redundant (nr) and Pfam (release 24.0)(see comment on Table S1) databases [34]. Signal peptides signal and transmembrane helices were the predicted using the signalP 3.0 [35] and TMHMM v.2.0 [36] servers, respectively.

Bacterial strains, plasmids and growth

Strains, primers and plasmids are listed in Tables S2, S3 and S4. See Tables S2, S3 and S4 for strains and their mode of construction. *Myxococcus xanthus* strains were grown at 32°C in CYE rich media as previously described [37]. Plasmids were introduced in *M. xanthus* by electroporation. Mutants and transformants were obtained by homologous recombination based on a previously reported method [37]. *Escherichia coli* cells were grown under standard laboratory conditions in Luria-Bertani broth supplemented with antibiotics, if necessary.

Bacterial two-hybrid experiments

Bacterial two-hybrid experiments, plate and ß-Galactosidase assays were performed as previously described [5] and as recommended by the manufacturer instructions (Euromedex).

Determination of spore titers

Sporulation was induced by adding glycerol to a final concentration of 0.5 M directly to a flask of CYE-grown *Myxococcus* cells (OD_{600} of 0.5) as previously described [14]. Viable spore titers were determined after 24 hours based on resistance to heat and sonication. For this, 10 mL cells were harvested, pelleted at 5000 × g during 5 minutes at room temperature, re-suspended in 10 ml sterile water, incubated at 50°C for 2 hours, and sonicated three times (30 pulses, output 3, 50% duty) in ice water. The surviving spores were counted directly on the microscope after 10 min incubation in a DAPI staining solution (formaldehyde 4% - DAPI 1 µg/mL) with a detection limit of 10^2 spores/ml.

Western blotting and spore protein extraction

Protein lysates for western Blot analysis were generated by harvesting sporulating cells. Spores were pelleted and resuspended in Tris-HCl 50 mM pH 7,8 supplemented with

benzonase (Sigma) and phenylmethanesulfonylfluoride (PMSF, Sigma). Spores were lysed in a Fast-Prep-24 at 6.5 $m.s^{-1}$ for 45 seconds, 8 times (matrix lysing B, MP Biomedicals, France). Protein concentrations were determined by Bradford assay (Bio-Rad) according to the manufacturer's instructions. Lysates were solubilized in Laemmli sample buffer and resolved by sodium-dodecyl sulfate polyacrylamide gel electrophoresis (SDS-PAGE) using 8% polyacrylamide concentration for GltD. Proteins were transferred to nitrocellulose membrane (0,45 µm, Bio-Rad) using a tank transfer system (Bio-Rad) and probed with anti-GltD rabbit polyclonal antibody [5] at a 1:1000 dilution and HRP-conjugated goat anti-rabbit secondary antibodies (Bio-Rad) at 1:5000. The signals were revealed with a SuperSignal West Pico Chemiluminescent Substrate (Thermo Scientific) and imaged in a LAS4000 Luminescent Image Analyzer (GE Healthcare).

Live microscopy sporulation assay

Commercial microscopy chambers (Ibitreat uncoated, Biovalley) were filled with 100 µL of carboxymethylcellulose sodium salt (Medium viscosity, Sigma-Aldrich) solution (1.5 mg/mL) diluted in de-ionized water and left 15 minutes at room temperature. The excess of coating solution was removed by flushing with de-ionized water first, followed by flushing with TPM buffer (10 mM Tris pH 7.6; 8 mM $MgSO_4$; 1 mM KH_2PO_4). The channels were then filled with 100 µL of a CYE-grown cell suspension (OD_{600} = 0.5) previously washed and re-suspended in TPM solution and left at room temperature during 20 minutes. Non-adhering cells were flushed with TPM, sporulation was induced by adding glycerol to a final concentration of 0.5 M directly on the microscope stage. Time-lapse experiments and image processing were performed as previously described using an inverted Nikon TE2000-E-PFS inverted epifluorescence microscope [38].

All image analysis was performed under Image J (NIH). Fluorescence quantifications were performed by integrating fluorescence intensities and normalizing over the level of background fluorescence measured for cells that do not express fluorescent proteins. Kymographs were obtained as follows: a typical NfsD-mCherry cluster path was obtained by summing a stack of time-lapse images. Kymographs were then computed by re-slicing along that path, defined with the "Segmented Line" selection tool.

To measure the fluorescence areas and discriminate GSL-I staining in various mutants, we first defined the specific signal by thresholding and removing background fluorescence, by subtraction. For each cell, the total area of GSLI specific fluorescence was measured and normalized by the total area of the cell. box plots were then computed under R.

In drug experiments, Carbonyl Cyanine-M-Chlorophenylhydrazone (CCCP, 1 mM, Sigma Aldrich), and A22 (50 µg/ml, Calbiochem) were injected manually into the flow chamber. For lectin staining, a Griffonia (Bandeiraea) simplicifolia (GSL)-FITC conjugated 2 mg/mL stock solution (CliniSciences) was diluted 1:100 in TPM containing 1 mM of $CaCl_2$ and 100 µg/mL of bovine serum albumin (BSA, Sigma-Aldrich) immediately prior to injection. The mixture was then injected. The unbound lectin was washed (TPM, $CaCl_2$ 1 mM, BSA 100 µg/mL) out of the flow chamber after 40 minutes of incubation.

Sub-pixel resolution tracking of fluorescent foci at the surface of sporulating cells

For each experiment, stacks of images were first normalized to correct for background fluctuations over time. If required, the background intensity of phase contrast images was subtracted to optimize auto-thresholding operations. Cells boundary, major and minor axis were detected using a specifically developed plug-in for ImageJ. Briefly, cells were detected using an auto-thresholding function and sub-pixel resolution refined cell contours were obtained using a cubic spline-fitting algorithm. Major axis were deduced from the skeleton and expended in both directions to the most probable point maximizing the cell-boundary curvature and minimizing the angle between the centerline and the cell boundary. Fluorescent foci were detected using a local and sub-pixel resolution maxima detection algorithm. The position of each focus is first determined using a polar coordinate system (r, θ) where the radial distance (r) represents the distance from the focus position and the cell center and the angular coordinate (θ) represents the angle formed between the major cell axis and the focus (Figure S5). Since sporulating cells are spherical and NsfD-mCherry foci form close to the cell surface, the polar coordinate system was extended to a 3D spherical coordinate system (p, θ, φ) where the radial distance (p) represents the distance from the cell center to the cell boundary, the angular coordinate (θ) represents the angle formed between the major cell axis and the orthogonal projection of the focus position on the focus plane and the azimuthal angle (φ) is deduced using the relation $\varphi = \arccos(r/p)$ (Figure S5). The distance between 2 points at the surface of a spherical spore of respective spherical coordinates (p1, θ1, φ1) and (p2, θ2, φ2) was deduced from the relation $d = p \cdot \arccos(\cos(\theta 1) \cdot \cos(\varphi 1) \cdot \cos(\theta 2) \cdot \cos(\varphi 2) + \sin(\theta 1) \cdot \cos(\varphi 1) \cdot \sin(\theta 2) \cdot \cos(\varphi 2) + \sin(\varphi 1) \cdot \sin(\varphi 2))$. By convention, a positive angular coordinate means that the angle θ is measured counter-clockwise from the polar axis formed by the major axis.

Fluorescent foci were tracked over time with a specifically developed plug-in for ImageJ. Briefly, cells are tracked with an optimized nearest-neighbor linking algorithm using the polar

(r, θ) or the spherical coordinates (p, θ, φ). From foci trajectories, the distance between two temporal points was used to calculate instantaneous speeds shown in Figure 4B and combined with the cumulated distance and the distance from the origin to compute the Mean Square Displacement (MSD). For WT cells, the mean velocity and the diffusion coefficient were extracted from the second order fit of the MSD. For each condition tested, the MSD of at least 15 individual foci trajectory was calculated.

Transmission Electron Microscopy (TEM)

Myxococcus xanthus cells were fixed for 1 hour with glutaraldehyde 2.5% in CYE medium and postfixed 1 hour in 2% OsO_4. Then cells were dehydrated in ethanol, and embedded in epon. Ultrathin sections were stained with aqueous uranyl acetate for 10 minutes and lead citrate for 5 minutes. Sample observations were performed on a Tecnai-G2 LaB6 microscope (FEI Company) operating at 200 kV.

Bead tracking

Custom microscopy chambers were made of a 1 mm-thick coverslide and a thin coverslip (#1, thickness 100 µm) separated by a double layer of double-sided sticky tape (Scotch). Chambers were immersed using 1.5%-agarose in DMSO (6 M, Sigma-Aldrich) for 15 min. Then, chambers were extensively washed with TPM containing 10 mM glucose. The chambers were filled with CYE-grown cell suspension (OD_{600} = 0.8) exposed to glycerol (final concentration of 0.5 M) 2 h or 4 h prior to experiments, and washed and re-suspended in TPM solution directly before infusion. After 30 min, access was washed out, leaving sporulated and non-sporulated *M. xanthus* stuck to the surfaces of the microscopy chamber. Sub-micron sized polystyrene beads (diameter 520 nm) were gently placed atop the sporulating cells using an optical trap system as previously described [4]. A low-powered tracking laser (< 1 mW power at the sample, wavelength 855 nm) was focused on a spore-attached bead. The forward scattered laser light was collected on a position-sensitive photodiode (Model 2931, New Focus). The bead position was recorded and used to update the stage position using a PID feedback at a frequency of 50 Hz. The accuracy of this technique was measured to be better than 4 nm. Simultaneously, we used an EMCCD camera (iXon, Andor) to record time-lapsed videos at 1 Hz [4]. Video and high-resolution tracking data were recorded for several hours for all experimental conditions.

Acknowledgements

We thank Patrick Viollier for critical reading and comments about the manuscript. We thank Alain Bernadac and Leon Espinosa at the plateforme de biophotonique (LCB, FRM) for their help with data processing and microscopy. We thank Rym Agrebi for phylogenetic analysis and Yonathan Arfi for help with figures. We also thank Annick Doan and Marie-Pierre Forquin for help with spore protein extraction.

References

1. Gitai Z (2005) The new bacterial cell biology: Moving parts and subcellular architecture. Cell 120: 577–586.

2. Shapiro L, McAdams HH, Losick R (2009) Why and how bacteria localize proteins. Science 326: 1225–1228.

3. Ingerson-Mahar M, Gitai Z (2012) A growing family: the expanding universe of the bacterial cytoskeleton. FEMS Microbiol Rev 36: 256–266. doi:10.1111/j.1574-6976.2011.00316.x.

4. Sun M, Wartel M, Cascales E, Shaevitz JW, Mignot T (2011) Motor-driven intracellular transport powers bacterial gliding motility. Proc Natl Acad Sci USA 108: 7559–7564. doi:10.1073/pnas.1101101108.

5. Luciano J, Agrebi R, Le Gall AV, Wartel M, Fiegna F, et al. (2011) Emergence and modular evolution of a novel motility machinery in bacteria. PLoS Genet 7: e1002268. doi:10.1371/journal.pgen.1002268.

6. Mauriello EM, Mignot T, Yang Z, Zusman DR (2010) Gliding motility revisited: how do the myxobacteria move without flagella? Microbiol Mol Biol Rev 74: 229–249.

7. Zhang Y, Ducret A, Shaevitz J, Mignot T (2012) From individual cell motility to collective behaviors: insights from a prokaryote, Myxococcus xanthus. FEMS Microbiol Rev 36: 149–164. doi:10.1111/j.1574-6976.2011.00307.x.

8. Nan B, Bandaria JN, Moghtaderi A, Sun I-H, Yildiz A, et al. (2013) Flagella stator homologs function as motors for myxobacterial gliding motility by moving in helical trajectories. Proc Natl Acad Sci USA 110: E1508–1513. doi:10.1073/pnas.1219982110.

9. Mauriello EM, Mouhamar F, Nan B, Ducret A, Dai D, et al. (2010) Bacterial motility complexes require the actin-like protein, MreB and the Ras homologue, MglA. Embo J 29: 315–326.

10. Nan B, Mauriello EM, Sun IH, Wong A, Zusman DR (2010) A multi-protein complex from Myxococcus xanthus required for bacterial gliding motility. Mol Microbiol 76: 1539–1554.

11. Nan B, Chen J, Neu JC, Berry RM, Oster G, et al. (2011) Myxobacteria gliding motility requires cytoskeleton rotation powered by proton motive force. Proc Natl Acad Sci USA 108: 2498–2503. doi:10.1073/pnas.1018556108.

12. Kaimer C, Berleman JE, Zusman DR (2012) Chemosensory signaling controls motility and subcellular polarity in Myxococcus xanthus. Curr Opin Microbiol 15: 751–757. doi:10.1016/j.mib.2012.10.005.

13. Ducret A, Valignat M-P, Mouhamar F, Mignot T, Theodoly O (2012) Wet-surface-enhanced ellipsometric contrast microscopy identifies slime as a major adhesion factor during

bacterial surface motility. Proc Natl Acad Sci USA 109: 10036–10041. doi:10.1073/pnas.1120979109.

14. Muller FD, Treuner-Lange A, Heider J, Huntley SM, Higgs PI (2010) Global transcriptome analysis of spore formation in Myxococcus xanthus reveals a locus necessary for cell differentiation. BMC Genomics 11: 264.

15. Higgins D, Dworkin J (2012) Recent progress in Bacillus subtilis sporulation. FEMS Microbiol Rev 36: 131–148. doi:10.1111/j.1574-6976.2011.00310.x.

16. McCormick JR, Flärdh K (2012) Signals and regulators that govern Streptomyces development. FEMS Microbiology Reviews 36: 206–231. doi:10.1111/j.1574-6976.2011.00317.x.

17. Lee B, Mann P, Grover V, Treuner-Lange A, Kahnt J, et al. (2011) The Myxococcus xanthus spore cuticula protein C is a fragment of FibA, an extracellular metalloprotease produced exclusively in aggregated cells. PLoS ONE 6: e28968. doi:10.1371/journal.pone.0028968.

18. Kottel RH, Bacon K, Clutter D, White D (1975) Coats from Myxococcus xanthus: characterization and synthesis during myxospore differentiation. J Bacteriol 124: 550–557.

19. Sutherland IW, Mackenzie CL (1977) Glucan common to the microcyst walls of cyst-forming bacteria. J Bacteriol 129: 599–605.

20. Müller FD, Schink CW, Hoiczyk E, Cserti E, Higgs PI (2012) Spore formation in Myxococcus xanthus is tied to cytoskeleton functions and polysaccharide spore coat deposition. Mol Microbiol 83: 486–505. doi:10.1111/j.1365-2958.2011.07944.x.

21. Lescar J, Loris R, Mitchell E, Gautier C, Chazalet V, et al. (2002) Isolectins I-A and I-B of Griffonia (Bandeiraea) simplicifolia. Crystal structure of metal-free GS I-B(4) and molecular basis for metal binding and monosaccharide specificity. J Biol Chem 277: 6608–6614. doi:10.1074/jbc.M109867200.

22. Dinh T, Bernhardt TG (2011) Using superfolder green fluorescent protein for periplasmic protein localization studies. J Bacteriol 193: 4984–4987. doi:10.1128/JB.00315-11.

23. Bui NK, Gray J, Schwarz H, Schumann P, Blanot D, et al. (2009) The peptidoglycan sacculus of Myxococcus xanthus has unusual structural features and is degraded during glycerol-induced myxospore development. J Bacteriol 191: 494–505.

24. Kron SJ, Toyoshima YY, Uyeda TQ, Spudich JA (1991) Assays for actin sliding movement over myosin-coated surfaces. Meth Enzymol 196: 399–416.

25. Van Teeffelen S, Wang S, Furchtgott L, Huang KC, Wingreen NS, et al. (2011) The bacterial actin MreB rotates, and rotation depends on cell-wall assembly. Proc Natl Acad Sci USA 108: 15822–15827. doi:10.1073/pnas.1108999108.

26. Garner EC, Bernard R, Wang W, Zhuang X, Rudner DZ, et al. (2011) Coupled, circumferential motions of the cell wall synthesis machinery and MreB filaments in B. subtilis. Science 333: 222–225. doi:10.1126/science.1203285.

27. Domínguez-Escobar J, Chastanet A, Crevenna AH, Fromion V, Wedlich-Söldner R, et al. (2011) Processive movement of MreB-associated cell wall biosynthetic complexes in bacteria. Science 333: 225–228. doi:10.1126/science.1203466.

28. Kimura Y, Yamashita S, Mori Y, Kitajima Y, Takegawa K (2011) A Myxococcus xanthus bacterial tyrosine kinase, BtkA, is required for the formation of mature spores. J Bacteriol 193: 5853–5857. doi:10.1128/JB.05750-11.

29. Grangeasse C, Nessler S, Mijakovic I (2012) Bacterial tyrosine kinases: evolution, biological function and structural insights. Philos Trans R Soc Lond, B, Biol Sci 367: 2640–2655. doi:10.1098/rstb.2011.0424.

30. Luciano J, Agrebi R, Le Gall AV, Wartel M, Fiegna F, et al. (2011) Emergence and modular evolution of a novel motility machinery in bacteria. PLoS Genet 7: e1002268. doi:10.1371/journal.pgen.1002268.

31. Dong C, Beis K, Nesper J, Brunkan-Lamontagne AL, Clarke BR, et al. (2006) Wza the translocon for E. coli capsular polysaccharides defines a new class of membrane protein. Nature 444: 226–229.

32. Finnigan GC, Hanson-Smith V, Stevens TH, Thornton JW (2012) Evolution of increased complexity in a molecular machine. Nature 481: 360–364. doi:10.1038/nature10724.

33. Abby SS, Rocha EPC (2012) The non-flagellar type III secretion system evolved from the bacterial flagellum and diversified into host-cell adapted systems. PLoS Genet 8: e1002983. doi:10.1371/journal.pgen.1002983.

34. Finn RD, Mistry J, Tate J, Coggill P, Heger A, et al. (2010) The Pfam protein families database. Nucleic Acids Res 38: D211–222. doi:10.1093/nar/gkp985.

35. Bendtsen JD, Nielsen H, von Heijne G, Brunak S (2004) Improved prediction of signal peptides: SignalP 3.0. J Mol Biol 340: 783–795. doi:10.1016/j.jmb.2004.05.028.

36. Krogh A, Larsson B, von Heijne G, Sonnhammer EL (2001) Predicting transmembrane protein topology with a hidden Markov model: application to complete genomes. J Mol Biol 305: 567–580. doi:10.1006/jmbi.2000.4315.

37. Bustamante VH, Martínez-Flores I, Vlamakis HC, Zusman DR (2004) Analysis of the Frz signal transduction system of Myxococcus xanthus shows the importance of the conserved C-terminal region of the cytoplasmic chemoreceptor FrzCD in sensing signals. Mol Microbiol 53: 1501–1513. doi:10.1111/j.1365-2958.2004.04221.x.

38. Ducret A, Maisonneuve E, Notareschi P, Grossi A, Mignot T, et al. (2009) A

microscope automated fluidic system to study bacterial processes in real time. PLoS ONE 4: e7282. doi:10.1371/journal.pone.0007282.

Figure Legends

Figure 1. The Nfs complex is a Glt-transducer-like complex. (A) Phylogenetic relationship between the *nfs* and *glt* complexes inside the *Myxococcales* order. Shown is a rooted Bayesian phylogenetic tree of concatenated alignments of GltD, E and G extracted from [5]. (B) Genetic organization of *agl*, *glt* and *nfs* genes and predicted structures of the Agl-Glt and Nfs machineries from (5) and (13). Paralogous genes are shown in specific colors. The PG is not represented because its connection to Glt and Nfs proteins is unknown.

Figure 2. The Agl interacts with Nfs to promote spore coat assembly. (A) Sporulation titers after heat and sonication counted by DAPI staining in various strains. Corresponding DAPI-staining images are shown. Note the 10^2 spores/ml detection limit of the assay. Scale bar = 5 µm. **(**B) Thin sections of myxospores observed by transmission electron microscopy. WT, *aglQ*, *nfsD* and *exoA* strains were observed 24 hours after the induction of sporulation. Arrows point to spore coat material that detaches from the surface of sporulating cells in *aglQ* and *nfsD* mutants. Scale bars = 0.1 µm. (C) GSLI-FITC staining of the spore coat material. WT, *aglQ*, *nfsD* and *exoA* strains were observed 4 hours after the induction of sporulation. Scale bar = 1 µm. (D) AglR interacts with GltG and NfsG in a bacterial two hybrid assay.

Figure 3. The Agl-Nfs machinery is sporulation-specific. (A) *nfs* and *glt* genes are differentially regulated during sporulation. Expression of NfsD, GltD and AglQ as inferred from the measurements of relative single cell mCherry/sfGFP fluorescence intensities over time after sporulation induction. Shown are the average fluorescence intensity ratios (measured intensity/maximum intensity) of 25 cells for each time points. (B) Time course of AglQ-sfGFP (left), GltD-mCherry (middle panel) and NfsD-mCherry (right panel) dynamics during sporulation.

Figure 4. The AglRQS motor rotates the Nfs complex around the spore surface. (A) NfsD-mCherry moves in orbital trajectories around the surface of 4h old spores. Observation of dynamic NfsD-mCherry clusters at different focal planes, middle (i) and top (ii) sections of a spore. For each time lapse, trajectories were computed by summing the different time points in consecutive frames and shown in "fire" colors to the right. Scale bar = 1 µm. (B) Instantaneous speed histogram of tracked NfsD-mCherry clusters over time in WT spores and in the different mutants. (C) Distance from the origin of NfsD-mCherry clusters in WT spores

and different mutants. (D) Mean square displacement (MSD) of NfsD-mCherry clusters over time in WT spores and in the different mutants. (E) NfsD-mCherry rotation is abolished by CCCP. (F) Rotation of NfsD-mCherry requires AglQ. (G) Movement of NfsD-mCherry in the *exoA* mutant.

Figure 5. The Nfs complex transports the spore coat polymer at the surface of the developing spores. (A) Snapshots of two beads moving on spore surface. Two beads are attached to a WT spore, another bead is stuck to bottom of flow chamber providing a fixed reference. The bead in focus is tracked using the low-powered laser as in the methods section. Both beads move independently at different times (arrows). Scale bar = 1 µm. (B) Speed histogram of tracked polystyrene beads at the spore surface: WT spores, *exoA* spores, *exoA* spores in the presence of CCCP (10 µM), and *exoA aglQ* spores. WT spores in the presence of CCCP and *aglQ* spores yielded similar results as the *exoA* CCCP and *exoA aqlQ* spores and are therefore not represented for improved clarity. (C) Dynamics of NfsD-mCherry and GSLI-FITC on a sporulating cell. A time lapse of a 4h old sporulating cell is shown with its corresponding kymograph. The white arrow points to the dissociation of the red and green signals. Scale bar = 1 µm.

Figure 6. The Exo export system localizes at discrete sites around the spore surface. (A) Predicted structure of the Exo export apparatus and genetic organization of the *exoA-I* operon. White genes have no know homologs in the databases. Gene accession numbers (MXAN) are shown. (B) Projection of a Z-stack of a 4h sporulating cells and associated BtkA-sfGFP foci. Scale bar = 1 µm. (C) Z-sections of a sporulating cell and localization of BtkA-sfGFP (D) Snapshots of a 3D-reconstruction of a cell expressing BtkA-sfGFP. The spore membrane was stained with FM4-64. 90° rotations are shown. Scale bar = 1 µm. (E) BtkA-sfGFP foci do not co-localize with NfsD-mCherry foci. Shown are 3D dimensional projections of z-sections for BtkA-sfGFP, NfsD-mCherry foci and the corresponding merge. For each probe, the individual z-sections are shown in Figure S8. Scale bar = 1 µm.

Figure 7. Phase specific interactions between Agl and Glt/Nfs promote motility or sporulation. The Agl motor (yellow), a three protein MotAB-like channel harvests the pmf and interacts either with Glt (orange) or Nfs (light blue) to transport slime (red) or the Exo polymer (blue) depending on the growth phase. Both Glt and Nfs are shown spanning the entire cell surface because they both contain predicted inner and outer membrane proteins.

The connection between the Glt complex and the MreB cytoskeleton is shown in black. IM: inner membrane, OM: outer membrane, the PG is not represented because its connection with Glt is unresolved and spores apparently lack PG. In both cases, the transport mechanism remains to be elucidated. In motile cells, the current model proposes that Glt proteins and attached slime (Orange-red dots circled in black) traffic along a closed loop helix (grey) and generate propulsion as they interact with the underlying substratum. At the lagging cell pole, the motility complexes become de-activated (orange circles), potentially by removing their connection to slime, which thus becomes deposited on the substrate. In spores, Nfs proteins may associate with Exo polymers following their secretion by the Exo export machinery (green). Distributed Agl motor units could move Exo-linked Nfs complexes from one motor to the next, guided by the Exo polymer.

Figure S1. Loose anchoring of the main spore coat polymer in the *aglQ* mutant. Box plot representations of the ratio between the area of GSL-I fluorescence and a cell total area (Fluorescence area ratio) are shown. For each strain, measurements were performed over 20 cells**.**

Figure S2. Sporulation of *Myxococcus* cells in the microfluidic chamber. (A) Sporulation kinetics after addition of glycerol. Following induction, cell rounding is observed with kinetics similar to cell rounding in liquid flasks. Aberrant cell shapes are observed both with the *aglQ* and *nfsD* mutants as described by [20]. Scale bar = 1 µm. (B) Germination after CYE (rich) medium injection. Spores germinate indicating that the observed round cells are indeed spores and not spheroplasts.

Figure S3. AglQ-sfGFP, NfsD-mCherry and BtkA-sfGFP are fully functional for sporulation. Spore titers were determined and expressed as in Figure 2A.

Figure S4. GltD expression is down-regulated during sporulation. (A) Detection of GltD by western blotting during a sporulation time course using GltD-specific antibodies. Extracts from a *gltD* mutants are shown as a specificity control. A non-specific cross-reactive specie is

shown as a control for comparable protein loading in all lanes. (B) Quantifications of the relative amounts of detectable GltD protein of the experiment shown in (A).

Figure S5. Tracking NfsD-mCherry at the surface of sporulating cells. (A) subpixel-resolution NfsD-mCherry foci tracking and methodology. Tracking of a rotating NfsD-mCherry cluster in the focal plane is shown. In this example, the NfsD-mCherry cluster is moving in the macroscope focal plane and therefore the orthodromic distance can be directly inferred from the images (orange and green). When clusters move out of the focal plane, orthodromic distances are calculated form euclidian distances (purple). (B) Geometric projections used to calculate orthodromic distances from Euclidian distances.

Figure S6. The MreB cytoskeleton is not required for the function of Agl-Nfs. (A) Addition of A22 immediately after Glycerol induction blocks cell rounding of WT but not $mreB_{V323A}$ cells. (B) Addition of A22 after cell rounding initiation does not block sporulation. (C) The rotation of NfsD-mCherry is not affect by the addition of A22. Scale bar = 1 µm.

Figure S7. NfsD-mCherry movement depends on Agl motor activity in absence of Exo secretion. (A) NfsD-mCherry movement in an *exoA aglQ* mutant. Time-lapse recording was obtained on 4h old sporulating cells. Scale bar = 1 µm. (B) and (C) NfsD-mCherry movement is abolished by CCCP in the *exoA* mutant.

Figure S8. Individual *z*-sections of BstkA-sfGFP and NfsD-mCh localization in the cell shown in Figure 6E.

Figure S9. Modular architecture of Agl-Glt/Nfs machineries in bacteria.

Movie S1. Sporulation of *Myxococcus* cells in the microfluidic chamber. Sporulation kinetics after addition of glycerol. The movie is accelerated by a factor of 720.

Movie S2. Rotation of NfsD-mCherry. The time-lapse recording was obtained on a 4h old sporulating cell. The movie is accelerated by a factor of 480.

Movie S3. Rotation of NfsD-mCherry is abolished in presence of CCCP (1 mM). The time-lapse recording was obtained on a 4h old sporulating cell. The movie is accelerated by a factor of 480.

Movie S4. Co-rotation of NfsD-mCherry and GSLI-FITC on a sporulating cell. The time-lapse recording was obtained on a 4h old sporulating cell. The movie is accelerated by a factor of 360.

Movie S5. 3D-reconstruction of a spore expressed BtkA-sfGFP and stained by FM4-64. The Z-stack recording was obtained on a 4h old sporulating cell. Each image corresponds to a 10° rotation of the cell.

Table S1. Bioinformatic analysis of the Glt and the Nfs clusters.

Table S2. Strains used in this study.

Table S3. Primers used in this study.

Table S4. Plasmids used in this study.

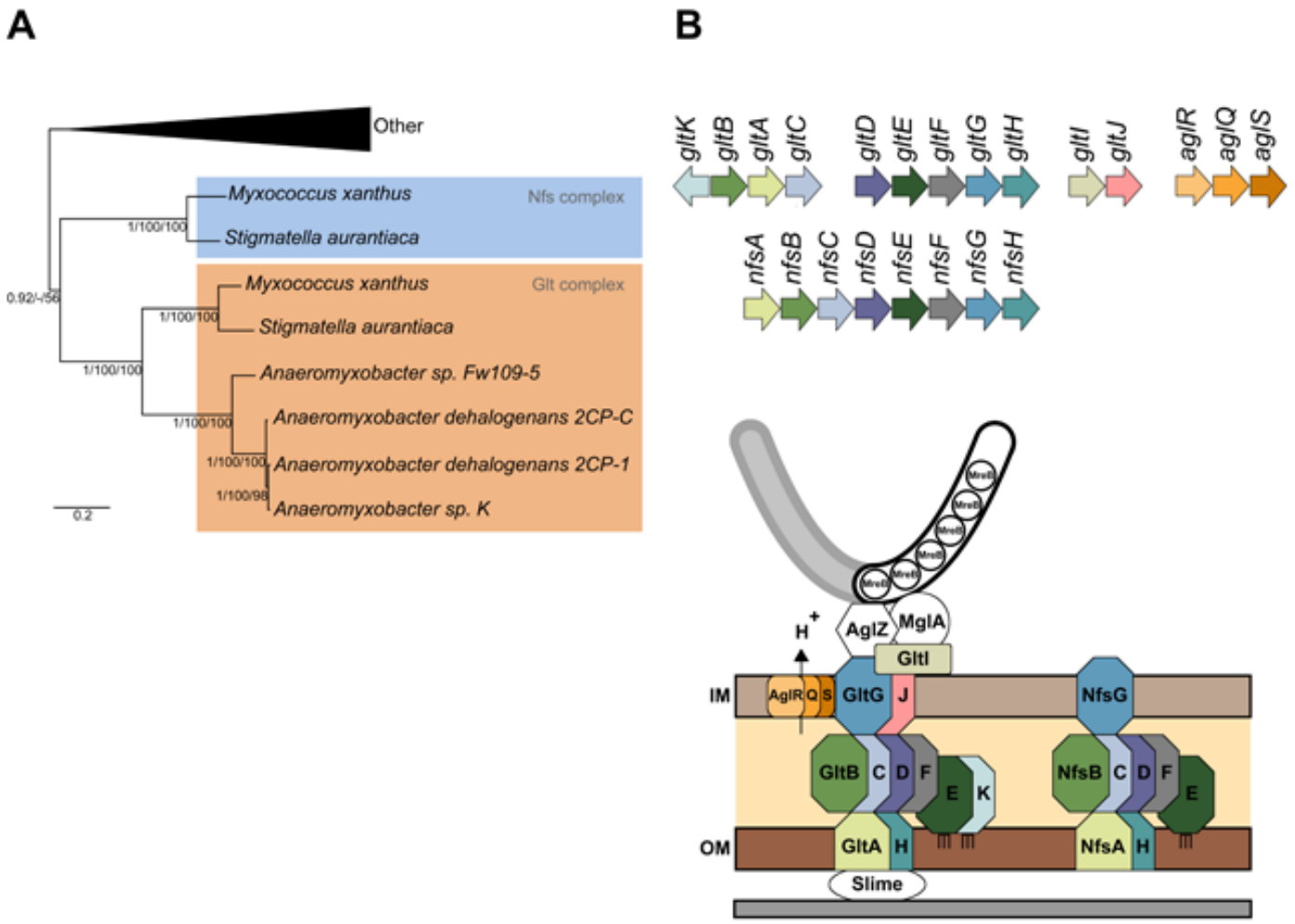
A
Other
Myxococcus xanthus
Nfs complex
Stigmatella aurantiaca
Myxococcus xanthus
Glt complex
Stigmatella aurantiaca
Anaeromyxobacter sp. Fw109-5
Anaeromyxobacter dehalogenans 2CP-C
Anaeromyxobacter dehalogenans 2CP-1
Anaeromyxobacter sp. K
1/100/100
1/100/100
1/100/100
1/100/100
1/100/100
1/100/98
0.92/-/56
0.2
B
gltK gltB gltA gltC
gltD gltE gltF gltG gltH
gltI gltJ
aglR aglQ aglS
nfsA nfsB nfsC nfsD nfsE nfsF nfsG nfsH
MreB
AglZ
MglA
GltI
H+
IM
AglR Q S
GltG
J
NfsG
GltB C D F E K
NfsB C D F E
OM
GltA H
NfsA H
Slime

Figure 1

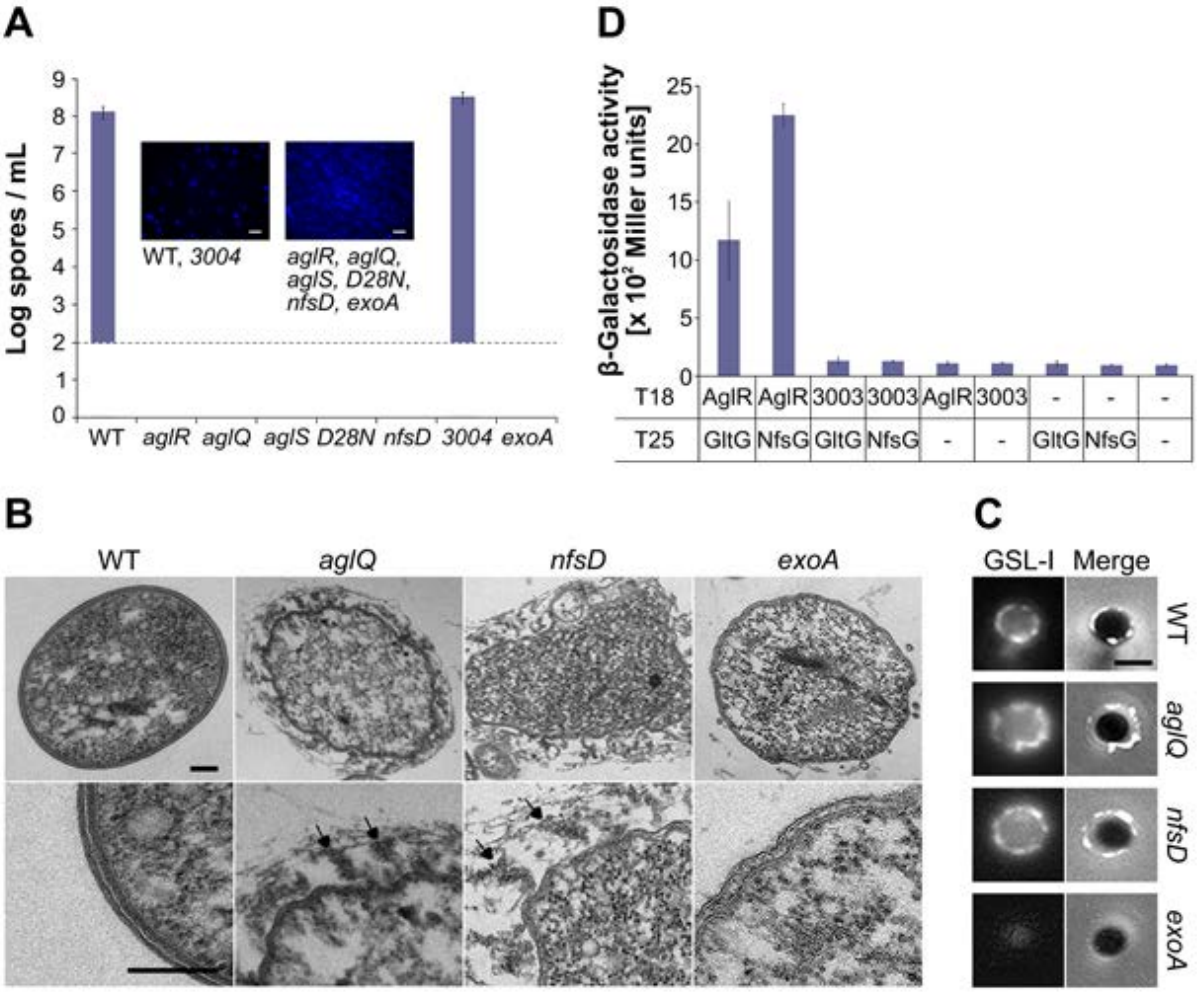
A
Log spores / mL
9
8
7
6
5
4
3
2
1
0
WT, 3004
aglR, aglQ, aglS, D28N, nfsD, exoA
WT aglR aglQ aglS D28N nfsD 3004 exoA
D
β-Galactosidase activity [x 10² Miller units]
25
20
15
10
5
0
T18 AglR AglR 3003 3003 AglR 3003 - - -
T25 GltG NfsG GltG NfsG - - GltG NfsG -
B
WT
aglQ
nfsD
exoA
C
GSL-I
Merge
WT
aglQ
nfsD
exoA

Figure 2

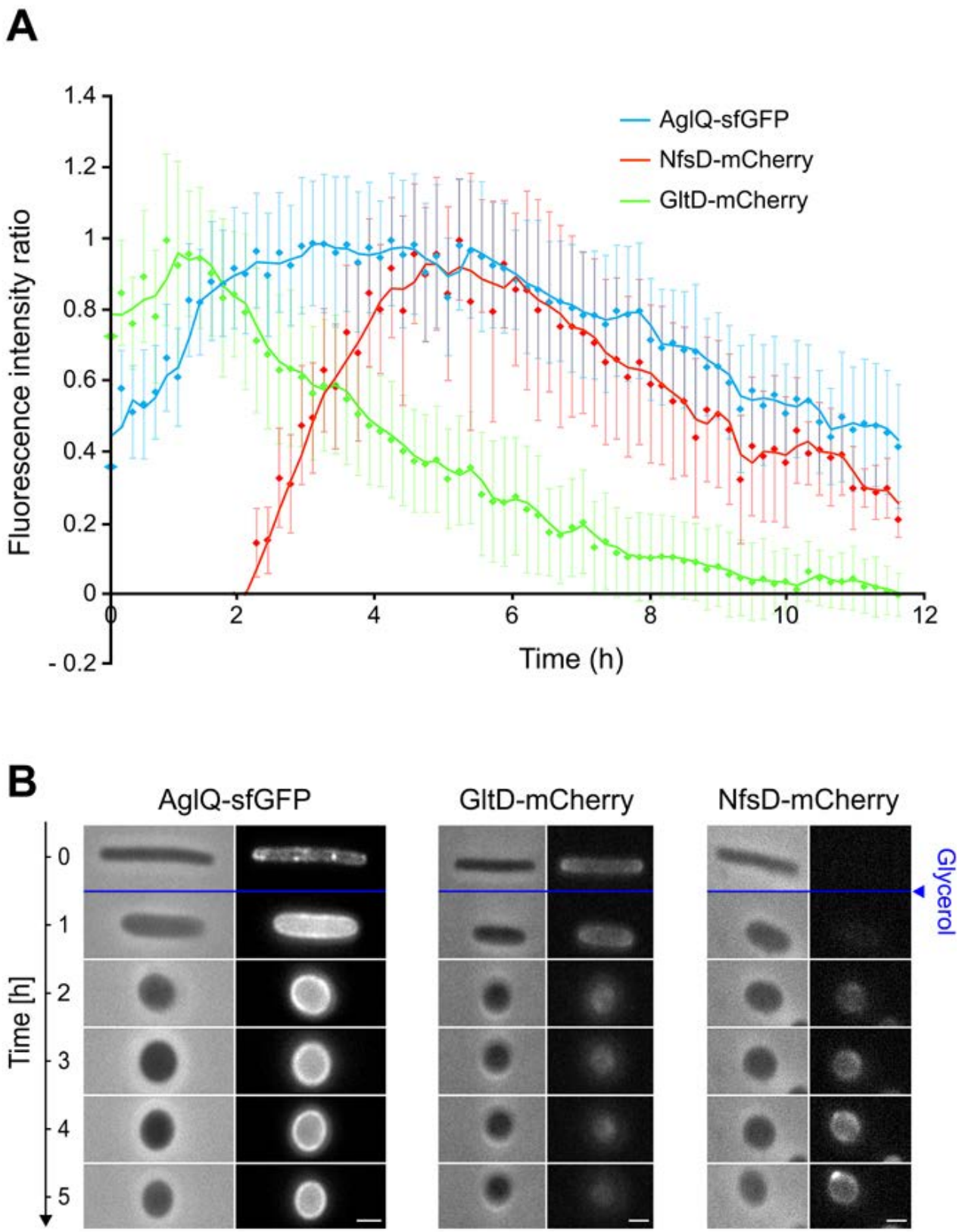
A
AglQ-sfGFP
NfsD-mCherry
GltD-mCherry
Fluorescence intensity ratio
1.4
1.2
1
0.8
0.6
0.4
0.2
0
- 0.2
0
2
4
6
8
10
12
Time (h)
B
AglQ-sfGFP
GltD-mCherry
NfsD-mCherry
Glycerol
Time [h]
0
1
2
3
4
5

Figure 3

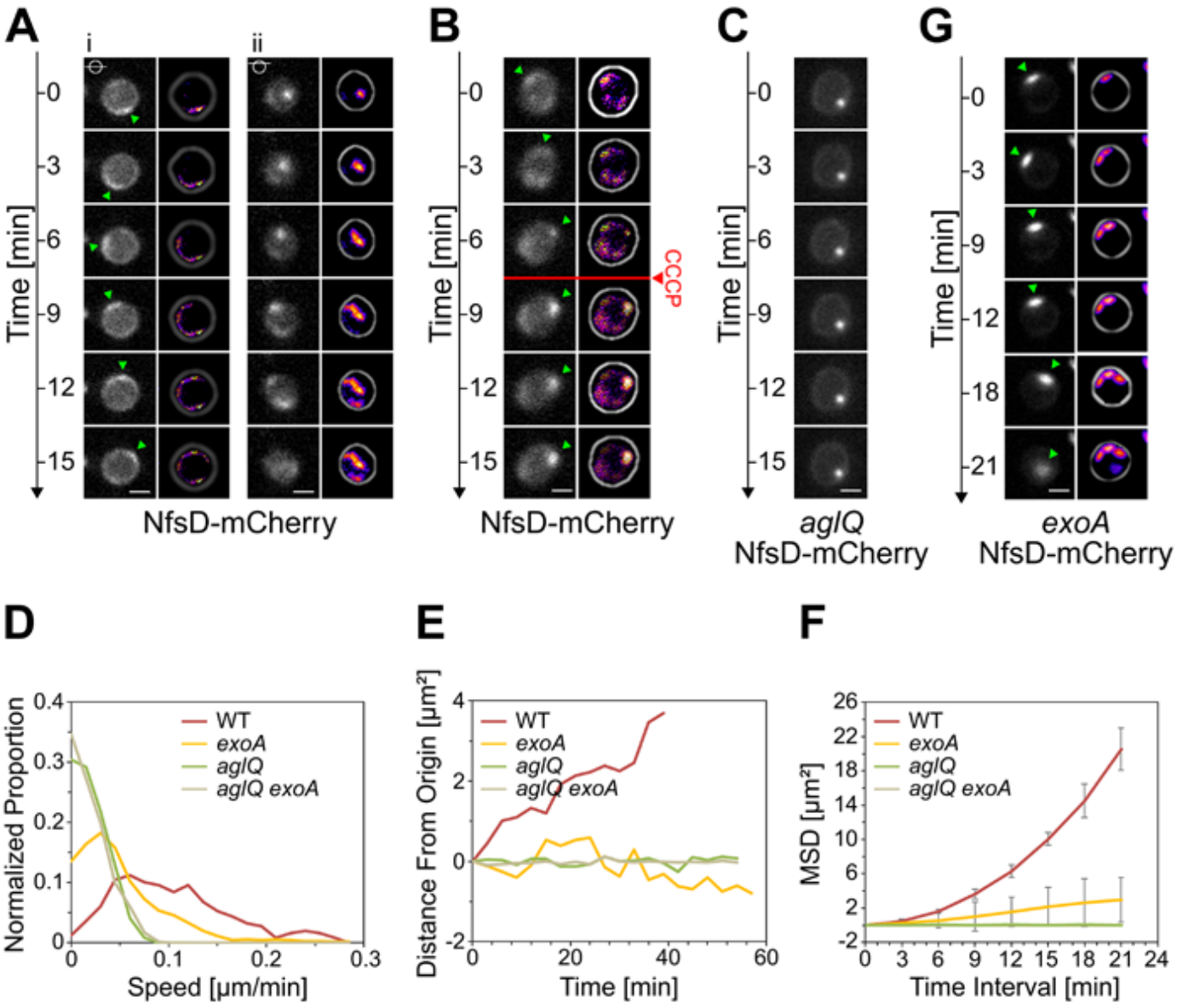
A
i
ii
Time [min]
0
3
6
9
12
15
NfsD-mCherry
B
CCCP
NfsD-mCherry
C
aglQ
NfsD-mCherry
G
18
21
exoA
NfsD-mCherry
D
Normalized Proportion
0.4
0.3
0.2
0.1
0
0.1
0.2
0.3
Speed [μm/min]
WT
exoA
aglQ
aglQ exoA
E
Distance From Origin [μm²]
4
2
0
-2
20
40
60
Time [min]
F
MSD [μm²]
26
22
18
14
10
6
2
-2
3
6
9
12
15
18
21
24
Time Interval [min]

Figure 4

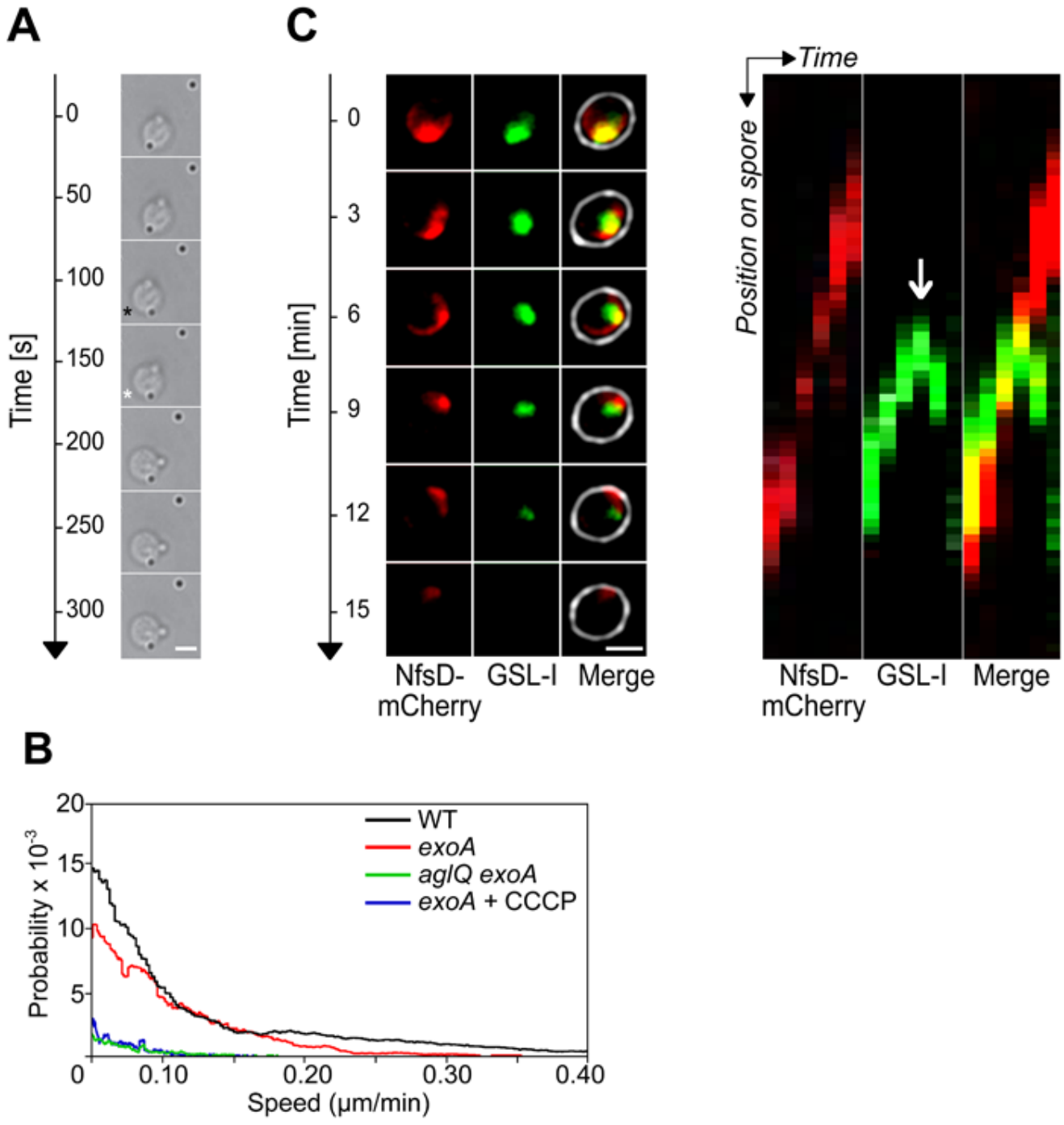
A
Time [s]
0
50
100
150
200
250
300
C
Time [min]
0
3
6
9
12
15
NfsD-mCherry
GSL-I
Merge
Time
Position on spore
NfsD-mCherry
GSL-I
Merge
B
Probability x 10-3
20
15
10
5
0
0.10
0.20
0.30
0.40
Speed (µm/min)
WT
exoA
aglQ exoA
exoA + CCCP

Figure 5

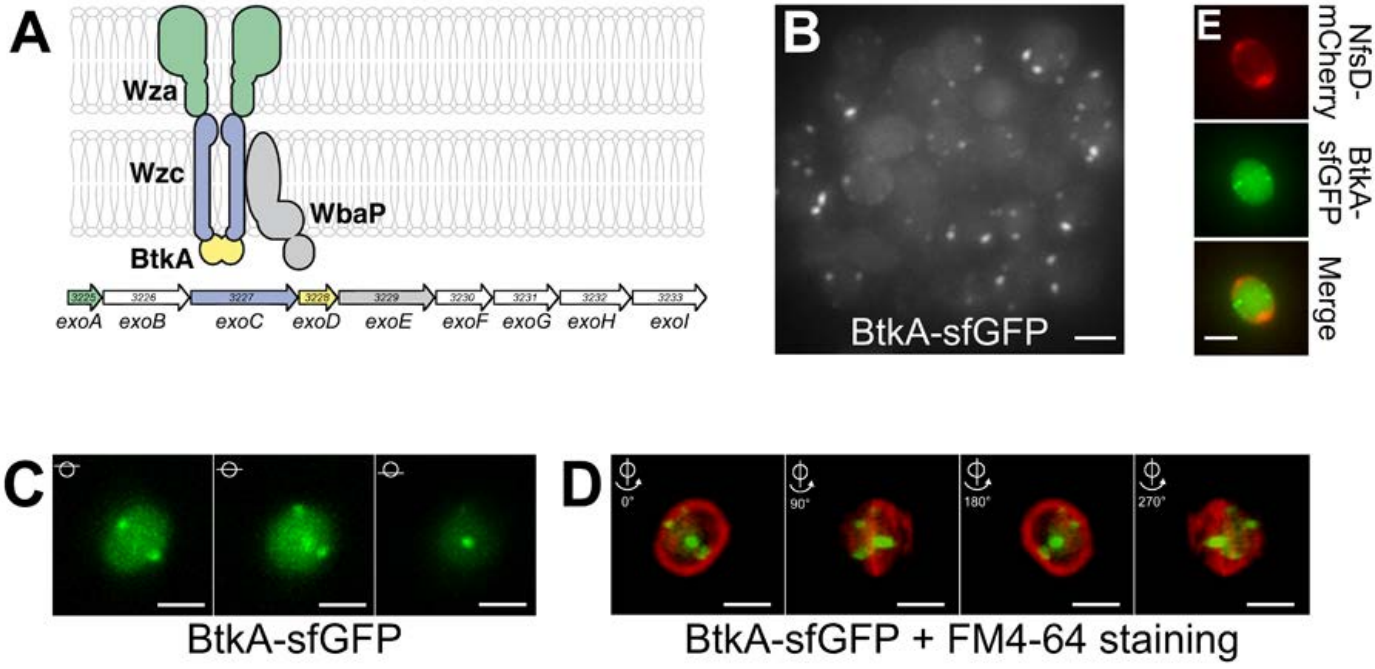
A
Wza
Wzc
WbaP
BtkA
3225
3226
3227
3228
3229
3230
3231
3232
3233
exoA
exoB
exoC
exoD
exoE
exoF
exoG
exoH
exoI
B
BtkA-sfGFP
E
NfsD-mCherry
BtkA-sfGFP
Merge
C
BtkA-sfGFP
D
0°
90°
180°
270°
BtkA-sfGFP + FM4-64 staining

Figure 6

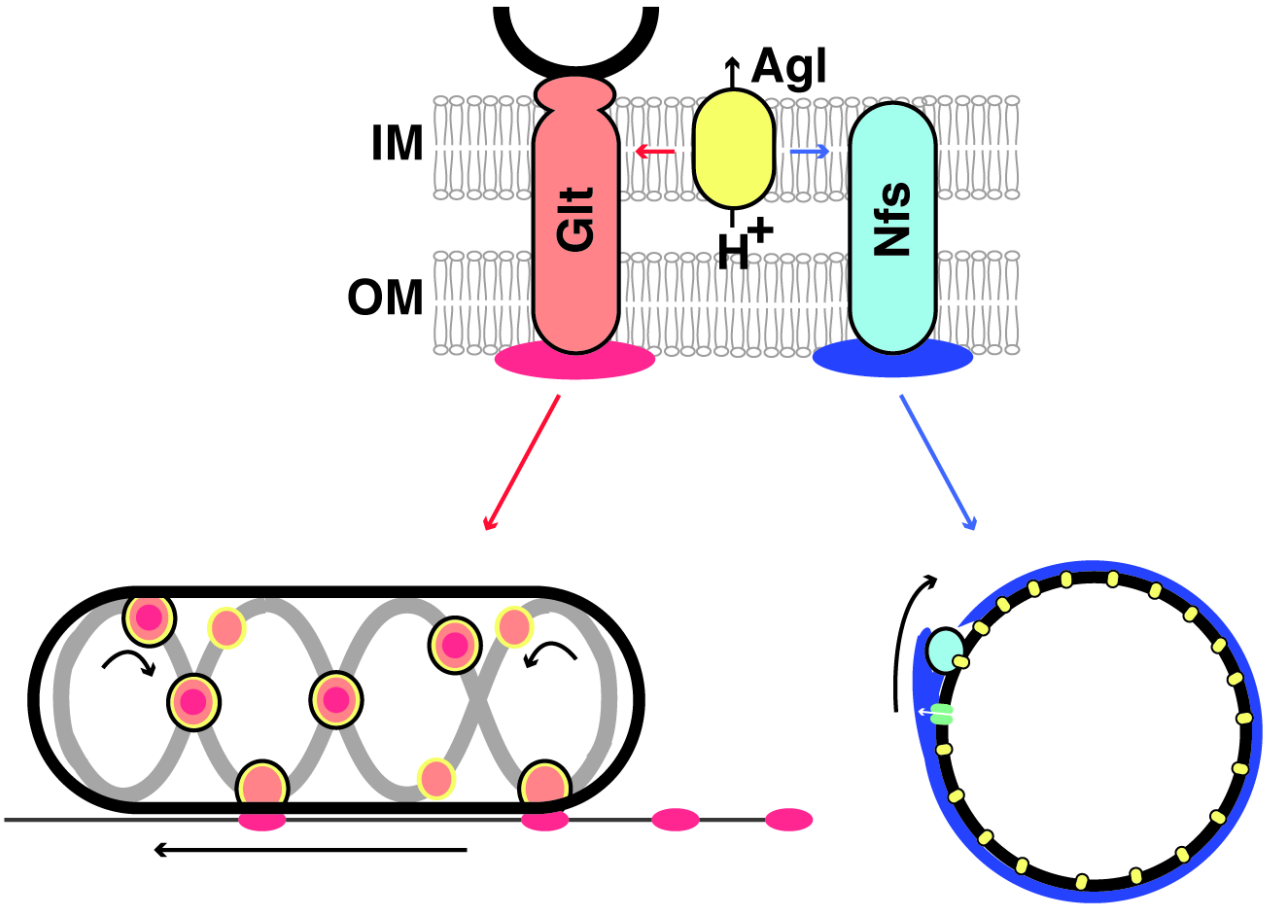

Figure 7

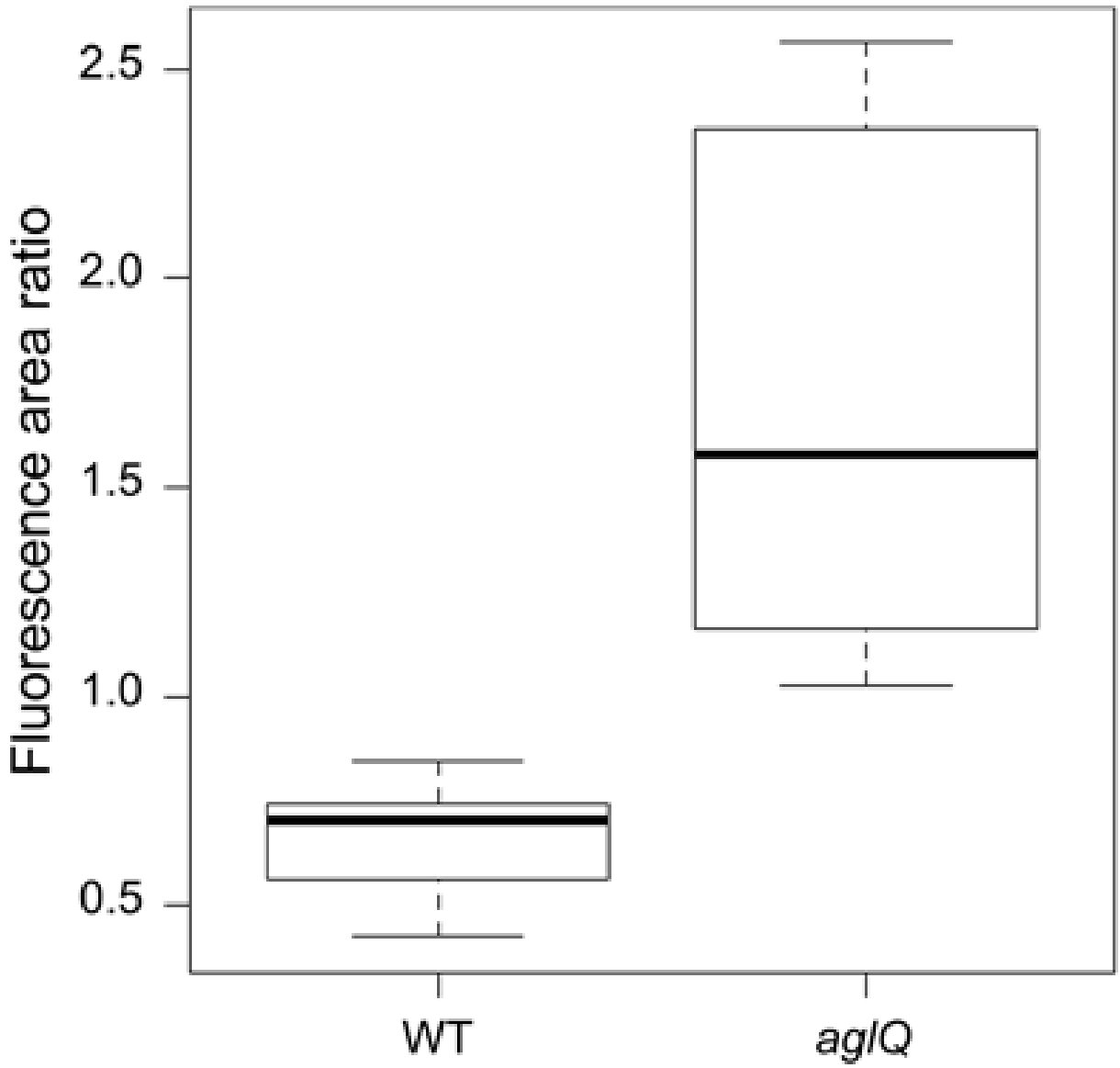

Figure S1

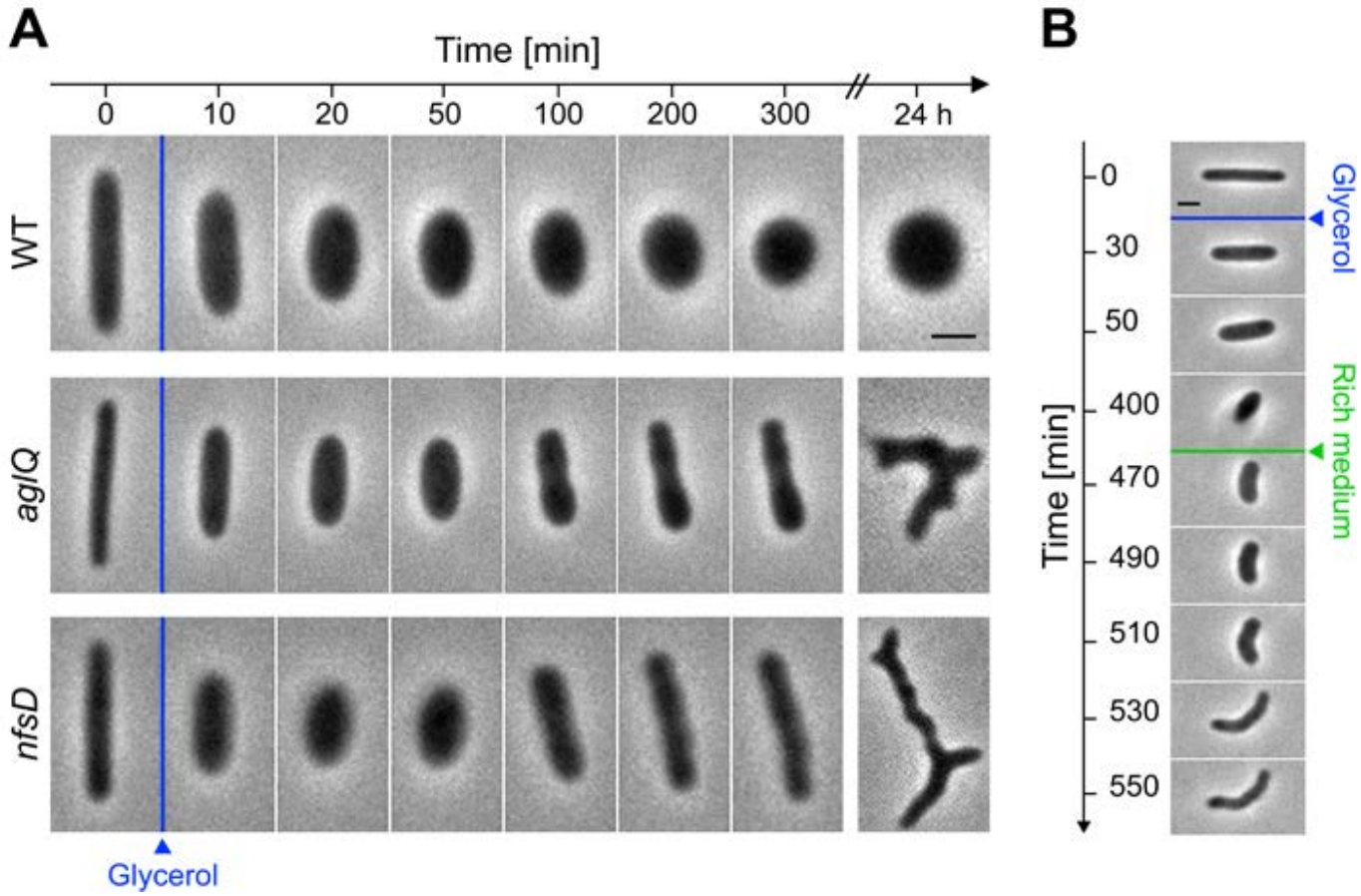
A
Time [min]
0
10
20
50
100
200
300
24 h
WT
aglQ
nfsD
Glycerol
B
Time [min]
0
30
50
400
470
490
510
530
550
Glycerol
Rich medium

Figure S2

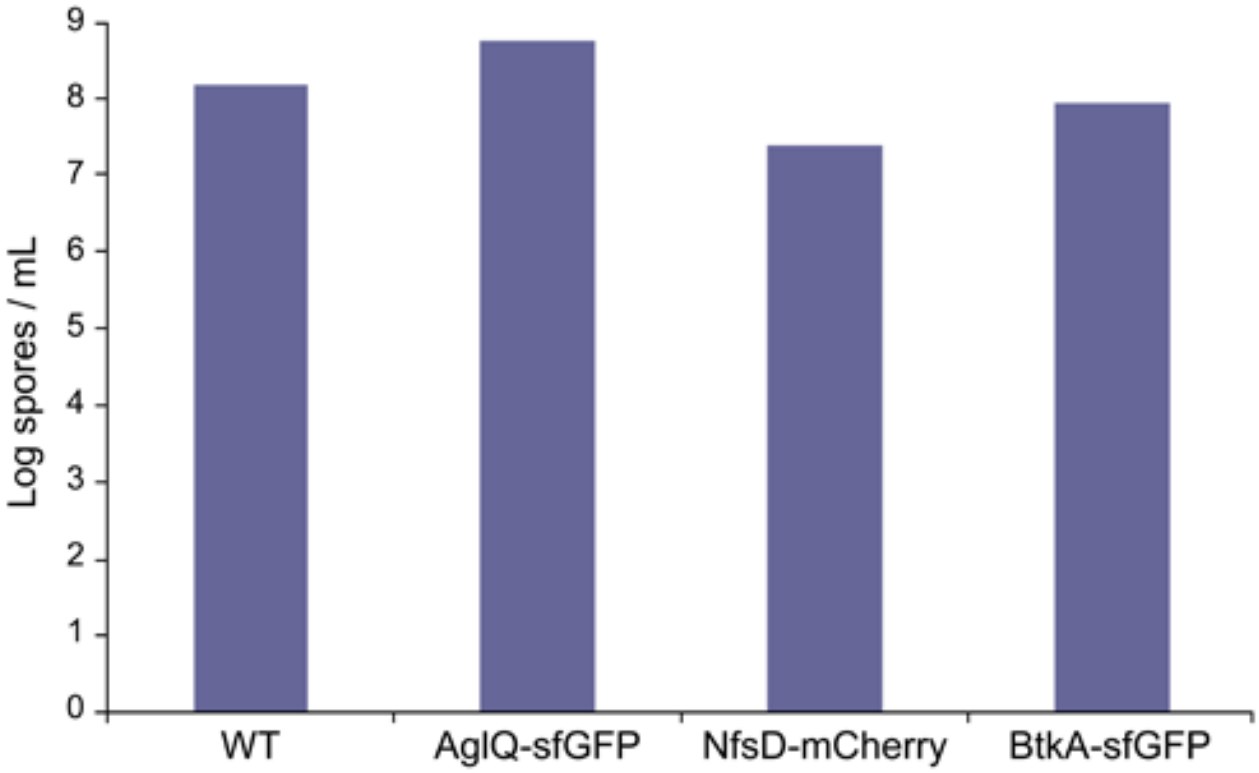
Log spores / mL
0
1
2
3
4
5
6
7
8
9
WT
AglQ-sfGFP
NfsD-mCherry
BtkA-sfGFP

Figure S3

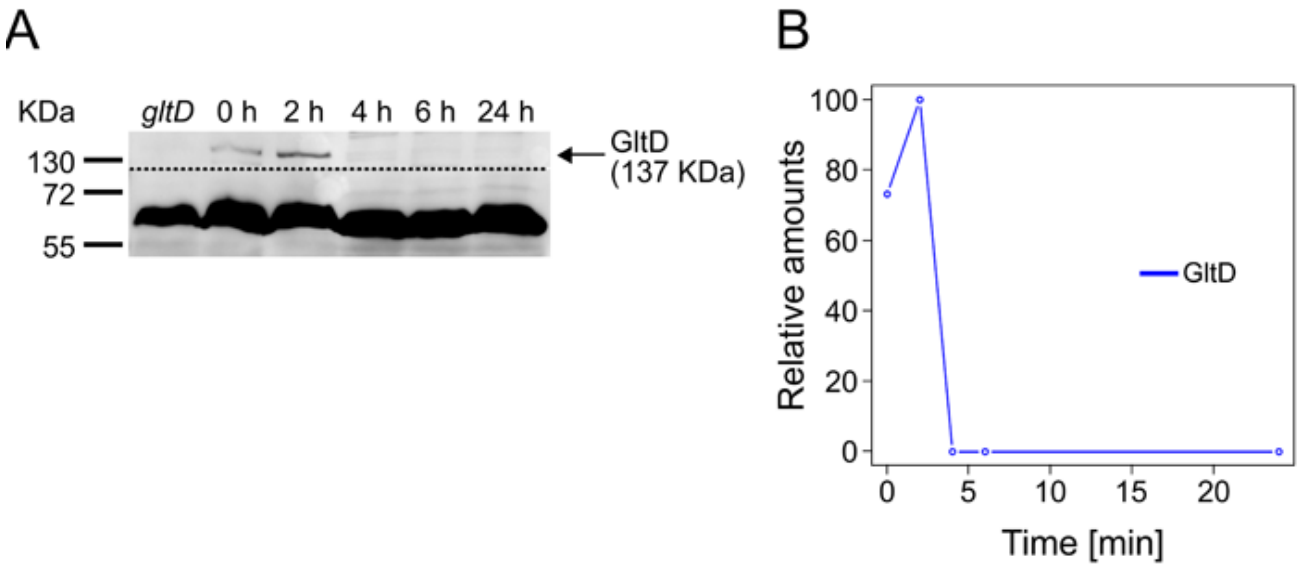
A
KDa
gltD
0 h
2 h
4 h
6 h
24 h
130
72
55
GltD
(137 KDa)
B
Relative amounts
100
80
60
40
20
0
0
5
10
15
20
Time [min]
GltD

Figure S4

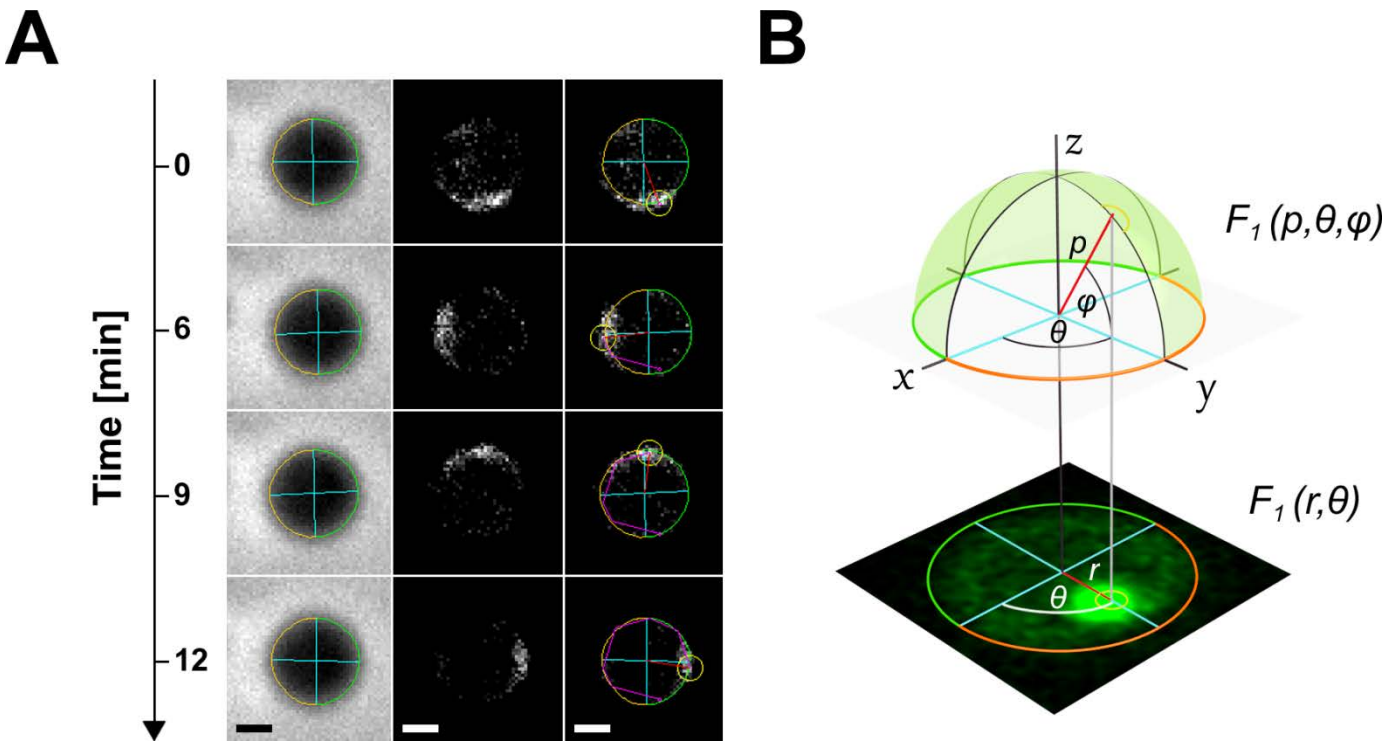

Figure S5

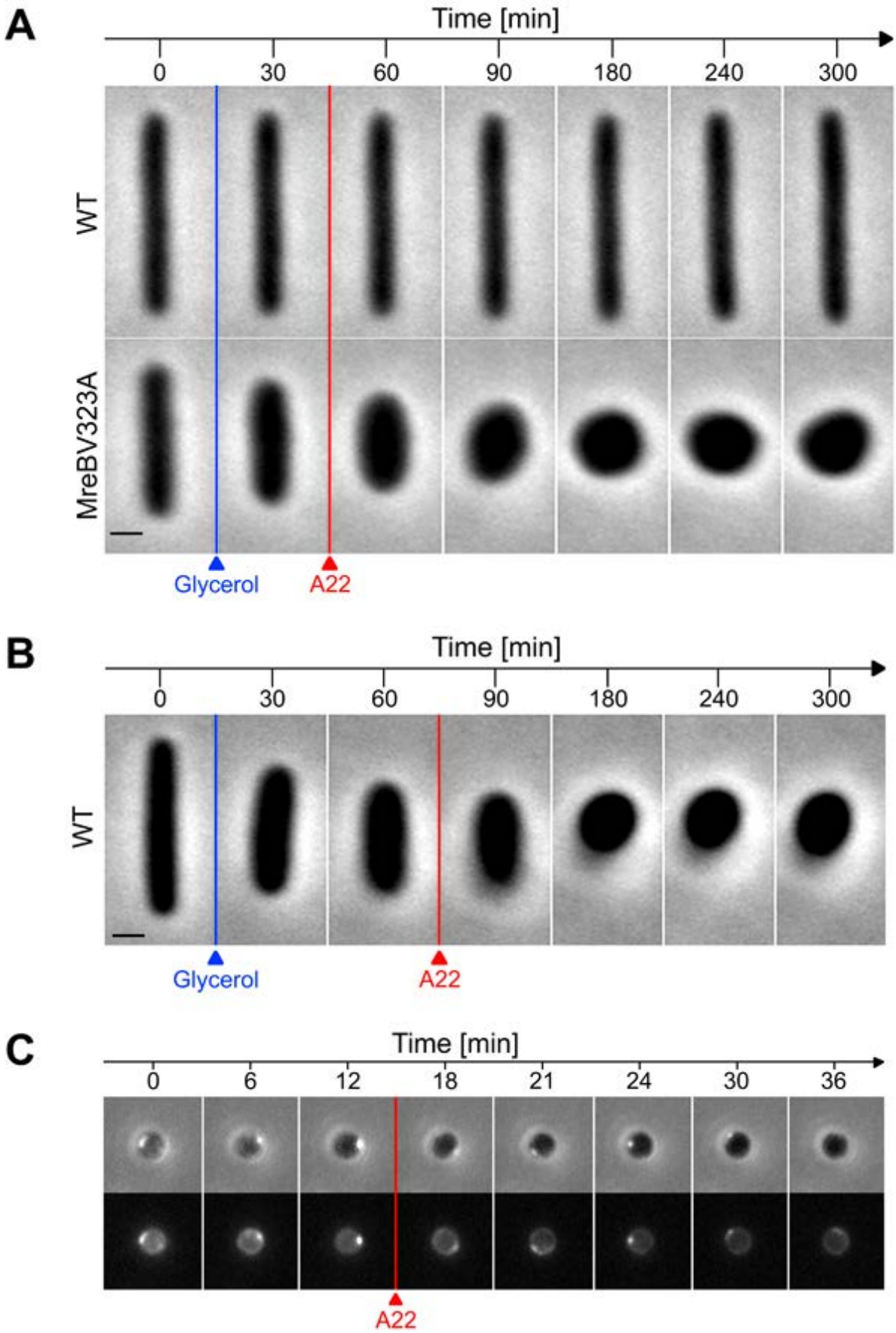
A
Time [min]
0
30
60
90
180
240
300
WT
MreBV323A
Glycerol
A22
B
Time [min]
0
30
60
90
180
240
300
WT
Glycerol
A22
C
Time [min]
0
6
12
18
21
24
30
36
A22

Figure S6

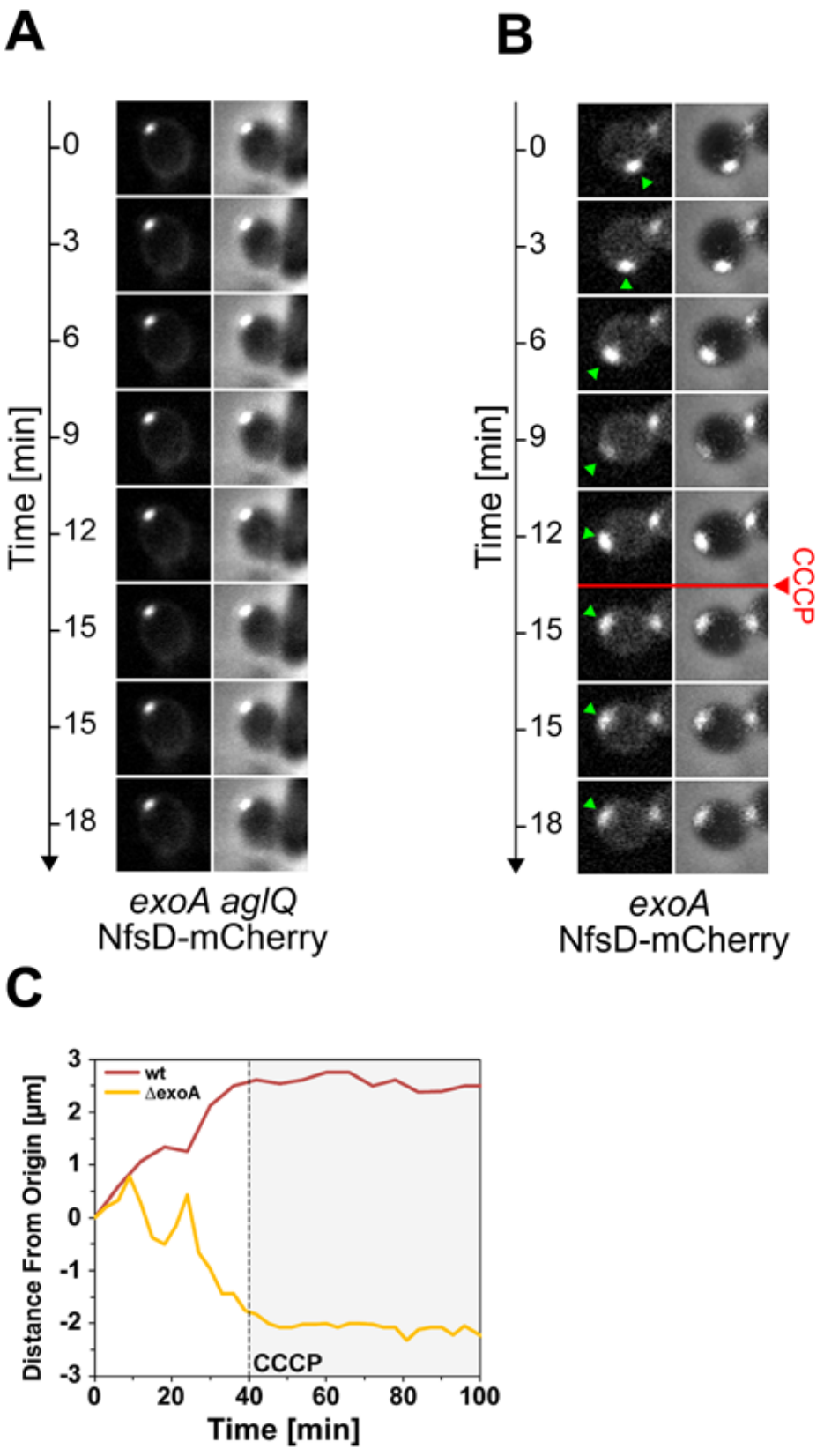
A
B
C
Time [min]
0
3
6
9
12
15
15
18
CCCP
exoA aglQ
NfsD-mCherry
exoA
NfsD-mCherry
wt
ΔexoA
Distance From Origin [µm]
3
2
1
0
-1
-2
-3
0
20
40
60
80
100
Time [min]

Figure S7

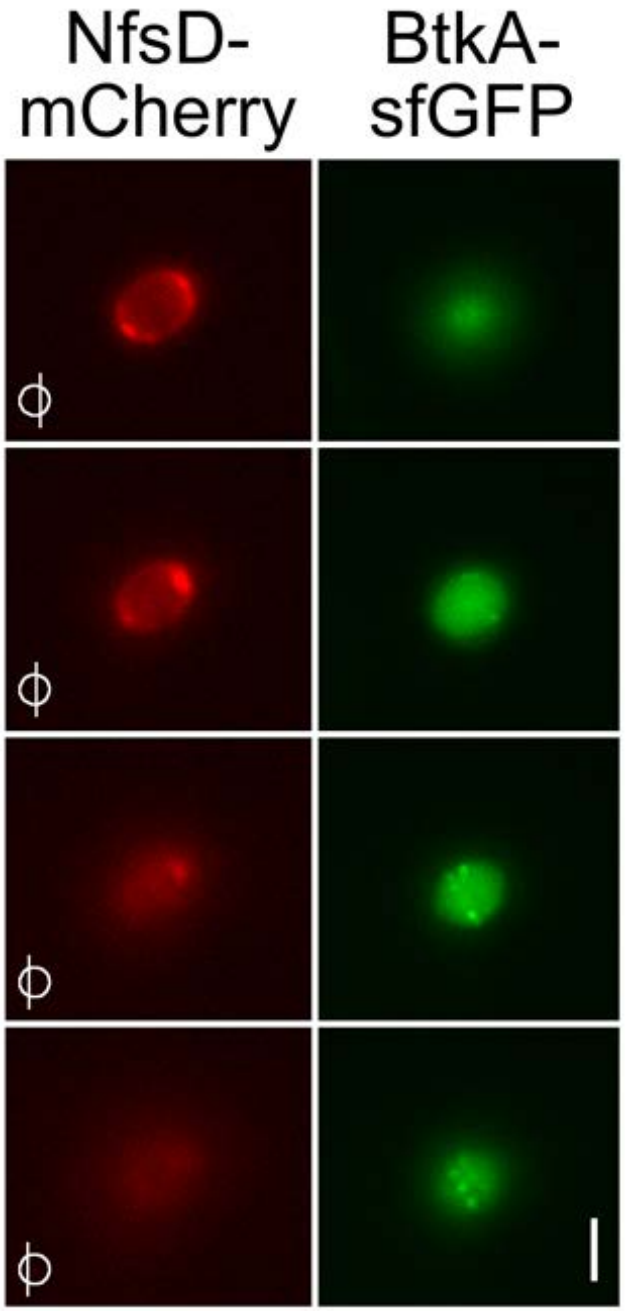

Figure S8

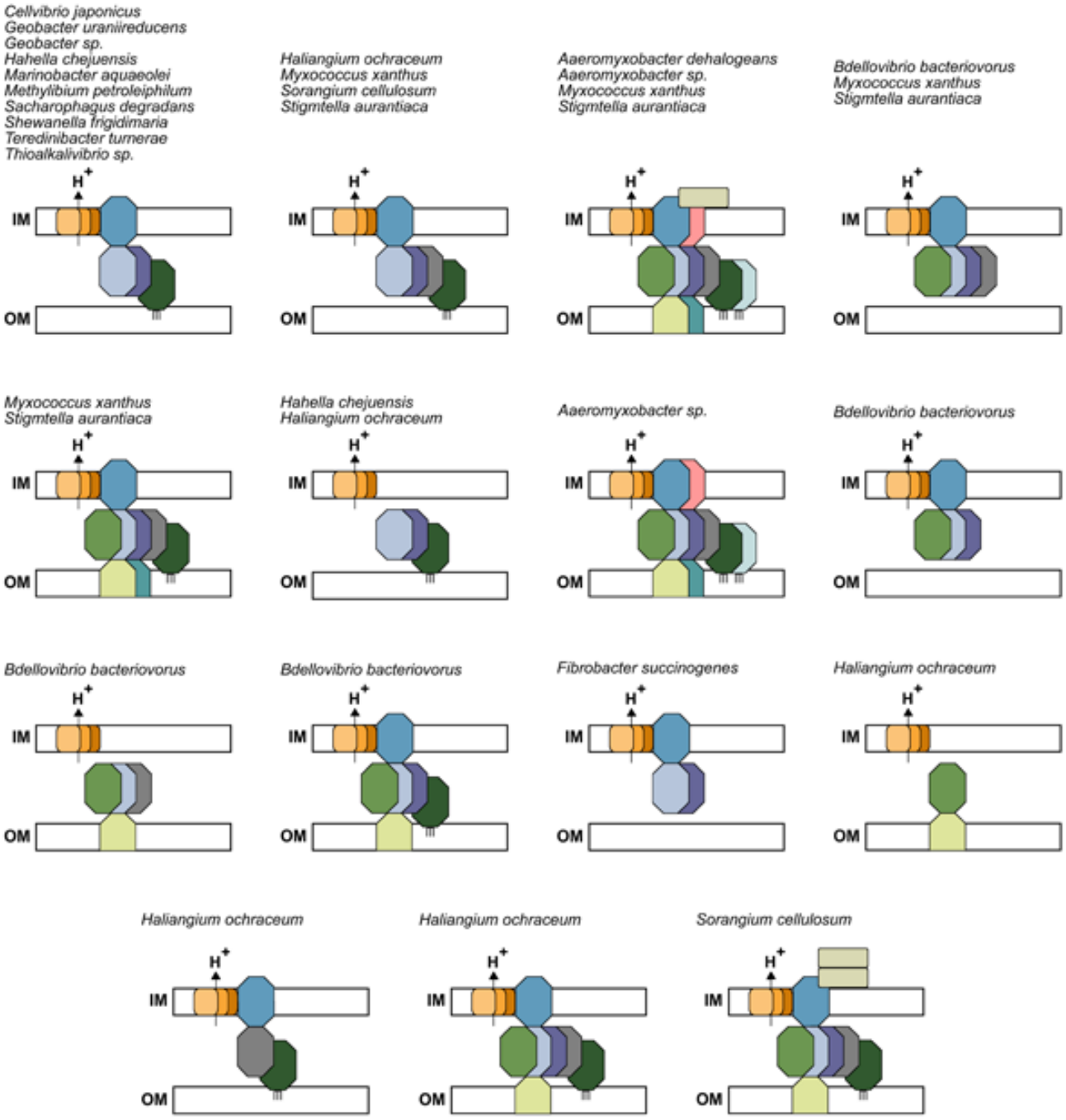
Cellvibrio japonicus
Geobacter uraniireducens
Geobacter sp.
Hahella chejuensis
Marinobacter aquaeolei
Methylibium petroleiphilum
Sacharophagus degradans
Shewanella frigidimaria
Teredinibacter turnerae
Thioalkalivibrio sp.
Haliangium ochraceum
Myxococcus xanthus
Sorangium cellulosum
Stigmtella aurantiaca
Aaeromyxobacter dehalogeans
Aaeromyxobacter sp.
Myxococcus xanthus
Stigmtella aurantiaca
Bdellovibrio bacteriovorus
Myxococcus xanthus
Stigmtella aurantiaca
Myxococcus xanthus
Stigmtella aurantiaca
Hahella chejuensis
Haliangium ochraceum
Aaeromyxobacter sp.
Bdellovibrio bacteriovorus
Bdellovibrio bacteriovorus
Bdellovibrio bacteriovorus
Fibrobacter succinogenes
Haliangium ochraceum
Haliangium ochraceum
Haliangium ochraceum
Sorangium cellulosum
H+
IM
OM

Figure S9

Table S1. Bioinformatic analysis of the Glt and the Nfs clusters.

Protein in the Glt complex	Paralog in the Nfs complex	Identities	Positives	Functional domain (Pfam)	Signal peptide	Transmembrane domain	Lipoprotein signal peptide
GltA (MXAN_2540)	NfsA (MXAN_3371)	29 %	43 %	OmpA-like transmembrane domain	+	-	-
GltB (MXAN_2539)	NfsB (MXAN_3372)	30 %	46 %	-	+	-	-
GltC (MXAN_2541)	NfsC (MXAN_3373)	23 %	45 %	Tetratricopeptide repeat	+	-	-
GltD (MXAN_4870)	NfsD (MXAN_3374)	28 %	46 %	Tetratricopeptide repeat	+	-	-
GltE (MXAN_4869)	NfsE (MXAN_3375)	28 %	47 %	Tetratricopeptide repeat	+	-	+
GltF (MXAN_4868)	NfsF (MXAN_3376)	42 %	70 %	-	+	-	-
GltG (MXAN_4867)	NfsG (MXAN_3377)	35 %	50 %	FHA domain Gram-negative; bacterial TonB protein	-	+	-
GltH (MXAN_4866)	NfsH (MXAN_3378)	28 %	43 %	Autotransporter β-domain	+	-	-
GltI (MXAN_4863)	-	-	-	Tetratricopeptide repeat	-	-	-
GltJ (MXAN_4862)	-	-	-	-	-	+	-
GltK (MXAN_2538)	-	-	-	-	+	-	+

Table S2. Strains used in this study.

Strain	Description	Source	Genotype
DZ2	Wild type	Laboratory collection	WT
TM146	DZ2 Δ*aglQ* (pBJΔ*aglQ*)	[1]	Δ*aglQ*
TM247	DZ2 *gltD-mCherry* (pBJ*gltD-mCherry*)	[2]	*gltD-mCherry*
TM312	TM146 $mx8_{att}$*::aglQ*$_{D28N}$*-HA* (pSW*aglQ*$_{D28N}$*-HA*)	[1]	Δ*aglQ aglQ*$_{D28N}$*-HA*
TM357	TM146 Δ*pilA* (pBJΔ*pilA*)	This work	Δ*aglQ* Δ*pilA*
TM363	DZ2 Δ*3004* (pBJΔ*3004*)	[1]	Δ*3004*
TM384	DZ2 Δ*aglR* (pBJΔ*aglR*)	[1]	Δ*aglR*
TM452	DZ2 Δ*aglS* (pBJΔ*aglS*)	[1]	Δ*aglS*
TM484	DZ2 Δ*exoA* (pBJΔ*exoA*)	[3]	Δ*exoA*
TM526	DZ2 *nfsD-mCherry* (pBJ*nfsD-mCherry*)	This work	*nfsD-mCherry*
TM541	TM357 $mx8_{att}$*::aglQ-sfGFP* (pSW*aglQ-sfGFP*)	This work	Δ*aglQ* Δ*pilA aglQ-sfGFP*
TM578	DZ2 Δ*nfsD* (pBJΔ*nfsD*)	This work	Δ*nfsD*
TM628	TM541 *nfsD-mCherry* (pBJ*nfsD-mCherry*)	This work	Δ*aglQ* Δ*pilA aglQ-sfGFP nfsD-mCherry*
EC153	Top 10 *T18-aglR* (pU*T18N-aglR*)	This work	*aglR-T18*
EC156	Top 10 *T25-gltG* (pK*T25-gltG*)	This work	*T25-gltG*
EC176	Top 10 *T25-nfsG* (pK*T25-nfsG*)	This work	*T25-nfsG*
EC208	Top 10 *T18-3003* (pU*T18N-3003*)	This work	*3003-T18*

1. Sun M, Wartel M, Cascales E, Shaevitz JW, Mignot T (2011) Motor-driven intracellular transport powers bacterial gliding motility. Proc Natl Acad Sci USA 108: 7559–7564.

2. Nan B, Mauriello EM, Sun IH, Wong A, Zusman DR (2010) A multi-protein complex from Myxococcus xanthus required for bacterial gliding motility. Mol Microbiol 76: 1539–1554.

3. Ducret A, Valignat M-P, Mouhamar F, Mignot T, Theodoly O (2012) Wet-surface-enhanced ellipsometric contrast microscopy identifies slime as a major adhesion factor during bacterial surface motility. Proc Natl Acad Sci USA 109: 10036–10041.

Table S3. Primers used in this study.

Primer	Sequences of primers (5'-3')
3374-mCherry-1	CCCAAGCTTGAGAAGGAGAAGAAGTGGAG
3374-mCherry-2	CTCGCCCTTGCTCACTCGCAGCACCTCCCCGCG
3374-mCherry-3	GGGGAGGTGCTGCGAGTGAGCAAGGGCGAGGAG
3374-mCherry-4	CGGGATCCTTACTTGTACAGCTCGTCC
3374-mCherry-5	CGGGATCCAGCTGTTTCGCATCGATTC
3374-mCherry-6	GGAATTCTCCAGCTTCAGGTAGACCATG
AglR-3	CGGGATCCGAAGTCCTTCGGGAACCCG
GmoBSFGFP-1	TTCTTCACCTTTAGAGCCCATCGCCGCGGACAC
GmoBSFGFP-2	TCCGCGGCGATGGGCTCTAAAGGTGAAGAACTGTTC
GmoBSFGFP-3	CCCAAGCTTTTATTTGTAGAGCTCATCCATG
D3374-1	GGAATTCCGCTTATGAGCGAGTGCCG
D3374-2	CGGGATCCGCGAGCTCCTGCCGTGAAG
D3374-3	CGGGATCCAGCTGTTTCGCATCGATTC
D3374-4	CCCAAGCTTACCTTCTCGAACGCCTCGC
gmoA-O1	CCCAAGCTTGGACCTGGCGTCTGTGAC
gmoA-O2	GGAATTCTCCTCCTCGTCGCGAG
4867-O1	GCTCTAGACGCCGTTCCTCTGACACTC
4867-O2	GGAATTCCTATTCGCCGGACTGCTTG
3377-O1	GCTCTAGACGCGGCGGCGAAGAACAAC
3377-O2	GGAATTCTCACCCTCCCGCGCCAGCG
3003-O1	CCCAAGCTTGATGGGCGCGCCCCG
3003-O2	GGAATTCCGCGAAGCGCGCGCCTC

Table S4. Plasmids used in this study.

Plasmid	Construction scheme*
pBJ114 *nfsD-mCherry*	Primer pairs 3374-mCherry-1/3374-mCherry-2 and 3374-mCherry-5/3374-mCherry-6 were used to amplify respectively the last 1 kb of *nfsD* gene (fragment 1) and the 1 kb downstream *nfsD* gene (fragment 3) from the DZ2 chromosome. Primer pair 3374-mCherry-3/3374-mCherry-4 is used to amplify *mCherry* from a plasmid containing the *mCherry* gene (fragment 2). Fragments 1 and 2 were fused by SOE-PCR and cloned at the HindIII and BamHI restriction sites of the pBJ114 (pBJ114-fragment1-2). Then, the fragment 3 is cloned at the BamHI and EcoRI restriction sites of the pBJ114-fragment1-2.
pSWU30 *aglQ-sfGFP*	Primer pair AglR-3/GmoBSFGFP-1 is used to amplify the *aglQ* gene and its promoter from the DZ2 chromosome (fragment 1). Primer pair GmoBSFGFP-2/ GmoBSFGFP-3 is used to amplify the *sfGFP* from a plasmid containing the *sfGFP* gene (fragment 2). Both fragments fused by SOE-PCR and cloned at the BamHI and HindIII restriction sites of the pSWU30.
pBJΔ*nfsD*	Primer pairs D3374-1/ D3374-2 and D3374-3/ D3374-4 were used to amplify respectively a 1 kb fragment upstream and downstream of the *nfsD* open reading frame. The upstream fragment was first cloned at the EcoRI and BamHI restriction sites of the pBJ114 (pBJ114-upstream). Then, the downstream fragment was cloned at the BamHI and HindIII restriction sites of the pBJ114-upstream.
pU*T18N-aglR*	A fragment encompassing *aglR* was amplified from the DZ2 chromosome with primers gmoA-O1/gmoA-O2 and cloned at the HindIII and EcoRI sites of pUT18N.
pK*T25-gltG*	A fragment encompassing *gltG* was amplified from the DZ2 chromosome with primers 4867-O1/4867-O2 and cloned at the XbaI and EcoRI sites of pKT25.
pK*T25-nfsG*	A fragment encompassing *nfsG* was amplified from the DZ2 chromosome with primers 3377-O1/3377-O2 and cloned at the XbaI and EcoRI sites of pKT25.
pU*T18N-3003*	A fragment encompassing *3003* was amplified from the DZ2 chromosome with primers 3003-O1/3003-O2 and cloned at the HindIII and EcoRI sites of pUT18N.

*All plasmid inserts were sequenced to ensure the absence of PCR-introduced mutations.

DISCUSSION

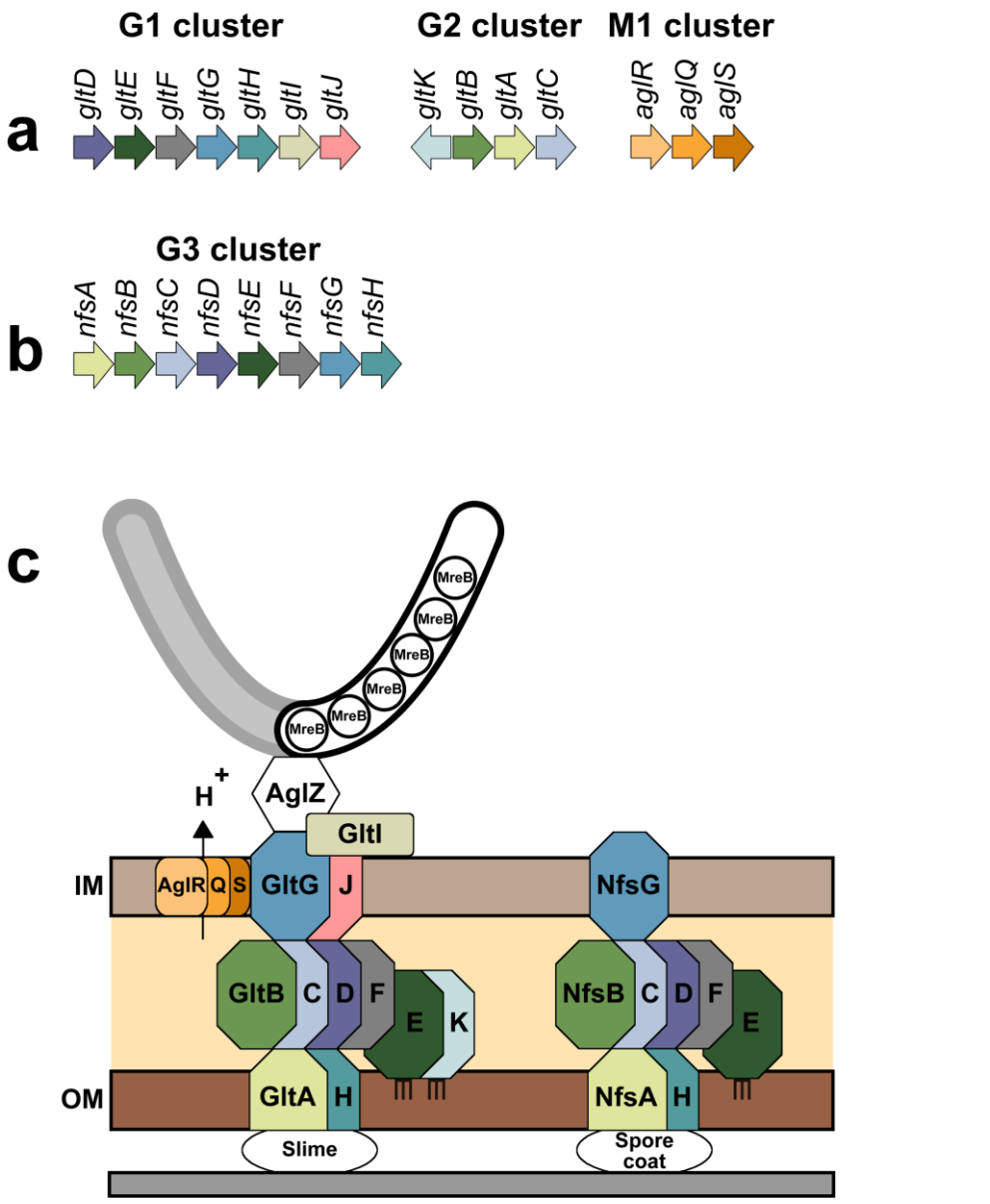

Figure 29. Glt and Nfs complexes are paralogous. a. Genetic organization of the 14 genes encoding the components of the gliding machinery in *Myxococcus xanthus*. The G1 and G2 clusters correspond to the *glt* genes, and M1 cluster corresponds to the *aglRQS* genes. b. Genetic organization of the G3 cluster, corresponding to the *nfs* locus. c. Predicted structures of the Agl-Glt and Nfs machineries. The PG is not represented because its connection to Glt and Nfs proteins is unknown. The color code indicates paralogous genes.

In 2009, when I started my PhD in Tâm Mignot's group, the mechanism of gliding motility in *M. xanthus* was a mystery and conflicting models were proposed to explain this form of motility on surface independent of any known bacterial structures: the "slime secretion" model and the "focal adhesion complexes" (FACs) model. According to the first model, gliding resulted from the secretion of a polysaccharide, the slime, at the back of the cells. On the other hand, the FACs model proposed that gliding machinery units were assembled at distributed sites along the cell body. Adhesion of the gliding machinery at these sites would create friction and thrust (Figure 27c) (Mignot et al., 2007).

The first objective of my thesis was to characterize the gliding motor, an essential part of the gliding machinery. We hypothesized that the identification and localization of the gliding motor would provide key evidences to solve the debate between the two conflicting models. Moreover, we supposed that characterization of the gliding motor could be a starting point for the identification of the entire gliding machinery and the characterization of the motility mechanism.

1. The Gliding Motility Mechanism

1.1. The Gliding Motility Machinery

During the first part of my thesis, a combination of fluorescence imaging, force microscopy and genetic experiments, led to the identification of a gliding motor formed by the AglRQS proteins (Sun et al., 2011). We then subsequently identified the rest of the motility complex by a phylogenomic approach rooted on characterization of the motor. We demonstrated that this gliding machinery localizes at the FACs, which strongly argues in favor of the FACs model.
We now propose that during motility, mechanical work from the AglRQS motor located in the inner membrane is transduced through the cell envelope to the cell surface by the associated Glt complex (Figure 29c) (Luciano et al., 2011). However many questions remain: How does transmission occur at the molecular level? What is the function of slime? What is at the origin of directionality? In the first part of this discussion section, I will address each of these questions and propose future research perspectives.

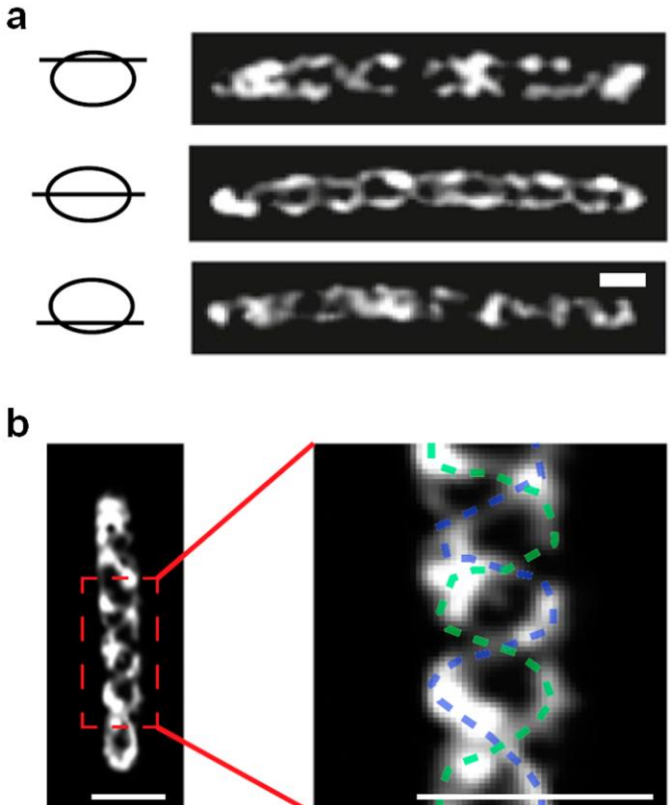

Figure 30. GltD and AglR decorate a helix. a. Deconvolved images of one fixed *gltD-mCherry* cell (Nan et al., 2011). b. Structure illumination microscopy (SIM) images of fixed *aglR-pamCherry* cell (Nan et al., 2013). Scale bar = 1 μm.

A rigid track must support motor activity

To promote motility, the Agl-Glt complex (stator) must be immobilized against the substratum and thread along a rigid rotor connected to the entire cell body. What could be the identity of such track?

The MreB cytoskeleton was initially proposed to be the rigid structure on which the motility motor moves, based on A22 experiments by Mauriello *et al.* (Section 3.2.1.2., Introduction) (Mauriello et al., 2010). Other evidence connects MreB to motility: (i), bead movements driven by the motility apparatus are immediately stopped by A22 (Sun et al., 2011). (ii), Nan *et al.* showed that both GltD and AglR move with helical trajectories and the rotation is blocked by A22 (see below, Nan et al., 2011, 2013). Even though MreB may be important for motility, it may not constitute the motility rotor. Indeed, the AglRQS motor is similar to the TolQR complex and this complex energizes envelope processes in the periplasmic space. Specifically, in the Tol-Pal system, the interaction between TolQR and TolA, the suspected energy transducer, likely allows dynamic contacts with the outer membrane through the Pal lipoprotein (Cascales et al., 2000). Since GltG interacts with AglR, the TolQ homologue and GltG is a TolA-like protein with an extended periplasmic domain, this suggests that AglRQS activity is transduced toward the periplasm and not the cytosol.

Thus, the question of MreB essentiality during gliding remains. Similar to its function in cell wall synthesis (Section 2.2.4.2., Introduction), MreB could act as a scaffold to recruit the Glt machinery. Alternatively, due to its interaction with the cell wall synthesis machinery, MreB could facilitate the insertion of the motility machinery in the cell envelope and specifically in the cell wall. Unpublished work from our lab suggests that MreB recruits the gliding machinery at the FACs directly and independently from its function in cell wall synthesis (Hot *et al.*, in preparation).

Work form the Zusman group recently provided evidence for the existence of a helical track. GltD-mCherry and AglR-pamCherry fusions appear to traffic along a closed helical loop that spans the entire cell length (Figure 30). Based on these rotary dynamics, the authors suggested a mechanism wherein the Agl motor powers the trafficking of the Glt complex along a looped helical track (see below, Section 1.2., Discussion). In our lab, we were not able to resolve any helical pattern of GltD-mCherry around the cell periphery, but rather, we observed that GltD-mCherry localized around the cell periphery and at FACs. This discrepancy could come from the fact that the Zusman group uses mathematical image-deconvolution processing to observe the GltD-mCherry helices. Deconvolution microscopy allows the visualization of fluorescent probes

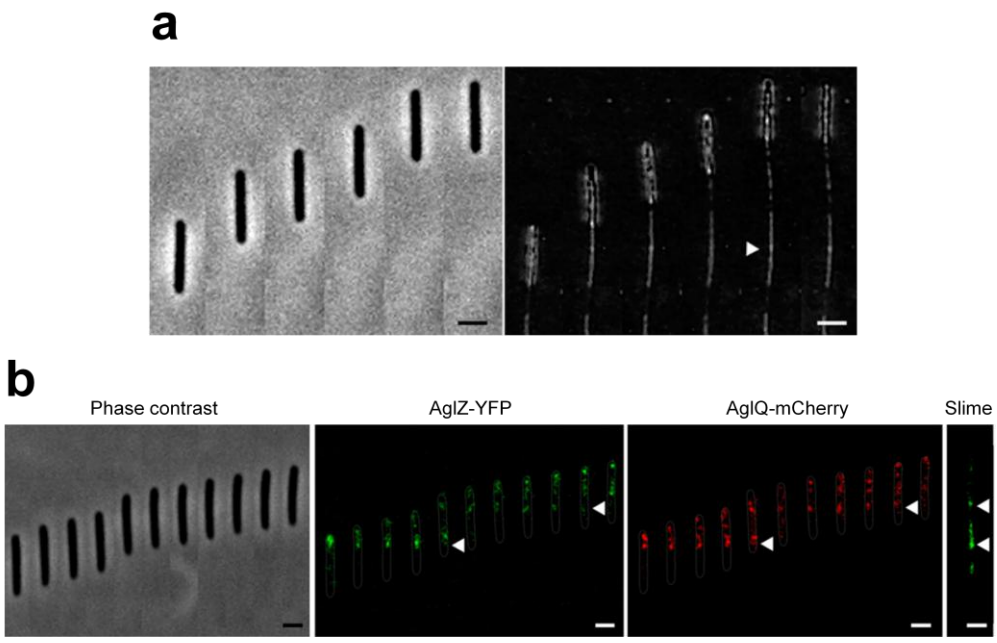

Figure 31. Slime is deposited by the Agl/Glt motility complexes. a. Phase contrast and Wet-SEEC images of slime deposition in the wake of a motile cell shown at different time points. Pictures were taken every 30 seconds. Triangle arrow points to the slime trail. b. Slime patches are deposited where the Agl/Glt machinery assembles. Time lapse of a cell expressing both AglZ-YFP and AglQ-mCherry is shown. Phase contrast and corresponding YFP and mCherry micrographs are shown. Slime was stained with a GFP-lectin after the cell left the positions shown on the Left. Triangular arrows point to fixed AglZ- and AglQ-bright motility complexes at positions where conspicuous slime patches were deposited. Fluorescent micrographs were taken every 15 seconds. Scale bar = 1 μm (Ducret et al., 2012).

or proteins at various planes along the sample depth and then the reconstruction of an image where the interference from obstructing light generated by excitation of the entire depth focus is reduced (Sibarita, 2005). This approach must be used carefully because it is highly artifact-prone. For example, it suggested that MreB forms a helix, and now, this organization seems to be controversial (Section 2.2.4.2., Introduction; Domínguez-Escobar et al., 2011). To confirm or infirm that GltD-mCherry forms a helix, we are now using TIRF microscopy to study the localization of GltD-mCherry in gliding cells. If this helical track exists, it appears to be independent from MreB because GltD-mCherry was still helical in the presence of A22 (Nan et al., 2011).

In fact, the only known rigid continuous structure in the bacterial cell is the PG itself and thus, it is tempting to propose that the PG itself constitutes the track. The Agl-Glt machinery could push against the PG during gliding and moves it like a caterpillar track. This could be tested by localizing PG components during cell movement by using specific PG probes (Kuru et al., 2012). Conversely, we could perturb the PG synthesis chemically or genetically and test how this affects gliding.

The role of slime

While slime appears not to mediate propulsion directly, it still has a function in motility. Recently, Ducret *et al.* addressed the role of the slime during *M. xanthus* gliding (Ducret et al., 2012). By using an optical microscopy method called surface enhanced ellipsometric contrast microscopy in wet condition (Wet-SEEC), they were able to image and quantify slime at unprecedented resolution (Figure 31a) (Ducret et al., 2012). This analysis revealed that slime is deposited at constant rates underneath the cell body and that during motility, slime patches are specifically bound by Agl-Glt gliding machinery (although the secretion of slime does not depend on the motility machinery, Figure 31b). Based on these results, it was proposed that slime acts as a sticky glue, bound to the outermost components of the motility machinery (possibly GltA, GltH, GltK, see below) and promoting its adhesion to the substrate on the ventral side of the cell (at the FACs). The exact composition of the slime and the identification of the machinery that produces and secretes will be helpful to understand how slime exactly contributes to the gliding mechanism.

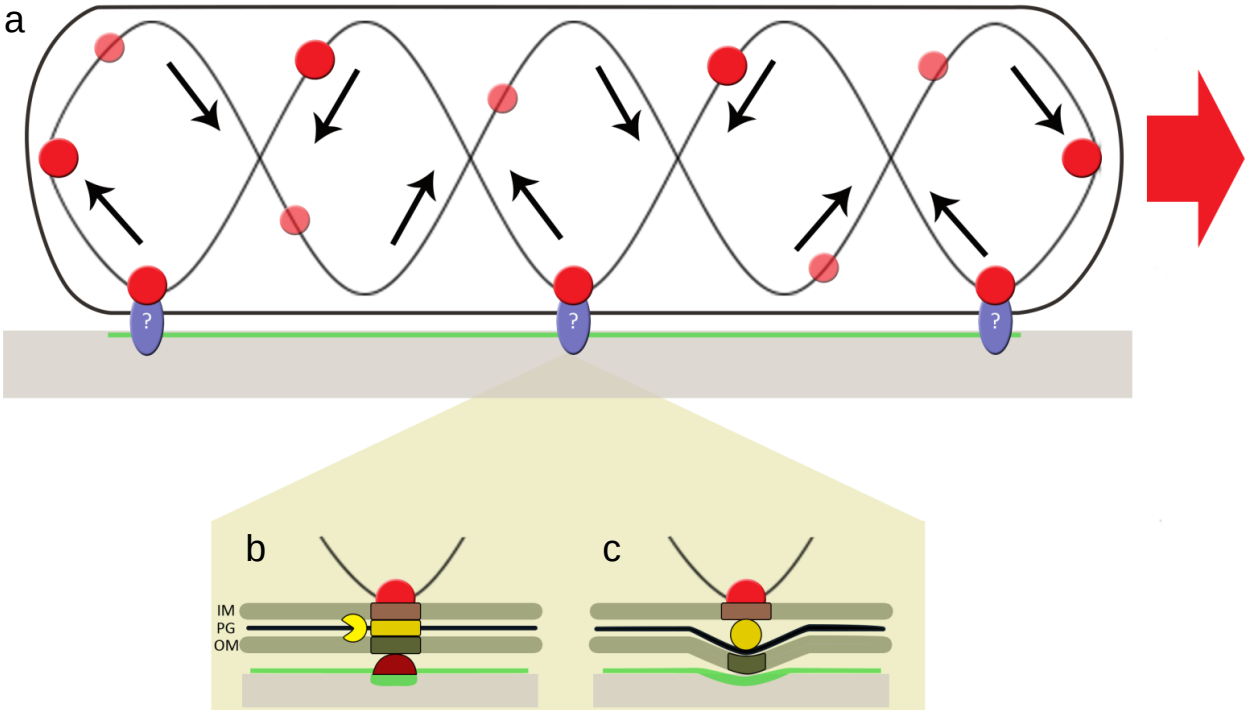

Figure 32. The gliding motility model. a. The red arrow represents the direction of movement. Motility motors loaded with the Glt complex (big dark red circles) or unloaded motors (small transparent red circles) translocate along an endless closed loop. Only the motors loaded with the Glt complex are proficient for movement. The machinery could afford the rigid PG by two different ways: b. The motility complex may span the entire cell envelope and a PG-hydrolase may facilitate insertion of the complex through the PG. c. Alternatively, the motility complex could deform the PG, creating surface depression and drag. Outer membrane proteins may in this system reinforce local contacts at the depressions.

Where does the directionality of the gliding machinery come from?

We showed that AglZ-YFP and beads are transported by the AglRQS motor in a directional manner from one pole to another. This unidirectional motion could be due to a periodic asymmetry of the unidentified rigid track on which the motor moves, like in the case of myosin V moving on actin tracks (Section 1.2.2.1., Introduction). MreB filaments for example may display such polarity if they act as a track. However evidences for a polarity of MreB filaments in bacterial cells are missing (Kim et al., 2006). Similarly, there is no evidence that PG exhibits any sort of intrinsic polarity.

Another possibility would be that slime constitutes a directionality factor during gliding. When slime links Agl-Glt-complexes to the substratum, it may become tightly bound and could thus act as a molecular ratchet, preventing the gliding machinery to step back. This hypothesis is inspired by the fact that the Exo polymer is required for Nfs movement directionality (see below). Unfortunately and contrarily to the spore coat for which the biosynthesis and secretion machinery has been identified, the slime polymer has not been characterized yet and this hypothesis may not be tested.

1.2. Current Gliding Motility Models

Based on all the experiments conducted these last five years by the Zusman and Mignot groups, an updated model can be proposed to explain gliding motility in *M. xanthus*. We propose that the AglRQS motor, a proton channel, harvests the energy from the proton flux, and this energy is converted to a mechanical output at the cell surface through the Glt transducer complex (Figure 29c). Thus, the AglRQS motor powers motility by trafficking Glt transducer complexes along a close looped helix, from the leading pole to the lagging pole (Figure 32a). The Agl motor could move along the closed helix in two conformations: it could form an active machinery when it is loaded with the Glt complex. In this conformation, the active gliding machinery could interact with the substratum, allowing cell movement. The other conformation involves an unloaded motor, which is thus inefficient to promote cell gliding. According to the model, motors become loaded at the leading cell pole. When active motors carrying the Glt complex cargo reach the back of the cell, it unloads its cargo, which alleviates the connection with the substratum. Then, the unloaded motor moves along the closed loop toward the leading cell pole, to be available for a new cycle (Figure 32a). If the rigid track is a helix, the cell body should rotate with respect to its point of attachment to the substratum.

Connection between the gliding machinery and the underlying substratum could occur in two ways

The motility complexes could span the entire cell envelope (inner membrane, PG and outer membrane) and movement would occur when the outer membrane Glt subunits get in contact with the substratum at the ventral side of the cell (Figure 32b). This hypothesis is supported by the presence of gliding proteins in each envelope layer (Figure 29c) (Luciano et al., 2011; Sun et al., 2011), and by the observation that the slime, a surface polysaccharide (see above), is transported by the Agl-Glt machinery (Ducret et al., 2012). However, a difficulty with this model is that the Glt complexes must span the rigid PG layer. The motility machinery could include or could be associated with PG-hydrolases, to degrade the PG locally, allowing its insertion in the PG (Figure 32b). However, such hydrolase activity has yet to be found. Alternatively, as discussed above, MreB could facilitate the insertion of the gliding machinery in the PG.

In an alternative mechanism, the gliding machinery would not cross the cell wall but distorts it when it is loaded with the Glt complex. This distortion would push against the outer membrane and create contact zones against the substratum (Figure 32c). Consistent with this model, TIRF microscopy revealed periodic undulations of the distance between the cytoplasm and the glass, suggesting the presence of a helical track in the cell cytoplasm (Nan et al., 2011). However, this result is surprising because TIRF microscopy can only provides images of objects that are in up to 100 nm in depth from the cover-slip, which in the case of bacterial cells is not beyond the plasma membrane (Zenisek and Perrais, 2007). Since Nan *et al.* used GFP-tagged proteins expressed in the cytoplasm, it appears surprising that they could observe deep invaginations.
The "PG distortion" model does not explain the requirement for outer membrane proteins such as GltH and potentially GltA and GltK (based on bioinformatic predictions) (Figure 29c) as well as the linkage to slime and its trafficking at the cell surface (see also below the Section 2.2., Discussion). In the future, it will be necessary to characterize the outermost components of the machinery in detail to test which hypothesis is correct.

2. The Spore Coat Assembly Mechanism

During the phylogenomic study of the gliding machinery (Luciano et al., 2011), we demonstrated that the Glt gliding complex is homologous to the Nfs complex, which was described to be involved in the formation of a mature spore (Figure 29bc). It was proposed that the Nfs proteins function in a pathway involving the *exoA-I* genes, which encodes enzymes that drive spore coat

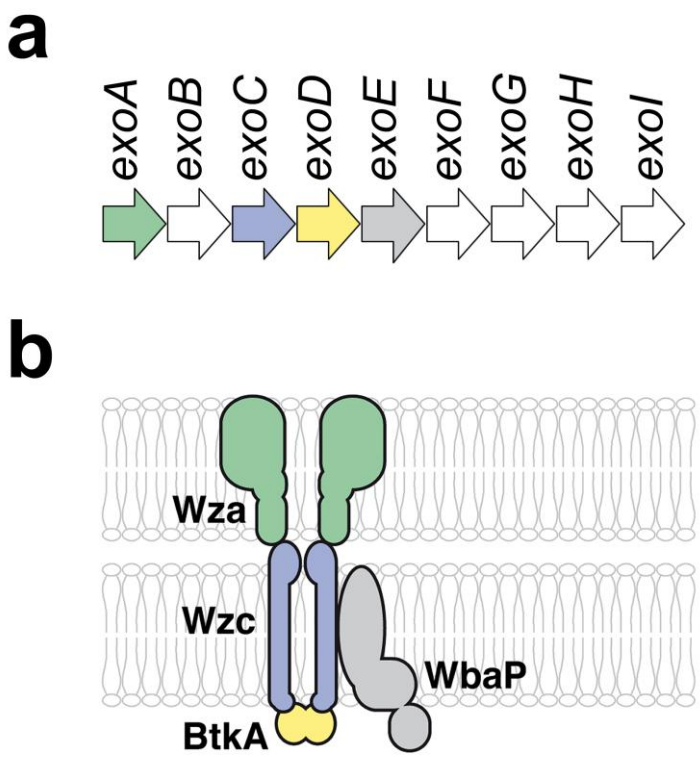

Figure 33. The ExoA-I export system produces and synthesizes the spore coat polymer. a. Genetic organization of the *exoA-I* operon. White genes have no know homologues in the databases. b. Predicted structure of the Exo export apparatus. The color code is the same in panel a and b. Thus, in the panel b, it indicated the name of the known homologues of *exo* genes.

synthesis and secretion (Figure 33ab) (Müller et al., 2012, 2010). Because gliding and sporulation are two distinct morphologically processes, but seem to involve similar machineries, we reasoned that studying the Nfs system might shed light into the function of Glt-like assemblages.

2.1. The Agl-Nfs Machinery is a Spore Coat Transporter

During sporulation, we showed that the AglRQS motor is distributed circumferentially around the spore surface to transport the Nfs complex directionally. Since the Nfs complex is linked directly to the spore coat polymer, Exo, we propose that the Agl-Nfs system is a spore coat transport system. In that case, how does the AglRQS motor transport directionally the Nfs complex?

The spore coat polymer guides the rotation of the Agl-Nfs machinery

In known molecular motor, directionality is generally dictated by the cognate track. For example, myosins V move directionally on the actin track because actin is polarized (Section 1.2.2.1., Introduction). In another example, SpoIIIE moves DNA directionally because SRS sequences are over-represented on the plus-strand of the chromosome. Indeed, SpoIIIE recognizes these sequences and uses them as a guide to accurately move the chromosome in the right direction (Section 2.3.3., Introduction). Remarkably, in the case of the Agl-Nfs system, the Exo polymer, that is the motor cargo, would also act as a directionality factor. In this process, we propose that the spore coat could act as an adhesive tape that prevents motor back steps when it becomes deposited. A better characterization of the spore coat composition, the identification and the characterization of the Nfs components that interact with the spore coat will be required to test this hypothesis. Yet, this hypothesis is seducing because it could also explain the directionality of the motility machinery as discussed above.

A model for spore coat assembly

Based on our results, we proposed a model explaining the sporulation process in *M. xanthus*. The spore coat is synthesized and secreted at the cell surface by the ExoA-I machinery. Then, this spore coat is recruited and transported around the spore surface by the Agl-Nfs machinery. Transport is ensured by (i), the circumferential distribution of the Agl motor and (ii), the directionality effect of the Exo polymer. This way, the Agl motor may transport Exo-linked Nfs complexes all around the spore from one Agl unit to the next and construct a homogenous, compact and resistant spore coat, like wrapping a strand of wool around a ball. However, how

exactly the Agl-Nfs machinery contributes to spore coat assembly at the molecular level is not clear. The Nfs complex could be required for the polymerization of the spore coat, it could facilitate cross-links between Exo strands at the spore surface, or it could even provide attachment sites for the spore coat in the outer membrane.

2.2. Agl-Glt/Nfs Machineries and the Origin of Bacterial Gliding Motility

The Agl-Glt and Agl-Nfs machineries perform very distinct tasks, yet they are very similar at the molecular level. Both the Nfs and Glt complex associate to the same molecular motor, the AglRQS proton channel, which in both cases results in their directional transport around the cell surface. In both cases, this transport activity is used to transport cell surface components, such as surface attached beads and cognate sugar polymers. We conclude that Agl-Glt/Nfs machineries form a novel class of directional surface sugar transport systems.

How have the Agl-Glt and Agl-Nfs machineries become specialized in gliding and sporulation in the course of evolution? Our phylogenomic data suggest that the motility machinery is more sophisticated as it contains homologues for all the *nfs* genes but also additional genes such as *gltI*, *gltJ*, and *gltK* (Figure 29abc). Are these three proteins giving the specificity of the gliding machinery? Proteins encoded by these genes are essential for motility and GltI and GltJ are predicted to localize in the cytoplasm and in the inner membrane respectively (Figure 29c). Besides, we previously showed that in the cytoplasm, the MreB cytoskeleton is essential for gliding motility whereas sporulation does not require it. These data suggest that GltI and/or GltJ connect MreB with the Agl/Glt machinery. Consistent with this, unpublished work from our lab showed that GltI might link the MreB cytoskeleton to the rest of the Glt machinery (Hot *et al.*, in preparation). Since this connection is essential to recruit the Agl-Glt system to FACs, we propose that proteins such as GltI and GltJ were key acquisitions to adapt an Agl-Glt/Nfs system to a motility function.

Globally, we propose that a surface sugar transporter, such as Nfs can be converted into a gliding machinery through its further recruitment to FACs by the connection to the bacterial cytoskeleton. This cytosolic connection is probably essential to concentrate force production at specific sites, a possible requirement for motility. This cytosolic connection could also provide a way to coordinate gliding motor activities which is essential for a robust motility. Indeed, when

the connection between the Agl-Glt machinery and the cytoskeleton is broken, we still observe motility, but in a highly inefficient way (Hot *et al.*, in preparation).
The presence of other proteins such as GltK, a predicted lipoprotein anchored into the outer membrane, with no homologue in the sporulation machinery also hints to other constraints. One of the major differences of cell envelope between a vegetative cell and a spore is the presence of the PG layer in vegetative cells only (Bui et al., 2009). Thus, GltK could enable interactions between the Glt machinery and the PG. However, until now, we have no evidence for a such role of GltK.

We also envision that we have not yet identified all the gliding components (and sporulation component too). Indeed, Nan *et al.* have identified other gliding proteins such as CglB (Nan et al., 2010), which is an outer membrane lipoprotein that may constitute a surface-exposed component of the motility complex. Identification of other gliding or sporulation components could bring more light on the mechanism that specializes Agl-Glt and Agl-Nfs machineries for gliding and sporulation respectively.
The remarkable adaptation of a surface sugar transporter (the Agl-Nfs machinery) to a motility machinery (the Agl-Glt machinery) as documented here may explain why gliding machineries are not conserved in bacteria: each gliding machinery might have evolved independently from a specific sugar transport machinery. Thus, a similar evolutive scenario might have occurred for the gliding machinery of *F. johnsoniae* (Section 3.1. and Figure 25, Introduction). Indeed, gliding motility in *F. johnsoniae* and *M. xanthus* shows intriguing similarities: (i), in both types of bacteria, micron-sized beads are propelled along the cell surface in a gliding machinery dependant manner. This suggests that in both cases, the motor propels a gliding complex along a helical closed looped (Section 3.1. and Figure 25, Introduction; Section 1.2. and Figure 32a, Discussion); (ii), in both species, it was shown that gliding proteins are able to link a sugar polymer. Indeed, it was shown that the adhesin RemA, essential for the gliding motility of *F. johnsoniae*, recognizes a surface polysaccharide synthesized and secreted among other by RemC, Wza and Wzc proteins, which are homologues of certain components of Exo machinery (see Article III, Results). As for the gliding motility and the slime in *M. xanthus*, it was shown that RemA is able to transport this polysaccharide along the cell (Shrivastava et al., 2012). These similarities between *M. xanthus* and *F. johnsoniae* gliding suggest that gliding motility in *F. johnsoniae* also evolved from an ancient sugar transport machinery.

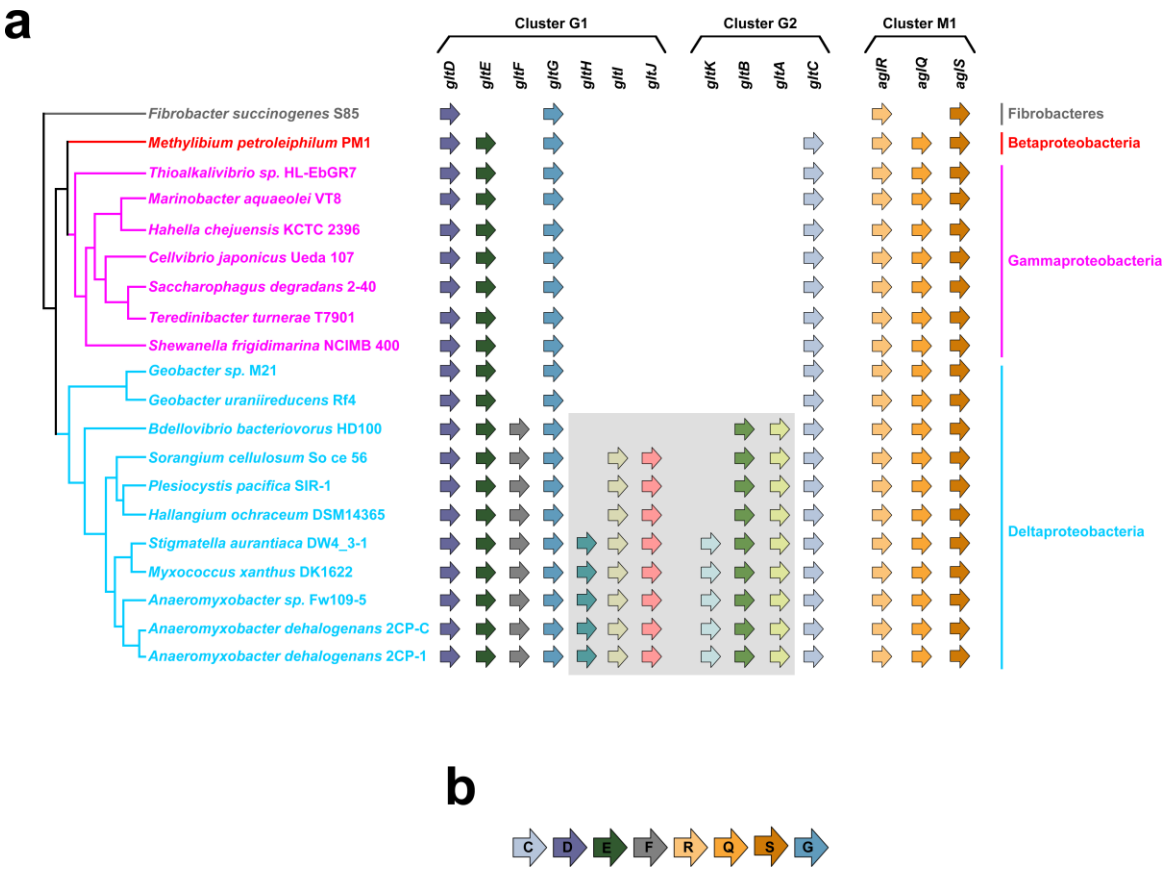

Figure 34. a. Taxonomic distribution of the closest homologues of the 14 genes composing the G1, G2, and M1 clusters. The relationships between the species carrying the different homologues of the genes are indicated by the phylogeny on the left. Based on their taxonomic distribution, the 14 genes can be divided into Group A (grey background) and Group B (white background). b. Genetic organization of the core complex (Adapted from Luciano et al., 2011).

3. The Agl-Glt/Nfs Machineries Evolved from a Core Complex with Broad Distribution in Bacteria

The phylogenomic study of the Agl-Glt/Nfs-like machineries suggests that they evolved from a more ancient core machinery. The AglRQS motor itself must be ancient, as it is a member of a ubiquitous bacterial motor family containing the flagellar stator MotAB, (Jarrell and McBride, 2008), TolQR from the Tol-Pal system which is required for outer membrane integrity and cell division (Gerding et al., 2007; Yeh et al., 2010; Zhang et al., 2009) and ExbBD that interacts with TonB to energize the transport of molecules across the outer membrane (Noinaj et al., 2010).

On the contrary, *glt* paralogues show a narrower distribution and are found in Beta-proteobacteria, Delta-proteobacteria, Gamma-proteobacteria and some representatives of Fibrobacteres (Figure 34a). As shown in article III, *agl-glt/nfs* genes can adopt many arrangements in bacterial genomes (Figure 35), suggesting that these machineries may cover many transport functions. However, one arrangement is overrepresented in these phyla and is composed by homologues of GltC, GltD, GltE, GltF and GltG. Because the *agl* genes co-occur systematically with these genes and are even clustered in a single genomic region in several bacteria (Figure 34b), we propose that *aglR*, *aglQ*, *aglS*, *gltC*, *gltD*, *gltE*, *gltF* and *gltG* genes encode a single functional unit, that could be the ancestral machinery (also called core machinery) of Agl-Glt/Nfs machineries (Luciano et al., 2011). Since Agl-Glt/Nfs are both sugar polymer transport machineries (slime and spore coat, respectively), we hypothesize that the ancestral machinery, consisting of an Agl-like molecular motor and a simplified Glt/Nfs-like complex, could constitutes a basal transport machinery. This ancestral machinery could form a sugar polymer transport system by itself, but it could also have been specialized in sugar polymer transport machinery later by the addition of other components *i.e.* GltA, GltB, and GltH homologues.

Thus, the core machinery may constitute a basal transport machinery that became specialized multiple times by the independent acquisition of new components. Theoretically, these systems may transport sugars but they could also transport other molecules, such as proteins and/or lipids. Moreover, these machineries could even transport molecules in the cytoplasm, or in the periplasm, and not only at the cell surface. For example, the AglZ protein is linked to the cytosolic face of the Agl-Glt complex and it is transported along with the rest of the machinery. Thus, theoretically, in a situation where an AglZ-like protein would be a major output of the system, then the function of the system would be to move a cytosolic protein inside the cell (for example, the transport of a DNA binding protein could be important for nucleoid organization).

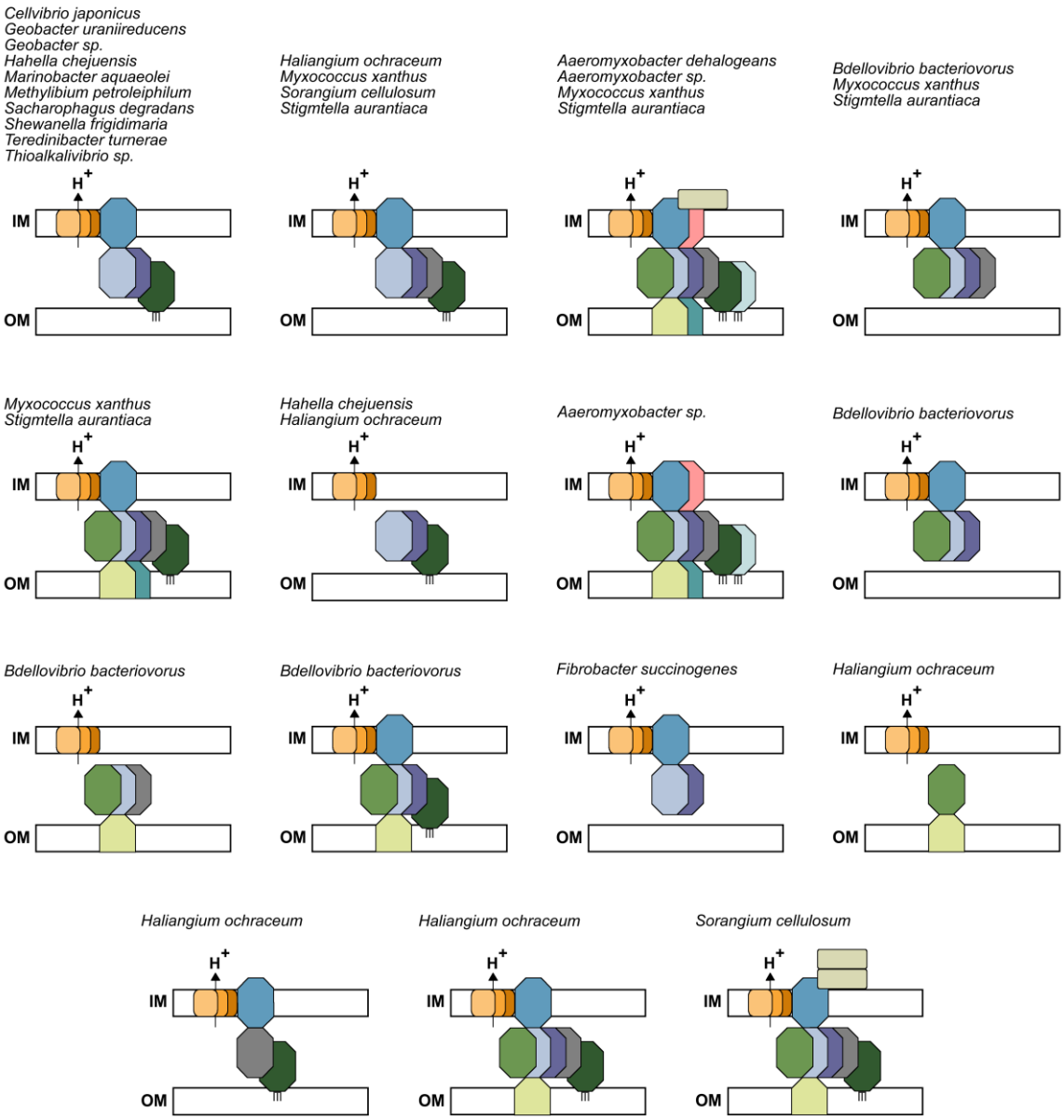

Figure 35. Modular architecture of Agl-Glt/Nfs machineries in bacteria.

To understand the potential role of the core machinery, we have started a reductive genetic approach on the Agl-Glt machinery to recreate an ancestral machinery by systematically deleting of all the non-core genes in the Glt machinery and test if the machinery still displays transport activity and if this transport is still directional. We also attempted to express the core machinery genes in heterologous hosts such as *E. coli* and test if the core proteins are sufficient to have a transport activity. Finally, starting from the core machinery, we could also recreate different arrangements of the machinery such those present in other bacteria (Figure 35), and test for their function. We hope that these experiments will give indications as for the function of the core machinery, and how this core machinery evolved potential other transport functions through the addition of new components. This study, by uncovering the role of each protein of the machinery, may also help us understanding the mechanism of gliding motility or sporulation.

4. An Unsuspected Wide Class of Bacterial Molecular Motor proteins?

The AglRQS motor constitutes an emerging subclass of TolQR, MotAB and ExbBD-like motors. For all the members of this family, it has been shown that the binding of protons to a conserved aspartate residue in the lumen of the channel is essential for the motor activity. It has been suggested that the binding of protons to this aspartate triggers the power stroke by generating a conformational change of motor associated proteins: TolA for TolQR, TonB for ExbBD, and FliG for MotAB. In our system, we suppose that the motor-associated transducer protein is GltG for the gliding and NfsG for the sporulation. This hypothesis is based on different observations: (i), with the AglRQS motor, GltG/NfsG protein is the only protein of the core machinery that is localized in the inner membrane, and the transducer protein is thought to be present in the core machinery; (ii), GltG/NfsG is showed to interact directly with the AglRQS motor which is also a requirement for a transducer protein. However, how the chemical energy is translated into mechanical energy is still unclear for all these motors, even for the flagellar rotor.

In the laboratory, we have systematically analyzed genomes for the presence of AglRQS-like complexes. We have found that this system is associated with many predicted envelope proteins across several bacterial lineages. In most cases, these proteins have no predicted function but this finding suggests that many envelope complexes use AglRQS-type motors (Agrebi *et al.*, in preparation).

Importantly, directional transport may not be a basic property of the motor because TolQR, MotAB, and ExbBD are not known to drive directional transport. In the MotAB system, MotB is

physically linked to the PG layer *via* a PG-binding motif (that TolQ, ExbD and AglQS, homologues of MotB, do not possess) (Yonekura et al., 2011). Thus, MotB holds the motor in place and the passage of protons through the channel causes a conformational change in MotA, which pushes FliG and spins the rotor (Morimoto et al., 2013). The mechanism underlying TolQR and ExbBD motor functions is less understood but appears to involve transient contacts with outer membrane proteins. Thus, it is more likely that AglRQS-type systems were converted into directional transport systems due to their linkage with Glt/Nfs parts. In conclusion, Tol/Exb/Mot/Agl-type molecular motors are ubiquitous and may govern a large array of functions. In the future, it will be interesting to study novel systems predicted with the bioinformatics to determine how diverse these functions are.

5. General Conclusions

Over the last decade, our view of the bacterial cell changed from a "chaotic soup" to exquisitely organized. In particular, the discovery of the bacterial cytoskeleton raised the question of the existence of processive motors akin to myosin, dynein and kinesin. However, despite an extensive search, such eukaryotic-like motors have never been found in bacteria. The absence of such devices could be explained by basic features of the bacterial cell: its size and the properties of the cytoplasm. Indeed, as discussed in the introduction (Section 1.1., Introduction), "super-diffusive" motors may be needed in the larger eukaryotic cell to direct large objects to specific locations but because bacteria are smaller organisms, these motors would not be useful.

In fact, this study reveals a new class of motors that apparently direct processes in the bacterial cell envelope. These motors mediate their tasks by moving directionally between subcellular regions and mediate functions as broad as motility and polysaccharide capsule synthesis. Because these types of motor appear mostly associated with proteins of unknown functions and are scarcely represented in standard bacterial laboratory models (although broadly distributed), we suggest that the function of this family in bacterial cell organization machines has been overlooked. A multitude of cargos may be transported: proteins and sugars, but potentially lipids, and even RNA and DNA. Testing this possibility will be a thrilling task for the future.

REFERENCES

Alberts, B., Johnson, A., Lewis, J., Raff, M., Roberts, K., and Walter, P. (2002). Molecular Biology of the Cell.

Ames, P., and Parkinson, J.S. (2006). Conformational suppression of inter-receptor signaling defects. Proc. Natl. Acad. Sci. U. S. A. *103*, 9292–9297.

Baluska, F., Volkmann, D., and Barlow, P.W. (2004). Eukaryotic cells and their cell bodies: Cell Theory revised. Ann. Bot. *94*, 9–32.

Barry, R.M., and Gitai, Z. (2011). Self-assembling enzymes and the origins of the cytoskeleton. Curr. Opin. Microbiol. *14*, 704–711.

Beebe, J.M. (1941). The Morphology and Cytology of Myxococcus xanthus, N. Sp. J. Bacteriol. *42*, 193–223.

Bernard, R., Marquis, K.A., and Rudner, D.Z. (2010). Nucleoid occlusion prevents cell division during replication fork arrest in Bacillus subtilis. Mol. Microbiol. *78*, 866–882.

Bernhardt, T.G., and de Boer, P.A.J. (2005). SlmA, a nucleoid-associated, FtsZ binding protein required for blocking septal ring assembly over Chromosomes in E. coli. Mol. Cell *18*, 555–564.

Braun, T.F., and McBride, M.J. (2005). Flavobacterium johnsoniae GldJ Is a Lipoprotein That Is Required for Gliding Motility. J. Bacteriol. *187*, 2628–2637.

Braun, T.F., Khubbar, M.K., Saffarini, D.A., and McBride, M.J. (2005). Flavobacterium johnsoniae gliding motility genes identified by mariner mutagenesis. J. Bacteriol. *187*, 6943–6952.

Brownhill, K., Wood, L., and Allan, V. (2009). Molecular motors and the Golgi complex: staying put and moving through. Semin. Cell Dev. Biol. *20*, 784–792.

Bui, N.K., Gray, J., Schwarz, H., Schumann, P., Blanot, D., and Vollmer, W. (2009). The peptidoglycan sacculus of Myxococcus xanthus has unusual structural features and is degraded during glycerol-induced myxospore development. J. Bacteriol. *191*, 494–505.

Burchard, R.P. (1981). Gliding motility of prokaryotes: ultrastructure, physiology, and genetics. Annu. Rev. Microbiol. *35*, 497–529.

Burton, B.M., Marquis, K.A., Sullivan, N.L., Rapoport, T.A., and Rudner, D.Z. (2007). The ATPase SpoIIIE transports DNA across fused septal membranes during sporulation in Bacillus subtilis. Cell *131*, 1301–1312.

Buss, F., Spudich, G., and Kendrick-Jones, J. (2004). MYOSIN VI: Cellular Functions and Motor Properties. Annu. Rev. Cell Dev. Biol. *20*, 649–676.

Cabeen, M.T., and Jacobs-Wagner, C. (2010). The bacterial cytoskeleton. Annu. Rev. Genet. *44*, 365–392.

Cabeen, M.T., Charbon, G., Vollmer, W., Born, P., Ausmees, N., Weibel, D.B., and Jacobs-Wagner, C. (2009). Bacterial cell curvature through mechanical control of cell growth. EMBO J. *28*, 1208–1219.

Cascales, E., Gavioli, M., Sturgis, J.N., and Lloubès, R. (2000). Proton motive force drives the interaction of the inner membrane TolA and outer membrane pal proteins in Escherichia coli. Mol. Microbiol. *38*, 904–915.

Charbon, G., Cabeen, M.T., and Jacobs-Wagner, C. (2009). Bacterial intermediate filaments: in vivo assembly, organization, and dynamics of crescentin. Genes Dev. *23*, 1131–1144.

Conde, C., and Cáceres, A. (2009). Microtubule assembly, organization and dynamics in axons and dendrites. Nat. Rev. Neurosci. *10*, 319–332.

Cowles, K.N., and Gitai, Z. (2010). Surface association and the MreB cytoskeleton regulate pilus production, localization and function in Pseudomonas aeruginosa. Mol. Microbiol. *76*, 1411–1426.

Divakaruni, A.V., Baida, C., White, C.L., and Gober, J.W. (2007). The cell shape proteins MreB and MreC control cell morphogenesis by positioning cell wall synthetic complexes. Mol. Microbiol. *66*, 174–188.

Doan, T., Marquis, K.A., and Rudner, D.Z. (2005). Subcellular localization of a sporulation membrane protein is achieved through a network of interactions along and across the septum. Mol. Microbiol. *55*, 1767–1781.

Doi, M., Wachi, M., Ishino, F., Tomioka, S., Ito, M., Sakagami, Y., Suzuki, A., and Matsuhashi, M. (1988). Determinations of the DNA sequence of the mreB gene and of the gene products of the mre region that function in formation of the rod shape of Escherichia coli cells. J. Bacteriol. *170*, 4619–4624.

Domínguez-Escobar, J., Chastanet, A., Crevenna, A.H., Fromion, V., Wedlich-Söldner, R., and Carballido-López, R. (2011). Processive movement of MreB-associated cell wall biosynthetic complexes in bacteria. Science *333*, 225–228.

Ducret, A., Valignat, M.-P., Mouhamar, F., Mignot, T., and Theodoly, O. (2012). Wet-surface-enhanced ellipsometric contrast microscopy identifies slime as a major adhesion factor during bacterial surface motility. Proc. Natl. Acad. Sci. U. S. A. *109*, 10036–10041.

DWORKIN, M., and GIBSON, S.M. (1964). A SYSTEM FOR STUDYING MICROBIAL MORPHOGENESIS: RAPID FORMATION OF MICROCYSTS IN MYXOCOCCUS XANTHUS. Science *146*, 243–244.

Dye, N.A., Pincus, Z., Theriot, J.A., Shapiro, L., and Gitai, Z. (2005). Two independent spiral structures control cell shape in Caulobacter. Proc. Natl. Acad. Sci. U. S. A. *102*, 18608–18613.

Dzink-Fox, J.L., Leadbetter, E.R., and Godchaux, W., 3rd (1997). Acetate acts as a protonophore and differentially affects bead movement and cell migration of the gliding bacterium Cytophaga johnsonae (Flavobacterium johnsoniae). Microbiol. Read. Engl. *143 (Pt 12)*, 3693–3701.

Ebersbach, G., Briegel, A., Jensen, G.J., and Jacobs-Wagner, C. (2008). A self-associating protein critical for chromosome attachment, division, and polar organization in caulobacter. Cell *134*, 956–968.

Egan, A.J.F., and Vollmer, W. (2013). The physiology of bacterial cell division. Ann. N. Y. Acad. Sci. *1277*, 8–28.

Elf, J., Li, G.-W., and Xie, X.S. (2007). Probing transcription factor dynamics at the single-molecule level in a living cell. Science *316*, 1191–1194.

Van den Ent, F., Amos, L.A., and Löwe, J. (2001). Prokaryotic origin of the actin cytoskeleton. Nature *413*, 39–44.

Erhardt, M., Namba, K., and Hughes, K.T. (2010). Bacterial nanomachines: the flagellum and type III injectisome. Cold Spring Harb. Perspect. Biol. *2*, a000299.

Errington, J. (2003). Regulation of endospore formation in Bacillus subtilis. Nat. Rev. Microbiol. *1*, 117–126.

Espeli, O., Mercier, R., and Boccard, F. (2008). DNA dynamics vary according to macrodomain topography in the E. coli chromosome. Mol. Microbiol. *68*, 1418–1427.

Eswaramoorthy, P., Erb, M.L., Gregory, J.A., Silverman, J., Pogliano, K., Pogliano, J., and Ramamurthi, K.S. (2011). Cellular architecture mediates DivIVA ultrastructure and regulates min activity in Bacillus subtilis. MBio *2*.

Fisher, J.K., Bourniquel, A., Witz, G., Weiner, B., Prentiss, M., and Kleckner, N. (2013). Four-dimensional imaging of E. coli nucleoid organization and dynamics in living cells. Cell *153*, 882–895.

Gagliano, J., Walb, M., Blaker, B., Macosko, J.C., and Holzwarth, G. (2010). Kinesin velocity increases with the number of motors pulling against viscoelastic drag. Eur. Biophys. J. EBJ *39*, 801–813.

Garner, E.C., Bernard, R., Wang, W., Zhuang, X., Rudner, D.Z., and Mitchison, T. (2011). Coupled, circumferential motions of the cell wall synthesis machinery and MreB filaments in B. subtilis. Science *333*, 222–225.

Gennerich, A., and Vale, R.D. (2009). Walking the walk: how kinesin and dynein coordinate their steps. Curr. Opin. Cell Biol. *21*, 59–67.

Gerding, M.A., Ogata, Y., Pecora, N.D., Niki, H., and de Boer, P.A.J. (2007). The trans-envelope Tol-Pal complex is part of the cell division machinery and required for proper outer-membrane invagination during cell constriction in E. coli. Mol. Microbiol. *63*, 1008–1025.

Gitai, Z., Dye, N., and Shapiro, L. (2004). An actin-like gene can determine cell polarity in bacteria. Proc. Natl. Acad. Sci. U. S. A. *101*, 8643–8648.

Goley, E.D., and Welch, M.D. (2006). The ARP2/3 complex: an actin nucleator comes of age. Nat. Rev. Mol. Cell Biol. *7*, 713–726.

Govindarajan, S., Nevo-Dinur, K., and Amster-Choder, O. (2012). Compartmentalization And Spatio-Temporal Organization Of Macromolecules In Bacteria. FEMS Microbiol. Rev.

Gupta, V., Palmer, K.J., Spence, P., Hudson, A., and Stephens, D.J. (2008). Kinesin-1 (uKHC/KIF5B) is required for bidirectional motility of ER exit sites and efficient ER-to-Golgi transport. Traffic Cph. Den. *9*, 1850–1866.

Hammer, J.A., 3rd, and Sellers, J.R. (2012). Walking to work: roles for class V myosins as cargo transporters. Nat. Rev. Mol. Cell Biol. *13*, 13–26.

Higgins, D., and Dworkin, J. (2012). Recent progress in Bacillus subtilis sporulation. FEMS Microbiol. Rev. *36*, 131–148.

Hodgkin, J., and Kaiser, D. (1977). Cell-to-cell stimulation of movement in nonmotile mutants of Myxococcus. Proc. Natl. Acad. Sci. U. S. A. *74*, 2938–2942.

Hodgkin, J., and Kaiser, D. (1979). Genetics of gliding motility in Myxococcus xanthus (Myxobacterales): Genes controlling movement of single cells. Mol. Gen. Genet. MGG *171*, 167–176.

Huitema, E., Pritchard, S., Matteson, D., Radhakrishnan, S.K., and Viollier, P.H. (2006). Bacterial birth scar proteins mark future flagellum assembly site. Cell *124*, 1025–1037.

Hunt, S.D., and Stephens, D.J. (2011). The role of motor proteins in endosomal sorting. Biochem. Soc. Trans. *39*, 1179–1184.

Ingerson-Mahar, M., and Gitai, Z. (2012). A growing family: the expanding universe of the bacterial cytoskeleton. FEMS Microbiol. Rev. *36*, 256–266.

Ingerson-Mahar, M., Briegel, A., Werner, J.N., Jensen, G.J., and Gitai, Z. (2010). The metabolic enzyme CTP synthase forms cytoskeletal filaments. Nat. Cell Biol. *12*, 739–746.

Jansen, R.-P., and Niessing, D. (2012). Assembly of mRNA-protein complexes for directional mRNA transport in eukaryotes--an overview. Curr. Protein Pept. Sci. *13*, 284–293.

Jarrell, K.F., and McBride, M.J. (2008). The surprisingly diverse ways that prokaryotes move. Nat. Rev. Microbiol. *6*, 466–476.

Jones, L.J., Carballido-López, R., and Errington, J. (2001). Control of cell shape in bacteria: helical, actin-like filaments in Bacillus subtilis. Cell *104*, 913–922.

Katahira, J. (2012). mRNA export and the TREX complex. Biochim. Biophys. Acta *1819*, 507–513.

Khvorova, A., Chary, V.K., Hilbert, D.W., and Piggot, P.J. (2000). The chromosomal location of the Bacillus subtilis sporulation gene spoIIR is important for its function. J. Bacteriol. *182*, 4425–4429.

Kikkawa, M. (2013). Big steps toward understanding dynein. J. Cell Biol. *202*, 15–23.

Kim, S.Y., Gitai, Z., Kinkhabwala, A., Shapiro, L., and Moerner, W.E. (2006). Single molecules of the bacterial actin MreB undergo directed treadmilling motion in Caulobacter crescentus. Proc. Natl. Acad. Sci. U. S. A. *103*, 10929–10934.

Klumpp, S., MüLler, M.J.I., and Lipowsky, R. (2006). COOPERATIVE TRANSPORT BY SMALL TEAMS OF MOLECULAR MOTORS. Biophys. Rev. Lett. *01*, 353–361.

Köhler, A., and Hurt, E. (2007). Exporting RNA from the nucleus to the cytoplasm. Nat. Rev. Mol. Cell Biol. *8*, 761–773.

Komeili, A. (2012). Molecular mechanisms of compartmentalization and biomineralization in magnetotactic bacteria. FEMS Microbiol. Rev. *36*, 232–255.

Kottel, R.H., Bacon, K., Clutter, D., and White, D. (1975). Coats from Myxococcus xanthus: characterization and synthesis during myxospore differentiation. J. Bacteriol. *124*, 550–557.

Kroos, L. (2007). The Bacillus and Myxococcus developmental networks and their transcriptional regulators. Annu. Rev. Genet. *41*, 13–39.

Kruse, T., Møller-Jensen, J., Løbner-Olesen, A., and Gerdes, K. (2003). Dysfunctional MreB inhibits chromosome segregation in Escherichia coli. EMBO J. *22*, 5283–5292.

Kühn, J., Briegel, A., Mörschel, E., Kahnt, J., Leser, K., Wick, S., Jensen, G.J., and Thanbichler, M. (2010). Bactofilins, a ubiquitous class of cytoskeletal proteins mediating polar localization of a cell wall synthase in Caulobacter crescentus. EMBO J. *29*, 327–339.

Kull, F.J., and Endow, S.A. (2013). Force generation by kinesin and myosin cytoskeletal motor proteins. J. Cell Sci. *126*, 9–19.

Kuru, E., Hughes, H.V., Brown, P.J., Hall, E., Tekkam, S., Cava, F., de Pedro, M.A., Brun, Y.V., and VanNieuwenhze, M.S. (2012). In Situ Probing of Newly Synthesized Peptidoglycan in Live Bacteria with Fluorescent D-Amino Acids. Angew. Chem. Int. Ed. *51*, 12519–12523.

De La Cruz, E.M., Wells, A.L., Rosenfeld, S.S., Ostap, E.M., and Sweeney, H.L. (1999). The kinetic mechanism of myosin V. Proc. Natl. Acad. Sci. U. S. A. *96*, 13726–13731.

Lam, H., Schofield, W.B., and Jacobs-Wagner, C. (2006). A landmark protein essential for establishing and perpetuating the polarity of a bacterial cell. Cell *124*, 1011–1023.

Lécuyer, E., Yoshida, H., Parthasarathy, N., Alm, C., Babak, T., Cerovina, T., Hughes, T.R., Tomancak, P., and Krause, H.M. (2007). Global analysis of mRNA localization reveals a prominent role in organizing cellular architecture and function. Cell *131*, 174–187.

Lenarcic, R., Halbedel, S., Visser, L., Shaw, M., Wu, L.J., Errington, J., Marenduzzo, D., and Hamoen, L.W. (2009). Localisation of DivIVA by targeting to negatively curved membranes. EMBO J. *28*, 2272–2282.

Levin, P.A., Margolis, P.S., Setlow, P., Losick, R., and Sun, D. (1992). Identification of Bacillus subtilis genes for septum placement and shape determination. J. Bacteriol. *174*, 6717–6728.

Li, Y., Sun, H., Ma, X., Lu, A., Lux, R., Zusman, D., and Shi, W. (2003). Extracellular polysaccharides mediate pilus retraction during social motility of Myxococcus xanthus. Proc. Natl. Acad. Sci. U. S. A. *100*, 5443–5448.

López, D., and Kolter, R. (2010). Functional microdomains in bacterial membranes. Genes Dev. *24*, 1893–1902.

Loubéry, S., Wilhelm, C., Hurbain, I., Neveu, S., Louvard, D., and Coudrier, E. (2008). Different Microtubule Motors Move Early and Late Endocytic Compartments. Traffic *9*, 492–509.

Luciano, J., Agrebi, R., Le Gall, A.V., Wartel, M., Fiegna, F., Ducret, A., Brochier-Armanet, C., and Mignot, T. (2011). Emergence and modular evolution of a novel motility machinery in bacteria. PLoS Genet. *7*, e1002268.

Margolin, W. (2005). FtsZ and the division of prokaryotic cells and organelles. Nat. Rev. Mol. Cell Biol. *6*, 862–871.

Mattick, J.S. (2002). Type IV pili and twitching motility. Annu. Rev. Microbiol. *56*, 289–314.

Mauriello, E.M.F., Mouhamar, F., Nan, B., Ducret, A., Dai, D., Zusman, D.R., and Mignot, T. (2010). Bacterial motility complexes require the actin-like protein, MreB and the Ras homologue, MglA. EMBO J. *29*, 315–326.

McBride, M.J. (2001). Bacterial gliding motility: multiple mechanisms for cell movement over surfaces. Annu. Rev. Microbiol. *55*, 49–75.

McBride, M.J., and Zhu, Y. (2013). Gliding motility and Por secretion system genes are widespread among members of the phylum bacteroidetes. J. Bacteriol. *195*, 270–278.

Ménétrey, J., Bahloul, A., Wells, A.L., Yengo, C.M., Morris, C.A., Sweeney, H.L., and Houdusse, A. (2005). The structure of the myosin VI motor reveals the mechanism of directionality reversal. Nature *435*, 779–785.

Mercier, R., Petit, M.-A., Schbath, S., Robin, S., El Karoui, M., Boccard, F., and Espéli, O. (2008). The MatP/matS site-specific system organizes the terminus region of the E. coli chromosome into a macrodomain. Cell *135*, 475–485.

Mierzejewska, J., and Jagura-Burdzy, G. (2012). Prokaryotic ParA-ParB-parS system links bacterial chromosome segregation with the cell cycle. Plasmid *67*, 1–14.

Mignot, T. (2007). The elusive engine in Myxococcus xanthus gliding motility. Cell. Mol. Life Sci. CMLS *64*, 2733–2745.

Mignot, T., and Shaevitz, J.W. (2008). Active and passive mechanisms of intracellular transport and localization in bacteria. Curr. Opin. Microbiol. *11*, 580–585.

Mignot, T., Shaevitz, J.W., Hartzell, P.L., and Zusman, D.R. (2007). Evidence that focal adhesion complexes power bacterial gliding motility. Science *315*, 853–856.

Mika, J.T., and Poolman, B. (2011). Macromolecule diffusion and confinement in prokaryotic cells. Curr. Opin. Biotechnol. *22*, 117–126.

Mileykovskaya, E., and Dowhan, W. (2009). Cardiolipin membrane domains in prokaryotes and eukaryotes. Biochim. Biophys. Acta *1788*, 2084–2091.

Misteli, T. (2001). Protein dynamics: implications for nuclear architecture and gene expression. Science *291*, 843–847.

Miyata, M. (2010). Unique centipede mechanism of Mycoplasma gliding. Annu. Rev. Microbiol. *64*, 519–537.

Montero Llopis, P., Jackson, A.F., Sliusarenko, O., Surovtsev, I., Heinritz, J., Emonet, T., and Jacobs-Wagner, C. (2010). Spatial organization of the flow of genetic information in bacteria. Nature *466*, 77–81.

Morimoto, Y.V., Nakamura, S., Hiraoka, K.D., Namba, K., and Minamino, T. (2013). Distinct roles of highly conserved charged residues at the MotA-FliG interface in bacterial flagellar motor rotation. J. Bacteriol. *195*, 474–481.

Müller, F.D., Schink, C.W., Hoiczyk, E., Cserti, E., and Higgs, P.I. (2012). Spore formation in Myxococcus xanthus is tied to cytoskeleton functions and polysaccharide spore coat deposition. Mol. Microbiol. *83*, 486–505.

Müller, F.-D., Treuner-Lange, A., Heider, J., Huntley, S.M., and Higgs, P.I. (2010). Global transcriptome analysis of spore formation in Myxococcus xanthus reveals a locus necessary for cell differentiation. BMC Genomics *11*, 264.

Muretta, J.M., Petersen, K.J., and Thomas, D.D. (2013). Direct real-time detection of the actin-activated power stroke within the myosin catalytic domain. Proc. Natl. Acad. Sci. U. S. A. *110*, 7211–7216.

Nakane, D., Sato, K., Wada, H., McBride, M.J., and Nakayama, K. (2013). Helical flow of surface protein required for bacterial gliding motility. Proc. Natl. Acad. Sci. U. S. A. *110*, 11145–11150.

Nan, B., and Zusman, D.R. (2011). Uncovering the mystery of gliding motility in the myxobacteria. Annu. Rev. Genet. *45*, 21–39.

Nan, B., Mauriello, E.M.F., Sun, I.-H., Wong, A., and Zusman, D.R. (2010). A multi-protein complex from Myxococcus xanthus required for bacterial gliding motility. Mol. Microbiol. *76*, 1539–1554.

Nan, B., Chen, J., Neu, J.C., Berry, R.M., Oster, G., and Zusman, D.R. (2011). Myxobacteria gliding motility requires cytoskeleton rotation powered by proton motive force. Proc. Natl. Acad. Sci. U. S. A. *108*, 2498–2503.

Nan, B., Bandaria, J.N., Moghtaderi, A., Sun, I.-H., Yildiz, A., and Zusman, D.R. (2013). Flagella stator homologs function as motors for myxobacterial gliding motility by moving in helical trajectories. Proc. Natl. Acad. Sci. U. S. A. *110*, E1508–1513.

Nelson, S.S., Bollampalli, S., and McBride, M.J. (2008). SprB is a cell surface component of the Flavobacterium johnsoniae gliding motility machinery. J. Bacteriol. *190*, 2851–2857.

Nevo-Dinur, K., Nussbaum-Shochat, A., Ben-Yehuda, S., and Amster-Choder, O. (2011). Translation-independent localization of mRNA in E. coli. Science *331*, 1081–1084.

Nevo-Dinur, K., Govindarajan, S., and Amster-Choder, O. (2012). Subcellular localization of RNA and proteins in prokaryotes. Trends Genet. TIG *28*, 314–322.

Nogales, E., and Wang, H.-W. (2006). Structural mechanisms underlying nucleotide-dependent self-assembly of tubulin and its relatives. Curr. Opin. Struct. Biol. *16*, 221–229.

Noinaj, N., Guillier, M., Barnard, T.J., and Buchanan, S.K. (2010). TonB-dependent transporters: regulation, structure, and function. Annu. Rev. Microbiol. *64*, 43–60.

Odronitz, F., and Kollmar, M. (2007). Drawing the tree of eukaryotic life based on the analysis of 2,269 manually annotated myosins from 328 species. Genome Biol. *8*, R196.

Park, H., Li, A., Chen, L.-Q., Houdusse, A., Selvin, P.R., and Sweeney, H.L. (2007). The unique insert at the end of the myosin VI motor is the sole determinant of directionality. Proc. Natl. Acad. Sci. U. S. A. *104*, 778–783.

Phair, R.D., and Misteli, T. (2000). High mobility of proteins in the mammalian cell nucleus. Nature *404*, 604–609.

Pierobon, P., Achouri, S., Courty, S., Dunn, A.R., Spudich, J.A., Dahan, M., and Cappello, G. (2009). Velocity, processivity, and individual steps of single myosin V molecules in live cells. Biophys. J. *96*, 4268–4275.

Pollard, T.D., and Borisy, G.G. (2003). Cellular motility driven by assembly and disassembly of actin filaments. Cell *112*, 453–465.

Potma, E.O., de Boeij, W.P., Bosgraaf, L., Roelofs, J., van Haastert, P.J., and Wiersma, D.A. (2001). Reduced protein diffusion rate by cytoskeleton in vegetative and polarized dictyostelium cells. Biophys. J. *81*, 2010–2019.

Ptacin, J.L., Nollmann, M., Becker, E.C., Cozzarelli, N.R., Pogliano, K., and Bustamante, C. (2008). Sequence-directed DNA export guides chromosome translocation during sporulation in Bacillus subtilis. Nat. Struct. Mol. Biol. *15*, 485–493.

Ramamurthi, K.S., and Losick, R. (2009). Negative membrane curvature as a cue for subcellular localization of a bacterial protein. Proc. Natl. Acad. Sci. U. S. A. *106*, 13541–13545.

Ramamurthi, K.S., Lecuyer, S., Stone, H.A., and Losick, R. (2009). Geometric cue for protein localization in a bacterium. Science *323*, 1354–1357.

Rhodes, R.G., Nelson, S.S., Pochiraju, S., and McBride, M.J. (2011). Flavobacterium johnsoniae sprB is part of an operon spanning the additional gliding motility genes sprC, sprD, and sprF. J. Bacteriol. *193*, 599–610.

Rief, M., Rock, R.S., Mehta, A.D., Mooseker, M.S., Cheney, R.E., and Spudich, J.A. (2000). Myosin-V stepping kinetics: a molecular model for processivity. Proc. Natl. Acad. Sci. U. S. A. *97*, 9482–9486.

Roberts, M.A.J., Wadhams, G.H., Hadfield, K.A., Tickner, S., and Armitage, J.P. (2012). ParA-like protein uses nonspecific chromosomal DNA binding to partition protein complexes. Proc. Natl. Acad. Sci. U. S. A. *109*, 6698–6703.

Rodrigues, C.D.A., and Harry, E.J. (2012). The Min system and nucleoid occlusion are not required for identifying the division site in Bacillus subtilis but ensure its efficient utilization. PLoS Genet. *8*, e1002561.

Romantsov, T., Battle, A.R., Hendel, J.L., Martinac, B., and Wood, J.M. (2010). Protein localization in Escherichia coli cells: comparison of the cytoplasmic membrane proteins ProP, LacY, ProW, AqpZ, MscS, and MscL. J. Bacteriol. *192*, 912–924.

Rudner, D.Z., and Losick, R. (2010). Protein subcellular localization in bacteria. Cold Spring Harb. Perspect. Biol. *2*, a000307.

Rudner, D.Z., Pan, Q., and Losick, R.M. (2002). Evidence that subcellular localization of a bacterial membrane protein is achieved by diffusion and capture. Proc. Natl. Acad. Sci. U. S. A. *99*, 8701–8706.

Sakamoto, T., Wang, F., Schmitz, S., Xu, Y., Xu, Q., Molloy, J.E., Veigel, C., and Sellers, J.R. (2003). Neck length and processivity of myosin V. J. Biol. Chem. *278*, 29201–29207.

Scialdone, A., and Nicodemi, M. (2010). Diffusion-based DNA target colocalization by thermodynamic mechanisms. Dev. Camb. Engl. *137*, 3877–3885.

Shaevitz, J.W., and Gitai, Z. (2010). The structure and function of bacterial actin homologs. Cold Spring Harb. Perspect. Biol. *2*, a000364.

Shapiro, L., McAdams, H.H., and Losick, R. (2009). Why and how bacteria localize proteins. Science *326*, 1225–1228.

Sherratt, D.J., Arciszewska, L.K., Crozat, E., Graham, J.E., and Grainge, I. (2010). The Escherichia coli DNA translocase FtsK. Biochem. Soc. Trans. *38*, 395–398.

Shih, Y.-L., Kawagishi, I., and Rothfield, L. (2005). The MreB and Min cytoskeletal-like systems play independent roles in prokaryotic polar differentiation. Mol. Microbiol. *58*, 917–928.

Shrivastava, A., Rhodes, R.G., Pochiraju, S., Nakane, D., and McBride, M.J. (2012). Flavobacterium johnsoniae RemA is a mobile cell surface lectin involved in gliding. J. Bacteriol. *194*, 3678–3688.

Shrivastava, A., Johnston, J.J., van Baaren, J.M., and McBride, M.J. (2013). Flavobacterium johnsoniae GldK, GldL, GldM, and SprA are required for secretion of the cell surface gliding motility adhesins SprB and RemA. J. Bacteriol. *195*, 3201–3212.

Sibarita, J.-B. (2005). Deconvolution microscopy. Adv. Biochem. Eng. Biotechnol. *95*, 201–243.

Sladewski, T.E., Bookwalter, C.S., Hong, M.-S., and Trybus, K.M. (2013). Single-molecule reconstitution of mRNA transport by a class V myosin. Nat. Struct. Mol. Biol.

Sliusarenko, O., Zusman, D.R., and Oster, G. (2007). The motors powering A-motility in Myxococcus xanthus are distributed along the cell body. J. Bacteriol. *189*, 7920–7921.

Speese, S.D., Ashley, J., Jokhi, V., Nunnari, J., Barria, R., Li, Y., Ataman, B., Koon, A., Chang, Y.-T., Li, Q., et al. (2012). Nuclear envelope budding enables large ribonucleoprotein particle export during synaptic Wnt signaling. Cell *149*, 832–846.

Strahl, H., and Hamoen, L.W. (2012). Finding the corners in a cell. Curr. Opin. Microbiol. *15*, 731–736.

Sun, H., Yang, Z., and Shi, W. (1999). Effect of cellular filamentation on adventurous and social gliding motility of Myxococcus xanthus. Proc. Natl. Acad. Sci. U. S. A. *96*, 15178–15183.

Sun, M., Wartel, M., Cascales, E., Shaevitz, J.W., and Mignot, T. (2011). Motor-driven intracellular transport powers bacterial gliding motility. Proc. Natl. Acad. Sci. U. S. A. *108*, 7559–7564.

Sweeney, H.L., and Houdusse, A. (2010). Myosin VI rewrites the rules for myosin motors. Cell *141*, 573–582.

Van Teeffelen, S., Wang, S., Furchtgott, L., Huang, K.C., Wingreen, N.S., Shaevitz, J.W., and Gitai, Z. (2011). The bacterial actin MreB rotates, and rotation depends on cell-wall assembly. Proc. Natl. Acad. Sci. U. S. A. *108*, 15822–15827.

Thompson, S.R., Wadhams, G.H., and Armitage, J.P. (2006). The positioning of cytoplasmic protein clusters in bacteria. Proc. Natl. Acad. Sci. U. S. A. *103*, 8209–8214.

Tonthat, N.K., Arold, S.T., Pickering, B.F., Van Dyke, M.W., Liang, S., Lu, Y., Beuria, T.K., Margolin, W., and Schumacher, M.A. (2011). Molecular mechanism by which the nucleoid occlusion factor, SlmA, keeps cytokinesis in check. EMBO J. *30*, 154–164.

Tonthat, N.K., Milam, S.L., Chinnam, N., Whitfill, T., Margolin, W., and Schumacher, M.A. (2013). SlmA forms a higher-order structure on DNA that inhibits cytokinetic Z-ring formation over the nucleoid. Proc. Natl. Acad. Sci. U. S. A. *110*, 10586–10591.

Toro, E., and Shapiro, L. (2010). Bacterial chromosome organization and segregation. Cold Spring Harb. Perspect. Biol. *2*, a000349.

Tumbarello, D.A., Kendrick-Jones, J., and Buss, F. (2013). Myosin VI and its cargo adaptors - linking endocytosis and autophagy. J. Cell Sci. *126 Pt 12*, 2561–2570.

Typas, A., Banzhaf, M., Gross, C.A., and Vollmer, W. (2012). From the regulation of peptidoglycan synthesis to bacterial growth and morphology. Nat. Rev. Microbiol. *10*, 123–136.

Valens, M., Penaud, S., Rossignol, M., Cornet, F., and Boccard, F. (2004). Macrodomain organization of the Escherichia coli chromosome. EMBO J. *23*, 4330–4341.

Verkman, A.S. (2002). Solute and macromolecule diffusion in cellular aqueous compartments. Trends Biochem. Sci. *27*, 27–33.

Viollier, P.H., Thanbichler, M., McGrath, P.T., West, L., Meewan, M., McAdams, H.H., and Shapiro, L. (2004). Rapid and sequential movement of individual chromosomal loci to specific subcellular locations during bacterial DNA replication. Proc. Natl. Acad. Sci. U. S. A. *101*, 9257–9262.

Wachi, M., Doi, M., Tamaki, S., Park, W., Nakajima-Iijima, S., and Matsuhashi, M. (1987). Mutant isolation and molecular cloning of mre genes, which determine cell shape, sensitivity to mecillinam, and amount of penicillin-binding proteins in Escherichia coli. J. Bacteriol. *169*, 4935–4940.

Wade, R.H. (2009). On and around microtubules: an overview. Mol. Biotechnol. *43*, 177–191.

Warshaw, D.M. (2012). Tilting and twirling as myosin V steps along actin filaments as detected by fluorescence polarization. J. Gen. Physiol. *139*, 97–100.

Warshaw, D.M., Kennedy, G.G., Work, S.S., Krementsova, E.B., Beck, S., and Trybus, K.M. (2005). Differential labeling of myosin V heads with quantum dots allows direct visualization of hand-over-hand processivity. Biophys. J. *88*, L30–32.

Wells, A.L., Lin, A.W., Chen, L.Q., Safer, D., Cain, S.M., Hasson, T., Carragher, B.O., Milligan, R.A., and Sweeney, H.L. (1999). Myosin VI is an actin-based motor that moves backwards. Nature *401*, 505–508.

Werner, J.N., Chen, E.Y., Guberman, J.M., Zippilli, A.R., Irgon, J.J., and Gitai, Z. (2009). Quantitative genome-scale analysis of protein localization in an asymmetric bacterium. Proc. Natl. Acad. Sci. U. S. A. *106*, 7858–7863.

Wolgemuth, C., Hoiczyk, E., Kaiser, D., and Oster, G. (2002). How myxobacteria glide. Curr. Biol. CB *12*, 369–377.

Wu, L.J., and Errington, J. (1994). Bacillus subtilis SpoIIIE protein required for DNA segregation during asymmetric cell division. Science *264*, 572–575.

Wu, S.S., and Kaiser, D. (1995). Genetic and functional evidence that Type IV pili are required for social gliding motility in Myxococcus xanthus. Mol. Microbiol. *18*, 547–558.

Wu, L.J., Ishikawa, S., Kawai, Y., Oshima, T., Ogasawara, N., and Errington, J. (2009). Noc protein binds to specific DNA sequences to coordinate cell division with chromosome segregation. EMBO J. *28*, 1940–1952.

Yeates, T.O., Kerfeld, C.A., Heinhorst, S., Cannon, G.C., and Shively, J.M. (2008). Protein-based organelles in bacteria: carboxysomes and related microcompartments. Nat. Rev. Microbiol. *6*, 681–691.

Yeh, Y.-C., Comolli, L.R., Downing, K.H., Shapiro, L., and McAdams, H.H. (2010). The caulobacter Tol-Pal complex is essential for outer membrane integrity and the positioning of a polar localization factor. J. Bacteriol. *192*, 4847–4858.

Ben-Yehuda, S., Fujita, M., Liu, X.S., Gorbatyuk, B., Skoko, D., Yan, J., Marko, J.F., Liu, J.S., Eichenberger, P., Rudner, D.Z., et al. (2005). Defining a centromere-like element in Bacillus subtilis by Identifying the binding sites for the chromosome-anchoring protein RacA. Mol. Cell *17*, 773–782.

Yildiz, A., Forkey, J.N., McKinney, S.A., Ha, T., Goldman, Y.E., and Selvin, P.R. (2003). Myosin V walks hand-over-hand: single fluorophore imaging with 1.5-nm localization. Science *300*, 2061–2065.

Yonekura, K., Maki-Yonekura, S., and Homma, M. (2011). Structure of the flagellar motor protein complex PomAB: implications for the torque-generating conformation. J. Bacteriol. *193*, 3863–3870.

Youderian, P., Burke, N., White, D.J., and Hartzell, P.L. (2003). Identification of genes required for adventurous gliding motility in Myxococcus xanthus with the transposable element mariner. Mol. Microbiol. *49*, 555–570.

Yu, R., and Kaiser, D. (2007). Gliding motility and polarized slime secretion. Mol. Microbiol. *63*, 454–467.

Zenisek, D., and Perrais, D. (2007). Principles of Total Internal Reflection Microscopy (TIRFM). CSH Protoc. *2007*, pdb.top24.

Zhang, X.Y.-Z., Goemaere, E.L., Thomé, R., Gavioli, M., Cascales, E., and Lloubès, R. (2009). Mapping the interactions between escherichia coli tol subunits: rotation of the TolR transmembrane helix. J. Biol. Chem. *284*, 4275–4282.

Zimmerman, S.B., and Trach, S.O. (1991). Estimation of macromolecule concentrations and excluded volume effects for the cytoplasm of Escherichia coli. J. Mol. Biol. *222*, 599–620.

Zupancic, M.L., Tran, H., and Hofmeister, A.E. (2001). Chromosomal organization governs the timing of cell type-specific gene expression required for spore formation in Bacillus subtilis. Mol. Microbiol. *39*, 1471–1481.

Résumé

De part leur petite taille, les bactéries ont longtemps été considérées comme des organismes non-organisés, dans lesquels les protéines diffusaient simplement à travers le cytoplasme afin d'atteindre aléatoirement leur site d'action. Cependant, les récentes améliorations en imagerie cellulaire ont révélé que de façon similaire aux eucaryotes, les bactéries sont spatialement organisées : l'ADN, les ARNs et les protéines sont adressés à des régions subcellulaires spécifiques dans les bactéries, où elles pourront exercer leur fonction. Différents mécanismes permettent aux bactéries de localiser correctement leurs molécules en des sites subcellulaires spécifiques, mais la majorité de ces mécanismes semblent être passifs. En effet, il semble que seule la ségrégation de l'ADN nécessite des mécanismes de transport actif.

Dans cette thèse, grâce à l'étude de la motilité chez la bactérie *Myxococcus xanthus*, nous avons découvert une nouvelle classe de moteur processif permettant de transporter de manière directionnelle des complexes protéiques dans l'enveloppe cellulaire. En effet, dans la première partie de cette thèse, nous avons démontré que la motilité chez *M. xanthus* est énergisée par un moteur de type canal à protons, composé par les protéines AglRQS. Ce moteur coopère avec le cytosquelette d'actine bactérien pour transporter le complexe de l'enveloppe Glt à la surface de la cellule. Ce transport est traduit en motilité car les complexes Glt transportés interagissent avec un polysaccharide de surface : le « slime ». Ce « slime » agit comme une colle et immobilise les complexes Glt transportés contre le substrat, produisant ainsi le mouvement.

Au cours de cette étude, nous avons fait l'étonnante découverte que le moteur AglRQS est essentiel non seulement à la motilité, mais également à la sporulation, processus cellulaire durant lequel les cellules s'arrondissent et sont recouvertes d'un épais polysaccharide (le « spore coat »). Ce « spore coat » confère à la bactérie une résistance face à des conditions environnementales défavorables. Nous avons identifié le mécanisme et démontré une interaction directe entre le moteur AglRQS et le complexe de l'enveloppe Nfs, un proche homologue du complexe Glt. Nous avons démontré que le moteur AglRQS transporte le complexe Nfs de manière directionnelle autour de la spore. Le « spore coat » étant sécrété en différents *foci* autour de la surface de la spore, son transport par la machinerie Agl-Nfs assure la formation d'une couche de « spore coat » compacte et dense autour de la future spore.

En conclusion, ces résultats ont démontré pour la première fois l'existence d'un moteur bactérien impliqué dans le transport directionnel de complexes protéiques associés à des sucres. Ces moteurs étant présents dans d'autres *phyla* bactérien, nous proposons que cette classe de protéines pourrait avoir un rôle général dans l'organisation de la bactérie et pourrait transporter une multitude de cargos : des protéines et des sucres, mais également des lipides, des ARNs et/ou de l'ADN.

Abstract

Because of their small sizes, bacteria have been mostly considered as non-organized cells, wherein proteins simply diffuse throughout the cytoplasm to reach randomly their sites of action. However, improvements in cell imaging revealed that, akin to eukaryotic cells, bacteria are spatially organized: DNA, RNA and proteins are targeted to specific subcellular regions where they are spatially constricted to exert their function. Bacteria have evolved several mechanisms to localize properly molecules to subcellular sites, which appear to be mostly diffusion-driven. In fact, active processive transport mechanisms have only been described for DNA segregation.

In this thesis, by studying the motility system of the bacterium *Myxococcus xanthus*, we have found a new class of processive transport systems allowing to move protein complexes directionally in the cell envelope. In the first part of this thesis, we demonstrated that *M. xanthus* motility is driven by a proton channel composed by the AglRQS proteins. This motor cooperates with the bacterial actin cytoskeleton to transport an envelope-spanning Glt motility protein complex at the cell surface. This transport is translated into motility because the surface tip of the Glt complex is bound to a glue-type polysaccharide (the slime) that immobilizes the motility complex against the underlying substratum.

In the course of this study, we also made the surprising discovery that the AglRQS motor is essential not only for motility but also for sporulation, a cellular process during which the cells become surrounded by a thick polysaccharide (the spore coat) that confers resistance during unfavourable environmental conditions. We identified the mechanism and demonstrated a direct interaction between the AglRQS motor and a previously identified Nfs envelope complex, a close homolog of the Glt complex. We demonstrated that the AglRQS motor rotates the Nfs complex directionally around the spore surface. Since the main spore coat polymer is secreted at discrete sites around the spore surface, its transport by the Agl-Nfs machinery ensures the formation of a compact and dense spore coat layer around the future spore.

In total, these results demonstrated the existence of a new type of bacterial motor complex involved in the directional transport of sugar polymers at the cell surface. Because this type of motor is present in other bacterial lineages, this class of proteins might play general functions in the organization of the bacterial cell and could transport a multitude of cargos: proteins and sugars, but potentially lipids, RNA and/or DNA.